



HAL
open science

Traitement des DNAPL dans les eaux souterraines par injection de solutions de polymères : étude expérimentale et numérique

Amir Hossein Mohammadi Alamooti

► **To cite this version:**

Amir Hossein Mohammadi Alamooti. Traitement des DNAPL dans les eaux souterraines par injection de solutions de polymères : étude expérimentale et numérique. Mécanique des fluides [physics.class-ph]. HESAM Université, 2023. Français. NNT : 2023HESAE073 . tel-04445743

HAL Id: tel-04445743

<https://pastel.hal.science/tel-04445743v1>

Submitted on 8 Feb 2024

HAL is a multi-disciplinary open access archive for the deposit and dissemination of scientific research documents, whether they are published or not. The documents may come from teaching and research institutions in France or abroad, or from public or private research centers.

L'archive ouverte pluridisciplinaire **HAL**, est destinée au dépôt et à la diffusion de documents scientifiques de niveau recherche, publiés ou non, émanant des établissements d'enseignement et de recherche français ou étrangers, des laboratoires publics ou privés.

ÉCOLE DOCTORALE SCIENCES DES MÉTIERS DE L'INGÉNIEUR
[I2M – TREFLE ENSAM UMR 8508 – Campus de Bordeaux]

THÈSE

présentée par : **Amir Hossein MOHAMMADI ALAMOOTTI**

soutenue le : 27 novembre 2023

pour obtenir le grade de : **Docteur d'HESAM Université**

préparée à : **École Nationale Supérieure d'Arts et Métiers**

Spécialité : **Mécanique des fluides**

Remediation of DNAPL saturated aquifers by injecting polymer solutions: Experimental and numerical study

THÈSE dirigée par :
Mme. AHMADI-SENICHAULT Azita
M. DAVARZANI Dorian

et co-encadrée par :
M. COLOMBANO Stéfan

Jury

M. Henri BERTIN , Directeur de Recherche CNRS, Université de Bordeaux	Président
Mme. Linda ABRIOLA , Professeur, Brown University (Etats-Unis)	Rapporteuse
M. Richard MARTEL , Professeur, INRS, Université du Québec (Canada)	Rapporteur
Mme. Irina PANFILOVA , Maître de Conférence, Université de Lorraine	Examinatrice
M. Eric van HULLEBUSCH , Professeur, Université Paris Cité	Examinateur
Mme. Azita AHMADI-SÉNICHAULT , Professeure, Arts et Métiers	Examinatrice
M. Dorian DAVARZANI , Ingénieur de recherche, BRGM	Examinateur
M. Stéfan COLOMBANO , Ingénieur de recherche, BRGM	Examinateur
M. Guillaume MASSELOT , Ingénieur, ADEME	Invité
M. David CAZAUX , Responsable remédiation environnementale, INOVYN	Invité

زندگی چیست؟

عشق ورزیدن

زندگی را به عشق بخشیدن

زنده است آن که عشق می ورزد

دل و جانش به عشق می ارزد

هـ.ا. سایه

Acknowledgments

"No one who achieves success does so without acknowledging the help of others. The wise and confident acknowledge this help with gratitude."

Alfred North Whitehead
Mathematician

To begin, I express my gratitude to BRGM and ADEME (through PAPIRUS project) for their contribution to the funding of this PhD research.

I would like to acknowledge my thesis supervision committee Dr. Stéfán Colombano, Dr. Dorian Davarzani, and Prof. Azita Ahmadi.

Stéfán, you've not only served as an advisor but also as a mentor, providing me with invaluable insights. You have been always open to new ideas, and your office door was always open, fostering endless technical brainstorming between us. I couldn't envision an advisor with a greater sense of compassion and humanity.

Dorian, I want to convey my sincere thanks for your valuable input on my publications and your readiness to offer assistance when needed. Your efforts and support have been instrumental in helping me achieve my current position, and for that, I'm deeply appreciative.

Azita, you've been an invaluable mentor to me in multiple aspects; scientifically, professionally, and personally. Your kindness, and wealth of knowledge have been truly inspiring. I've thoroughly enjoyed experiencing these qualities in you.

I would like to extend my thanks to Prof. Abriola and Prof. Martel for graciously agreeing to invest their time in reviewing my thesis. I'd like to express my gratitude to Prof. van Hullebusch and Prof. Panfilova for serving as examiners of my thesis, as well as to Mr. Masselot and Dr. Cazaux for being esteemed invited guests on my thesis jury. A special thanks to Prof. Bertin, for his valuable comments and suggestions during the last three years as well as being the president of jury.

I want to thank our colleagues in BRGM who have helped me during these three years, Clément, Fabien, Michaëlle, Stéphane, Thibault, Stéphanie, and Cédric. I would like to thank Hamza, Zacks, Vikas, Abbas, and Idriss for their assistance in the experiments. Additionally, a big thank-you goes to my friends at BRGM —Sagyn, Maxime, Behshad, Adil, Ali, Bexultan and Lazzat for the kindness and friendliness. I want to thank my other friends who have always been a source of comfort for me and encouraged me through my Ph.D. Thank you Moji, Mehdi, and Armin.

I'd like to extend my deepest and warmest gratitude to my family for their unwavering support and unconditional love. To my mom, Zari, whom I deeply miss, whose spirit continues to reside within me, and whose memory will forever be etched in my heart. To my lovely father, Hormat, your wisdom and guidance have been my North Star throughout this journey. To my siblings, Mahnaz, Maryam, Hassan, and Behnaz, your encouragement and camaraderie have been invaluable to me; your support has lifted me up at every turn. And to my nephew, Arius, your youthful enthusiasm and love add joy to me.

Finally, my heartfelt appreciation goes to my soulmate Fereshteh. *You are the soul of Universe and your name is Love.* Over the past three years, your unwavering support has been more than I could have ever hoped for, and I aspire to one day reciprocate the boundless love and support you've so generously given.

Abstract

The remediation of soils contaminated with DNAPL (Dense non-aqueous phase liquid) near groundwater is a crucial environmental issue due to the significance of water resources. Injection of polymer solutions into the contaminated zones has been used as a promising method for soil aquifer remediation. The existing literature lacks a comprehensive numerical and experimental examination of the non-Newtonian properties of polymer solutions used for displacing DNAPL in single or multi-layer systems. There's also an underexplored area concerning the reduction of residual DNAPL in layered systems following the primary introduction of a polymer solution. Furthermore, addressing the challenge of density-driven concerns in an unconfined system during polymer injection remains necessary. In order to evaluate the efficiency of this technology, a variety of experimental and numerical analyses has been performed. The non-Newtonian behavior of polymer solutions, along with other chemical substances including suspended particles, surfactant, salt, and alcohols in bulk and in porous media, was examined. The 1-column and 2D-tank as the experimental setups were used for displacement studies, and COMSOL Multiphysics was used for numerical analysis. To address the density-driven issue during the displacement of DNAPL a gravity-driven remediation method is evaluated in which the polymer solution is densified either by suspended barite particles or the salts. The impact of densifying the polymer solution with suspended particles or soluble salt showed that the polymer densification can improve DNAPL recovery factor up to 4 times. Clogging of suspended particles in porous media during densified polymer suspension injection was characterized; a reduction in permeability up to 70% was observed. For the case of injection of densified brine polymer solution, densification of polymer solution in 2D two-phase experiments could result in improvement of propagation aspect ratio (ratio of lateral to vertical radius) in the system from 0.38 to 1.2. Two-phase flow numerical simulations in porous media were employed to assess various scenarios during the displacement of DNAPL using polymer solutions. The injection of polymer solution in an unconfined domain has been analyzed experimentally and numerically in order to mimic the conditions as close as possible to a real polluted site. The performance of polymer solutions with and without surfactant on the remediation of a DNAPL-polluted multilayer system has been investigated. 2D experiments revealed that the displacement of DNAPL in multilayer zones was affected by permeability difference and density contrast of fluids in a heterogeneous soil. To minimize the residual saturation of DNAPL in the multilayer system, the efficiency of post-injection mixtures of polymer/alcohol/surfactant was evaluated. Density analysis of the samples obtained from displacement experiments in single-layer column and the multilayer 2D tank shows that the mobilization mechanism can improve the recovery factor from 91% (achieved by primary flushing) to 99% in 1D column and from 86% to 94% in 2D tank. This thesis provides the promising results for remediation of real polluted aquifers by DNAPL, by shedding light on the non-Newtonian properties of polymer solutions and considering the impact of density-driven flow on DNAPL displacement in both single-layer and multilayer systems.

Résumé

La dépollution des nappes phréatiques contaminées par les DNAPLs (en anglais, «Dense Non-Aqueous Phase Liquid») est un enjeu environnemental crucial en raison de l'importance des ressources en eau. L'injection de solutions de polymères constitue une technique prometteuse pour le traitement de ces aquifères. La littérature existante ne dispose pas d'un examen numérique et expérimental complet des propriétés non newtoniennes des solutions polymères utilisées pour déplacer le DNAPL dans des systèmes monocouches ou multicouches. Il existe également un domaine sous-exploré relatif à la diminution du DNAPL résiduel dans les systèmes en couches suite à l'introduction primaire d'une solution de polymère. De plus, il est nécessaire de relever le défi des problèmes liés à la densité dans un système non confiné lors de l'injection de polymère. Diverses analyses expérimentales et numériques ont été effectuées afin d'évaluer l'efficacité de cette technologie. Des essais rhéologiques ont été effectués avec différents types de polymères en solution (sans et avec milieu poreux), ainsi que d'autres substances chimiques incluant les microparticules en suspension, le tensioactif, le sel (iodure de sodium) et les alcools. Une colonne 1D et un bac 2D ont été utilisés pour les études expérimentales de dépollution, et COMSOL Multiphysics a été utilisé pour l'analyse numérique. L'impact de la densification de la solution de polymère avec des particules en suspension ou du sel soluble a été évalué ; il a été démontré que la densification du polymère permet d'améliorer l'efficacité du déplacement du DNAPL jusqu'à un facteur 4. De plus, le dépôt de matières en suspension dans les milieux poreux lors de l'injection de suspension de polymère densifiée a été caractérisé ; une réduction de la perméabilité allant jusqu'à 70% a été observée. Dans le cas de l'injection de solution de polymère densifiée avec de la saumure, la densification de la solution de polymère dans des expériences bidimensionnelles à deux phases entraîne une amélioration du rapport d'aspect (ratio du rayon latéral/ rayon vertical de propagation) dans le système passant de 0,38 à 1,2. Des simulations numériques de l'écoulement diphasique en milieu poreux ont été réalisées pour évaluer divers scénarios de déplacement des DNAPLs à l'aide de solutions de polymères. L'injection de solution de polymères dans un milieu non confiné a été étudiée expérimentalement et numériquement afin de reproduire les conditions les plus proches possibles d'un site pollué. Les performances des solutions de polymères, avec et sans tensioactif, sur la dépollution d'un système multicouche pollué par des DNAPLs ont été étudiées. Les expériences en bac 2D ont révélé que le déplacement des DNAPLs dans les zones multicouches était affecté par la différence de perméabilité et le contraste de densité des fluides dans un sol hétérogène. Par ailleurs, l'efficacité des mélanges post-injection de polymère/alcool/tensioactif a été évaluée afin de diminuer la saturation résiduelle des DNAPL en milieu hétérogène. Les analyses de la densité des échantillons obtenus à partir des expériences en colonne 1D monocouche et en bac 2D multicouche montrent que le mécanisme de mobilisation peut améliorer l'efficacité de récupération de 91% (atteint par le rinçage primaire) à 99% en colonne 1D, et de 86% à 94% en bac 2D. Cette thèse fournit des résultats prometteurs pour la réhabilitation d'aquifères réellement pollués par DNAPL, en mettant en lumière les propriétés non newtoniennes des solutions polymères et en considérant l'impact de l'écoulement basé sur la densité sur le déplacement de DNAPL dans les systèmes monocouches et multicouches.

Table of content

List of Figures	vii
Nomenclature	xii
Part 1 – Substantial summary in French	1
1. Introduction	3
2. Matériel et méthodes : expérimental	8
2.1. Matériel et consommables expérimentaux	8
2.2. Expériences en colonnes 1D.....	9
2.3. Expériences en bac 2D	10
2.4. Mélanges et solutions	13
3. Modélisation numérique.....	14
3.1. Écoulement diphasique en milieu poreux.....	14
3.2. Modèle de transport de soluté.....	16
4. Résultats et discussions	18
4.1. Comportement rhéologique	18
4.1.1. Xanthane et SDBS.....	18
4.1.2. Xanthane, SDBS et alcools.....	19
4.1.3. CMC et barytine	20
4.1.4. Xanthane et sel (NaI).....	21
4.2. Déplacement unidimensionnel (colonne 1D)	22
4.2.1. Xanthane et SDBS.....	22
4.2.2. Xanthane, SDBS et alcools.....	24
4.2.3. Xanthane et NaI.....	26
4.3. Écoulement bidimensionnel (bac 2D)	27
4.3.1. Xanthane et SDBS dans système multicouche	27
4.3.2. Xanthane, SDBS et alcools dans système multicouche.....	30
4.3.3. CMC et Barytine dans système non confiné	35
4.3.4. Xanthane et NaI dans système non confiné.....	39
Conclusion.....	42
Part 2 – Dissertation in English	49
1. General introduction	50
1.1 Introduction	51
1.2 Overview on polluted sites in France	52
1.3 French public policy for contaminated sites.....	53
1.4 PAPIRUS project	55
1.4.1. Tavaux polluted site	56
1.4.2. Composition of DNAPL in Tavaux site	58

2. Literature Review	60
2.1 Introduction	61
2.2 Properties of porous media.....	64
2.2.1. Porous media	64
2.2.2. Scale	64
2.2.2.1. Molecular Scale.....	65
2.2.2.2. Pore-Scale.....	65
2.2.2.3. Representative Elementary Volume (REV)	65
2.2.2.4. Darcy Scale.....	66
2.2.3. Porosity.....	66
2.2.4. Permeability.....	66
2.2.5. Saturation.....	67
2.2.6. Wettability	67
2.2.7. Capillary pressure.....	68
2.2.8. Relative permeability.....	70
2.3 Fluid flow in porous media.....	72
2.3.1. Single phase flow	72
2.3.2. Multiphase flow.....	73
2.3.3. Finite element method	74
2.4 Polymers.....	75
2.4.1. Polysaccharides	75
2.4.1.1. Xanthan	76
2.4.2. Polymer Conformation and Entanglement	77
2.5 Polymer transport in porous media.....	78
2.5.1. Retention	78
2.5.1.1. Mechanical entrapment	79
2.5.1.2. Hydrodynamic retention.....	79
2.5.1.3. Polymer bridging	79
2.5.1.4. Adsorption	80
2.5.1.5. Adsorption measurement.....	82
2.5.1.6. Adsorption kinetic and isotherm models	83
2.5.2. Diffusion.....	84
2.5.3. Dispersion.....	85
2.5.4. Advection	86
2.5.5. Advection dispersion reaction	87
2.6 Rheology	88
2.6.1. Viscosity.....	88

2.6.2.	Non-Newtonian fluids	89
2.6.2.1.	Viscoelasticity	89
2.6.2.2.	Time-dependent viscosity.....	90
2.6.2.3.	Shear-rate dependent viscosity	90
2.6.2.4.	Shear-thinning fluids	91
2.6.2.5.	Non-Newtonian fluid models	92
2.6.3.	Rheological behavior of xanthan.....	93
2.6.4.	Rheological behavior of polymer solutions in porous media	95
2.7	Polymer for polluted aquifer remediation	97
2.8	Density-driven issue during DNAPL displacement	99
2.9	Dimensionless numbers and Lenormand curve.....	101
2.10	Objectives and structure of the thesis	103
3.	Remediation of multilayer DNAPL contaminated aquifers by injection of polymer solutions: primary injection of polymer/polymer-surfactant, post-injection of polymer-alcohol mixture	106
	Summary	107
3.1.	Remediation of multilayer soils contaminated by heavy chlorinated solvents using biopolymer-surfactant mixtures: two-dimensional flow experiments and simulations.....	109
3.1.1.	Abstract	111
3.1.2.	Introduction	112
3.1.3.	Materials and methods: experimental and numerical	115
3.1.3.1.	Experimental materials.....	115
3.1.3.2.	Column experiments.....	116
3.1.3.3.	2D tank experiments.....	117
3.1.3.4.	Error and uncertainty estimations.....	118
3.1.3.5.	Polymer/surfactant solutions	118
3.1.3.6.	Numerical modeling	118
3.1.4.	Results and discussion.....	122
3.1.4.1.	Rheological behavior and polymer surfactant interactions	122
3.1.4.2.	One dimensional displacement.....	125
3.1.4.3.	Two-Dimensional displacement	128
3.1.5.	Conclusion.....	134
3.1.6.	Appendix	135
3.1.6.1.	DNAPL composition and properties	135
3.1.6.2.	Single phase flow experiments.....	140
3.2.	Enhancing Remediation of Residual DNAPL in Multilayer Aquifers: Post-Injection of Alcohol-Surfactant-Polymer Mixtures	146
3.2.1.	Abstract	148

3.2.2.	Introduction	150
3.2.3.	Materials and methods.....	154
3.2.3.1.	Experimental materials.....	154
3.2.3.2.	Batch experiment.....	155
3.2.3.3.	1D column	156
3.2.3.4.	2D tank	157
3.2.4.	Results and discussion.....	158
3.2.4.1.	Partitioning behavior alcohol-surfactant mixture and DNAPL	158
3.2.4.2.	Selection of the flushing mixtures	162
3.2.4.3.	1 D column experiments.....	164
3.2.4.4.	Evaluating different injection scenarios for DNAPL mobilization mechanism in columns	167
3.2.4.5.	2D tank experiments.....	168
3.2.5.	Conclusion.....	172
3.2.6.	Appendix	174
4.	Remediation of DNAPL Polluted Aquifers by injection of Densified Biopolymer Suspension/solution	181
	Summary	182
4.1.	Influence of the injection of densified polymer suspension on the efficiency of DNAPL displacement in contaminated saturated soils	183
4.1.1.	Abstract	185
4.1.2.	Environmental Implication.....	185
4.1.3.	Introduction	186
4.1.4.	Material and methods (experimental and numerical)	190
4.1.4.1.	1D column experiments.....	190
4.1.4.2.	2D tank experiments.....	191
4.1.4.3.	Suspensions preparation	194
4.1.4.4.	Image interpretation.....	195
4.1.4.5.	Governing equations.....	196
4.1.5.	Results	201
4.1.5.1.	Rheological behavior of the densified polymer suspension	201
4.1.5.2.	Experiments on clogging of barite particles in sandpacks.....	203
4.1.5.3.	Experimental results of DNAPL displacement using barite-CMC suspension ...	204
4.1.5.4.	Effect of the boundaries on the DNAPL recovery factor (closed or open system)	206
4.1.6.	Discussion	208
4.1.6.1.	Characterization of the clogging of barite particles by finding attachment/detachment parameters	208

4.1.6.2.	Numerical simulation results of DNAPL displacement using barite-CMC suspension	210
4.1.6.3.	Analysis of the transition zone in displaced zone.....	213
4.1.6.4.	Difference between closed and open systems	214
4.1.7.	Conclusions	215
4.1.8.	Appendix	216
4.1.8.1.	Experimental materials.....	216
4.1.8.2.	DNAPL.....	216
4.1.8.3.	Barite-polymer suspension	217
4.1.8.4.	Soil physics.....	217
4.2.	Gravity-Driven Remediation of DNAPL Polluted Aquifers using Densified Biopolymer Brine Solution: Two-Dimensional Flow Experiments and Simulations	222
4.2.1.	Abstract	224
4.2.2.	Introduction	224
4.2.3.	Materials and methods (experimental and numerical).....	230
4.2.3.1.	Experimental materials.....	230
4.2.3.2.	Column and 2D tank experiments	231
4.2.3.3.	Xanthan-NaI solutions.....	234
4.2.3.4.	Numerical modeling	235
4.2.3.5.	Image analysis	239
4.2.4.	Results and discussion.....	240
4.2.4.1.	Rheological behavior in bulk and porous media	240
4.2.4.2.	Two-phase flow columns experiments	244
4.2.4.3.	Two-dimensional flow (2D tank)	245
4.2.4.4.	Gravity number analysis.....	251
4.2.4.5.	DNAPL displacement in confined two-layer system by densified polymer solution	252
4.2.4.6.	Sensitivity analysis	256
4.2.5.	Conclusions	258
5.	Conclusions and perspectives	260
5.1.	Conclusions	261
5.2.	Perspectives	266
	List of Publications Scientific papers.....	269
	Contribution of authors in research papers in this thesis.....	272
	References	274

List of Figures

Figure 1-1 Main pollutants found in contaminated sites across France (Report of French Ministry of Ecological Transition, 2015)	53
Figure 1-2 Investment distribution across sectors for the preservation and improvement of soil, groundwater, and surface water in the year 2018.	54
Figure 1-3 Map of factory location and source site for the study (Cazaux et al., 2014)	57
Figure 1-4 Hydrogeological cross section and schematic representation of Tavaux site adapted from Cazaux et al. (2014).....	57
Figure 1-5 Migration of the DNAPL (orange phase) from the storage sector to the plume area in a) 1989 and b) 2009 (Cazaux et al., 2014)	58
Figure 2-1 Different scales: Molecular scale, pore scale, REV and Darcy scale.....	65
Figure 2-2 Schematic of capillary pressure curve for imbibition and drainage	69
Figure 2-3 Schematic of relative permeability curves for a water-wet porous media	71
Figure 2-4 1D slab of porous medium	72
Figure 2-5 chemical structure of xanthan gum (García-Ochoa et al., 2000).....	77
Figure 2-6 Schematic of different mechanisms of polymer retention mechanisms in porous media	79
Figure 2-7 Schematic of adsorption of species in liquid phase (blue color) onto the solid surface (dashed gray grain in the middle)	81
Figure 2-8 Polymer and tracer breakthrough curves in a column test.....	83
Figure 2-9 Schematic of Couette parallel flow	89
Figure 2-10 Classification of fluids with shear stress as a function shear rate	91
Figure 2-11 Rheological behavior of a shear-thinning fluid	92
Figure 2-12 Schematic comparison of in-situ and bulk rheology	96
Figure 2-13 Phase-diagram of multiphase domain displacement	103
Figure 3.1-1 Rheological behavior of the mixture of xanthan and SDBS solution at fixed xanthan concentration of 800 mg/L and various concentrations of SDBS and Carreau models fitted on experimental data	123
Figure 3.1-2 SEM micrographs. (a) SDBS 1265 mg/L, (b) xanthan 800 mg/L, and (c) mixture of xanthan 800 mg/L and SDBS 1265 mg/L.....	124
Figure 3.1-3 Performance of injection of polymer solutions in two sand packs of different permeabilities. (a) Recovery factor, (b) Capillary number versus injected PV	127
Figure 3.1-4 DNAPL displacement in a 2D multilayer system by injection of xanthan solution (first row) and mixture of xanthan-SDBS (second row) at different pore volumes of injected fluids.....	129
Figure 3.1-5 Comparison between the numerical and experimental results of DNAPL displacement by xanthan solution in a 2D multilayer system, first row: experimental results shown; second row simulation results depicted.	132
Figure 3.1-6 Crossflow between the layers after 0.66 PV injection of xanthan in a 2D multilayer system. (a) xanthan-DNAPL distribution in the system, the arrows show the direction of crossflow and the star shows zero cross flow, (b) pressure gradient along the layers	132

Figure 3.1-7 DNAPL displacement by xanthan solution (black-blue) in a 2D multilayer system where the contaminated zone is blocked by the injection of a densified polymer suspension (pink) through a horizontal well	134
Figure 3.1-8 Schematic of polymer-DNAPL displacement experimental setup (2D tank) as well as the layers configurations. (a) unconfined system, and (b) confined system	138
Figure 3.1-9 Schematic of boundary and initial conditions for numerical simulations. (a) 1D column, and (b) 2D tank.....	138
Figure 3.1-10 Rheological behavior of the xanthan solutions at different concentrations.....	139
Figure 3.1-11 Apparent viscosity compared with those obtained from rheometer. (a) pure xanthan solution for the fine sand, (b) pure xanthan solution for coarse sand, (c) mixture of xanthan and SDBS for fine sand, and (d) mixture of xanthan and SDBS for coarse sand	140
Figure 3.1-12 Breakthrough curves for tracer, xanthan and mixture of xanthan-SDBS in 1D columns. (a) Fine sand, and (b) Coarse sand.....	141
Figure 3.1-13 Apparent viscosity versus pressure gradient for fine and coarse sand in 1D columns	141
Figure 3.1-14 Comparison of results obtained from experiments and simulations for xanthan-DNAPL displacement for different soils in 1D columns. (a) Recovery factor versus injected PVs, (b) Differential pressure versus injected PVs	142
Figure 3.1-15 Results obtained from injection of polymer solutions into the multilayer 2D system. (a) Recovery factor, (b) Differential pressure	143
Figure 3.1-16 Comparison between the numerical and experimental results. (a) Recovery factor, (b) differential pressure for xanthan-DNAPL displacement in a confined multilayer 2D system.....	144
Figure 3.1-17 DNAPL displacement by densified polymer ($\rho= 1.66$ g/mL) solution in a multilayer system after injection period for (a) 0.33 PV, (b) 0.5 PV, and (c) 0.66 PV.....	145
Figure 3.1-18 DNAPL displacement by non-densified polymer ($\rho= 1$ g/mL) injection by considering an open boundary on the upper side (unconfined system) after injection of 1 PV	145
Figure 3.2-1 Schematic of polymer-surfactant injection (container 1) followed by ASP mixture injection (container 2) for DNAPL displacement in 1D column.....	157
Figure 3.2-2 Schematic of polymer-surfactant injection (container 1) followed by ASP mixture (container 2) injection for DNAPL displacement in the 2D tank (multilayer system)	158
Figure 3.2-3 Dissolution of DNAPL in contact with AS mixtures containing solely 1-propanol (a) graph showing the dissolution rates, and (b) schematic of dissolution: tubes on the left represent the state before mixing, while those on the right depict the state after mixing. The gray color indicates the AS mixture prior to mixing. DNAPL is represented by the black color, and the brownish phase signifies the aqueous phase post-mixing	160
Figure 3.2-4 a) Swelling factor of organic phase versus volume ratio of 1-propanol:1-hexanol for various water/alcohol and DNAPL volume fractions (b) schematic of dissolution for the case 0:1	161
Figure 3.2-5 Viscosities of different ASP mixtures containing xanthan with concentration of 2 g/L, as well as XS mixture	164

Figure 3.2-6 Experimental results of post-injection of ASP mixtures in columns: (a) recovery factor for low permeable layer, (b) differential pressure for low permeable layer, (c) recovery factor for high permeable layer, and (d) differential pressure for high permeable layers.....	167
Figure 3.2-7 DNAPL displacement in a 2D multilayer system by injection of XS solution (first row) and subsequent injection of C ₃ mixture (second row) against the number of PVs injected of each solution.....	170
Figure 3.2-8 DNAPL displacement in a 2D multilayer system by injection of XS solution (first row) and subsequent injection of C ₃ -C ₆ mixture (second and third rows) against the number of PVs of each solution injected, mobilized ganglia are shown by red circles.....	171
Figure 3.2-9 Densities of organic phase versus volume ratio of 1-propanol:1-hexanol	174
Figure 3.2-10 Partitioning of 1-propanol into organic phase versus volume ratio of 1-propanol: 1-hexanol.....	174
Figure 3.2-11 Samples (from left to right) chronologically obtained from the post-injection of C ₃ -C ₆ mixture in a high-permeability layer at residual DNAPL saturation (the corresponding PVs of post-injection are shown above the samples).....	175
Figure 3.2-12 DNAPL content/densities of organic phase produced during mobilization /solubilization mechanisms. (a) C ₃ mixture post-injection in low permeable layer, (b) C ₃ mixture post-injection in high permeable layer, (c) C ₃ -C ₆ mixture post-injection in low permeable layer, (d) C ₃ -C ₆ mixture post-injection in high permeable layer, (e) C ₆ mixture post-injection in low permeable layer, and (f) C ₆ mixture post-injection in high permeable layer.....	176
Figure 3.2-13 Evaluating different injection scenarios for DNAPL mobilization mechanism in columns. (a) Low permeable layer, and (b) High permeable layer	177
Figure 3.2-14 Experimental data for primary injection of XS and post injection of C ₃ mixture into multilayer system. (a) Recovery factor versus PV, and (b) differential pressure versus PV	178
Figure 3.2-15 Experimental data for primary injection of XS and post injection of C ₃ -C ₆ mixture into multilayer system. (a) Recovery factor versus PV, and (b) differential pressure versus PV.....	179
Figure 4.1-1 Schematic of barite-polymer solution injection in 1D column	191
Figure 4.1-2 Schematic of 2D tank (configurations of fluids and sands)	192
Figure 4.1-3 Schematic of barite-polymer solution-DNAPL displacement experimental setup (2D tank)	194
Figure 4.1-4 Rheological behavior of barite-CMC mixtures with different densities	202
Figure 4.1-5 Comparison of the propagation of the barite-CMC solutions with different densities, the left images are the raw images, and the right images are those interpreted by image analysis. (a) pure polymer injection with density of 1 g/mL, barite-CMC injection with density of (b) 1.3 g/mL, (c) 1.66 g/mL, and (d) 1.9 g/mL. The injection is from bottom.....	206
Figure 4.1-6 schematic of configuration and displacement of DNAPL by barite-polymer suspension with the density of 1.66 g/mL in a closed system.....	207
Figure 4.1-7 Comparison between the outlet densities obtained from simulation and experiments after breakthrough time.....	210
Figure 4.1-8 Geometry used for modeling and the corresponding boundary conditions.....	211

Figure 4.1-9 Comparison between the numerical and experimental results for the end of displacement of DNAPL by barite-CMC suspension, the first row images are from the simulation and the second row images are extracted from the image analysis of experiments. (a) pure polymer injection with density of 1 g/mL after 94 min, barite-CMC injection with density of (b) 1.3 g/mL after 234 min, (c) 1.66 g/mL after 240 min, and (d) 1.9 g/mL after 220 min.....	212
Figure 4.1-10 Comparison between the experimental displacement efficiencies for various densities of invading phases (obtained using mass balance) and those obtained from simulation results.....	213
Figure 4.1-11 Propagation of the barite-polymer solutions with density of 1.66 g/mL in a closed system after (a) 20 min, (b) 23 min, (c) 34 min, (d) 49 min, (e) 64 min, (f) 70 min, and (g) the one after 70 min interpreted by image analysis.	219
Figure 4.1-12 Images of fully displaced and transition zones in the right hand side of 2D tank for the barite-CMC injection with density (a1-4) 1.3 g/mL at 50, 95, 145, 234 min after injection respectively, (b1-4) 1.66 g/mL 38, 99, 161, 240 min after injection respectively , and (c1-4) 1.9 g/mL 65, 100, 135, 220 min after injection respectively.....	221
Figure 4.1-13 Dynamics of the growth of the transition zone during the injection of barite-CMC in the 2D tank	221
Figure 4.2-1 Schematic of polymer-DNAPL displacement experimental setup. (a) 1D column setup,(b) unconfined 2D tank, and (c) confined multilayer 2D tank.....	234
Figure 4.2-2 Schematic of boundary and initial conditions for numerical simulations in 2D tank. (a) unconfined single layer 2D tank, (b) confined two-layer 2D tank	239
Figure 4.2-3 Rheological behavior of xanthan solution at a concentration of 800 mg/L and mixture of xanthan and NaI with xanthan concentration of 590 mg/L and NaI concentration of 960.11 g/L as well as Carreau models fitted on experimental data. Experiments have been triplicated and error bars are calculated by determining the mean (average) of the data points and the standard deviation.....	242
Figure 4.2-4 Apparent viscosity compared with those obtained from rheometer. (a) mixture of xanthan and NaI, (b) pure xanthan solution	243
Figure 4.2-5 Performance of injection of different solutions. (a) Recovery efficiency, (b) Capillary number versus injected PV	245
Figure 4.2-6 Comparison of the propagation of three solutions at the end of injection through the contaminated zone, DNAPL appears black and displaced zone is bright. (a) Mixture of xanthan and NaI, (b) pure NaI brine, and (c) xanthan solution.....	246
Figure 4.2-7 Dynamic of propagation of the fluids during injection through the DNAPL contaminated zone. (a) fully displaced zone for injection of mixture of xanthan and NaI, (b) transition displaced zone for injection of mixture of xanthan and NaI, (c) displaced zone for injection of NaI brine solution, and (d) displaced zone for injection of xanthan solution.....	247
Figure 4.2-8 Comparison of recovery factor obtained from experiments and simulations for injection of different solutions including mixture of xanthan and NaI solution, pure NaI solution, and xanthan solution.....	248
Figure 4.2-9 Comparison between the numerical and experimental results at the end of the displacement of DNAPL by different solutions, the first row images are extracted from the	

image analysis of experiments and the second row images are from the simulation. (a) Mixture of NaI and xanthan (b) pure NaI, (c) and pure xanthan.....	249
Figure 4.2-10 Comparison of the propagation of invading solutions and DNAPL in 2D tank at different times, (a) mixture of xanthan and NaI solution, (b) pure NaI solution, and (c) pure xanthan solution	250
Figure 4.2-11 Changes in aspect ratio of invaded fluid based on gravity number using numerical simulations in 2D tank domain.....	252
Figure 4.2-12 DNAPL displacement in a 2D multilayer system by injection of pure xanthan solution (first row), mixture of xanthan-NaI (second row) and numerical simulation for xanthan-NaI (third row) at different pore volumes of injected fluids	253
Figure 4.2-13 Recovery efficiency curve for experiments of injection of pure xanthan and xanthan-NaI mixture into multilayer system and results from numerical simulation for xanthan-NaI mixture injection	254
Figure 4.2-14 Effect of permeability contrast on propagation of invading xanthan-NaI solution in DNAPL saturated two-layer system.....	255
Figure 4.2-15 Effect of L/H ratios on propagation of invading xanthan-NaI solution in DNAPL saturated two-layer system.....	256
Figure 4.2-16 Sensitivity analysis of numerical simulation parameters compared with selected experiment. (a) non wetting phase relative permeability saturation exponent, (b) non wetting phase maximum relative permeability, (c) wetting phase relative permeability saturation exponent, (d) wetting phase maximum relative permeability, (e) threshold pressure, (f) pore size distribution, and (g) transport equation.....	257

Nomenclature

Latin symbols

		Units
A	Global Stiffness matrix,	
\mathbf{b}	Global load vector	
c	Concentration	(kg/m ³)
c_b	Barite particle concentration in the bulk of suspension	(kg/m ³)
C_e	Equilibrium concentration of the adsorbate	(mg/L)
c_s	Concentration of barite particles deposited on the sand grain surfaces per unit pore volume	(kg/m ³)
D	Hydrodynamic dispersion	(m ² /s)
\mathbf{D}	Dispersion tensor	
D_0	Molecular diffusion coefficient	(m ² /s)
D_{eff}	Effective diffusion coefficient	(m ² /s)
D_m	Mechanical dispersion	(m ² /s)
\mathbf{g}	gravity vector	(m/s ²)
\mathbf{I}	Identity matrix	
I_0	Initial luminous intensity	
I_r	Reflected luminous intensity	
J_{adv}	Advective mass flux	(kg/m ² /s)
J_{disp}	Dispersive mass flux	(kg/m ² /s)
J_{diff}	Diffusive mass flux per unit area	(kg/m ² /s)
k	scalar absolute permeability	(m ²)
k_0	Initial absolute permeability	(m ²)
k_1	rate constant of the first-order adsorption	(1/s)
k_L	Langmuir constant	(L/mg)
k_{rd}	Relative permeability of defending phase	(-)
k_{rin}	Relative permeability of invading phase	(-)
k_{rnw}	Non-wetting phase relative permeability	(-)
k_{rnw}^{max}	Maximum relative permeability of non-wetting phase	(-)
k_{rw}	Wetting phase relative permeability	(-)
k_{rw}^{max}	Maximum relative permeability of wetting phase	(-)
l	Power index of Carreau fluid model	(-)
N_{ca}	Capillary number	(-)
N_G	Gravity number	(-)
n	Flow behavior index	
\mathbf{n}	Outward normal direction	
O_d	Optical density of reflected light	
p	Pressure	(Pa)
P_c	Capillary pressure	(Pa)
p_{th}	Threshold pressure	(Pa)
p_{nw}	Pressure of non-wetting phase	(Pa)
p_w	Pressure of wetting phase	(Pa)
q	Adsorbed mass on the solid surface	(g/g)
q_e	Amounts of adsorbate adsorbed at equilibrium in in mass of adsorbate	mg/g
q_t	Amounts of adsorbate adsorbed at time (t) in in mass of adsorbate	mg/g
r	Average pore radius	m

R_{eq}	Average pore throat radius	(m)
S_{nw}	Non- wetting phase saturation	(-)
S_{nwe}	Effective saturations of non-wetting phase	(-)
S_{nwr}	Residual saturation of the non-wetting phase	(-)
S_w	Wetting phase saturation	(-)
S_{we}	Effective saturations of wetting phase	(-)
S_{wir}	Irreducible saturation of the wetting phase	(-)
t	Time	s
\mathbf{u}	Velocity vector	(m/s)
u	Darcy velocity	(m/s)

Greek symbols

		Units
α	Empirical shifting parameter of apparent viscosity	(-)
α	Dispersivity	(m)
α_L	Longitudinal dispersivity	(m)
α_T	Transverse dispersivity	(m)
β	Particle detachment coefficient	(s ⁻¹)
$\dot{\gamma}$	Shear rate	(s ⁻¹)
ϵ_{nw}	Saturation exponents for non-wetting phases	(-)
ϵ_w	Saturation exponents for wetting phases	(-)
θ	Particle attachment coefficient	(s ⁻¹)
κ	Flow consistency index	(Pa.s ⁿ)
λ	Index of the pore size distribution	(-)
μ	Viscosity	(Pa.s)
μ_0	Viscosity at zero shear rate	(Pa.s)
μ_d	Viscosity of defending phase	(Pa.s)
μ_{in}	Viscosity of invading phase	(Pa.s)
μ_{inf}	Viscosity at infinite shear rate	(Pa.s)
v	Test function	
ρ	Density	(kg/m ³)
ρ_B	Bulk density	(kg/m ³)
ρ_b	Solid barite density	(kg/m ³)
ρ_{nw}	Density of non-wetting phase	(kg/m ³)
ρ_t	Ratio of reflected luminous intensity and the initial luminous intensity	
ρ_w	Density of wetting phase	(kg/m ³)
σ	Interfacial tension	N/m
τ	Tortuosity factor	(-)
τ_f	Fluid shear stress	(Pa)
\emptyset	Porosity	(-)
\emptyset_0	Initial porosity	(-)
χ	Relaxation time	(s)
ω	Contact angle	(°)
Ω	Domain of solution	

Acronyms

ADR	Advection-Dispersion-Reaction equation
AOI	Area of interest
AS	Alcohol-Surfactant mixture
ASP	Alcohol-Surfactant-Polymer mixture
BDF	Backward differentiation formula
CBLA	Colloidal biliquid aphron
CMC	Carboxymethyl cellulose
COC	Chlorinated organic compounds
DNAPL	Dense Non-Aqueous Phase Liquids
EOR	Enhanced Oil Recovery
FEM	Finite element method
HBCD	Hexachlorobutadiene
HCA	Hexachloroethane
HPAM	Hydrolyzed polyacrylamide
IFT	Interfacial tension
LNAPL	Light Non-Aqueous Phase Liquids
MRE	Mean relative error
MUMPS	Multifrontal massively parallel sparse direct solver
NAPL	Non-Aqueous Phase Liquids
PAH	Polycyclic Aromatic Hydrocarbons
PAM	Polyacrylamide
PCE	Perchloroethylene
PDE	Partial differential equations
PeCB	Penta-chlorobenzene
PFO	Pseudo-first-order adsorption kinetic model
PSO	Pseudo-second-order model adsorption kinetic model
PV	Pore volume
REV	Representative elementary volume
SEM	Scanning electron microscopic
SDBS	Sodium dodecylbenzenesulfonate
SDS	Sodium dodecyl sulfate
TCE	Trichloroethylene
TCM	Carbon tetrachloride
TOC	Total organic carbon
XS	Xanthan-SDBS mixture

Part 1 – Substantial summary in French

Résumé

La dépollution des nappes phréatiques contaminées par les DNAPLs (en anglais, « Dense Non-Aqueous Phase Liquid ») est un enjeu environnemental crucial en raison de l'importance des ressources en eau. L'injection de solutions de polymères constitue une technique prometteuse pour le traitement de ces aquifères. La littérature existante ne dispose pas d'un examen numérique et expérimental complet des propriétés non newtoniennes des solutions polymères utilisées pour déplacer le DNAPL dans des systèmes monocouches ou multicouches. Il existe également un domaine sous-exploré relatif à la diminution du DNAPL résiduel dans les systèmes en couches suite à l'introduction primaire d'une solution de polymère. De plus, il est nécessaire de relever le défi des problèmes liés à la densité dans un système non confiné lors de l'injection de polymère. Diverses analyses expérimentales et numériques ont été effectuées afin d'évaluer l'efficacité de cette technologie. Des essais rhéologiques ont été effectués avec différents types de polymères en solution (sans et avec milieu poreux), ainsi que d'autres substances chimiques incluant les microparticules en suspension, le tensioactif, le sel (iodure de sodium) et les alcools. Une colonne 1D et un bac 2D ont été utilisés pour les études expérimentales de dépollution, et COMSOL Multiphysics a été utilisé pour l'analyse numérique. L'impact de la densification de la solution de polymère avec des particules en suspension ou du sel soluble a été évalué ; il a été démontré que la densification du polymère permet d'améliorer l'efficacité du déplacement du DNAPL jusqu'à un facteur 4. De plus, le dépôt de matières en suspension dans les milieux poreux lors de l'injection de suspension de polymère densifiée a été caractérisé ; une réduction de la perméabilité allant jusqu'à 70% a été observée. Dans le cas de l'injection de solution de polymère densifiée avec de la saumure, la densification de la solution de polymère dans des expériences bidimensionnelles à deux phases entraîne une amélioration du rapport d'aspect (ratio du rayon latéral/ rayon vertical de propagation) dans le système passant de 0,38 à 1,2. Des simulations numériques de

l'écoulement diphasique en milieu poreux ont été réalisées pour évaluer divers scénarios de déplacement des DNAPLs à l'aide de solutions de polymères. L'injection de solution de polymères dans un milieu non confiné a été étudiée expérimentalement et numériquement afin de reproduire les conditions les plus proches possibles d'un site pollué. Les performances des solutions de polymères, avec et sans tensioactif, sur la dépollution d'un système multicouche pollué par des DNAPLs ont été étudiées. Les expériences en bac 2D ont révélé que le déplacement des DNAPLs dans les zones multicouches était affecté par la différence de perméabilité et le contraste de densité des fluides dans un sol hétérogène. Par ailleurs, l'efficacité des mélanges post-injection de polymère/alcool/tensioactif a été évaluée afin de diminuer la saturation résiduelle des DNAPL en milieu hétérogène. Les analyses de la densité des échantillons obtenus à partir des expériences en colonne 1D monocouche et en bac 2D multicouche montrent que le mécanisme de mobilisation peut améliorer l'efficacité de récupération de 91% (atteint par le rinçage primaire) à 99% en colonne 1D, et de 86% à 94% en bac 2D. Cette thèse fournit des résultats prometteurs pour la réhabilitation d'aquifères réellement pollués par DNAPL, en mettant en lumière les propriétés non newtoniennes des solutions polymères et en considérant l'impact de l'écoulement basé sur la densité sur le déplacement de DNAPL dans les systèmes monocouches et multicouches.

1. Introduction

Des composés organiques chlorés tels que le trichloroéthène (TCE) et le tétrachloroéthène (PCE) ont été utilisés à diverses fins industrielles ces dernières décennies (pour le nettoyage des vêtements, le dégraissage des métaux, etc.). Ces solvants ont entraîné toute une série de désordres environnementaux en raison de leur consommation intensive et de leur gestion inappropriée. Typiquement, les solvants chlorés s'infiltrent dans le sous-sol sous forme de liquides non aqueux denses en phase (DNAPLs). Les DNAPLs sont des liquides non miscibles plus denses que l'eau et peu solubles dans l'eau. Par conséquent, les DNAPLs peuvent migrer

sous forme de phases liquides distinctes (phase pure) à des profondeurs considérables dans la nappe phréatique (Langwaldt et Puhakka, 2000a ; Zhang et Smith, 2002). Ils se dissolvent progressivement dans l'eau souterraine, donnant naissance à des panaches de contamination dans la phase aqueuse (Roy et al., 2004). Malgré la faible solubilité des solvants chlorés dans l'eau, leurs concentrations dans les eaux souterraines dépassent parfois de plusieurs ordres de grandeur les normes pour l'eau potable. Par conséquent, même de faibles quantités de DNAPL libérées dans le sous-sol peuvent entraîner une contamination d'importants volumes d'eau. De nombreux solvants chlorés possèdent également une pression de vapeur suffisante pour permettre leur vaporisation dans le gaz du sol, entraînant des panaches de contamination dans la phase vapeur (Kueper et al., 2014).

Une "zone source de solvant chloré" fait référence à une zone du sous-sol avec ou ayant précédemment contenu des solvants chlorés sous forme de DNAPL (produit pur), contenant suffisamment de masse de solvant pour générer des concentrations dépassant les limites réglementaires dans l'eau souterraine. Cette définition reconnaît que le DNAPL peut ne pas persister de manière uniforme dans le sous-sol, et qu'il pourrait être totalement épuisé en raison de processus naturels ou de méthodes de dépollution. Comprendre la nature et l'étendue des solvants chlorés dans le sous-sol, et ce qui constitue exactement une zone source, est d'une grande importance. Kueper et al. (2014) ont considéré cinq étapes pour le cycle de vie d'une zone source de solvant chlorés : a) la libération initiale de DNAPL, b) la redistribution du DNAPL, c) la dissolution continue et le vieillissement du DNAPL, d) l'épuisement complet du DNAPL, et e) la désorption et la diffusion inverse. La durée de vie d'une source de pollution de DNAPL pourrait être de l'ordre de plusieurs centaines d'années dans certains cas (absence de dépollution, grande libération de DNAPL dans des milieux de perméabilité faible à modérée, solubilité du DNAPL, vitesse de l'eau souterraine et degré de biodégradation) (Gerhard et al., 2007; Kueper et al., 2014, 1993).

Les efforts de dépollution sur les sites de solvants chlorés ont été mis en première approche sur l'installation de systèmes de pompage et de traitement, principalement parce que c'est accessible et facile à concevoir. Une revue de 849 sites Superfund aux États-Unis (zones contaminées par des matériaux dangereux) de 1980 à 2004 montre que 63 % des sites pollués par du DNAPL ont fait l'objet des systèmes de pompage et de traitement (Kovalick, 2008). Les limitations du système de pompage et de traitement sont devenues évidentes en raison de la persistance de la contamination après le début de l'activité de dépollution (Travis et Doty, 1990), entraînant un coût élevé par unité de contaminant éliminé. L'inefficacité du pompage et du traitement pour l'élimination de la masse de DNAPL est bien documentée (Kavanaugh et al., 2003).

Les experts et les chercheurs ont essayé de développer des méthodes de dépollution plus avancées/adaptées pour les sites pollués par des solvants chlorés que les méthodes classiques de pompage et de traitement. Ces méthodes concernent l'excavation en vue d'un traitement on site ou hors site (McGuire et al., 2006; USEPA, 2009), le venting (Kim et al., 2022; Reddy et Tekola, 2004; Unger et al., 1995), le traitement thermique *in situ* (Beyke et Fleming, 2005; Colombano et al., 2021, 2020; Davarzani et al., 2022; Philippe et al., 2021, 2020; Xie et al., 2019), les dépollutions chimiques *in situ* incluant l'oxydation (Huling et Pivetz, 2006; Johansson et al., 2022, 2020; Siegrist et al., 2011; Tsitonaki et al., 2010) ou la réduction (Bossa et al., 2017; Cheng et Wu, 2000; Crane et Scott, 2012; Rodrigues et al., 2017a), le traitement biologique *in situ* (Langwaldt et Puhakka, 2000b; Maire et al., 2019), le lavage *in situ* par tensioactif ou cosolvant (Lee et al., 2005; Pennell et al., 1993; Pennell et Abriola, 2017; Ramsburg et al., 2003; Walker et al., 2022; Wang et Mulligan, 2004), et le déplacement hydraulique assisté (Kilbane et al., 1997; Martel et al., 1998; Miller et al., 2000; Omirbekov et al., 2023; Pennell et al., 1996; Robert et al., 2006).

Le déplacement hydraulique assisté peut permettre d'éliminer une masse importante de DNAPL dans le cas où celui-ci est présent sous forme de produit pur au fond de l'aquifère (pool : piscine)

(Alexandra et al., 2012). Cette technologie a principalement été utilisée dans l'industrie pétrolière, où le lavage à l'eau (waterflooding) (Craig, 1972 ; Willhite, 1986), l'injection de polymère (Alamooti et Malekabadi, 2018 ; Sorbie et Seright, 1992 ; Wei et al., 2020 ; Wever et al., 2011), et ou l'injection de mousse (Adebanjo et Olusegun, 2015 ; Ardakani et al., 2020 ; Falls et al., 1988) ont été utilisées pour déplacer le pétrole du réservoir en tant que méthode de récupération assistée de pétrole (EOR : enhanced oil recovery). Cette méthode peut être employée avec des puits d'injection, où le fluide sélectionné est injecté à travers la source de pollution pour la pousser vers les puits de récupération. Bien que le lavage à l'eau (waterflooding) soit moins coûteuse que les autres méthodes de déplacement hydraulique, et simple à mettre en œuvre, son efficacité peut diminuer lorsqu'il s'agit de DNAPL visqueux en raison de problèmes potentiels de fingering (digitations) (Giese et Powers, 2002 ; Kueper et Frind, 1988). Un autre élément crucial dans la conception d'une technique de dépollution par déplacement hydraulique assisté est la prise en compte de l'hétérogénéité de la zone contaminée. Dans les zones à plusieurs couches de perméabilités différentes, les zones à faible perméabilité peuvent être contournées si l'on n'utilise pas un fluide rhéofluidifiant. Avec le waterflooding, l'eau injectée s'écoule principalement à travers les pores les plus grands, négligeant une quantité significative de DNAPL potentiellement mobile dans les pores plus fins. Le contournement du DNAPL se produit à la fois au niveau des pores et à des échelles plus grandes, en fonction de la variabilité de la structure des pores (Giese et Powers, 2002). Le polymère et la mousse en tant que fluides rhéofluidifiants peuvent permettre de surmonter les problèmes de digitations visqueuses et peuvent déplacer le DNAPL dans des couches de perméabilités différentes (Hirasaki et al., 1997b, 1997a ; Maire et al., 2015 ; Martel et al., 1998, 2004 ; Omirbekov et al., 2020 ; Robert et al., 2006 ; Silva et al., 2013).

Un des défis de la conception et de la formulation des mousses est de garantir de bonnes performances d'injection de mousse et donc une bonne stabilité en présence de solvants chlorés (Kilbane et al., 1997 ; Wang et Mulligan, 2004).

Plusieurs biopolymères rhéofluidifiants sont potentiellement utilisables pour la dépollution des zones polluées par du DNAPL : gomme de guar, gomme de xanthane et carboxyméthylcellulose (CMC) (Omirbekov et al., 2023). Il est nécessaire de bien comprendre de nombreux phénomènes afin de maîtriser la dépollution de DNAPL (sous forme de produit pur) à l'aide de ces biopolymères : écoulements monophasiques et multiphasiques dans les milieux poreux, propriétés rhéologiques des polymères en solution et en milieu poreux avec et sans polluant.

L'objectif principal de cette thèse était d'étudier la dépollution des aquifères contaminés par le DNAPL à l'aide de l'injection de solutions de polymères. Un éventail de techniques expérimentales, y compris l'analyse rhéologique, les tests en batchs, les études en colonne 1D, les expériences en bac 2D, ainsi que la modélisation des écoulements biphasiques, ont été employés pour aborder principalement les objectifs suivants :

- Analyse du comportement rhéologique des solutions de polymères lorsqu'elles sont combinées à d'autres additifs tels que les tensioactifs, les alcools, les particules et les sels, à la fois en solution et en milieux poreux.
- Évaluation du transport des polymères en milieux poreux et de leur performance sur le déplacement du DNAPL à l'aide d'expériences en colonnes 1D.
- Examen de l'efficacité des solutions de polymères pour déplacer le DNAPL dans des systèmes non confinés et confinés, à une seule couche et multicouches à travers des expériences en bac 2D.

- Utilisation de la modélisation des écoulements diphasiques pour acquérir une compréhension plus profonde des mécanismes physiques sous-jacents aux résultats expérimentaux et pour évaluer différents scénarios de dépollution.

L'efficacité de l'injection de solutions polymères dans des aquifères multicouches saturés en DNAPL à des fins de dépollution est examinée dans la première étude. La première partie de la thèse examine le déplacement du DNAPL dans des aquifères multicouches saturés à l'aide de solutions polymères avec ou sans tensioactifs, en utilisant des approches numériques et expérimentales. Puis, la performance de la post-injection de mélanges polymères-alcool-tensioactifs est évaluée à l'aide de divers outils expérimentaux dans le but d'améliorer la dépollution du DNAPL résiduel au sein de systèmes multicouches.

Par la suite, l'influence des forces gravitationnelles sur le déplacement du DNAPL par l'injection de solutions polymères est examinée ; une approche de dépollution dirigée par la gravité est introduite. La première partie de cette étude traite de l'impact de l'injection de suspensions de polymères densifiées sur le déplacement du DNAPL. Puis, la dépollution du DNAPL à l'aide d'injection de saumure de polymères densifiées est abordée.

2. Matériel et méthodes : expérimental

2.1. Matériel et consommables expérimentaux

Dans l'étude multicouche, du sable de marbre (un carbonate) de deux fractions granulométriques (0,2-0,3 mm avec une perméabilité de 35 ± 5 Darcy et 0,4-0,6 mm avec une perméabilité de 105 ± 10 Darcy) a été utilisé dans des expériences en colonnes 1D et 2D. Pour l'étude sur la densification dirigée par la gravité, du sable avec des tailles de grain comprises entre 0,63 mm et 0,8 mm ont été employés, avec une perméabilité de 182 ± 10 Darcy et une porosité de $0,395 \pm 0,01$. Ils ont été tamisés et lavés à l'eau déionisée puis séchés dans un four à $105 \text{ }^\circ\text{C}$. Le DNAPL utilisé dans ces études était principalement composé d'hexachlorobutadiène-HCBD (58 %), d'hexachloroéthane-HCA (14 %) et de penta-

chlorobenzène (3,5 %), ainsi que de tétrachlorure de carbone (4 %). Il y a d'autres composés dans le mélange de DNAPL présents en quantité plus faible ou qui ne sont pas quantifiables. Pour l'étude multicouche, de la gomme xanthane (biopolymère) et du dodécylbenzènesulfonate de sodium – SDBS (tensioactif biodégradable) ont été utilisés en solution pour le déplacement primaire du DNAPL. De plus, du 1-propanol et du 1-hexanol ont été utilisés comme alcools solubles et insolubles dans l'eau pour les expériences de post-rinçage, tous deux avec une pureté de 99 %.

La barytine BariStar® 9015 (taille moyenne des particules ~ 3,5 µm) a été utilisée pour la densification de la solution de polymères avec matières en suspension (fournisseur : Mineralia, pureté : 97,68 % de BaSO₄). De plus, du sel d'iodure de sodium (NaI) en poudre (avec une pureté > 99 %) a été utilisé comme agent densifiant soluble. La carboxyméthylcellulose (CMC) a été utilisée comme biopolymère pour obtenir une densification avec des matériaux en suspension, tandis que la gomme xanthane a été utilisée pour la densification soluble. Tous les polymères, tensioactifs et alcools ont été fournis par Sigma-Aldrich.

Le rhéomètre rotatif Haake Mars 60 équipé de la géométrie cône-plaque a été utilisé pour analyser le comportement rhéologique des solutions de polymères. La tension interfaciale (IFT) entre les solutions de polymères et le DNAPL a été mesurée à l'aide de l'appareil d'analyse de forme de goutte (DSA-100, KRUSS).

Toutes les expérimentations ont été réalisées à température ambiante (22 ± 1 °C).

2.2. Expériences en colonnes 1D

Des expériences sur colonnes ont été menées pour étudier le déplacement du DNAPL par différentes solutions dans un système unidimensionnel (1D). La procédure expérimentale impliquait l'utilisation de colonnes en verre de 4 cm de diamètre et de 30 cm de longueur. Les colonnes ont été rincées avec du gaz CO₂, puis saturées verticalement avec de l'eau déionisée à un débit de 0,1 mL/min pendant 2 VP (Volumes de Pores). Ensuite, du DNAPL a été injecté

verticalement dans la colonne à un débit de 1 mL/min jusqu'à ce qu'aucune production d'eau ne soit observée. Enfin, les solutions ont été injectées individuellement horizontalement dans les colonnes à un débit de 1 mL/min à l'aide de pompes péristaltiques numériques Reglo ICC (Ismatec®). Pour l'étude avec plusieurs couches de sables différentes (étude multicouche), une injection primaire a été réalisée individuellement dans chaque couche avec un mélange de xanthane (0.8 g/L) et de SDBS (odium dodecyl benzenesulfonate) (1.265 g/L) à un débit constant de 1 mL/min jusqu'à atteindre la saturation résiduelle en DNAPL ; par la suite, un mélange d'alcools a été injecté au même débit pendant 2 PV. Les effluents ont été recueillis dans des tubes en propylène de 15 mL, tandis que la pression différentielle le long de la colonne était surveillée à l'aide des transmetteurs de pression KELLER PR33X. La récupération du DNAPL lors de l'injection primaire a été mesurée par mesure de volume. Pour le post-rinçage avec le mélange d'alcools, les volumes de la phase organique et aqueuse ont été enregistrés et leurs densités mesurées. Ensuite, les phases organiques et aqueuses de 3 à 4 tubes ont été individuellement combinées, diluées, et analysées par chromatographie en phase gazeuse (AGILENT 8890). Un schéma de l'écoulement multiphasique dans les expériences en colonnes 1D est présenté Figure 1.

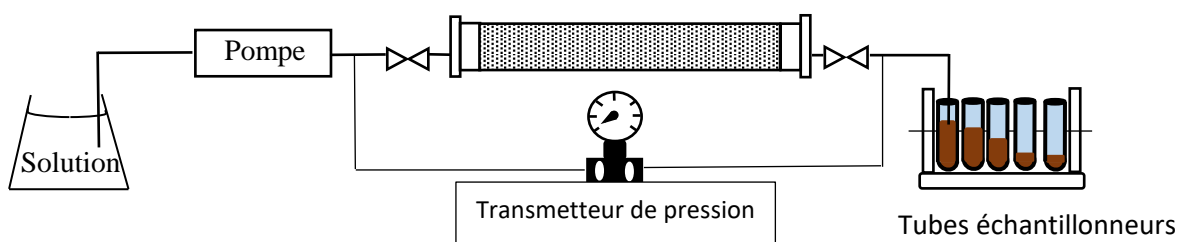


Figure 1 Schéma du dispositif expérimental de déplacement polymère-DNAPL en colonne 1D

2.3. Expériences en bac 2D

Un bac 2D confiné (i.e. avec un couvercle dans la partie sommitale), permettant de mesurer la pression le long des couches, a été utilisé pour évaluer l'efficacité de l'injection de solutions de

polymères dans un système hétérogène multicouche. Deux couches séparées, chacune ayant une hauteur de 5 cm, ont été mises en place dans le bac. Le sable a été compacté à l'intérieur du bac tandis que l'eau était continuellement injectée par le bas. Les deux couches ont été entièrement saturées d'eau. Par la suite, le DNAPL a été injecté uniformément à partir de trois orifices situés dans la partie inférieure du bac à un débit de $3 \times 0,5$ mL/min. Les solutions polymères ont été injectées à partir de deux orifices sur le côté gauche du bac à un débit de $2 \times 0,5$ mL/min ; le DNAPL a été produit naturellement dans l'effluent par l'injection du polymère (méthode similaire à celle des colonnes). Le schéma du bac 2D confiné est présenté en Figure 2.

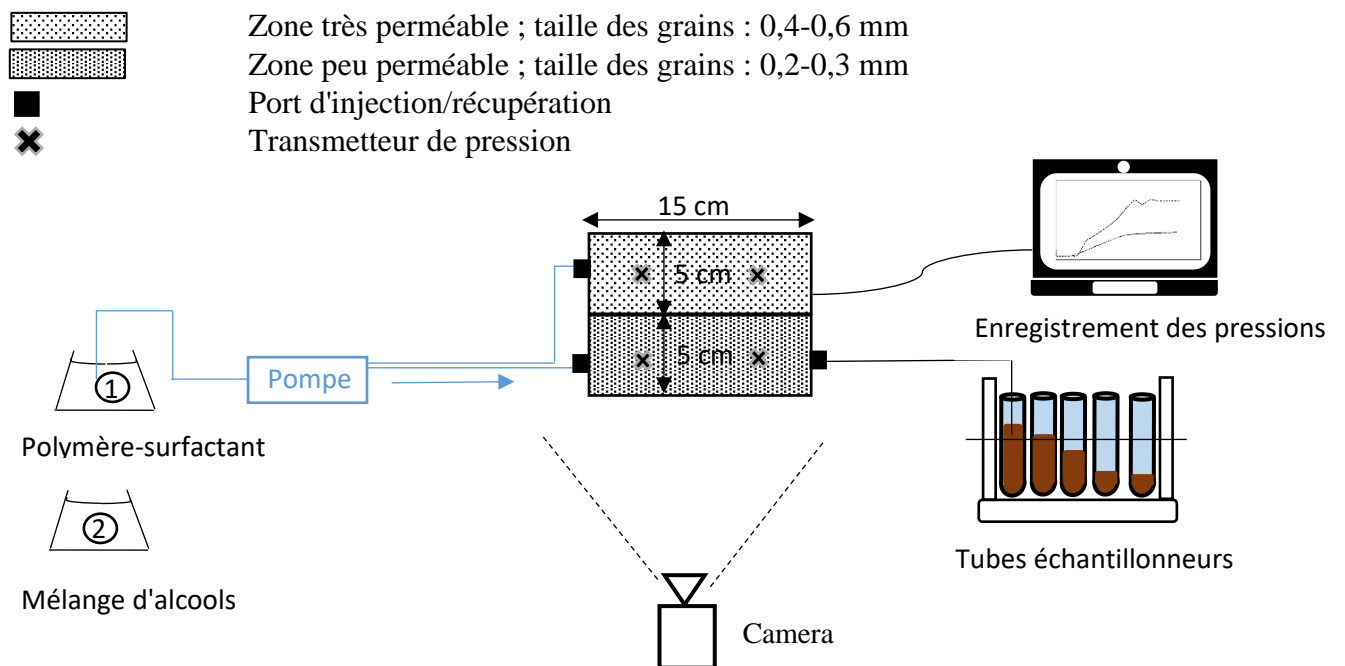


Figure 2 Schéma de l'injection de polymère/polymère-surfactant (réipient 1) suivie de l'injection d'un mélange d'alcool (réipient 2) pour le déplacement des DNAPL dans le réservoir 2D confiné (système multicouche)

En ce qui concerne l'étude sur la densification des polymères, des expériences en bac 2D non confiné (i.e. sans couvercle dans la partie sommitale) ont été menées pour évaluer l'efficacité du déplacement du DNAPL en utilisant différentes solutions (dans un système proche du site réellement pollué). Les expériences ont été réalisées dans un bac 2D mesurant 50 cm de

longueur, 30 cm de hauteur et 2 cm d'épaisseur. Initialement, le sable a été compacté sous l'eau, puis le DNAPL a été injecté (par la partie basale du bac) dans le milieu poreux saturé d'eau jusqu'à ce qu'il atteigne une hauteur de 20 cm. Ensuite, différentes solutions ont été injectées individuellement dans la zone contaminée par le DNAPL par un port situé dans la partie centrale inférieure du bac à un débit de 2 mL/min. Le niveau de DNAPL a été maintenu constant dans le système pendant l'injection des fluides de dépollution à l'aide de pompes péristaltiques reliées à des contre-canaux des deux côtés du bac.

Dans le cas de l'injection de polymère densifié par matières en suspension (polymère densifié par particules), les configurations des couches de sable ont été légèrement différentes de celles utilisées pour le polymère densifié par solution. La partie centrale près du point d'injection de la suspension de polymère a été séparée à l'aide de deux plaques (2 cm × 30 cm) pendant la phase de remplissage du bac (avec le sable et l'eau). Ensuite, le sable de taille de grain comprise entre 0,6 et 0,8 mm a été compacté des deux côtés latéraux du bac. Le sable plus grossier a ensuite été compacté dans la partie centrale ; les plaques ont été retirées progressivement pendant cette phase. Lorsque le niveau de sable a atteint une hauteur de 6 cm dans le bac 2D, le sable plus grossier a été recouvert de 3 cm de hauteur de sable fin dans la partie centrale. Le sable de taille de grain compris entre 0,6 et 0,8 mm était, quant à lui, compacté dans les autres parties du bac 2D. Les deux plaques ont été complètement retirées du bac 2D.

L'injection des deux types de polymères (avec suspension et solution), a été poursuivie jusqu'à ce qu'il n'y ait plus de DNAPL à récupérer ou que les fronts de solution atteignent les limites latérales du système. La masse de DNAPL récupéré a été mesurée à l'aide d'une balance (Sartorius Cubis MSE8201S-000-D0). Les acquisitions des données relatives aux masses et aux pressions ont été effectuées en temps réel. Ces données ont été complétées par des prises d'images régulières du bac 2D à l'aide d'un appareil photo Nikon D810 équipé d'un objectif

NIKKOR 105. Ces images ont permis d'analyser la propagation des fluides. Un schéma des expériences multiphasiques dans le bac 2D est présenté en Figure 3.

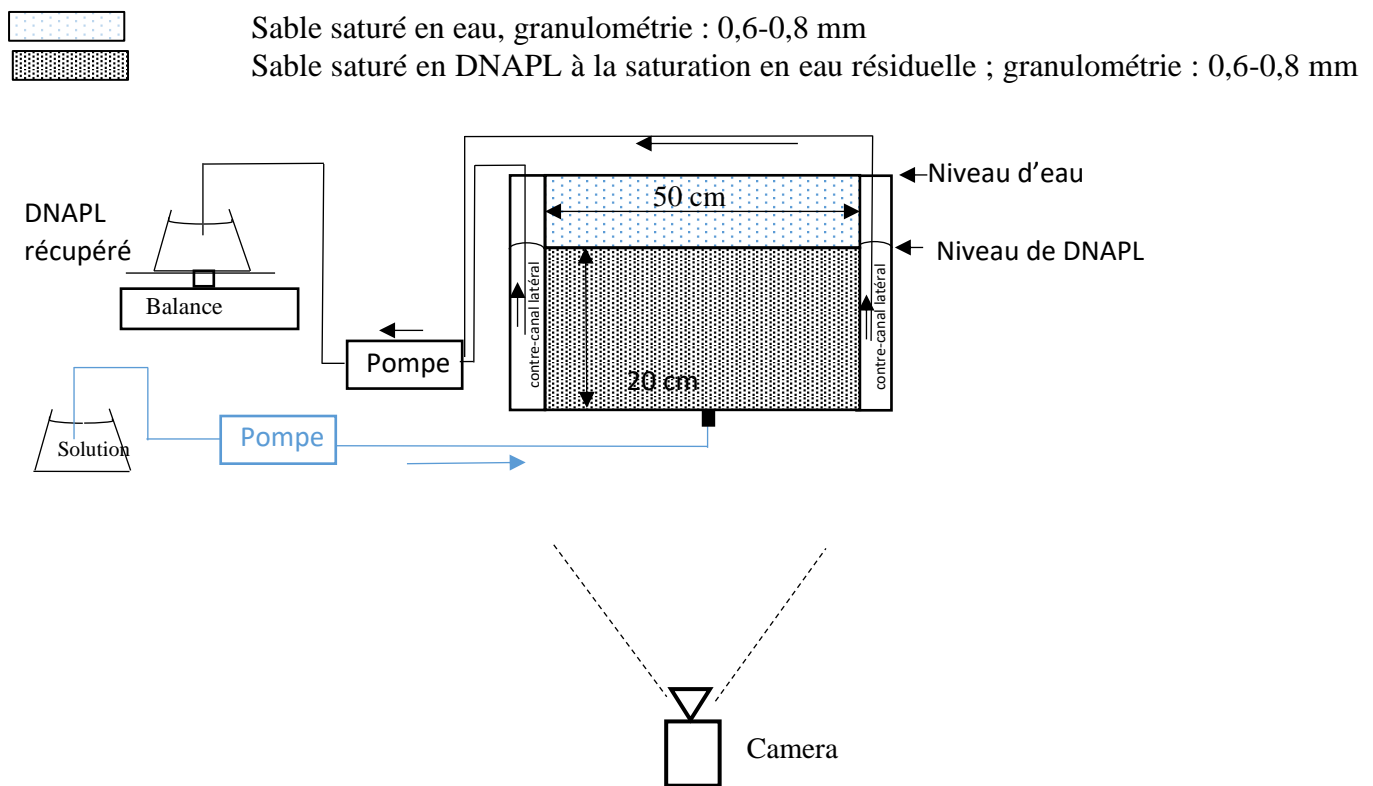


Figure 3 : Schéma de l'injection de polymère densifié pour le déplacement du DNAPL dans le réservoir 2D non confiné

2.4. Mélanges et solutions

L'efficacité de l'injection du polymère (xanthane) et du polymère-tensioactif (xanthane-SDBS) a été comparée dans l'étude multicouche (analyse primaire). Pour éviter le phénomène de digitation visqueuse (Lenormand et al., 1988) et pour obtenir un front de déplacement stable, nous avons choisi une concentration en xanthane de 0,8 g/L et un débit d'injection de 1 mL/min. La concentration de SDBS utilisée était de 1265 mg/L, soit 5 fois la concentration micellaire critique, ce qui provoque une très légère solubilisation du DNAPL à un niveau de 40 mg/L (Colombano et al., 2021 ; Rodrigues et al., 2017b).

En ce qui concerne la post-injection du système multicouche à saturation résiduelle de DNAPL, trois mélanges ont été sélectionnés. Ces mélanges incluent des solutions composées de 50 % en volume de 1-propanol et de 50 % de solution de xanthane-SDBS (mélange C3), de 25 % de 1-

propanol, de 25 % de 1-hexanol et de 50 % de solution de xanthane-SDBS (mélange C3-C6), et également de 50 % de 1-hexanol et de 50 % de solution de xanthane-SDBS (mélange C6). Les concentrations de xanthane et de SDBS dans le mélange étaient respectivement de 2 et 1 g/L.

Un mélange de barytine et de polymère a été utilisé pour l'injection de suspension densifiée. Le polymère a été utilisé non seulement pour fournir une viscosité élevée mais aussi pour générer une suspension stable. Le CMC a montré la meilleure efficacité pour la stabilisation de cette suspension. Trois suspensions polymères avec des densités de 1,3, 1,66 (équivalente à la densité du DNAPL) et 1,9 kg/L à une concentration fixe de CMC de 4 g/L ont été utilisées.

En ce qui concerne la solution de polymère-saumâtre densifiée, une solution de saumure dense a été préparée en mélangeant de l'iodure de sodium avec de l'eau pour atteindre une densité proche de celle du DNAPL à 1,7 kg/L. Une solution de xanthane a été préalablement préparée à une concentration de 0,8 g/L. Ensuite, de la poudre d'iodure de sodium a été ajoutée à cette solution pour atteindre une densité de 1,7 kg/L, ce qui correspond à une concentration de 960,11 g/L.

3. Modélisation numérique

3.1. Écoulement diphasique en milieu poreux

Le sol est considéré comme un milieu poreux uniforme et isotrope contenant de l'eau et du DNAPL en tant que phases incompressibles et non miscibles. L'équation de continuité pour chaque phase peut être considérée comme suit (Bear, 2013) :

$$\frac{\partial}{\partial t}(\phi \rho_i S_i) + \nabla \cdot (\rho_i \mathbf{u}_i) = 0 \text{ avec } i = w, nw \quad 1$$

où les indices "w" et "nw" se réfèrent respectivement aux phases mouillantes et non mouillantes.

La porosité est représentée par le symbole ϕ (-), le temps par t (s), tandis que la densité, la saturation et la vitesse de Darcy de la phase i sont respectivement désignées par ρ_i (kg/m^3), S_i

(-) et \mathbf{u}_i (m/s). La loi de Darcy généralisée pour l'écoulement de deux phases en milieu poreux isotrope est donnée par :

$$\mathbf{u}_i = -\frac{k k_{ri}}{\mu_i} (\nabla p_i - \rho_i \mathbf{g}) \quad 2$$

où k (m^2) représente la perméabilité absolue scalaire du milieu poreux isotrope, et k_{ri} (-) désigne la perméabilité relative pour la phase i . La viscosité et la pression de la phase i sont représentées respectivement par μ_i (Pa.s), p_i (Pa), et le vecteur de gravité est représenté par \mathbf{g} (m/s^2). Comme le volume de l'espace vide dans un milieu poreux rigide est considéré comme constant, il est exclusivement occupé par des phases aqueuses et non aqueuses ; par conséquent, la somme des saturations des phases mouillantes et non mouillantes est toujours égale à 1. Les fonctions de Brooks et Corey sont utilisées pour présenter la pression capillaire, qui reflète la différence de pression entre les phases aqueuses et non aqueuses, ainsi que les courbes de perméabilité relative dans le modèle (Brooks et Corey, 1964) :

$$p_c = p_{th} S_{we}^{-\frac{1}{\lambda}} \quad 3$$

$$k_{rw} = k_{rw}^{max} S_{we}^{\epsilon_w} \quad 4$$

$$k_{rnw} = k_{rnw}^{max} S_{nwe}^{\epsilon_{nw}} \quad 5$$

où l'indice de la distribution de la taille des pores est représenté par λ (-) et p_{th} désigne la pression seuil (Pa). Les valeurs maximales de la perméabilité relative, ou points finaux, pour les phases mouillantes et non mouillantes sont indiquées respectivement par k_{rw}^{max} et k_{rnw}^{max} . ϵ_w et ϵ_{nw} indiquent les exposants de saturation pour les phases mouillantes et non mouillantes, respectivement. Les saturations effectives des phases mouillantes et non mouillantes sont désignées par S_{we} (-) et S_{nwe} (-) et peuvent être exprimées comme suit :

$$S_{we} = \frac{S_w - S_{wr}}{1 - S_{nwr} - S_{wr}} \quad 6$$

$$S_{nwe} = \frac{S_{nw} - S_{nwr}}{1 - S_{nwr} - S_{wr}} \quad 7$$

où les saturations irréductibles mouillantes et les saturations résiduelles non mouillantes sont représentées respectivement par S_{wr} (-) et S_{nwr} (-).

3.2. Modèle de transport de soluté

Dans les milieux poreux, le transport de soluté est décrit par l'équation différentielle classique d'advection-dispersion (O'Carroll et al., 2013; Tsakiroglou et al., 2018) :

$$\underbrace{\frac{\partial(\phi S_w c_i)}{\partial t}}_{\text{Accumulation}} - \underbrace{\nabla \cdot (\phi S_w \mathbf{D} \cdot \nabla c_i)}_{\text{Dispersion}} + \underbrace{\mathbf{u}_w \cdot \nabla c_i}_{\text{Advection}} = R_i + \dot{m} \quad 8$$

où la concentration du composant i (kg/m^3) est représentée par c_i , \mathbf{D} désigne le tenseur de dispersion, le terme de réaction pour le composant i est indiqué par R_i et \dot{m} signifie le terme source. L'adsorption du xanthane (en tant que polymère anionique) et du NaI (en tant que traceur) sont négligées. Les termes principaux et croisés du tenseur de dispersion pour un milieu poreux isotrope peuvent être représentés comme suit (Auset et Keller, 2004; Bear, 2013) :

$$\mathbf{D} = (\alpha_T |\mathbf{U}_w| + D_{eff}) \mathbf{I} + (\alpha_L - \alpha_T) \frac{U_{wx} U_{wy}}{|\mathbf{U}|} \quad 9$$

$$D_{eff} = \frac{D_0}{\tau} \quad 10$$

où la matrice identité est notée \mathbf{I} , le coefficient de diffusion efficace dans les milieux poreux est représenté par D_{eff} (m^2/s). Le coefficient de diffusion moléculaire est indiqué par " D_0 (m^2/s), et τ fait référence à la tortuosité. De plus, α_L et α_T sont utilisés pour représenter les dispersivités longitudinale et transversale, respectivement. A travers la formule suivante, il est possible de dériver le coefficient de diffusion moléculaire du xanthane (qui est un polysaccharide) (Kono, 2014) :

$$D_0 = 8.2 \times 10^{-9} M_w^{-0.49} \quad 11$$

où M_w ($g.mol^{-1}$) est le poids moléculaire du polysaccharide (xanthane ou CMC). Dans le cas de l'injection de suspension de polymère, le processus d'obstruction était couplé avec des variations de densité à l'intérieur de la zone déplacée et une réduction de la perméabilité/porosité. Selon l'équation 8, la formulation du transport des particules de barytine dans les milieux poreux peut être décrite comme suit (Zheng et al., 2014) :

$$\frac{\partial(\phi c_b + c_s)}{\partial t} + \mathbf{u}_w \cdot \nabla c_b - \nabla \cdot (\phi S_w \mathbf{D} \cdot \nabla c_b) = 0 \quad 12$$

où c_b est la concentration en particules de barytine dans la suspension (kg/m^3), et c_s est la concentration en particules de barytine déposées sur les surfaces des grains de sable par unité de volume de pore (kg/m^3). Selon le processus d'attachement et de détachement des particules dans les milieux poreux, le mécanisme de dépôt des particules de barytine en suspension peut être décrit comme suit (Herzig et al., 1970) :

$$\frac{\partial c_s}{\partial t} = \theta c_b - \beta c_s \quad 13$$

où θ est le coefficient d'attachement des particules (s^{-1}) et β est le coefficient de détachement des particules (s^{-1}). Durant l'injection de la suspension de barytine-polymère, les particules de barytine peuvent facilement être capturées par les surfaces des grains de sable, entraînant ainsi une réduction de l'espace des pores (porosité) :

$$\phi = \phi_0 - \frac{c_s}{\rho_b} \quad 14$$

où ϕ_0 est la porosité initiale et ρ_b est la densité solide de la barytine (kg/m^3). Pour corrélérer les changements de perméabilité-porosité dans la zone déplacée, la relation de Carman-Kozeny a été utilisée (Hommel et al., 2018; Voronov et al., 2010) :

$$k = k_0 * CF * \frac{\phi^3}{(1 - \phi)^2} * \frac{(1 - \phi_0)^2}{\phi_0^3} \quad 15$$

où k_0 est la perméabilité absolue initiale, et CF est un facteur de correction pour incorporer les changements de sphéricité et de diamètres des particules de sable après le dépôt des particules de barytine. Pour la modélisation numérique, les erreurs relatives absolues moyennes ont été

considéré comme : $\left(\frac{1}{\text{Nombre de points}} \left| \frac{\text{Efficacité du déplacement}_{Exp} - \text{Efficacité du déplacement}_{Sim}}{\text{Efficacité du déplacement}_{Exp}} \right| \right)$.

4. Résultats et discussions

4.1. Comportement rhéologique

4.1.1. Xanthane et SDBS

Des solutions de polymères en combinaison avec différents additifs, y compris du tensioactif, du sel, des matières en suspension et des alcools, ont été utilisées à des fins de dépollution des aquifères. Les résultats concernant le comportement rhéologique du mélange de xanthane et de solution de SDBS à une concentration fixe de xanthane de 800 mg/L et diverses concentrations de SDBS sont présentés en Figure 4.

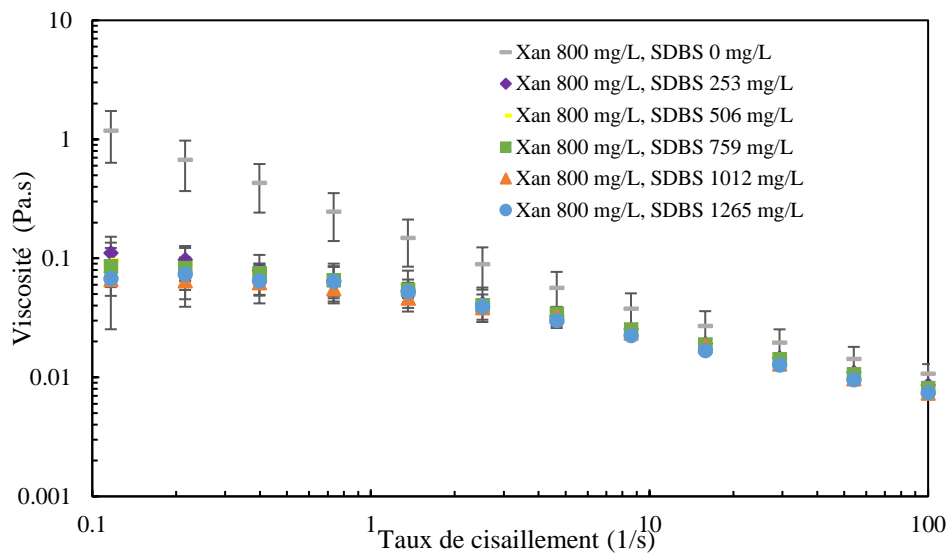


Figure 4 Comportement rhéologique du mélange de xanthane et de solution de SDBS à une concentration fixe de xanthane de 800 mg/L et différentes concentrations de SDBS

Comme on peut le voir sur la Figure 4, l'ajout du tensioactif SDBS à une concentration fixe de solution de xanthane diminue la viscosité (principalement à faible taux de cisaillement). Il

élargit également la plage de taux de cisaillement où la solution présente un comportement newtonien (à faibles taux de cisaillement), mais il n'y a pas de changements significatifs dans le comportement rhéologique à mesure que la concentration de SDBS augmente. La diminution de la viscosité s'explique par la rétraction des chaînes de xanthane en raison de l'existence de forces électrostatiques répulsives entre le xanthane et le SDBS (Yang et Pal, 2020). Plus la concentration en SDBS augmente, plus l'interaction entre les parties hydrophobes du xanthane et du SDBS contrebalance les forces répulsives, n'entraînant pas de changements supplémentaires notables dans la viscosité du mélange (Krstonošić et al., 2019).

4.1.2. Xanthane, SDBS et alcools

Le comportement rhéologique des mélanges d'alcool avec une concentration de xanthane de 2 g/L dans la solution de tensioactif est présenté en Figure 5. L'ajout d'alcools à la solution tensioactif-polymère (1 g/L de SDBS et 2 g/L de xanthane) a généré des viscosités plus élevées par rapport au fluide de dépollution primaire, c'est-à-dire au mélange polymère-tensioactif (1,265 g/L de SDBS et 0,8 g/L de xanthane) qui avait été choisi pour être injecté dans le sol saturé de DNAPL. Tous les mélanges ont montré un comportement de type rhéofluidifiant. Dans la plage de taux de cisaillement de travail, c'est-à-dire autour de 1-10 1/s, la viscosité la plus élevée été observée pour les mélanges C3-C6 et C6, qui ont une viscosité environ 17 fois supérieure à celle du mélange de dépollution primaire. Le mélange C3 a également une viscosité environ 5 fois supérieure à celle du mélange de dépollution primaire.

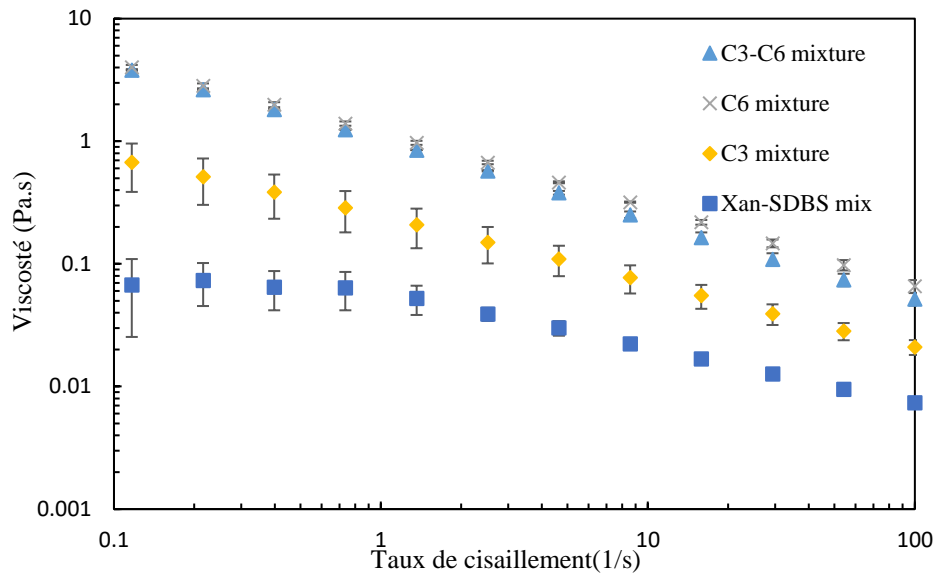


Figure 5 Viscosités de différents mélanges d'alcool contenant du xanthane à une concentration de 2 g/L, ainsi que du mélange xanthane-SDBS en tant que fluide de rinçage primaire

4.1.3. CMC et barytine

La Figure 6 montre la viscosité des suspensions de barytine-polymère pour différentes densités en fonction du taux de cisaillement sur une échelle log-log. On peut voir que la viscosité augmente avec la densité du mélange. Pour tous les mélanges de polymères avec ou sans particules de barytine dans la plage de taux de cisaillement utilisée dans cette étude, un comportement de rhéofluidification peut être observé, ce qui correspond à une moindre résistance à l'écoulement à des taux de cisaillement plus élevés. Dans le cas de la solution de CMC sans particules de barytine ($\rho=1$ g/mL), à faible taux de cisaillement, un comportement initial d'épaississement au cisaillement peut être noté. Cette augmentation de la viscosité à faible taux de cisaillement fait encore l'objet de controverses. Liu et al. (2007) ont attribué ce mécanisme à la "formation induite par l'écoulement d'associations macromoléculaires". Benchabane et Bekkour (Benchabane et Bekkour, 2008) ont observé ce comportement pour des concentrations élevées de solution de CMC à faible taux de cisaillement. Ils ont signalé que l'une des raisons les plus probables de ce comportement pourrait être l'augmentation des interactions intermoléculaires lors de l'augmentation du taux de cisaillement.

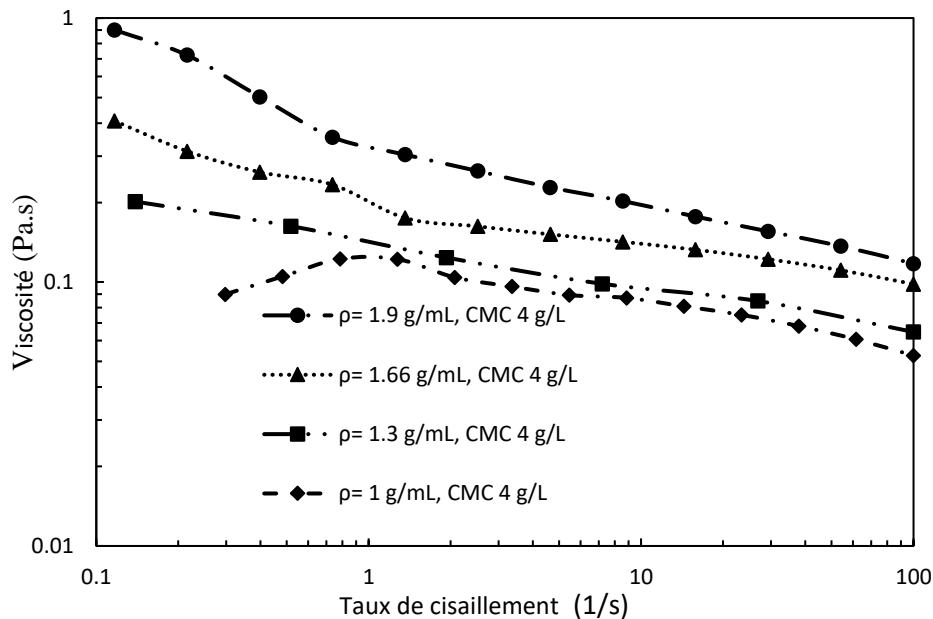


Figure 6 Comportement rhéologique des mélanges polymère-barytine à différentes densités

4.1.4. Xanthane et sel (NaI)

La Figure 7 illustre le comportement rhéologique de la solution de xanthane avec et sans NaI. Les résultats expérimentaux montrent que le xanthane conserve un comportement rhéofluidifiant avec le NaI, pour autant la viscosité de la solution est réduite (Najjari et al., 2016). Le xanthane, en tant que polysaccharide à longue chaîne, contient des groupes chimiques chargés négativement, tels que les groupes acétyle et pyruvate. La répulsion électrostatique entre ces charges négatives pousse les molécules de xanthane à s'étendre et à former une forme enroulée en raison de la répulsion électrostatique (Carrington et al., 1996). Cependant, lorsque des ions de sel sont présents, ils réduisent la répulsion électrostatique et provoquent une modification de la molécule de xanthane en une forme plus compacte et en forme de tige. Par conséquent, les groupes chargés négativement sont positionnés plus près du squelette de la molécule, ce qui entraîne une diminution de son volume hydrodynamique (Higiro et al., 2007; Rochefort et Middleman, 2000). Plus le volume hydrodynamique est faible, plus les molécules

de xanthane peuvent se déplacer facilement dans la solution ; ce qui entraîne une réduction de la viscosité. En conséquence, la viscosité du mélange de NaI et de xanthane est inférieure à celle de la solution pure de xanthane.

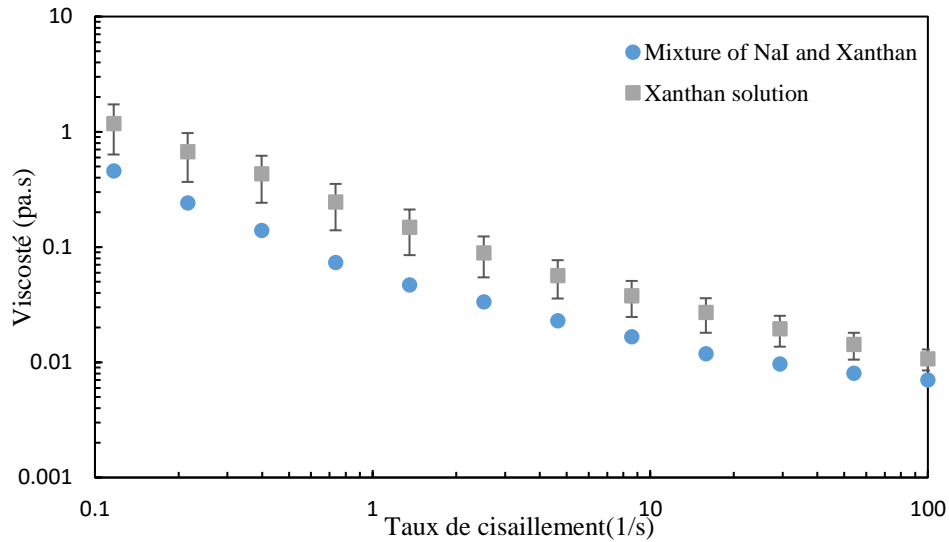


Figure 7 Comportement rhéologique de la solution de xanthane à une concentration de 800 mg/L et mélange de xanthane et de NaI à une concentration de xanthane de 590 mg/L et une concentration de NaI à 960,11 g/L

4.2. Déplacement unidimensionnel (colonne 1D)

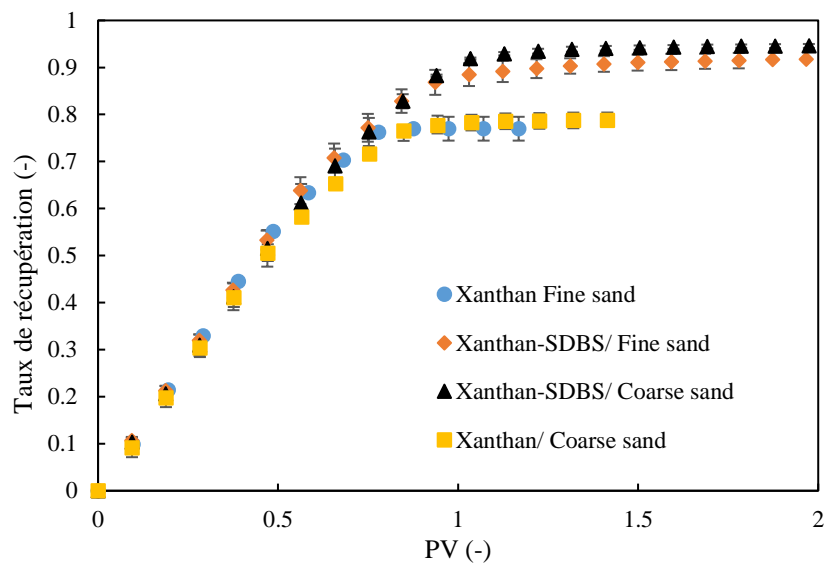
4.2.1. Xanthane et SDBS

Les expériences en colonne 1D ont été réalisées afin d'évaluer l'efficacité des solutions de polymères injectées pour récupérer le DNAPL. En ce qui concerne l'étude multicouche, les solutions de xanthane avec et sans SDBS (utilisées comme méthode de dépollution primaire) ont été injectées dans deux types de sable saturés de DNAPL. Les volumes de DNAPL récupérés ainsi que les différences de pression ont été enregistrés tout au long des expériences. Le nombre capillaire utilisé pour évaluer la performance de récupération de DNAPL pendant l'injection des solutions de polymères a été calculé comme suit (Chatzis et Morrow, 1984) :

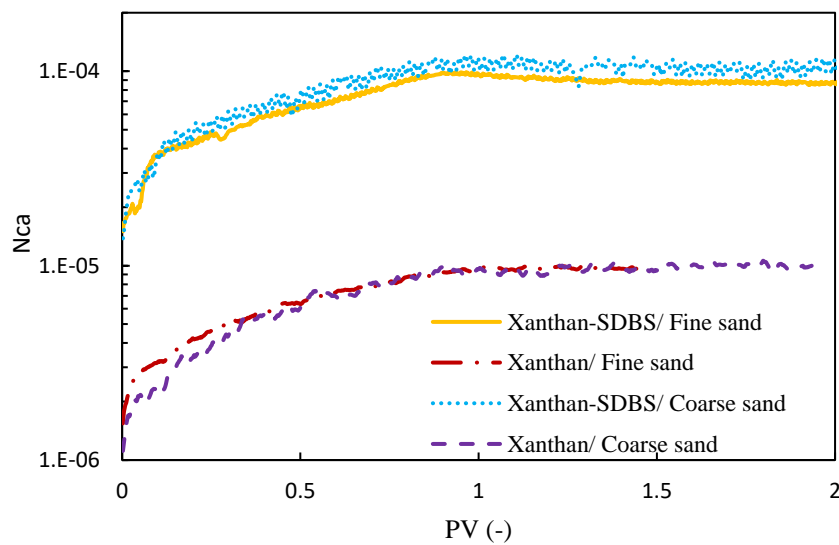
$$N_{ca} = \frac{k\nabla p}{\sigma}$$

16

où σ (mN/m) est la tension interfaciale (IFT) entre le DNAPL et les solutions. L'IFT pour la solution de xanthane et le mélange de xanthane-SDBS a été mesurée à environ $21,5 \pm 0,05$ et $1,5 \pm 0,05$ mN/m, respectivement. La Figure 8 présente le taux de récupération de DNAPL ((volume de DNAPL produit) / (volume initial de DNAPL dans le sable)) et les nombres capillaires par rapport au volume de pore injecté des solutions de polymères pour les deux types de sable.



(a)



(b)

Figure 8 Performance de l'injection de solutions polymères dans deux types de sable de perméabilités différentes. (a) Taux de récupération, (b) Nombre capillaire par rapport au volume de pore injecté.

Les courbes du taux de récupération (Figure 8a) montrent que la présence de surfactant dans la solution polymère augmente le rendement épuratoire d'environ 0,15 (de 0,77 à 0,91 pour le sable fin et de 0,79 à 0,95 pour le sable grossier). Le graphique relatif au nombre capillaire (Figure 8b) indique que le mélange xanthane-SDBS génère un nombre capillaire plus élevé, en raison de la plus faible tension interfaciale et de la plus faible viscosité menant à une pression différentielle plus basse.

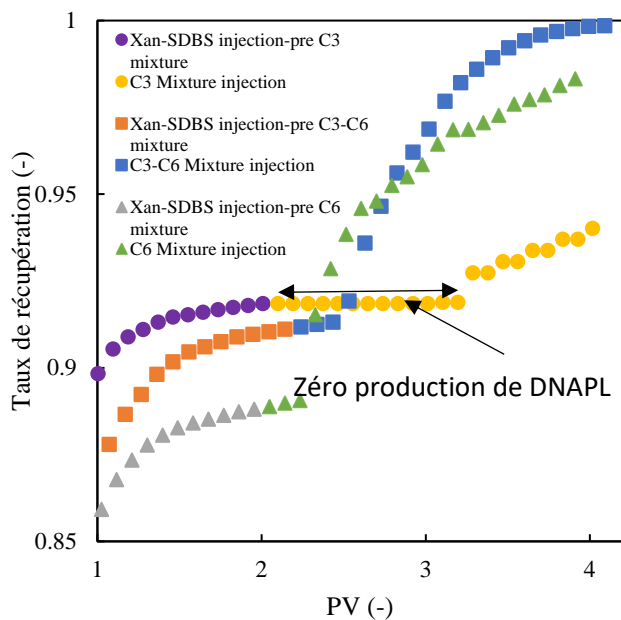
4.2.2. Xanthane, SDBS et alcools

La solution de xanthane-SDBS a été injectée préalablement à l'injection des solutions alcooliques dans des colonnes saturées de DNAPL remplies de sables grossier et fin afin d'évaluer la performance des mélanges d'alcool sélectionnés sur la dépollution des sols. La Figure 9 illustre le taux de récupération de DNAPL et la pression différentielle après 1 PV d'injection du mélange xanthane-SDBS, ainsi que l'injection postérieure des mélanges d'alcools en fonction des PV cumulatifs (pour les sables à grande et faible perméabilités).

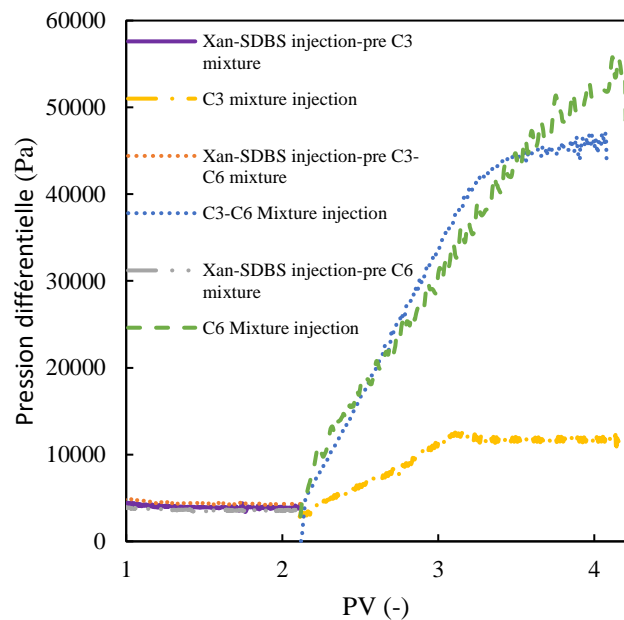
Ces résultats indiquent que les courbes de récupération de DNAPL pour l'injection postérieure des mélanges C3-C6 et C6 suivent une tendance similaire dans les colonnes 1D à grande et faible perméabilité. Dans les premiers stades de l'injection de solutions alcooliques contenant du 1-hexanol, il n'y a pas de production de DNAPL. Cependant, le DNAPL commence à apparaître dans l'effluent après environ 0,3 PV d'injection de mélange alcoolique. Ceci est attribué aux alcools se partitionnant dans les ganglions de DNAPL piégés dans l'espace poreux, les faisant gonfler et finalement coalescer pour former des gouttelettes plus grandes capables de migrer à travers le milieu poreux (St-Pierre et al., 2004). Par conséquent, une phase organique, contenant à la fois le DNAPL et les alcools, commence à apparaître dans l'effluent.

Cette phase, ayant une densité inférieure au DNAPL original, finit par se transformer en un LNAPL. Les courbes de pression différentielle pour les mélanges contenant du 1-hexanol sont cohérentes, reflétant le comportement similaire observé dans les mélanges C3-C6 et C6.

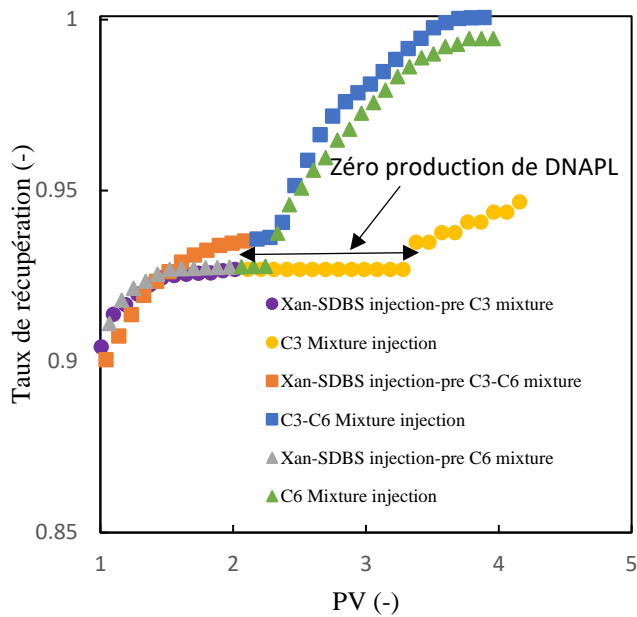
En revanche, l'introduction du mélange C3 dans des colonnes à la saturation résiduelle en DNAPL, entraîne l'émergence de la phase organique seulement après 1 PV d'injection postérieure, indiquant un mécanisme de solubilisation. Le mélange C3 commence à dissoudre le DNAPL résiduel dans la phase aqueuse, se déplaçant à travers le milieu poreux. Une fois que la solubilité maximale est atteinte dans la phase aqueuse, le piston postérieur du mélange C3 continue ce processus de dissolution. En conséquence, le DNAPL est absent dans l'effluent jusqu'après 1 PV d'injection postérieure, puis il est récupéré à un taux de récupération constant (pente fixe).



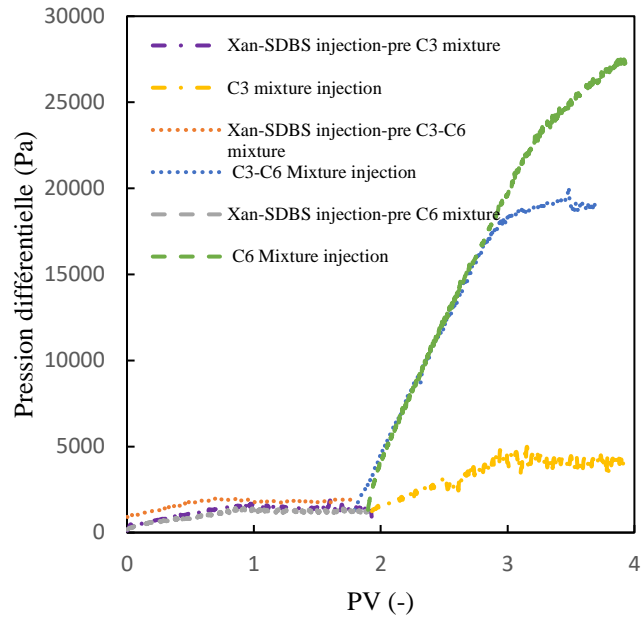
(a)



(b)



(c)



(d)

Figure 9 Résultats expérimentaux de l'injection postérieure de mélanges alcooliques dans les colonnes : (a) taux de récupération pour la couche à faible perméabilité, (b) pression différentielle pour la couche à faible perméabilité, (c) taux de récupération pour la couche à forte perméabilité, et (d) pression différentielle pour la couche à forte perméabilité

4.2.3. Xanthane et NaI

Des expériences en colonne ont été menées pour évaluer l'efficacité de l'injection de diverses solutions de polymère densifié pour déplacer le DNAPL dans un système horizontal fermé. Les résultats de la colonne 1D présentés en Figure 10a indiquent que le taux de récupération en fonction du PV pour les solutions de xanthane, avec ou sans NaI, sont presque identiques ; il faut noter que l'efficacité de la récupération est légèrement supérieure pour la solution pure de xanthane en raison de sa viscosité plus élevée que celle du mélange de xanthane-NaI. L'efficacité de la récupération pour la solution pure de NaI est plus faible, environ 0,74, car sa viscosité est nettement inférieure à celle des solutions de polymère.

Les graphiques du nombre capillaire (Figure 10b) montrent que le nombre capillaire à la fin de l'expérience en fonction du PV est presque identique pour l'injection de xanthane et le mélange

de xanthane-NaI. De plus, il est supérieur à la solution pure de NaI, ce qui est en accord avec les résultats de l'efficacité de la récupération de DNAPL.

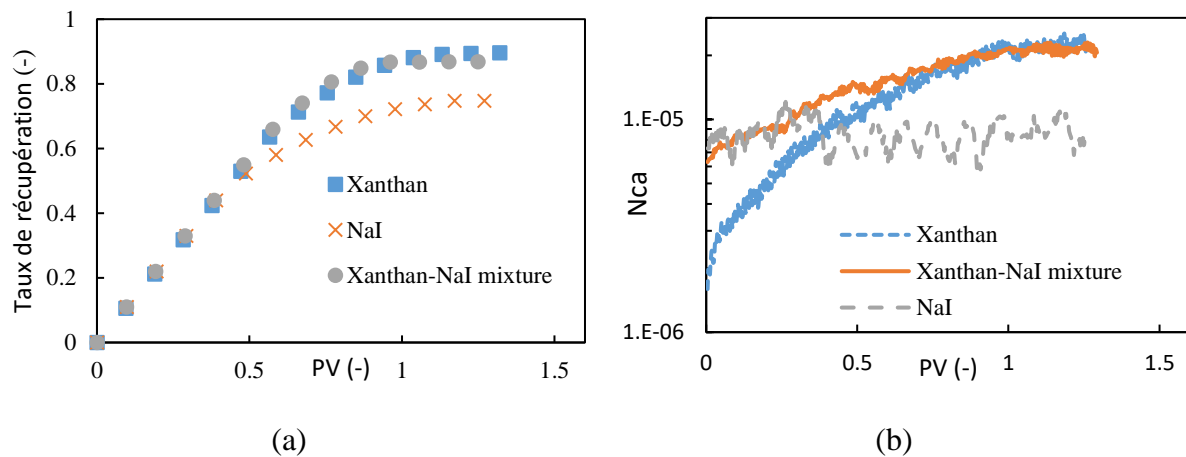


Figure 10 Performance de l'injection de différentes solutions ; mélange de xanthane-NaI, NaI pure, et xanthane pure. (a) Taux de récupération, (b) Nombre capillaire par rapport au PV injecté

4.3. Écoulement bidimensionnel (bac 2D)

4.3.1. Xanthane et SDBS dans système multicouche

Les expériences en bac 2D font suite aux expériences d'écoulement en colonne 1D ; elles ont été menées pour apporter des éclaircissements sur le déplacement du DNAPL dans des systèmes multicouches confinés (i.e. avec un couvercle dans la partie sommitale) et à couche unique non confinés (i.e. sans couvercle dans la partie sommitale). Pour l'étude multicouche, les solutions polymères ont été injectées à travers les couches contaminées, en suivant les étapes décrites dans la partie relative au matériel et méthodes. La Figure 11 illustre la distribution des solutions de polymères et du DNAPL à différents PV injectés. Les saturations résiduelles moyennes en DNAPL après injection de xanthane-SDBS et de xanthane sont respectivement de 0,13 et 0,195, ce qui est cohérent avec les expériences précédentes en colonnes. Le déplacement du DNAPL pour les deux types d'injection de solution de xanthane et de mélange xanthane-SDBS était similaire ; cependant, la présence de SDBS dans la solution polymère a abouti à une saturation

résiduelle plus faible. De plus, deux fronts de déplacement peuvent être observés dans le système en présence de SDBS dans la solution de xanthane, ce qui est probablement dû à la capacité du tensioactif à réduire la tension interfaciale et à améliorer la mobilisation de plus de DNAPL.

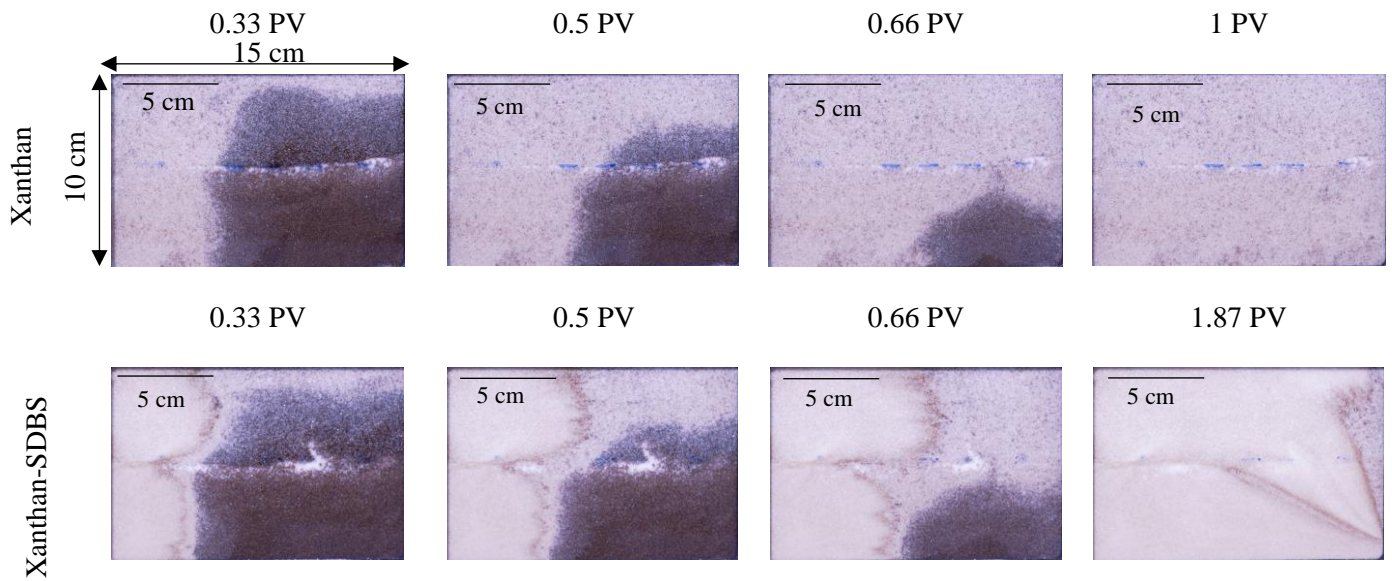


Figure 11 Déplacement du DNAPL dans un système multicouche 2D par injection de solution de xanthane (première rangée) et mélange de xanthane-SDBS (deuxième rangée) à différents volumes de pores de fluides injectés

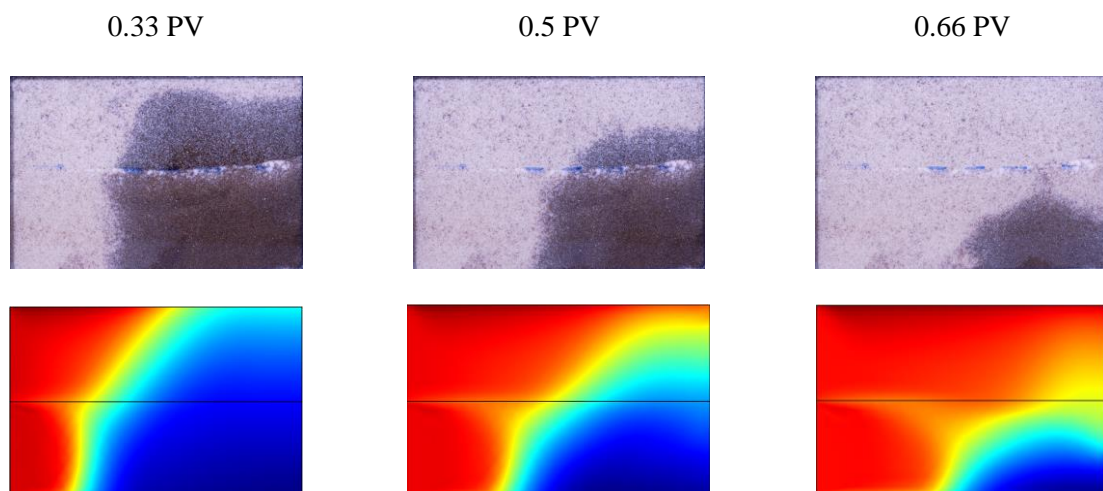
Le déplacement du DNAPL et des solutions polymères est influencé non seulement par le contraste de perméabilité mais aussi par la différence de densité entre les solutions polymères et le DNAPL. La solution envahissante a tendance à s'écouler en haut des couches à grande perméabilité, car les forces de flottabilité favorisent le mouvement vertical des solutions polymères. En effet, la comparaison des nombres sans dimension, y compris les nombres capillaires et de Bond, peut fournir un aperçu précieux de l'interaction complexe des forces qui entraînent le déplacement du DNAPL par les solutions de polymères. En évaluant les valeurs de ces nombres sans dimension, il est possible de déterminer l'influence relative de la gravité,

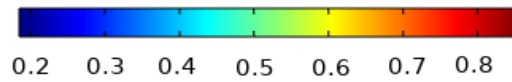
des forces capillaires et visqueuses sur le processus de déplacement. Le nombre de Bond est défini comme suit (Morrow et Songkran, 1981) :

$$N_{Bo} = \frac{\nabla \rho g k}{\sigma} \quad 17$$

Le rapport entre le nombre de Bond et le nombre capillaire, évalué à la fin de l'expérience, pour la couche à haute perméabilité, est de 7,15 et 8,57 respectivement pour les injections de xanthane et de xanthane-SDBS. Pour la couche à faible perméabilité, ce rapport est respectivement de 3,65 et 4,4 pour les injections de xanthane et de xanthane-SDBS. Cela montre que les forces gravitationnelles sont plus fortes que les forces visqueuses pour les deux couches et pour les solutions de polymères avec ou sans tensioactif.

La modélisation du déplacement du DNAPL dans un système multicouche à l'aide de solution de xanthane a été réalisée en utilisant les relations constitutives recueillies à partir des expériences en colonne en 1D. La figure 12 montre la bonne corrélation des profils de saturation obtenus numériquement et expérimentalement. La dynamique de propagation du front de déplacement (influencée par les forces gravitationnelles et capillaires) dans les deux couches a été relativement bien modélisée par le modèle numérique.





S_w

Figure 12 Comparaison entre les résultats numériques et expérimentaux du déplacement du DNAPL par une solution de xanthane dans un système multicouche en 2D, première rangée : résultats expérimentaux; deuxième rangée : résultats de la modélisation

4.3.2. Xanthane, SDBS et alcools dans système multicouche

La Figure 13 illustre la récupération du DNAPL dans un système multicouche, d'abord à l'aide de la solution de xanthane-SDBS puis du mélange C3. Cette figure montre que la solution de xanthane-SDBS déplace efficacement le DNAPL des deux couches. Ce déplacement est influencé par les différences de densité, la solution envahissante passant au-dessus du DNAPL, en réponse à la différence de densité entre les phases envahissante et déplacée. Lors de l'injection postérieure du mélange C3, deux zones distinctes apparaissent : les zones sombre et blanche. Celles-ci sont mises en évidence par des lignes en pointillés blancs et noirs, respectivement.

Conformément aux observations réalisées avec les expériences en colonne, l'injection du mélange C3 initie la dissolution du DNAPL, formant une zone sombre indiquant une solubilité proche du maximum. Cette zone sombre progresse grâce à la force motrice fournie par l'injection continue du mélange C3. Le mélange d'alcool à l'avant de la zone sombre est proche de la solubilité maximale du DNAPL, où toute dissolution supplémentaire du DNAPL devient négligeable, laissant derrière elle du DNAPL résiduel. Derrière le front de la zone sombre, le mélange d'alcool continue la dissolution du DNAPL restant. Ce phénomène donne naissance à une zone de transition, caractérisée par un gradient de concentration de DNAPL dans la phase aqueuse qui diminue de son maximum à l'avant à presque zéro à l'arrière. Suite à cette zone de transition se trouve la zone blanche, qui représente les régions où le DNAPL a été largement

dissous ou transporté par le mélange C3. La propagation de la zone sombre est directement corrélée au volume de pores injecté (par exemple, à 0,7 PV d'injection, la zone sombre couvre 60 % de la surface du réservoir) ; *a contrario*, l'avancement de la zone blanche est nettement plus lent, ne couvrant qu'un supplément de 20 % de la surface entre 1,58 et 2,1 PV.

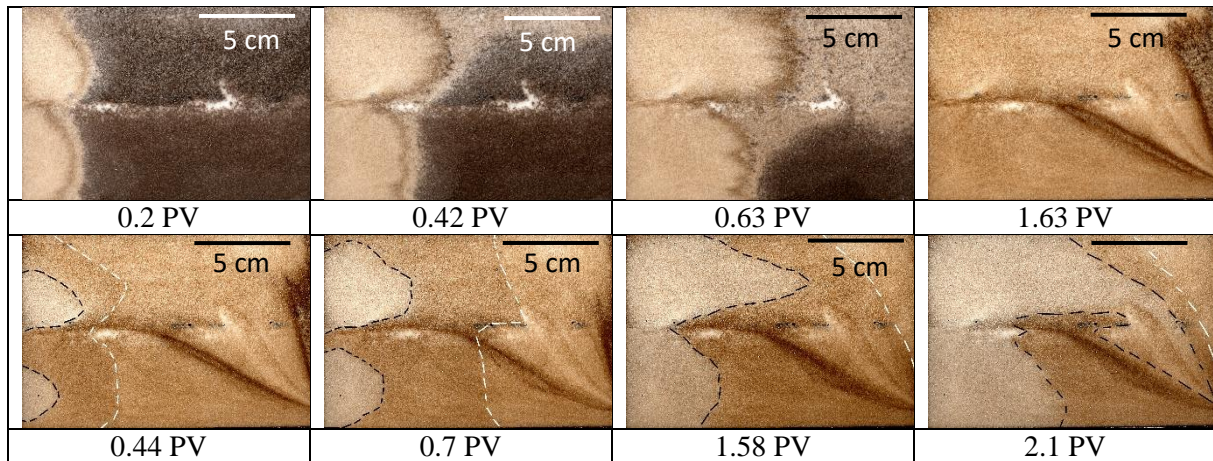
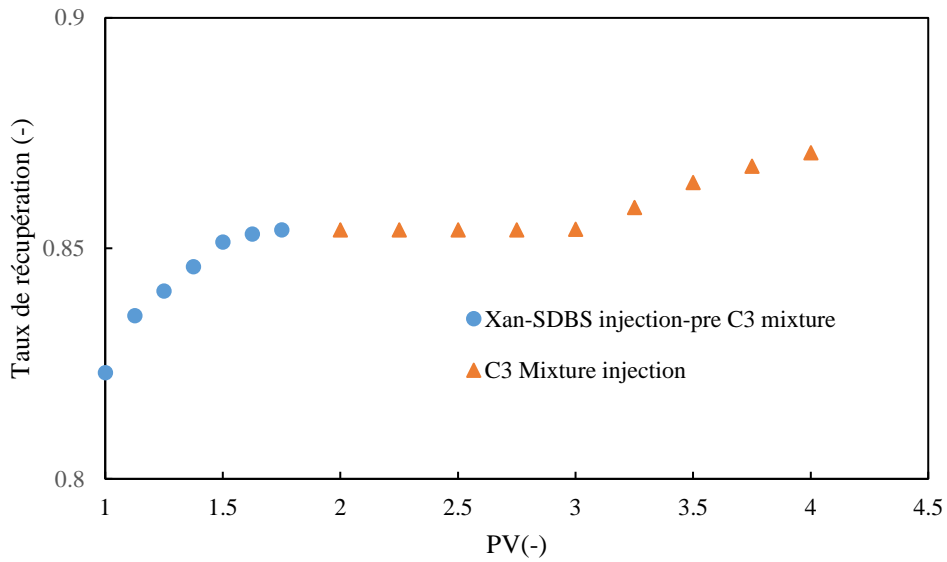


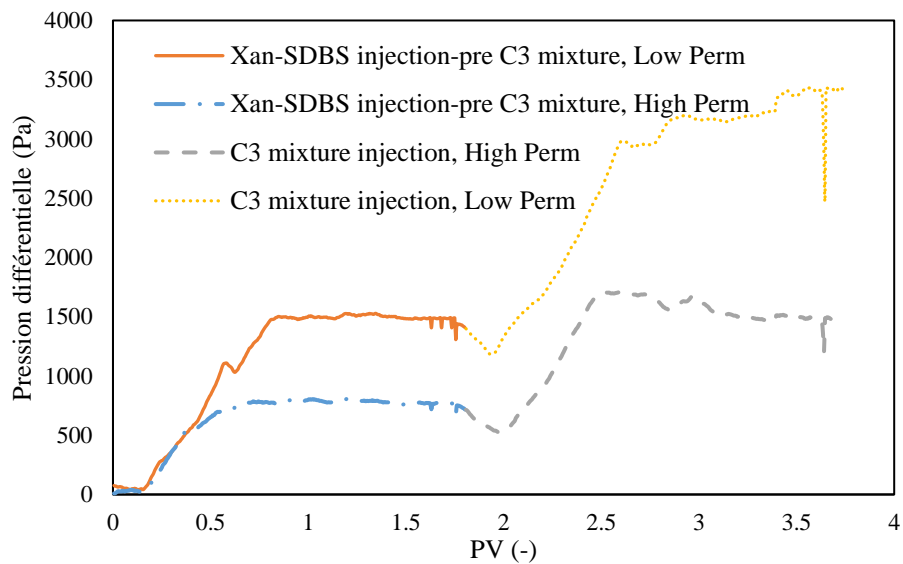
Figure 13 Déplacement du DNAPL dans un système multicouche 2D par injection de solution de xanthane-SDBS (première rangée) et injection postérieure du mélange C3 (deuxième rangée) en fonction du nombre de volumes de pores injectés pour chaque solution

La Figure 14 présente à la fois le taux de récupération et la pression différentielle pendant l'injection initiale de xanthane-SDBS et l'injection postérieure du mélange C3 dans le système multicouche. Comme observé dans les expériences en colonne, le DNAPL commence à apparaître dans l'effluent après 1 PV d'injection du mélange C3 et est récupéré à un taux constant. L'injection postérieure du mélange C3 a amélioré le facteur de récupération d'environ 0,02. Les résultats présentés en Figure 14 mettent en lumière que les courbes de pression différentielle entre les capteurs de pression dans chaque couche sont cohérents avec le processus d'injection ; on constate que le gradient de pression est plus élevé dans la couche moins perméable, et que ce gradient est nettement plus élevé pour l'injection postérieure du mélange

C3 que pour l'injection de xanthane-SDBS. Ceci peut s'expliquer par la viscosité des solutions injectées, qui est plus élevée dans le cas de l'injection de mélanges alcooliques.



(a)



(b)

Figure 14 Données expérimentales pour l'injection primaire de xanthane-SDBS et l'injection postérieure du mélange C3 dans le système multicouche. (a) taux de récupération en fonction des PV, et (b) pression différentielle en fonction des PV.

Le mode opératoire du bac 2D avec le mélange C3 a été reproduit avec le mélange C3-C6 : un mélange de xanthane-SDBS a d'abord été injecté jusqu'à ce qu'aucun DNAPL supplémentaire ne soit produit, puis le mélange C3-C6 a été introduit dans le système à saturation résiduelle de DNAPL. Dès que ce mélange a été introduit, les alcools qu'il contient ont commencé à pénétrer dans les ganglions de DNAPL, les faisant ainsi bouger et montrant ainsi le mécanisme de mobilisation. Comme on peut le voir sur la Figure 15, juste après l'injection de 0,3 PV du mélange C3-C6, des gouttelettes de DNAPL mobilisées sont arrivées au point de récupération. Ces gouttelettes sombres se sont progressivement éclaircies à mesure que davantage de mélange C3-C6 pénétrait dans les couches. Cela est dû au fait que plus la quantité de DNAPL restant dans les couches diminuait, plus la couleur sombre qui lui est associée a commencé à s'estomper.

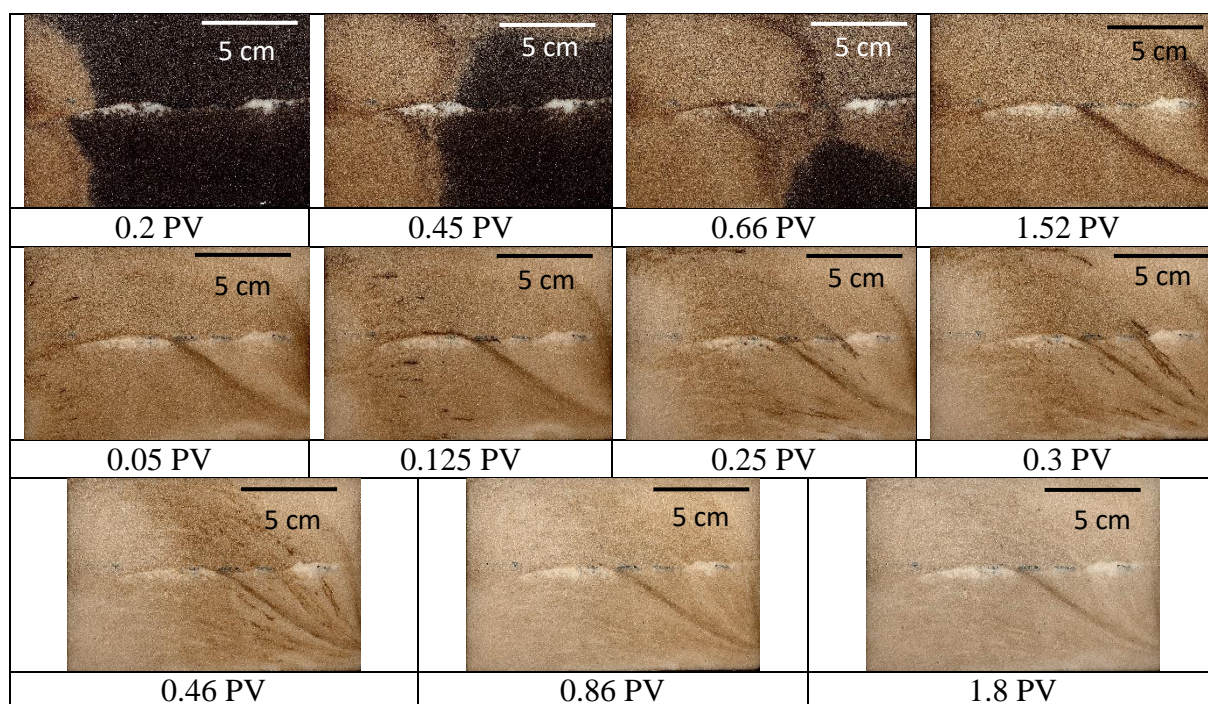
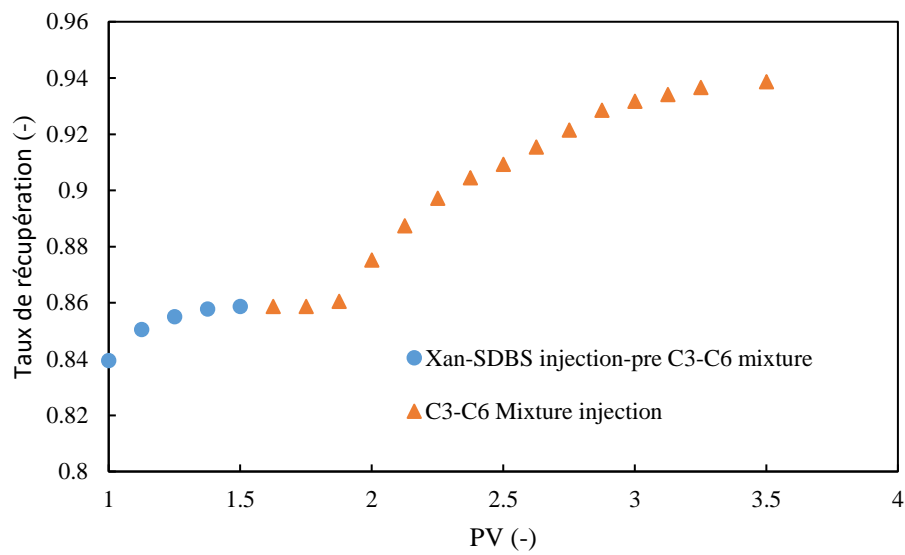


Figure 15 Déplacement de DNAPL dans un système multicouche 2D par injection de solution xanthan-SDBS (première rangée) et injection postérieure de mélange C3-C6 (deuxième et troisième rangées) en fonction du nombre de volumes de pore de chaque solution injectée

La Figure 16 présente respectivement le facteur de récupération et la pression différentielle dans chaque couche pour la post-injection du mélange C3-C6 dans le système multicouche. Il révèle que l'injection de ce mélange a amélioré le facteur de récupération d'environ 0,08. De même, les courbes de pression différentielle correspondent aux résultats obtenus dans les expériences en colonne.



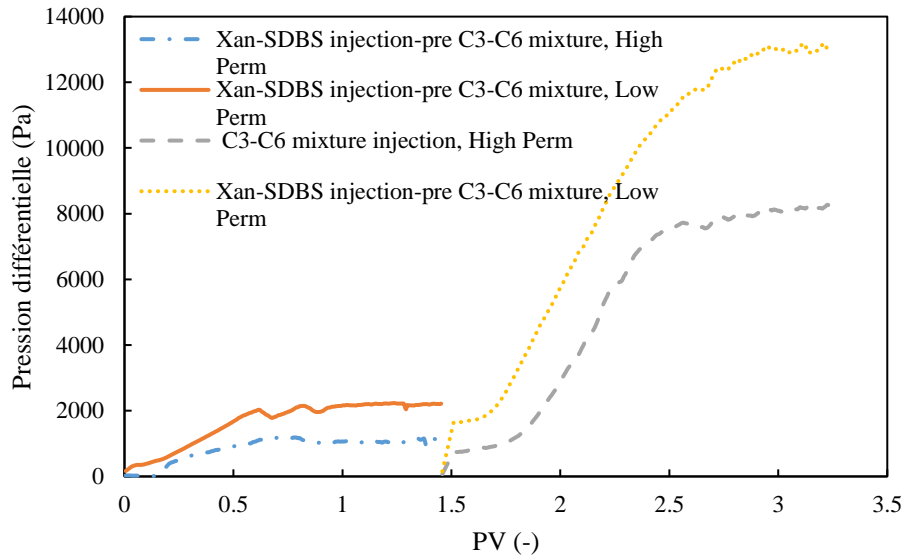
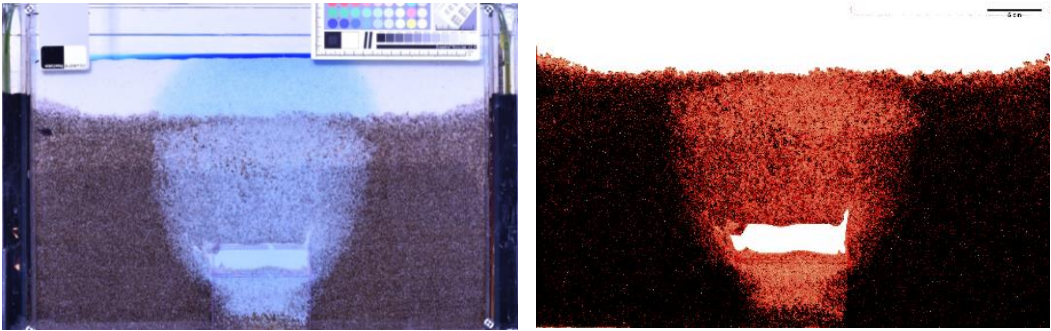


Figure 16 Données expérimentales pour l'injection primaire de la solution xanthane-SDBS et l'injection postérieure du mélange C3-C6 dans le système multicouche. (a) taux de récupération en fonction des PV, et (b) pression différentielle en fonction des PV

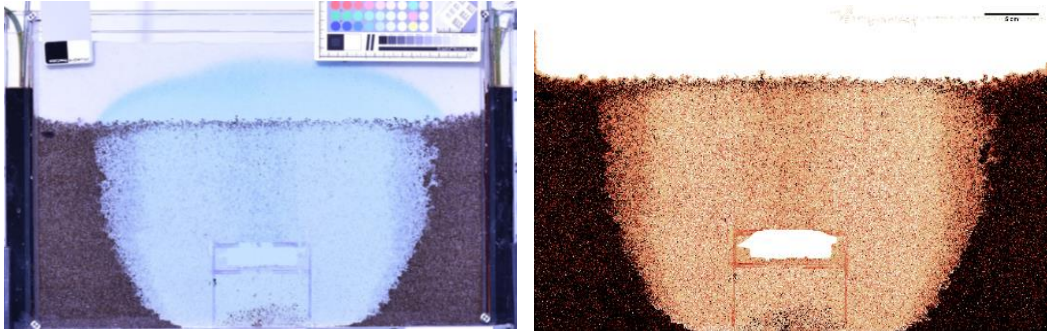
4.3.3. CMC et Barytine dans système non confiné

La dépollution de l'aquifère polluée par du DNAPL prenant en compte les effets gravitaires par injection d'une suspension de polymères a, par la suite, été étudiée en bac 2D. Trois densités différentes de suspension de barytine-CMC (1,3 g/mL, 1,66 g/mL et 1,9 g/mL) ont été prises en compte pour comparer l'efficacité de l'injection de mélanges de polymères avec et sans barytine sur le déplacement du DNAPL. Plusieurs mélanges de polymères de différentes densités ont été injectés dans le bac 2D saturé en DNAPL (à la saturation résiduelle en eau). La figure 17 montre la distribution du polymère et du DNAPL (images brutes et analysées) à la fin de l'expérience, c'est-à-dire lorsqu'il n'y a plus de production de DNAPL ou que la phase envahissante (suspension de barytine-CMC) s'est rapprochée des limites latérales. Dans le cas d'une injection de polymère pur en l'absence de particules de barytine, la phase envahissante se déplace verticalement. En augmentant la densité du mélange de polymères avec les particules de barytine, on observe un déplacement plus latéral du DNAPL, car les forces de flottabilité diminuent. Les résultats obtenus à partir des données du bilan de masse montrent que le taux

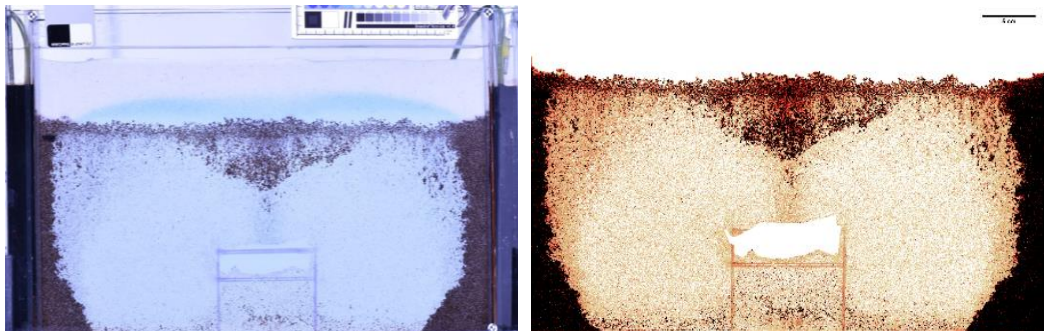
de récupération final dans le cas d'une solution de CMC sans particules est d'environ 0,095, tandis que pour les suspensions de barytine-CMC avec des densités de 1,3, 1,66 et 1,9 g/mL, les taux de récupération sont respectivement d'environ 0,3, 0,45 et 0,44.



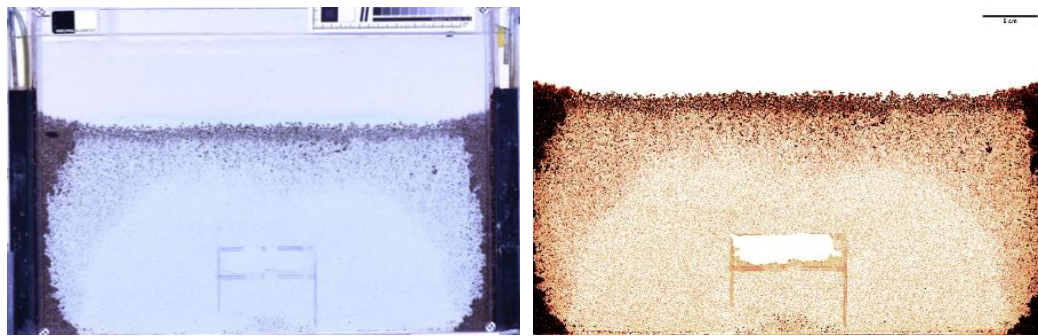
(a)



(b)



(c)



(d)

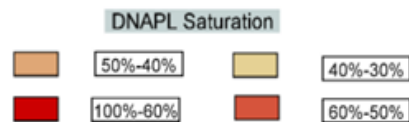


Figure 17 Comparaison de la propagation des solutions de barytine-CMC avec différentes densités, les images de gauche sont les images brutes, et les images de droite sont celles interprétées par analyse d'image. (a) injection de polymère pur avec une densité de 1 g/mL, injection de barite-CMC avec une densité de (b) 1,3 g/mL, (c) 1,66 g/mL, et (d) 1,9 g/mL. Les solutions sont injectées depuis le port situé dans la partie inférieure centrale du bac 2D

La Figure 18 montre la comparaison entre les résultats expérimentaux et numériques. Comme on peut le voir, la forme des fronts de déplacement de la suspension de barytine-CMC pour les différentes densités obtenues par simulation numérique est en corrélation avec les résultats expérimentaux. Comme mentionné précédemment, la grande zone transitoire près du front de la phase envahissante est attribuée au rôle de colmatage des particules de barytine et par conséquent à la variation de la densité.

Les taux de récupération résultant des expériences pour diverses densités des phases envahissantes sont comparés à ceux obtenus à partir des simulations numériques dans la Figure 19. Les erreurs relatives entre les résultats expérimentaux et les résultats des simulations sont respectivement d'environ 0,1, 0,045, 0,083 et 0,158 pour les densités de 1, 1,3, 1,6 et 1,9 g/mL.

La plus grande erreur pour les résultats avec les suspensions les plus denses peut être attribuée à la dépendance des fonctions de saturation (pression capillaire et perméabilités relatives) et à la concentration des particules de barytine qui colmatent le sable. Une autre raison pourrait être due au flux au-dessus de la couche peu perméable observé expérimentalement alors que nous l'avons considérée comme une zone imperméable dans notre modèle. Il est considéré que le polymère injecté a complètement envahi latéralement les deux côtés de la zone à haute perméabilité et aucun déplacement vertical ne se produit à partir de la zone à faible perméabilité.

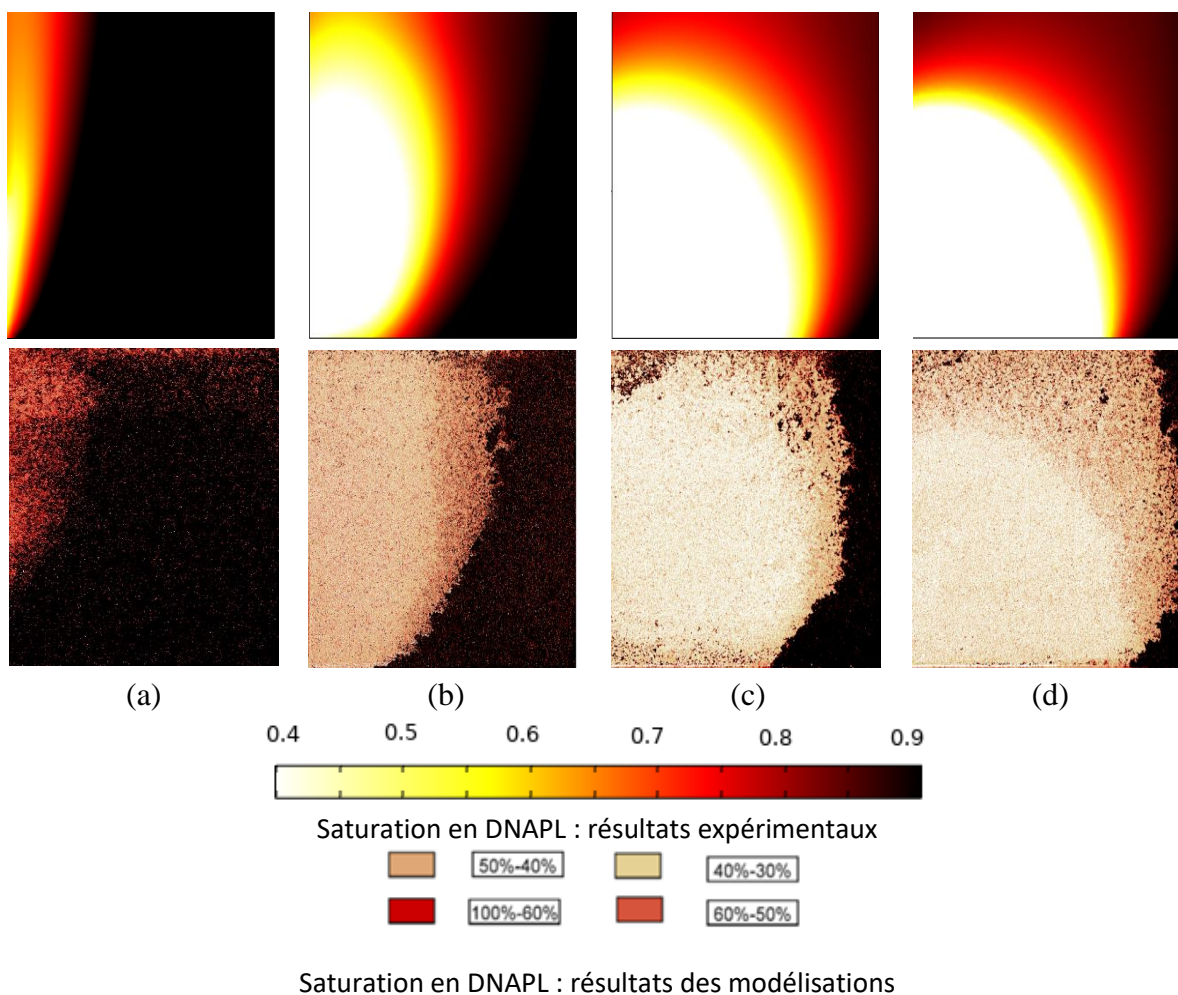


Figure 18 Comparaison entre les résultats numériques et expérimentaux à la fin du déplacement du DNAPL par la suspension de barytine-CCMC, les images de la première

rangée proviennent de la simulation et les images de la deuxième rangée sont extraites de l'analyse d'image des expériences. (a) injection de polymère pur avec une densité de 1 g/mL après 94 min, injection de barytine-CMC avec une densité de (b) 1,3 g/mL après 234 min, (c) 1,66 g/mL après 240 min, et (d) 1,9 g/mL après 220 min

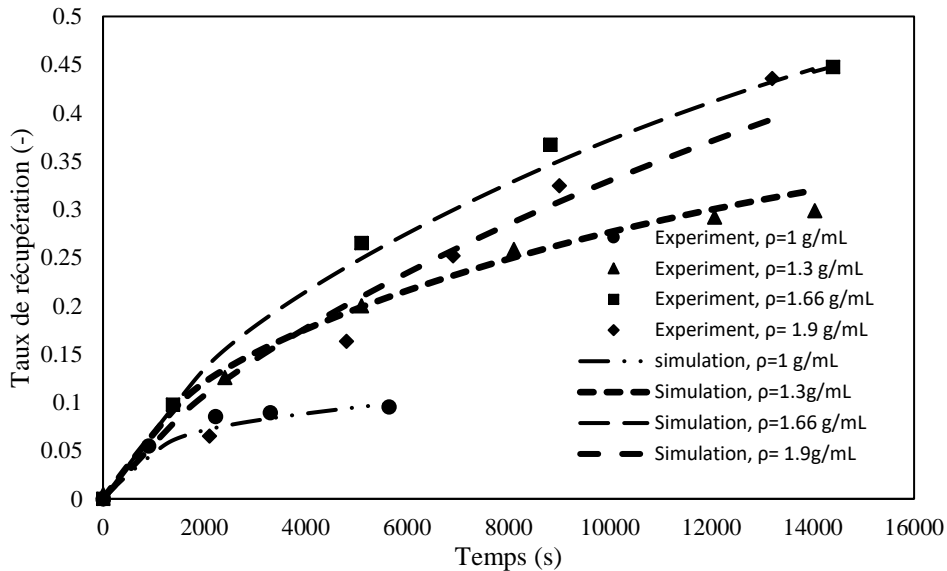


Figure 19 Comparaison entre les efficacités de déplacement expérimentales pour diverses densités de phases envahissantes (obtenues par bilan de masse) et celles obtenues à partir des résultats de simulation

4.3.4. Xanthane et NaI dans système non confiné

Des expériences en bac 2D ont aussi été menées pour étudier les effets bénéfiques de la densification de polymère (xanthane) à l'aide d'une solution saumâtre dense (NaI) sur les taux de récupération de DNAPL. La Figure 20 représente la propagation des différentes solutions injectées à la fin des expériences. L'interface entre la solution envahissante et le DNAPL est représentée par des lignes en pointillés blancs. Dans le cas d'un mélange de xanthane et de NaI (Figure 20a), deux lignes blanches sont présentes, représentant l'interface pour les zones complètement et partiellement déplacées.

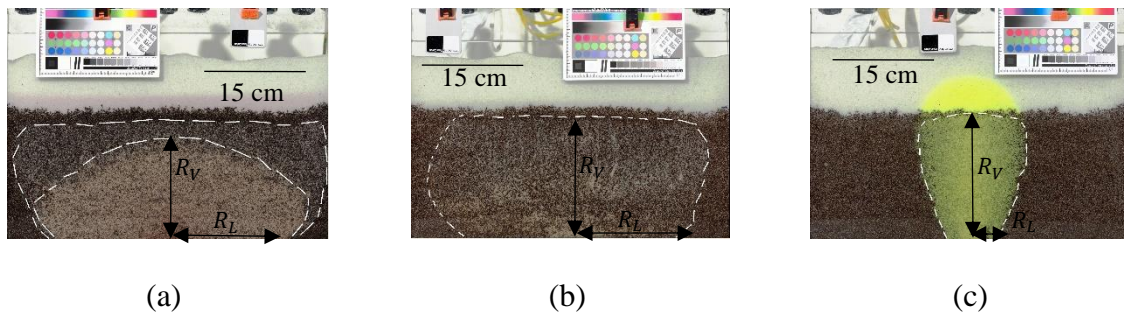


Figure 20 Comparaison de la propagation des trois solutions à la fin de l'injection à travers la zone contaminée, le DNAPL apparaît en noir et la zone déplacée est lumineuse. (a) mélange de xanthane et de NaI, (b) saumure pure de NaI, et (c) solution de xanthane. Les solutions sont injectées depuis le port situé dans la partie inférieure centrale du bac 2D

Lorsque le NaI est présent dans la solution de polymère, un déplacement latéral peut être observé (Figure 20a) ; cependant, en l'absence de xanthane dans la solution de NaI, le déplacement est moins efficace et il y a des zones où la couleur noire du DNAPL reste plus préminente (Figure 20b). L'injection de xanthane pur entraîne un mouvement principalement vertical (Figure 20c). Dans le cas de l'injection du mélange xanthane-NaI, une zone complètement déplacée et une zone de transition peuvent être observées (Figure 20a). Les courbes des taux de récupération de DNAPL en fonction du temps pour les différentes solutions injectées sont présentées dans la Figure 21. Ces taux sont respectivement de 0,46, 0,24 et 0,09 à la fin du déplacement pour le mélange de xanthane et de NaI, de NaI pur, et de solutions de xanthane.

La propagation de la solution envahissante dans la zone contaminée peut être décrite à travers les valeurs du rapport d'aspect (voir Figure 20), qui est défini comme le rapport du rayon latéral R_L au rayon vertical R_V (Davarzani et al., 2021). Il faut noter que, dans le cas où la zone de transition et la zone complètement déplacée sont présentes dans le système, les R_L et R_V pris en compte correspondent aux rayons de la zone complètement déplacée. Les rapports d'aspect sont respectivement d'environ 1,21, 1 et 0,38 pour le mélange de xanthane et de NaI, de NaI pur, et

de solutions de xanthane. Le faible rendement de récupération de DNAPL même lorsque le rapport d'aspect favorise le déplacement du DNAPL est attribué à la nature non confinée du système, qui est proche du site réellement pollué.

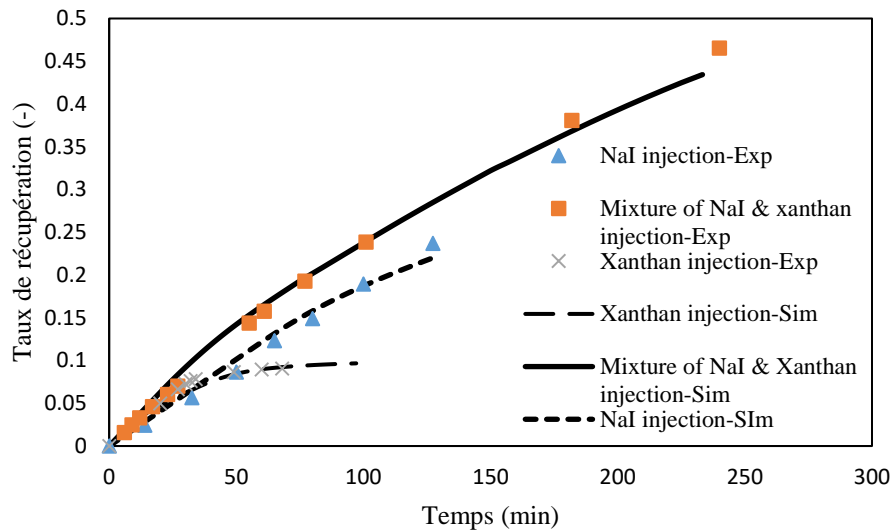
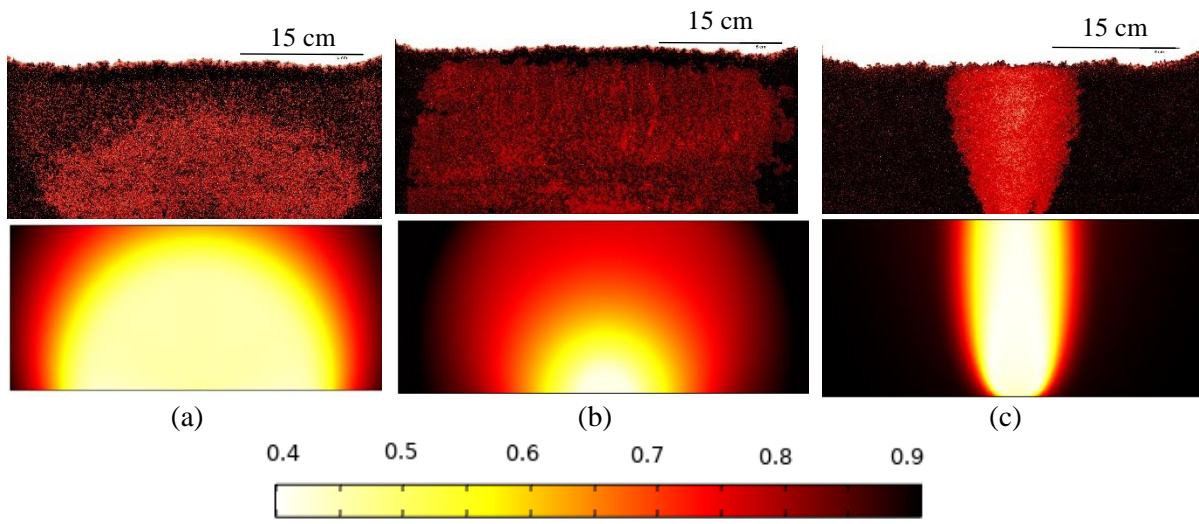
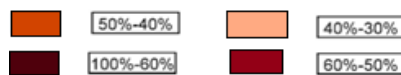


Figure 21 Comparaison du taux de récupération obtenu à partir des expériences et des simulations pour l'injection de différentes solutions : un mélange de solution de xanthane et de NaI, une solution de NaI pur, et une solution de xanthane

Une modélisation numérique a été effectuée pour mieux comprendre la physique sous-jacente derrière les expériences. Le déplacement du DNAPL à travers le bac 2D a été modélisé en utilisant les données obtenues à partir d'expériences en colonne 1D. La Figure 22 montre la comparaison entre les résultats numériques et expérimentaux après analyse d'image. Les courbes du taux de récupération obtenues à partir des expériences et de la modélisation sont présentées en Figure 21. Ces résultats démontrent que la modélisation numérique peut correctement prédire les résultats expérimentaux ; l'erreur absolue moyenne entre les résultats numériques et expérimentaux (en récupération du DNAPL) est d'environ 0,1.



Saturation en DNAPL : résultats expérimentaux



Saturation en DNAPL : résultats des modélisations

Figure 22 Comparaison entre les résultats numériques et expérimentaux à la fin du déplacement du DNAPL par différentes solutions, les images de la première rangée sont extraites de l'analyse d'image des expériences et les images de la deuxième rangée proviennent de la simulation. (a) Mélange de NaI et de xanthane (b) NaI pur, (c) et xanthane pur

Conclusion

Cette thèse visait à apporter de nouvelles perspectives dans l'étude de l'injection de polymères pour le traitement des nappes phréatiques polluées par le DNAPL. La performance de l'injection de polymères dans des systèmes poreux multicouches est examinée de manière exhaustive, et la thèse explore l'utilisation de solutions de polymères mélangées avec des tensioactifs et des alcools pour améliorer l'efficacité de la récupération de DNAPL. Un sujet clé discuté en détail est l'impact de l'écoulement densitaire sur le déplacement du DNAPL dans les systèmes poreux à une seule couche et multicouches. Une combinaison d'analyses expérimentales et numériques a été menée pour éclairer la dynamique de l'écoulement diphasique du déplacement du DNAPL par injection de polymères, en prenant en compte les propriétés non-newtoniennes des solutions

de polymères dans le fluide en solution et dans les milieux poreux. Diverses approches telles que l'augmentation de la densité de la solution de polymère en ajoutant des particules de barytine ou des sels solubles, ainsi que l'isolation des zones contaminées, ont été évaluées pour aborder le problème de la densité dans des systèmes poreux homogènes ou stratifiés,

Dans le cas de systèmes multicouches, l'accent initial était mis sur l'évaluation de l'efficacité de l'injection de solutions de xanthane, avec ou sans SDBS, pour le traitement de la nappe phréatique polluée par le DNAPL avec 2 couches de perméabilités différentes. Les résultats ont indiqué que le mélange de xanthane et de SDBS donnait des taux de récupération supérieurs dans les systèmes à une seule couche et multicouches. Par conséquent, ce mélange a été choisi comme fluide d'injection principal pour une étude ultérieure qui a évalué la performance des mélanges d'alcool en post-injection dans la réduction de la saturation résiduelle du DNAPL.

Les principales conclusions des études multicouches sont les suivants :

- La présence de SDBS a diminué la viscosité de la solution de xanthane, sans changements significatifs du comportement rhéologique à mesure que la concentration de SDBS augmentait. Les forces électrostatiques répulsives et l'interaction hydrophobe entre leurs molécules étaient responsables de ce comportement.
- L'ajout de SDBS à la solution de xanthane a entraîné une meilleure récupération du DNAPL en augmentant le nombre capillaire pendant l'injection du mélange, avec une amélioration d'environ 0,15 dans un système homogène 1D et 0,7 dans un système stratifié 2D. Les expériences 2D ont révélé que le déplacement du DNAPL était affecté par la différence de perméabilité et le contraste de densité.
- Les résultats de la simulation validés par les données expérimentales ont montré que, si la solution de polymère envahissante n'était pas densifiée et que le sol au-dessus du DNAPL n'était pas confiné (i.e. sans couvercle au-dessus du bac 2D), la récupération du

DNAPL était inférieure à la moitié de celle du système confiné (0,35 par rapport à 0,78). Dans un système expérimental 2D plus grand, l'injection de xanthane a conduit à une récupération de 0,87 du DNAPL lorsque les zones contaminées stratifiées étaient bloquées par un agent bloquant, suggérant que pour une application sur le terrain, la combinaison de l'injection d'un mélange de polymères avec le blocage de la zone contaminée peut conduire à un traitement prometteur des zones stratifiées contaminées par le DNAPL.

- Les expériences en batchs ont révélé que l'ajout de 1-hexanol dans le mélange d'alcools entraînait une partition de l'alcool dans la phase DNAPL, gonflant la phase organique. A l'inverse, lorsque le 1-propanol était le seul alcool dans le mélange, le DNAPL se dissolvait dans la phase aqueuse. L'analyse rhéologique a montré que, pour les mélanges d'alcools avec une fraction volumique de 50%, ceux contenant du 1-hexanol à 25% ou 50% de fraction volumique pouvaient avoir une viscosité trois fois supérieure à celle des mélanges ne contenant que du 1-propanol. L'analyse rhéologique a montré que l'ajout des alcools à la solution de polymère-tensioactif conservait le comportement non-newtonien.

- Les expériences en colonne 1D, réalisées après l'injection primaire de la solution de xanthane-SDBS, ont révélé deux mécanismes uniques. La post-injection de mélanges avec le 1-hexanol a entraîné l'apparition du DNAPL dans l'effluent après injection de 0,3 PV, indiquant un mécanisme de mobilisation dû à la partition de l'alcool dans le DNAPL piégé. En revanche, la post-injection du mélange C3 a initié la dissolution du DNAPL, signifiant un mécanisme de solubilisation. Ici, le DNAPL n'est apparu dans l'effluent qu'après 1 PV. Dans un ensemble d'expériences en colonne, une méthode de post-injection en "sandwich" du mélange de mobilisation a été proposée. Cette méthode

a amélioré le facteur de récupération d'environ 0,06 avec seulement 0,5 PV d'injection du mélange, comparé à 1 PV dans un scénario de post-injection complet.

- Les expériences en bac 2D ont été menées pour comparer visuellement les processus de solubilisation et de mobilisation. L'injection initiale du mélange de xanthane-SDBS a effectivement déplacé le DNAPL au travers deux couches. La post-injection du mélange C3 a initié la dissolution du DNAPL, formant une zone sombre avec un gradient de concentration en DNAPL, suivie d'une zone blanche où le DNAPL avait été largement dissous. La post-injection du mélange C3-C6 a mis en évidence le mécanisme de mobilisation, avec la partition de l'alcool dans le DNAPL provoquant sa mobilisation. Ceci a été illustré par la formation de gouttelettes de DNAPL en mouvement à l'intérieur des couches, où les ganglions de DNAPL gonflés sont devenus interconnectés, ont été mobilisés et ont atteint le point de récupération seulement après 0,3 PV. Au fur et à mesure que l'invasion du nouveau mélange d'alcool progressait, la couleur sombre de ces gouttelettes mobilisées s'estompa progressivement. La post-injection du mélange C3 a amélioré le facteur de récupération de 0,02 et a généré un gradient de pression plus faible par rapport au mélange C3-C6. En revanche, le mélange C3-C6 a entraîné une amélioration plus importante du facteur de récupération, environ 0,08. Ces résultats montrent que la post-injection d'un mélange d'alcool-tensioactif-polymère peut diminuer la saturation résiduelle du DNAPL dans un système stratifié.

Dans l'étude du traitement relatif aux effets gravitaires, nous avons étudié l'interaction entre les forces de flottabilité et les forces visqueuses qui influencent la distribution du DNAPL et de la phase envahissante. Les polymères utilisés pour traiter la nappe phréatique polluée par du DNAPL ont été densifiés à l'aide de particules de barytine (dans du CMC) et d'une solution de NaI (dans du xanthane).

- Il a été démontré qu'utiliser une solution de polymères seule ne permet pas d'avoir une efficacité de déplacement appropriée dans un système similaire au site réellement pollué (i.e. sans confinement au-dessus de la pollution). L'ajout de particules de barytine pour densifier la solution de polymères a permis d'améliorer l'efficacité de déplacement du DNAPL d'un facteur 4 fois.

- Le colmatage des particules de barytine en suspension dans les polymères densifiés a été analysé ; les paramètres liés au colmatage des particules de barytine ont été trouvés en utilisant des expériences en colonne 1D. De plus, il a été démontré que les suspensions de barytine-polymère peuvent entraîner une réduction de la perméabilité dans le sable allant jusqu'à 55%, 70% et 72% respectivement pour différentes suspensions avec des densités croissantes de 1,3, 1,66 et 1,9 g/mL. Il a été démontré que la viscosité de la suspension de polymère augmentait avec la densité du mélange. Pour tous les mélanges de polymères avec ou sans particules de barytine, un comportement rhéofluidifiant a été observé.

- Il a été démontré que pour un système confiné (qui n'est pas représentatif d'un site pollué réel), une efficacité de déplacement anormalement élevée peut être obtenue. Les résultats des simulations numériques, en utilisant la loi de Darcy généralisée et l'équation de continuité, étaient en corrélation avec les résultats expérimentaux. Ils ont montré que les fonctions de saturation pour les systèmes ouvert (non confiné) et fermé (confiné) sont différentes. La courbe de pression capillaire est plus élevée dans le cas d'un système fermé que dans un système ouvert. Les courbes de perméabilité relative à l'huile et à l'eau sont décalées vers la droite lorsque le système est fermé. Cette ignorance de la différence entre les saturations résiduelles dans les systèmes fermés et ouverts peut entraîner une surestimation de l'efficacité de la dépollution à l'échelle du terrain. Ainsi, il est fortement recommandé de prendre en compte le rôle de la limite supérieure de la

zone contaminée lors de la conception des méthodes de dépollution des sols à l'échelle du terrain.

- Les mesures rhéologiques ont montré que l'ajout de NaI comme densifiant n'affectait pas le comportement rhéofluidifiant du xanthane ; pour autant, la présence d'ions réduisait la viscosité d'un facteur 2,6 pour une gamme de taux de cisaillement intermédiaire. Le facteur de décalage pour la viscosité apparente était inférieur à l'unité, indiquant une déformation des molécules de polymère et une résistance accrue au flux en raison de contractions et d'expansions dans les milieux poreux. Des expériences en colonne confinée ont révélé des efficacités de récupération similaires d'environ 89% pour les solutions de xanthane quelle que soit la densité, tandis que la solution de saumure pure avait une efficacité de récupération plus faible d'environ 74%, cohérente avec l'analyse du nombre capillaire.

- Dans les expériences en bac 2D ouvert, les forces de gravité et visqueuses ont amélioré l'efficacité de déplacement du DNAPL. L'injection de solution de xanthane pure a montré un déplacement vertical avec un rapport d'aspect de 0,38 et un taux de récupération de 0,09, tandis que la solution de polymère densifiée a envahi la zone contaminée radialement avec un rapport d'aspect de 1,21 (pour un taux de récupération de 0,46). La solution de saumure pure a atteint la majeure partie de la zone contaminée, mais la couleur noire du DNAPL est restée plus proéminente dans la zone déplacée ; le taux de récupération est seulement de 0,24. Les simulations numériques ont indiqué qu'un nombre de gravité proche de zéro est nécessaire pour obtenir un rapport d'aspect autour de l'unité et éviter les problèmes de flux liés à la densité.

Ces résultats démontrent la nécessité de prendre en compte les effets gravitaires pour traiter les sols contaminés par des DNAPL chlorés lourds. Il est prouvé qu'une augmentation à la fois de

la viscosité et de la densité du fluide de déplacement conduit à une amélioration significative de l'efficacité de traitement des DNAPL chlorés lourds dans les sols.

Part 2 – Dissertation in English

Chapter 1

1. General introduction

1.1 Introduction

The pollution of groundwater by various anthropogenic organic compounds has become increasingly problematic in areas dominated by agricultural and industrial activities. Several organic environmental contaminants are persistent in the subsurface environment. Such persistent contaminants in the groundwater can spread, potentially leading to the infiltration of our primary drinking water sources. Chlorinated solvents are notable among these pollutants. While they serve multiple purposes, from machinery and clothing cleaning to chemical manufacturing, their widespread application and occasional careless disposal have led to notable environmental challenges. These pollutants generally have low water solubility and therefore are considered as Non-Aqueous Phase Liquids (NAPLs). Chlorinated solvents, in particular, are usually denser than water, categorizing them as Dense Non-Aqueous Phase Liquids (DNAPLs). Due to their density, these solvents can travel downward through soil and groundwater. They might appear as either static discontinuous blobs or ganglia of residual DNAPL or as continuous, near-saturated DNAPL zones (like pools or lenses) beneath the groundwater table. These zones can be mobile and are usually linked with capillary barriers.

This thesis, within the scope of the PAPIRUS (Pompage Assisté par Puits Inclinés avec Récupération par Upwelling et injection de Stabilisants in French; Enhanced Pumping by Inclined Wells with Recovery by Upwelling and Injection of Stabilizers in English) project, seeks to explore the remediation of DNAPL polluted aquifers by injecting polymer solutions in both experimental and numerical approaches for a polluted site in Tavaux located in eastern region of France. This chapter delves into the current state of polluted sites in France, examining French public policies regarding contaminated site and land management. It also briefly discusses the transport of chlorinated compounds in subsurface soil, various methods for remediation of aquifers contaminated by these components and proposes a brief overview on Tavaux polluted site and PAPIRUS project.

1.2 Overview on polluted sites in France

Pollution arising from chemicals, plastics, pesticides, and similar sources stands as one of the principal threats to soil integrity due to human actions alongside with soil overexploitation, water proofing, and erosion. Pollution (by chemicals, plastics, pesticides, etc.) is one of the 4 main threats to soils due to human activities, along with overexploitation, sealing and erosion. In 2021, more than 9,000 polluted sites are identified in France due to industrial activities in the past, particularly concentrated in former mining regions (ADEME, 2023). Pollution often turns out to be multiple on a site. The most frequently encountered pollutants in soils and groundwater are:

- Three categories of hydrocarbons (Total Petroleum Hydrocarbons (TPH), Chlorinated Hydrocarbons-CHC, Polycyclic Aromatic Hydrocarbons-PAH)
- Metals and metalloids such as arsenic, barium, cadmium, chromium, cobalt, copper, mercury, molybdenum, nickel, lead, selenium, and zinc
- Substances like benzene, toluene, ethylbenzene, xylene (BTEX), cyanides, and other contaminants like ammonium, chlorides, pesticides, non-halogenated solvents, and sulfates.

A statistical study conducted in 2015 in France underscores the prevalence of multi-contaminant pollution. Figure 1-1 illustrates the outcomes, indicating that hydrocarbons and metals are the most frequently detected pollutant families across the 5,991 compromised sites. Additionally, chlorinated hydrocarbons constitute approximately 14% of the identified pollutants (Report of French Ministry of Ecological Transition, 2015).

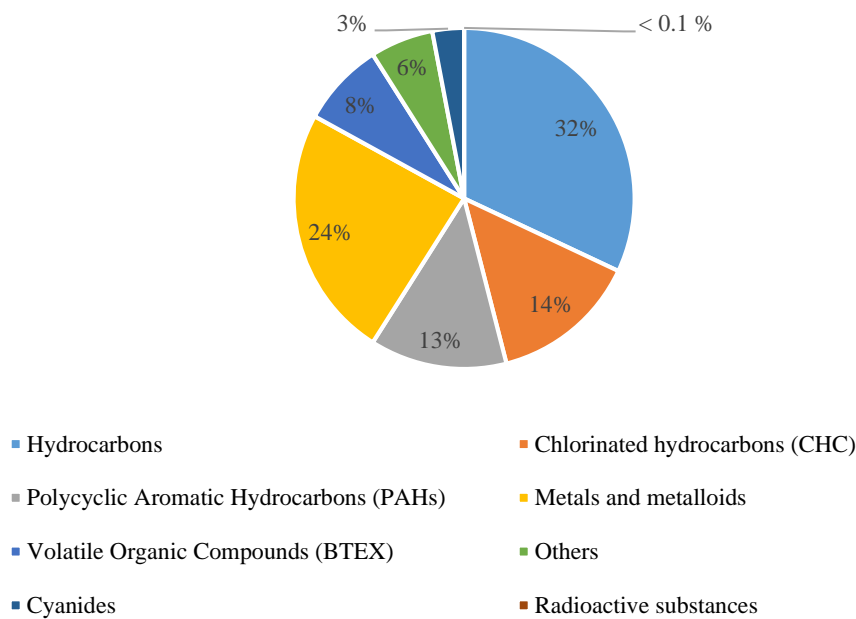


Figure 1-1 Main pollutants found in contaminated sites across France (Report of French Ministry of Ecological Transition, 2015)

1.3 French public policy for contaminated sites

As of 2021, over 9,000 polluted sites have been identified in France, with former mining regions being responsible for half of these cases. This contamination arises from either uncontrolled pollutant releases or incidents and inadequate containment measures. The protection of soil, groundwater, and surface water involves a collective effort from various economic players, spanning both the public and private sectors.

In 2018, 2.3 billion euros, i.e. nearly 4.5 % of environmental protection expenditure, were earmarked for actions to prevent and rehabilitate soil and water: prevention of pollution infiltration (52.2%), remediation (40.1%), environmental monitoring and assessments (3.6%) and protection of soils against erosion and other physical degradation (4.0%) (Figure 1-2). Since 2015, investments in the protection of soil, surface water, and groundwater have exhibited an upward trajectory. There was a 1% increase between 2015 and 2016, followed by robust growth of 17.6% in 2017 and a substantial rise of 19.0% in 2018. This expansion was largely attributed

to heightened agri-environmental subsidies (Annual Report of French Ministry of Ecological Transition, 2022).

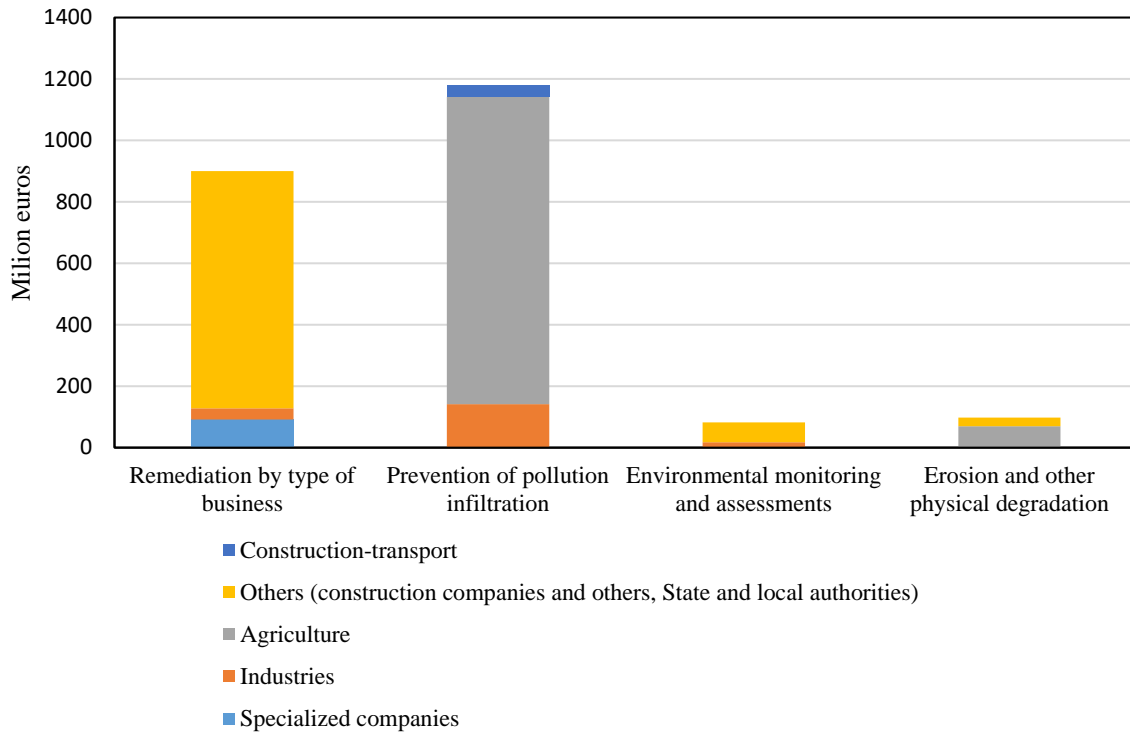


Figure 1-2 Investment distribution across sectors for the preservation and improvement of soil, groundwater, and surface water in the year 2018.

ADEME (The French Environmental Protection Agency) has recently published a report indicating the cost and implementation frequency of various remediation techniques (ADEME, 2014). According to this report, the majority of remediation techniques for chlorinated compounds involve extractive methods e.g. pump and treat (67%). The classic pumping/skimming approach has proven inefficient both technically and economically due to long treatment durations and poor remediation yields (Travis and Doty, 1990). The French Ministry of the Environment's methodology emphasizes thorough monitoring and testing (i.e. feasibility tests) before costly full-scale remediation. Many sites have been remediated without a clear understanding of pollution sources, particularly for chlorinated compounds, leading to

prolonged and ineffective pump and treat operations. New regulatory guidelines that mandate accurate pollution source monitoring are necessary to address this issue.

Hence, there's a growing demand for innovative remediation methods. The PAPIRUS project has been developed to assess the effectiveness of injecting polymers into aquifers saturated with DNAPL at one of the polluted sites in France. The following section delves into more detailed information about this project, the polluted site, and the characterization of DNAPL.

1.4 PAPIRUS project

The PAPIRUS project, initiated in 2020 and ending in 2023, has brought together a consortium of partners from both industry and academia. The collaborative team includes INEOS INOVYN (the vinyl chloride supplier and owner of the polluted site), SERPOL (a remediation company), GENDRY SERVICE LOCATION (a specialist in directional drilling), INTERA (focused on groundwater modeling), University of Poitiers, I2M Bordeaux (Institute of Mechanics and Mechanical Engineering, Art et Metiers Institute of Technology and the BRGM (French Geological Survey).

The principal aim of the PAPIRUS project was to combine tools and techniques for characterizing and remediating aquifers contaminated with chlorinated compounds through polymer solution injection. The project's various phases have been:

- Assessment of polymer solution injection's impact on DNAPL remediation at the laboratory scale, supplemented by numerical approaches.
- Field-scale modeling and numerical simulation.
- Remediation process monitoring using geophysical methods.
- Evaluation of techniques through technical-economic analysis and multi-criteria analysis.

This thesis primarily focuses on the first task within this project.

1.4.1. Tavaux polluted site

The project was conducted at the INEOS INOVYN plant located in Tavaux, situated in Bourgogne-Franche-Comté, France. The Tavaux site is a large chloroalkali chemical plant that covers an area of 300 hectares. The hydrogeological properties of the site are detailed in Table 1-1 (from uppermost to lowest).

Table 1-1 Hydrogeological properties of the Tavaux site (Cazaux et al., 2014)

Thickness	Lithology	Hydraulic conductivity (m.s-1)
2 to 4 m	Modern fine alluvium: superficial clays and loams	10^{-7} to 10^{-9}
5 to 10 m	Quaternary old alluvium (more or less clayey sands and gravel stones alluvial deposits)	10^{-2} to 10^{-4}
From a depth of 10 to 12 m	Marls	10^{-9}

The plant hosted a landfill between 1964 and 1986, serving as a dumping ground for production waste, particularly liquid waste (depicted in Figure 1-3). This landfill was constructed with a clay barrier. However, pollution was detected in 1987 during groundwater quality monitoring. Subsequent monitoring campaigns revealed the presence of approximately 20,000 metric tons of chlorinated compounds existing as free product within the underlying water table. This free product accumulated just above the substratum. Starting from the early 1980s until 2007, a historical DNAPL pool spanning several hectares was effectively confined, with its movement being closely observed (as shown in Figure 1-4).

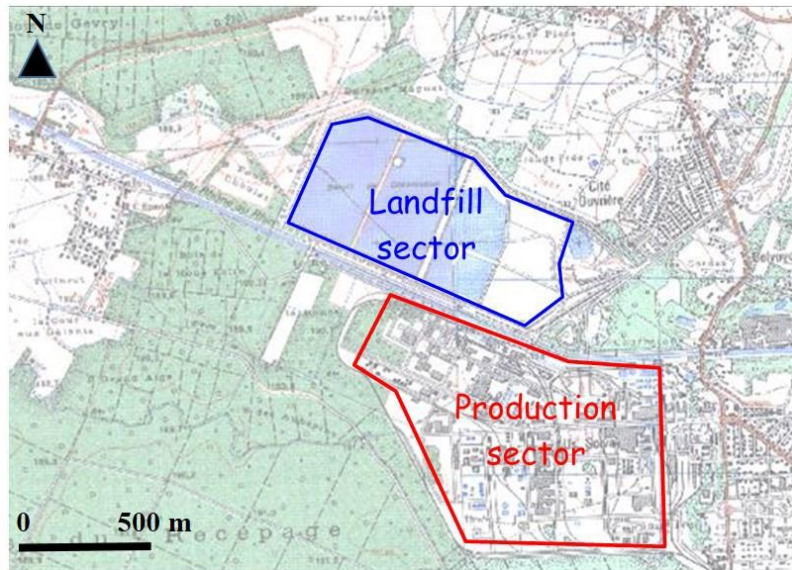


Figure 1-3 Map of factory location and source site for the study (Cazaux et al., 2014)

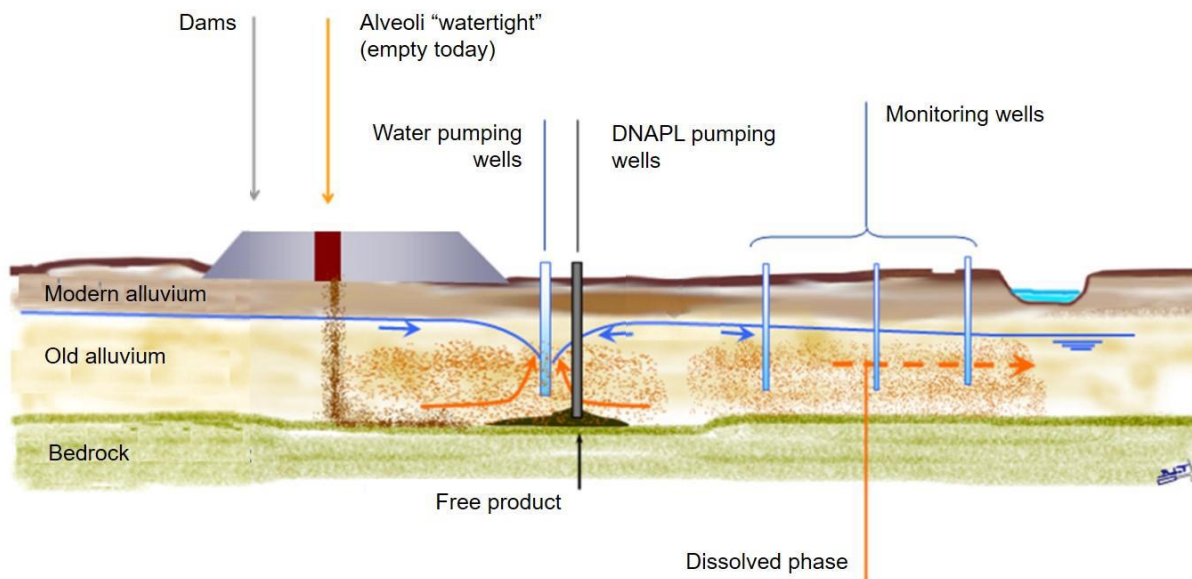


Figure 1-4 Hydrogeological cross section and schematic representation of Tavaux site adapted from Cazaux et al. (2014)

Following the migration of DNAPL from the landfill, a steady-state plume was formed within a shallow sandy aquifer above a clayey layer situated at a depth of 10 meters. The thickness of DNAPL ranged from 0.20 m to 1.50 m, aligning with the substratum's contours (Cazaux et al.,

2014). The movement of DNAPL was regulated by two water-pumping wells over the past three decades, inducing a lowering of the water table and an opposite gradient within the region. The hydraulic confinement achieved an average flow rate of $40 \text{ m}^3 \cdot \text{h}^{-1}$. Presently, the free product extends across multiple hectares, generating areas of pollution sources containing roughly 20,000 tons of pure DNAPL, along with impacted plume zones stretching for 15 km (displayed in Figure 1-5). Monitoring efforts for this have been in place since 1970.

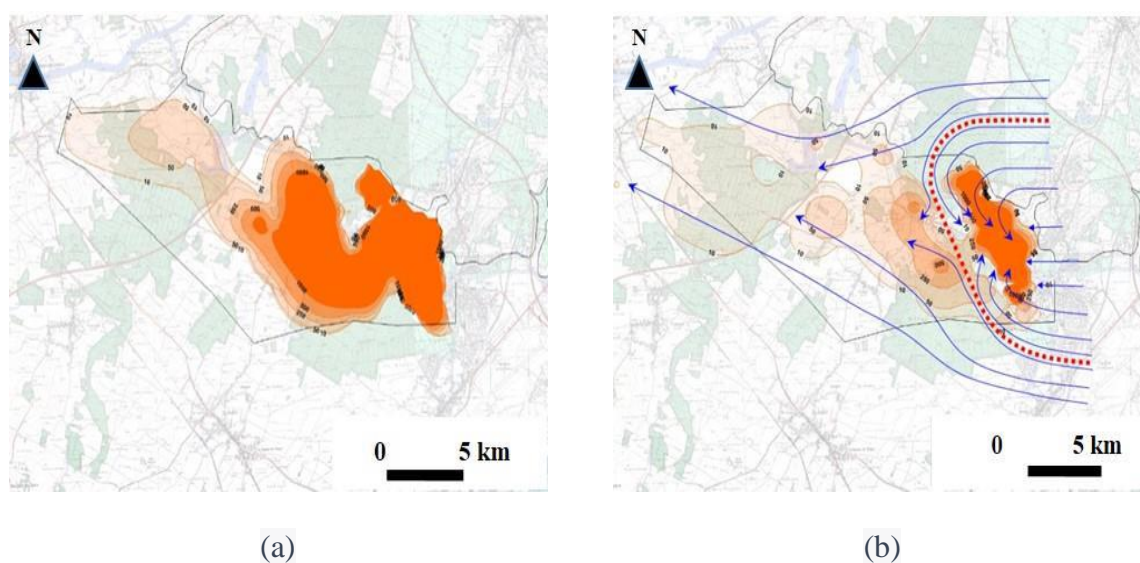


Figure 1-5 Migration of the DNAPL (orange phase) from the storage sector to the plume area in a) 1989 and b) 2009 (Cazaux et al., 2014)

1.4.2. Composition of DNAPL in Tavaux site

The DNAPL found in Tavaux site is a multicomponent chlorinated organic compound that is mainly made of hexachlorobutadiene (HBCD, C_4Cl_6) (58%), hexachloroethane (HCA, C_2Cl_6) (14%), and penta-chlorobenzene (PeCB, C_6HCl_5) (3.5%), carbon tetrachloride (TCM, CCl_4) (4%), and other conventional chlorinated organic compounds including perchloroethylene (PCE, C_2Cl_4) (8%), and trichloroethylene (TCE, C_2HCl_3) (2%). There are some other components in DNAPL mixture that are not quantifiable. The physical properties of DNAPL are mentioned in Table 1-2.

Table 1-2 Physical parameters of the DNAPL(Colombano et al., 2020)

Parameter	Density (kg.L ⁻¹)	Dynamic viscosity (mPa.s)	DNAPL/water interfacial tension (mN.m ⁻¹)	DNAPL/water/sand contact angle (°)
DNAPL, 20 °C	1.66±0.005	4.47±0.15	10.96±0.05	119.33±4.16

Chapter 2

2. Literature Review

2.1 Introduction

Chlorinated organic compounds like trichloroethene (TCE) and tetrachloroethene (PCE) have been utilized for various purposes over the years, including fabric cleaning and metal degreasing. Due to their extensive consumption in recent decades and improper disposal, these solvents have led to a range of environmental concerns. Typically, chlorinated solvents infiltrate the subsurface in the form of dense non-aqueous phase liquids (DNAPLs). DNAPLs are immiscible liquids denser than water and only slightly soluble in water. As a result, DNAPLs can migrate as separate liquid phases to considerable depths beneath the water table down to the bedrock if the mass of DNAPL is sufficient (Langwaldt and Puhakka, 2000a; Zhang and Smith, 2002). There, they gradually dissolve into flowing groundwater, giving rise to contamination plumes in the aqueous phase (Roy et al., 2004).

Despite the limited solubility of chlorinated solvent DNAPLs in water, their solubility usually surpasses typical drinking water standards by orders of magnitude. Consequently, even minor amounts of DNAPL released into the subsurface can lead to contamination in groundwater volumes several times larger. Many chlorinated solvents also possess sufficient vapor pressure to enable vaporization into soil gas, leading to contamination plumes in the vapor phase (Kueper et al., 2014).

A "chlorinated solvent source zone" refers to a subsurface area with or previously with chlorinated solvents in DNAPL form, containing enough solvent mass to maintain concentrations exceeding regulatory limits in soil or groundwater. This definition acknowledges that DNAPL might not uniformly persist across its original subsurface volume, and it could be fully depleted due to natural processes (if the natural conditions of the environment allow it: pH, electron acceptors/donors, etc.) or remediation methods. Understanding the nature and extent of chlorinated solvents in the subsurface, and what exactly

constitutes a source zone, is of great importance. Kueper et al. (2014) considered five stages for the life cycle of a chlorinated solvent source zone including a) initial DNAPL release, b) DNAPL redistribution, c) continued DNAPL dissolution and aging, d) complete DNAPL depletion, and e) desorption and back diffusion. In the absence of remediation efforts for a large volume of DNAPL release into low to moderate permeability media, depending on the DNAPL solubility, the groundwater velocity and the degree of biodegradation, the life span of DNAPL could be on the order of hundreds of years (Gerhard et al., 2007; Kueper et al., 2014, 1993).

The initial focus of remediation efforts at chlorinated solvent sites was to install pump-and-treat systems, largely because it has been accessible, and easy to design. A review of 849 US Superfund sites (areas contaminated with hazardous materials) from 1980 to 2004 shows that 63 % of these sites used pump-and-treat systems for DNAPL remediation (Kovalick, 2008). Pump-and-treat system limitations became evident due to contamination persisting after the start of remediation activity (Travis and Doty, 1990), resulting in high cost per removed unit of contaminant. The ineffectiveness of pump-and-treat for DNAPL mass removal is well-documented (Kavanaugh et al., 2003).

The experts and researchers tried to develop more advanced methods for the remediation of polluted sites by chlorinated solvents instead of implementing pump-and-treat systems. These methods could consist in a variety of categories such as excavation before disposal in off-site remediation centers (McGuire et al., 2006; USEPA, 2009), air sparging and soil vapor extraction (Kim et al., 2022; Reddy and Tekola, 2004; Unger et al., 1995), in situ thermal treatment (Beyke and Fleming, 2005; Colombano et al., 2021, 2020; Xie et al., 2019), in situ chemical reaction including oxidation (Huling and Pivetz, 2006; Johansson et al., 2022, 2020; Siegrist et al., 2011; Tsitonaki et al., 2010) or reduction (Bossa et al., 2017; Cheng and Wu, 2000; Crane and Scott, 2012; Rodrigues et al., 2017a), in situ bioremediation (Langwaldt and Puhakka, 2000b; Maire et al., 2019), in situ soil washing by surfactant or cosolvent (Lee et al.,

2005; Pennell et al., 1993; Pennell and Abriola, 2017; Ramsburg et al., 2003; Walker et al., 2022a; Wang and Mulligan, 2004), and hydraulic displacement (Alamooti et al., 2023, 2022; Kilbane et al., 1997; Martel et al., 1998; Miller et al., 2000; Omirbekov et al., 2023; Pennell et al., 1996; Robert et al., 2006).

For the cases where DNAPL is present in pools, the hydraulic displacement as a mass removal technology can effectively remediate the DNAPL pools in subsurface (Alexandra et al., 2012). This technology has been primarily used in the petroleum industry, where the waterflooding (Craig Jr, 1972; Willhite, 1986), polymer injection (Alamooti and Malekabadi, 2018; Sorbie and Seright, 1992; Wei et al., 2020; Wever et al., 2011), and or foam injection (Adebanjo and Olusegun, 2015; Ardakani et al., 2020; Falls et al., 1988) were used to displace the oil from the reservoir as an Enhanced Oil Recovery (EOR) method. This method can be employed using injection wells, where the selected fluid is injected through the contaminated zone to push it toward the recovery wells.

Although waterflooding is less expensive compared to other hydraulic displacement methods, and straightforward to be implemented, its efficiency can drop when dealing with viscous DNAPL due to potential viscous fingering issues (Giese and Powers, 2002; Kueper and Frind, 1988). Another crucial element in designing a hydraulic displacement remediation technique is the consideration of the heterogeneity of the contaminated zone. In multi-layered zones, low-permeability zones may be bypassed unless a shear-thinning fluid is used. With waterflooding, the injected water flows predominantly through larger pores, neglecting a significant amount of potentially mobile DNAPL in finer pores. DNAPL bypassing happens both at the pore level and on larger scales, depending on the variability in pore structure (Giese and Powers, 2002). Polymer and foam as shear thinning fluids can overcome viscous fingering and displace DNAPL from the multilayer zones (Hirasaki et al., 1997b, 1997a; Maire et al., 2015; Martel et al., 1998, 2004; Omirbekov et al., 2020b; Robert et al., 2006; Silva et al., 2013).

In the case of remediation by foam injection, the foam's stability especially when it is in contact with chlorinated solvents is one of the challenging issues in the process of design and the analysis of the performance of foam injection (Kilbane et al., 1997; Wang and Mulligan, 2004).

A variety of shear-thinning biopolymers including guar gum, xanthan gum, and carboxymethyl cellulose (CMC) are accessible to be used for remediation of DNAPL polluted zones (Omirebekov et al., 2023). For a successful polymer injection strategy to remediate DNAPL-contaminated soils, it is necessary to understand basics of single-phase and multiphase flow in porous media, the transport of polymers in the soil, and the polymer's non-Newtonian properties in both bulk and porous contexts. The subsequent sections delve into these concepts.

2.2 Properties of porous media

2.2.1. Porous media

Porous media refer to materials characterized by a solid structure interspersed with voids or pores, allowing the passage and storage of fluids (both liquids and gases). These interstitial spaces can be interconnected, facilitating fluid movement, or isolated. Examples of porous media span from natural substances like soils and rocks to engineered materials like foams and filters. The study of porous media is essential for diverse applications, including water filtration, oil recovery, and materials science.

2.2.2. Scale

Flow phenomena in porous media and free flows can be analyzed on various scales, including the molecular scale, pore scale, Representative Elementary Volume (REV) scale, and Darcy scale as depicted in Figure 2-1. These scales help comprehend different aspects of fluid behavior.

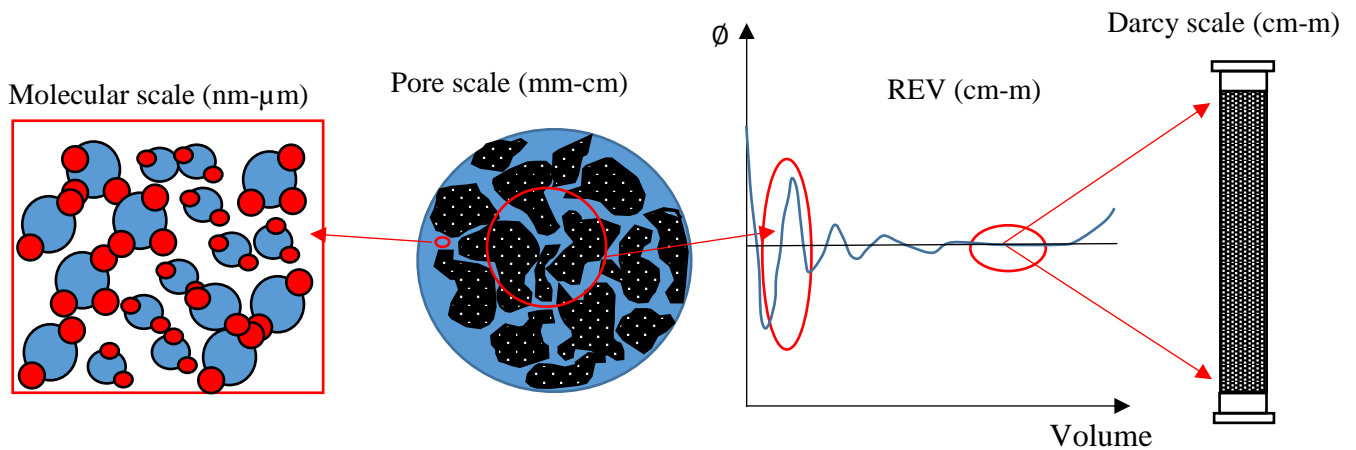


Figure 2-1 Different scales: Molecular scale, pore scale, REV and Darcy scale

2.2.2.1. Molecular Scale

The molecular scale is concerned with molecular motion and collisions in fluid phases. It determines chemical and physical fluid properties. Averaging over this scale generates parameters like density, pressure, and temperature, which are used in continuous descriptions where they vary smoothly in space (Bear, 2013).

2.2.2.2. Pore-Scale

At the pore scale (micrometers to centimeters), individual pores and their interactions with fluids are studied. Focus lies on pore properties like size, shape, connectivity, and surface attributes. Pore scale processes involve phenomena like capillary action, fluid-solid interactions, and molecular diffusion. The Navier-Stokes equations are a set of partial differential equations that describe the behavior of fluid flow at this scale. For incompressible flow, where the fluid density remains constant, the Navier-Stokes equations are hyperbolic. In this case, the system of equations describes the propagation of pressure waves and fluid velocity perturbations through the fluid.

2.2.2.3. Representative Elementary Volume (REV)

For practical applications over larger extents, averaged quantities are often required over Representative Elementary Volumes (REV). The REV bridges pore and Darcy scales, representing a volume where averaged properties of porous media are meaningful. REV's size balances microscopic variability (avoiding strong fluctuations) and macroscopic heterogeneity (Heinemann and Mittermeir, 2013).

2.2.2.4. Darcy Scale

The Darcy scale refers to the macroscopic level of porous media which is the focus of this work. It encompasses larger volumes and considers averaged properties such as permeability and porosity. Darcy's law establishes a link between fluid flow rate, pressure difference, and permeability at this scale, providing insights into how fluids flow through the material (Heinemann and Mittermeir, 2013; Vafai, 2015). The Darcy-continuity equation is used to describe the flow of fluid through porous media, such as groundwater flow in an aquifer. The Darcy-continuity equation is generally considered to be parabolic. This is because it describes the flow of fluid through porous media, where the flow is governed by diffusion-like processes.

2.2.3. Porosity

The porosity of a porous medium (soil here) indicates its ability to contain fluids, representing the space or voids within it. Quantitatively, porosity is defined as the proportion of the soil's void volume to its bulk volume. This important soil characteristic is determined using the given generalized relationship:

$$\emptyset = \frac{\text{Pore volume within a REV (mL)}}{\text{REV (mL)}} \quad \text{Eq 2-1}$$

where \emptyset is porosity (-). Effective porosity is that portion of the total void space of a porous material that is capable of transmitting a fluid.

2.2.4. Permeability

Permeability is a property of the porous medium and is a measure of the capacity of the medium to transmit fluids when only one fluid phase is present in the medium. For an isotropic homogenous porous medium, the permeability k can be determined using Darcy's law:

$$\mathbf{u} = -\frac{k}{\mu}(\nabla p - \rho \mathbf{g}) \quad \text{Eq 2-2}$$

where \mathbf{u} is the velocity (m/s), and k (m^2) refers to the scalar absolute permeability of the isotropic porous medium. The viscosity and the pressure as well as the gravity vector are represented by μ (Pa.s), p (Pa), and \mathbf{g} (m/s^2) respectively.

2.2.5. Saturation

When several phases like water, air, or oil are present in porous media, the fraction of the pore volume occupied by a particular phase is called saturation. This property can be expressed as:

$$\alpha - \text{Phase saturation} = \frac{\text{Total volume of the } \alpha - \text{phase in the REV (mL)}}{\text{Pore volume contained in the REV (mL)}} \quad \text{Eq 2-3}$$

The saturation of each individual phase ranges between zero to 1. By definition, the sum of the saturations of the different phases present in the porous medium is 1, and for a soil system composed of two phases, wetting and non wetting, we have:

$$S_w + S_{nw} = 1 \quad \text{Eq 2-4}$$

where S_w and S_{nw} represent wetting and non-wetting phases saturations respectively.

2.2.6. Wettability

Wettability is the tendency of a fluid to spread on or adhere to a solid surface in the presence of other immiscible fluids. The phase spreading over the solid surface is called the wetting phase. The angle at which the interface meets the solid surface is known as the contact angle. Surface tension is a property of the liquid-gas interface. It's the force acting at the surface of a

liquid that tends to minimize its surface area. It results from the greater attraction of liquid molecules to each other (due to cohesion). Interfacial tension is a similar concept for immiscible liquids at their boundary. However the main forces involved in interfacial tension are adhesive forces (tension) between the liquid phase of one substance and either a solid, liquid or gas phase of another substance.

2.2.7. Capillary pressure

When two immiscible fluids encounter each other within the pore spaces of a porous medium, a pressure contrast arises along the interface that separates them. This pressure distinction, referred to as capillary pressure (P_c), is determined by subtracting the pressure in the wetting phase from the pressure in the non-wetting phase (P_a). The Young-Laplace equation provides a formulation for capillary pressure:

$$P_c = \frac{2\sigma \cos \omega}{r} \quad \text{Eq 2-5}$$

where r is the average pore radius (m), σ is the interfacial tension (N/m), and ω is the contact angle. This expression is applicable to the pore-scale process. According to this expression, capillary pressure is influenced by the characteristics of both the porous medium (pore radius and wettability) and the fluid (interfacial tension). Capillary pressure equations have been developed based on a simplification involving a single, uniform capillary tube. However, real porous media consist of interconnected pores of diverse dimensions, resulting in capillary pressure variations based on fluid saturation levels. At Darcy scale the magnitude of capillary pressure relies on phase saturations, phase continuity, pore and pore throat shapes and sizes, as well as the prior saturation history and governing mechanisms related to the fluid configurations i.e. imbibition (the process where wetting phase saturation increases, wetting phase displaces the non-wetting one) and drainage (the process where non-wetting phase

saturation increases). Figure 2-2 illustrates the typical relationship between capillary pressure and saturation for both imbibition and drainage scenarios.

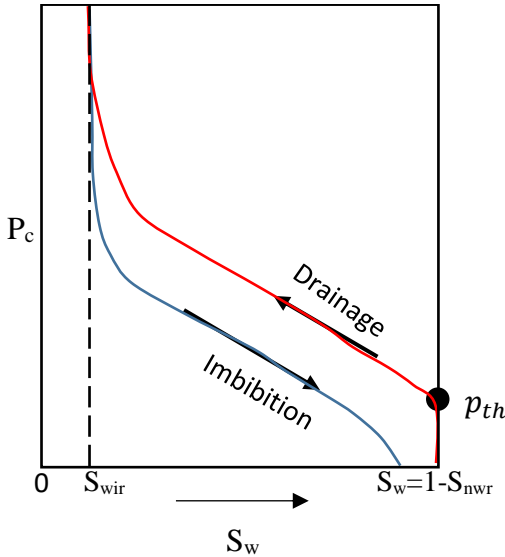


Figure 2-2 Schematic of capillary pressure curve for imbibition and drainage

The wetting irreducible saturation, S_{wir} , represents the saturation of the wetting phase that cannot be further decreased by increasing capillary pressure, reached at the end the drainage process in porous media. The non-wetting residual saturation, S_{nwr} , corresponds to the lowest attainable saturation of the non-wetting phase following the imbibition process. p_{th} (Pa) signifies the minimum pressure necessary for the non-wetting phase to enter into the porous media .

To describe the capillary pressure as the function of saturation several empirical models have been developed. Brooks-Corey model can describe capillary pressure as function of saturation as follows (Brooks and Corey, 1964):

$$p_c = p_{th} S_{we}^{-\frac{1}{\lambda}} \tag{Eq 2-6}$$

where λ is the index of the pore size distribution. The effective saturations of wetting phase is denoted by S_{we} (-) and can be expressed as:

$$S_{we} = \frac{S_w - S_{wir}}{1 - S_{nwr} - S_{wir}} \quad \text{Eq 2-7}$$

where, S_{wir} (-) and S_{nwr} (-) are the wetting irreducible and non-wetting residual saturations respectively.

2.2.8. Relative permeability

Relative permeability is a dimensionless measure of the permeability of a fluid phase as it flows through porous media in the presence of another fluid phase. Several methods have been developed in order to determine relative permeability curves from the unsteady state experimental data. These methods may be classified into two main explicit and implicit categories (Richmond and Watson, 1990). In both categories, production data and/or differential pressure along the porous media are required to obtain the relative permeability curves.

The explicit methods are mainly analytical and directly calculate the relative permeability from the flow data (Johnson et al., 1959; Jones and Roszelle, 1978; Li et al., 1994; Toth et al., 2002). In explicit method the simulation of multiphase flow is normally done by considering predetermined models of relative permeability and capillary pressure functions. Then simulation results are adjusted with the experimental data to find the unknown parameters of flow functions (Richmond and Watson, 1990). This method is also known as inverse modeling. For water-wet porous media, a number of models have been proposed to correlate capillary pressure and relative permeability with water saturation (Brooks and Corey, 1964; Kjosavik et al., 2000; Lomeland et al., 2005; Nono et al., 2014; Skjaeveland et al., 2000; Van Genuchten, 1980). Among them, Brooks and Corey model is one of the simplest and easiest to use. It has been widely used in the context of two-phase flow in porous media. For the relative permeabilities, this model can be expressed as:

$$k_{rw} = k_{rw}^{max} S_{we}^{\epsilon_w} \quad \text{Eq 2-8}$$

$$k_{rnw} = k_{rnw}^{max} S_{nwe}^{\epsilon_{nw}} \quad \text{Eq 2-9}$$

where k_{rw}^{max} and k_{rnw}^{max} are the maximum relative permeability values (end points) for the wetting and non-wetting phases, respectively. The saturation exponents for the wetting and non-wetting phases are given by ϵ_w and ϵ_{nw} . The effective saturations of the wetting and non-wetting phases are denoted by S_{we} and S_{nwe} (-) respectively and can be expressed as

$$S_{nwe} = \frac{S_{nw} - S_{nwr}}{1 - S_{nwr} - S_{wr}} \quad \text{Eq 2-10}$$

In a typical water-wet porous medium, the relative permeability curves often look like the schematic shown in Figure 2-3. Notably, the curve for the non-wetting phase tends to be more pronounced in its curvature compared to that of the wetting phase. The water saturation at which both phases exhibit identical relative permeabilities is greater than 0.50. Additionally, the maximum relative permeability for the wetting phase is less than that of the non-wetting phase (Anderson, 1987).

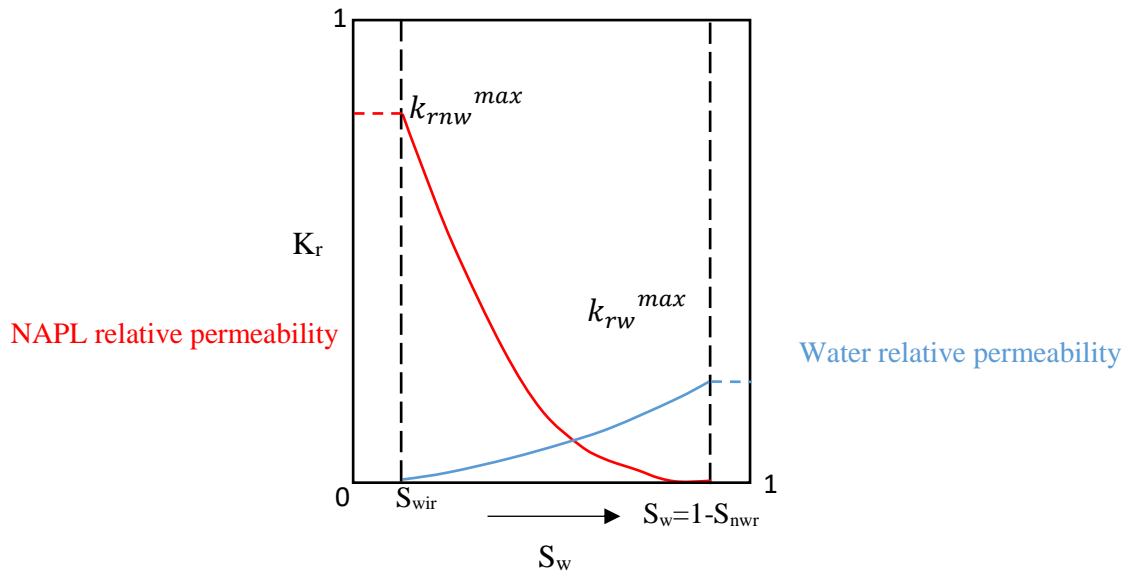


Figure 2-3 Schematic of relative permeability curves for a water-wet porous media

2.3 Fluid flow in porous media

2.3.1. Single phase flow

For one-dimensional isotropic homogenous porous medium like the 1D slab shown in Figure 2-4, mass conservation may be formulated across a control element of the slab, with one fluid of density ρ is flowing through it at a velocity u (m/s):

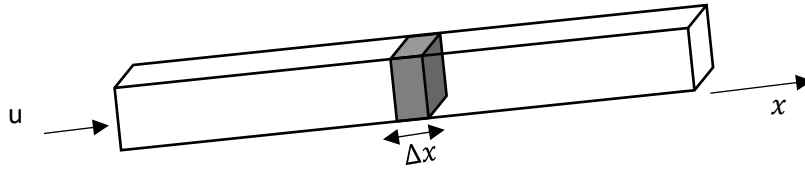


Figure 2-4 1D slab of porous medium

The mass balance for the control element is then written as:

$$\{\mathbf{u}\rho A\}_x - \{\mathbf{u}\rho A\}_{x+\Delta x} = \frac{\partial}{\partial t} \{\phi A \Delta x \rho\} \quad \text{Eq 2-11}$$

where A is the cross-sectional area (m^2). Dividing by Δx , and taking the limit as Δx goes to zero, and by considering a constant cross section, the conservation of mass or continuity equation can be written as:

$$-\frac{\partial(\rho \mathbf{u})}{\partial x} = \frac{\partial(\rho \phi)}{\partial t} \quad \text{Eq 2-12}$$

Conservation of momentum is normally simplified for low velocity flow in porous materials to be described by Darcy's equation. Thus, for incompressible single-phase flow, in a one-dimensional, horizontal system the continuity equation can be re-written as:

$$\frac{\partial}{\partial x} \left(\frac{k}{\mu} \left(\frac{\partial p}{\partial x} - \rho g \right) \right) = \frac{\partial(\phi)}{\partial t} \quad \text{Eq 2-13}$$

To solve this equation numerically, it's essential to have specific initial and boundary conditions. Dirichlet conditions are applied when there's a constant pressure boundary, while Neumann boundary conditions are used for scenarios with a constant flow rate.

2.3.2. Multiphase flow

For multiphase flow in porous media, in a similar way as for the single phase flow, the continuity equation can be written as:

$$\frac{\partial}{\partial t}(\phi \rho_i S_i) + \nabla \cdot (\rho_i \mathbf{u}_i) = 0 \text{ with } i = w, nw \quad \text{Eq 2-14}$$

where the subscripts w represents the wetting phase and nw denotes non-wetting phase.

Generalized Darcy's law for multi-phase flow in isotropic porous media is considered:

$$\mathbf{u}_i = -\frac{k k_{ri}}{\mu_i} (\nabla p_i - \rho_i \mathbf{g}) \quad \text{Eq 2-15}$$

where k_{ri} (-) is the relative permeability of phase i .

After substitution of the 1D generalized Darcy's law for each phase into the continuity equations, the following equations appear:

$$\frac{\partial}{\partial x} \left(\frac{k k_{rw}}{\mu_w} \left(\frac{\partial p_w}{\partial x} - \rho_w \mathbf{g} \right) \right) = \frac{\partial}{\partial t} (\phi S_w) \quad \text{Eq 2-16}$$

$$\frac{\partial}{\partial x} \left(\frac{k k_{rnw}}{\mu_{nw}} \left(\frac{\partial p_{nw}}{\partial x} - \rho_{nw} \mathbf{g} \right) \right) = \frac{\partial}{\partial t} (\phi S_{nw}) \quad \text{Eq 2-17}$$

To solve these partial differential equations (PDE) to find the unknown pressures and saturations, two other auxiliary equations are required which are:

$$p_c(S_w) = p_{nw} - p_w \quad \text{Eq 2-18}$$

$$S_{nw} + S_w = 1 \quad \text{Eq 2-19}$$

To solve this system of equations, various mathematical methods including finite difference and/or finite elements can be used. In the next part, a short description on the finite element method, which is used in the numerical part of this thesis, is given.

2.3.3. Finite element method

The Finite Element Method (FEM) is a powerful numerical technique utilized to approximate solutions to boundary value problems for partial differential equations (PDEs). It achieves this by dividing the entire problem domain into smaller, simpler parts called finite elements. These elements are connected at points termed nodes, and simple functions are chosen to represent the solution within each element. By employing a variational approach, the original PDE is recast into a form more amenable to approximation, termed the weak form. The solution is then sought in this weak form over the entire domain.

The weak formulation for the i-phase continuity equation is obtained by multiplying the equation by a test function v and integrating over the domain Ω :

$$\int_{\Omega} v \frac{\partial}{\partial t} (\phi \rho_i S_i) dx + \int_{\Omega} v \nabla (\rho_i \mathbf{u}_i) dx = 0 \quad \text{Eq 2-20}$$

Integration by parts (Green's theorem) is then applied to the second term, resulting in:

$$\int_{\Omega} v \frac{\partial}{\partial t} (\phi \rho_i S_i) dx + \int_{\Omega} \nabla v \cdot \rho_i \mathbf{u}_i dx - \int_{\partial\Omega} v (\rho_i \mathbf{u}_i \cdot \mathbf{n}) d\partial\Omega = 0 \quad \text{Eq 2-21}$$

Here, $\partial\Omega$ is the boundary of the domain Ω , and \mathbf{n} is the outward normal direction, which, in the 1D case, is either positive or negative unity vector, depending on the boundary orientation.

Introducing Darcy's equation into this equation, we get:

$$\int_{\Omega} v \frac{\partial}{\partial t} (\phi \rho_i S_i) dx - \int_{\Omega} \nabla v \cdot \rho_i \frac{k k_{ri}}{\mu_i} (\nabla p_i - \rho_i \mathbf{g}) dx + \int_{\partial\Omega} v \rho_i \frac{k k_{ri}}{\mu_i} ((\nabla p_i - \rho_i \mathbf{g}) \cdot \mathbf{n}) d\partial\Omega = 0 \quad \text{Eq 2-22}$$

In the context of the FEM, the choice of test function v and the approximate solution for S_i are typically based on simple polynomial functions (e.g., linear or quadratic) over each finite element. Through this methodology, the weak form is transformed into a system of algebraic equations, which can be solved using standard techniques to approximate the solution of the original PDE. For each element, a local matrix and vector are computed, representing the contributions of that element to the overall system. These local matrices/vectors are then assembled into a global system:

$$Ax = b \quad \text{Eq 2-23}$$

where A is the global stiffness matrix, and would be integrals involving the product of derivatives of the test functions, basis functions, and possibly other terms from the governing equations (two first integrals in equation 2-22), x is the vector of unknown nodal values (pressure and saturations here), and b is global load vector that encapsulates all the known loads or sources in the system (the last integral part in equation 2-22). This could be sources/sinks of phases, known values at boundaries (like injection rates/pressure).

2.4 Polymers

Polymers are high molecular weight chemical agents composed of small simple structural units or monomers. The term "polymer" indeed originates from the Greek words “πολύς” (polus), meaning “many” or “much,” and “μέρος” (meros), meaning “part”. In the context of chemistry and materials science, a polymer refers to chemical substances in the form of chains that are composed of long and repeated small units (monomers) through a process of polymerization. They can significantly increase the water viscosity by dissolving in aqueous phase even at low concentrations.

2.4.1. Polysaccharides

Polysaccharides, are naturally occurring polymers that are produced by microorganisms, plants, and animals (Nsengiyumva and Alexandridis, 2022). The most notable polysaccharides are xanthan gum (Nsengiyumva and Alexandridis, 2022), guar gum (Thombare et al., 2016), and cellulose (Alexandridis et al., 2018). The main chains of polysaccharides are comprised of diverse monosaccharide residues (i.e., glucose, mannose, and galactose) with various functional groups (e.g., hydroxyl, amide, carboxyl, acetyl, and pyruvate), that are connected through glycosidic linkages (Fittolani et al., 2020). Polysaccharides are commonly used for modifying the rheological properties of fluids tailored for petroleum applications, and aquifer remediation (Alamooti et al., 2023, 2022; Keykhosravi et al., 2021; Martel et al., 1998, 2004; Omirbekov et al., 2023).

Generally, biopolymer polysaccharides can exhibit either a double helix conformation (as seen in xanthan) or a triple helix conformation (found in scleroglucan and schizophyllan), depending on their arrangement when dissolved in a solution. This helical structure influences their rigidity, which, in turn, affects their ability to thicken solutions (viscosifying power), their resistance to cations (both mono and divalent) and their tolerance to elevated salinity and temperature while experiencing minimal mechanical degradation effects (Gbadamosi et al., 2022; Olajire, 2014).

2.4.1.1. Xanthan

This is one of the most common polysaccharides, known for its 'green' polymer nature resulting from microbial activity. Xanthan gum is a non-toxic and biodegradable polymer that is commercially synthesized through the activity of the *Xanthomonas campestris* bacterium, a microbial organism. This process involves the interaction of the bacterium with carbohydrate substrates (glucose or fructose), along with a protein supplement and an inorganic nitrogen source, known as fermentation (Barrere et al., 1986). The chemical structure of xanthan gum is

depicted in Figure 2-5, featuring a single glucuronic acid unit, two mannose units, and two glucose units in a molar ratio of 2.0, 2.0, and 2.8, respectively (García-Ochoa et al., 2000). The thickening ability of xanthan gum relies primarily on its high molecular weight (ranging from 2 to 50×10^6 g/mol) and the rigidity of its polymer chains (Muhammed et al., 2020). Beyond its applications in EOR (Enhanced Oil Recovery) and groundwater remediation, xanthan gum has applications in the food and cosmetic industries due to its effective gelling properties and non-toxic nature (Challen, 1994; Jamshidian et al., 2014; Mortensen et al., 2017; Singhvi et al., 2019). Xanthan as a long-chain polysaccharide contains negatively charged chemical groups, such as acetyl and pyruvate group (Carrington et al., 1996).

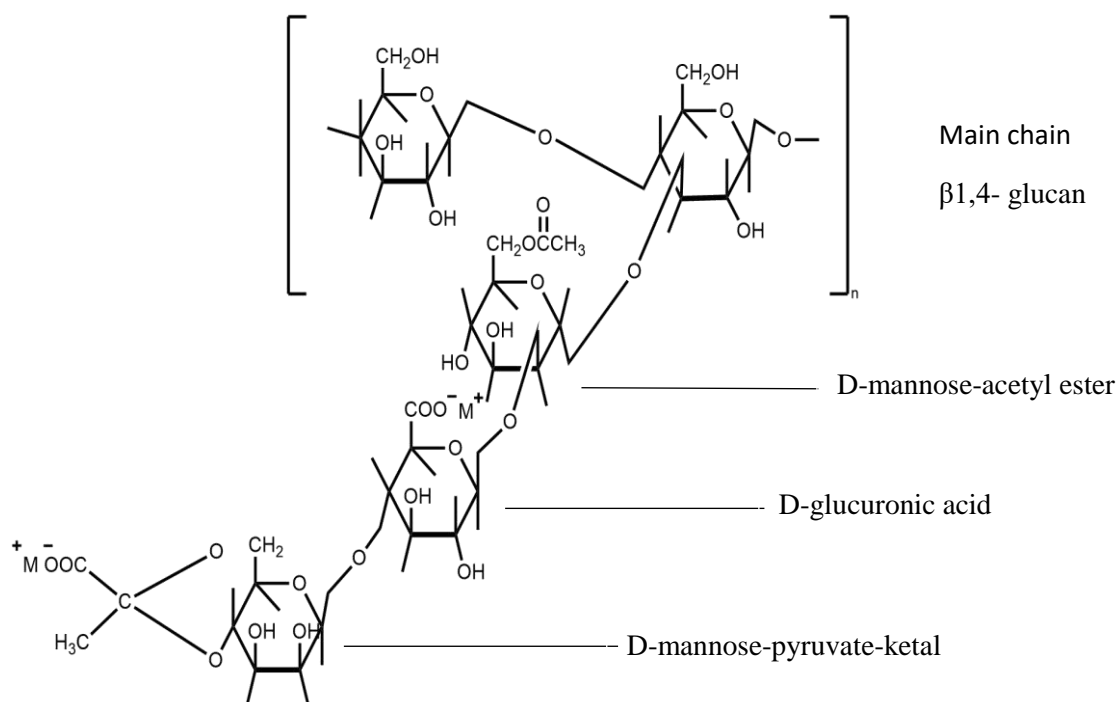


Figure 2-5 chemical structure of xanthan gum (García-Ochoa et al., 2000)

2.4.2. Polymer Conformation and Entanglement

Polymer conformation refers to the spatial arrangement and shape that a single polymer chain adopts in a given environment or under specific conditions. It describes how the chain folds, twists, and occupies three-dimensional space. The conformation is influenced by factors such

as chemical structure, intermolecular interactions, temperature, solvent conditions, and chain length. Different conformations, like random coils, globules, extended chains, helices, etc., are possible based on the combination of these factors. Polymer conformation is essentially about the shape of an individual polymer chain (Holzwarth, 1976).

For an ionic polymer like xanthan which is widely used in this study, it has been shown to exhibit two different conformational states: an ordered, helical conformation and a disordered conformation that can be described as a broken or imperfect helix (Bezemer et al., 1993; Holzwarth, 1976; Jansson et al., 1975). The conformation assumed by the xanthan molecules is highly dependent on the ionic content of the solvent. In salt-free solution, the xanthan backbone is disordered and highly extended due to electrostatic repulsions between charges on the side chains. In this state, the chains are relatively stiff, but retain some degree of flexibility (Wyatt and Liberatore, 2009).

Entanglement in a polymer solution occurs when the long chains of polymers, despite being dissolved individually in a liquid, become intertwined with one another due to their flexible nature. This can lead to a network-like structure within the solution, affecting its viscosity and other properties.

2.5 Polymer transport in porous media

2.5.1. Retention

Polymer retention in porous media can happen by main mechanisms of mechanical entrapment, hydrodynamic retention, polymer bridging, and adsorption (Dominguez and Willhite, 1977). Figure 2-6 schematically shows these main mechanisms from pore-scale point of view.

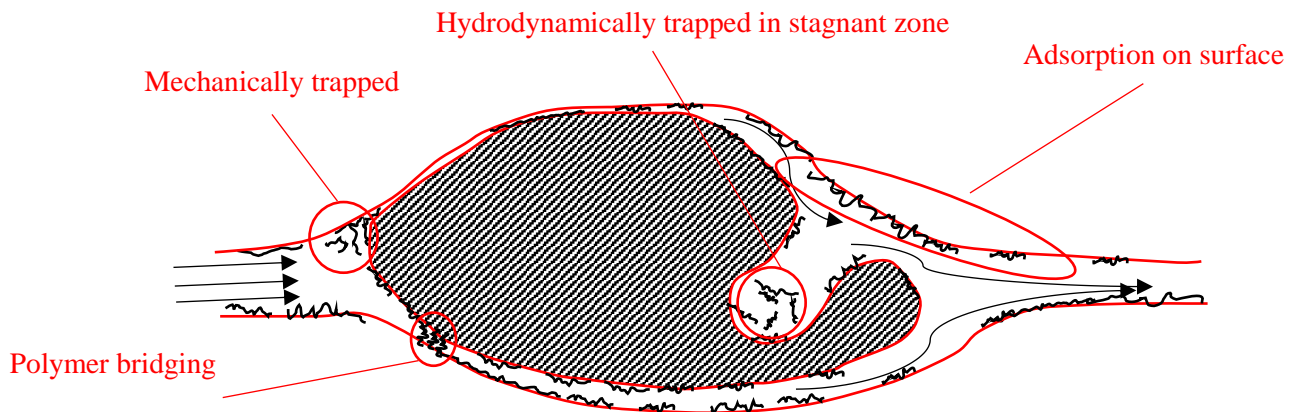


Figure 2-6 Schematic of different mechanisms of polymer retention mechanisms in porous media

2.5.1.1. Mechanical entrapment

Retention through entrapment takes place when larger polymer molecules get caught in constricted flow channels (Farajzadeh et al., 2016). These entrapments result in blockages, subsequently reducing the flow in these sections, which likely causes further entrapment of molecules upstream of these blockages. In larger pores, the likelihood of mechanical entrapment decreases, which can often be observed when polymers flow through highly permeable soils (Cohen and Christ, 1986a; Zitha et al., 1998).

2.5.1.2. Hydrodynamic retention

Some polymer molecules are believed to be trapped in stagnant regions like the dead-end shown in Figure 2-6 due to hydrodynamic drag forces. In these areas, the local polymer concentration might surpass that of the introduced fluid. Once steady-state conditions achieved during the retention test, the flow halts, and these molecules could diffuse into the primary flow paths. Upon flow resumption, a peak in polymer concentration can be observed (Chauveteau and Kohler, 1974; Dominguez and Willhite, 1977).

2.5.1.3. Polymer bridging

Some polymers can adsorb onto multiple sites simultaneously, forming a "bridge" between different surfaces or particles. This mechanism can be especially relevant in porous media when a stretched chain passes through a pore restriction the chain can be adsorbed on the sides of pore walls, thus forming bridges over pore restrictions. This mechanism is seen in very low permeable porous media (Denys et al., 2001; Zitha et al., 2001; Zitha and Botermans, 1998).

2.5.1.4. Adsorption

Surface adsorption is a process in which molecules of species existing in a fluid phase (e.g., gaseous or liquid phase) stick to solid surfaces. Following the selective transfer of species toward the adsorbent surface, which is mainly based on the nature of the bonds created between the adsorbed species and the functional groups of adsorbent surface, the adsorption phenomenon is classified as physical, chemical, and electrostatic adsorption (Pourhakkak et al., 2021). In physical adsorption, binding and accumulation of target species occur via attraction forces such as Van der Waals forces. Another type of adsorption in this category can be hydrophobic interactions. If the porous medium has hydrophobic regions (having organic content) and the species contain hydrophobic segments, these segments may preferentially adsorb onto hydrophobic sites to minimize their contact with the aqueous phase (Ishiguro and Koopal, 2016).

Chemical adsorption, is characterized by the formation of a chemical bond between the adsorbate and the adsorbent. Within this category, several types of bonding such as ionic, covalent and hydrogen bonding can occur (Králik, 2014). Electrostatic adsorption refers to the attraction between charged surfaces (like adsorbents) and ions in a solution. This is more of a surface phenomenon, and it doesn't lead to the formation of new compounds. If the porous medium has charged sites (due to ionizable groups or a net surface charge), and the species carry an opposite charge, there can be an electrostatic attraction between the species and the

surface (Letey, 1994; Malik and Letey, 1991). Figure 2-7 provides a schematic representation of various adsorption mechanisms of species on the solid/pore wall surface which is mainly at molecular scale.

For the polymers commonly used for soil remediation like the polysaccharides the main mechanisms of adsorption are the electrostatic interaction between the ionic parts of the polymers and the charged surface of the soil, and also the hydrophobic interactions with soils containing some organic contents (Cheraghian et al., 2014; Chiappa et al., 1999; Cohen and Christ, 1986b).

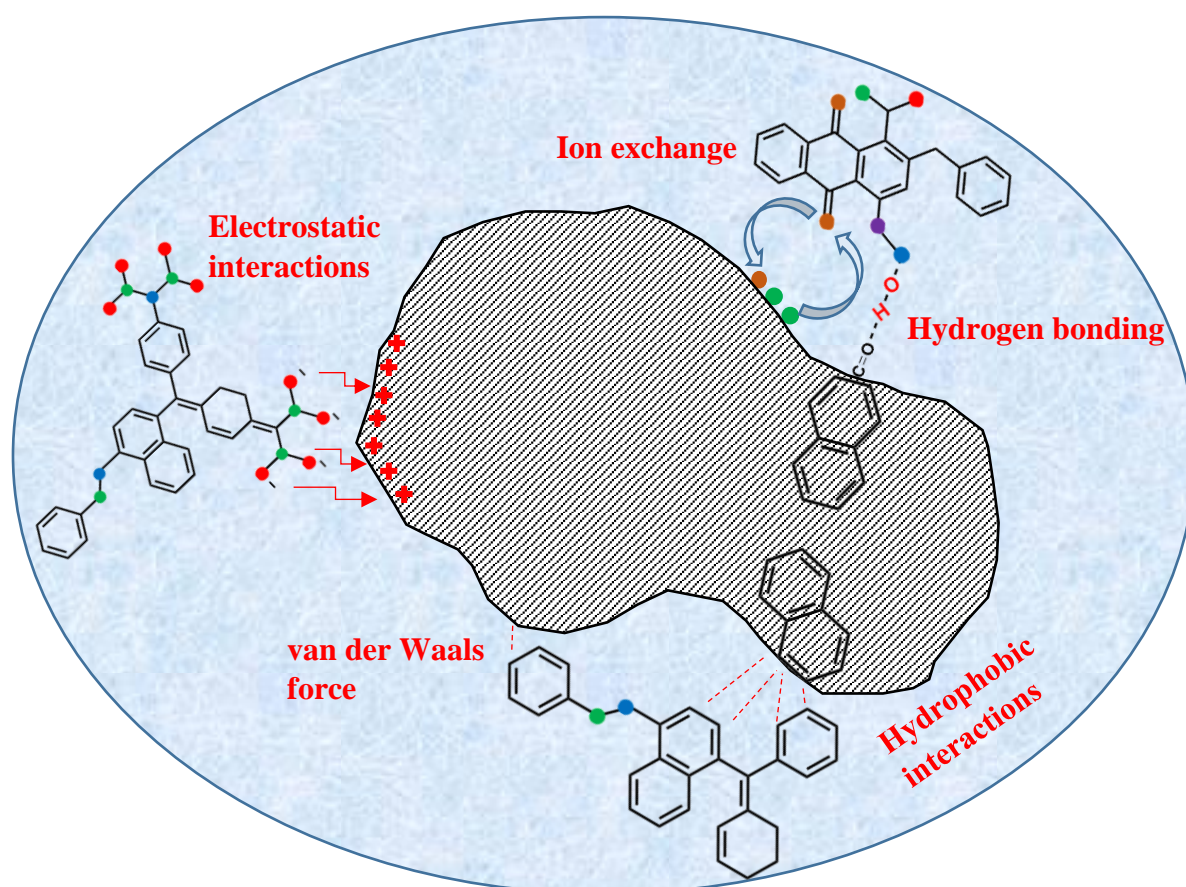


Figure 2-7 Schematic of adsorption of species in liquid phase (blue color) onto the solid surface (dashed gray grain in the middle)

2.5.1.5. Adsorption measurement

Polymer adsorption at the laboratory scale can be evaluated using both static and dynamic methods (Huang and Sorbie, 1992a). For static conditions, bulk adsorption measurements involve soaking soil particles (or crushed rock for core plugs) in a polymer solution. The adsorption is determined by observing the difference in the polymer concentration before and after the solution interacts with the particles. To study adsorption kinetics, the polymer solution is mixed with soil particles for varied time intervals in the batch experiments. By doing so, changes in adsorption levels can be chronologically quantified. This process continues until the polymer solution reaches equilibrium concentration. To assess the polymer concentration, several experimental techniques can be employed, including rheological analysis, spectrophotometric measurements of turbidity, gravimetric analysis, chromatography, and total organic carbon measurements (Dang et al., 2014).

To study adsorption in dynamic flow conditions which is more representative of real cases in subsurface soil, column experiments can be performed providing insights into breakthrough curves and system dynamics. The other mechanisms of retention (mechanical entrapment, hydrodynamic retention, polymer bridging, etc.) can only be seen during the dynamic test. Typically, a solution containing the target species, in this case, a polymer, is injected at a fixed rate into a water-saturated column. Subsequent samples are obtained from the column's effluent. To evaluate the adsorption of the species considered, a tracer a conservative (non reactive, non adsorbed, non biodegradable) tracer is simultaneously injected. The material balance calculation for the effluent concentration profiles is performed in order to determine the adsorption level. The level of adsorption can be determined by plotting the normalized concentrations of the polymer and the tracer in the effluents and analyzing the difference in their breakthrough curves. Figure 2-8 shows a schematic for breakthrough curves of the tracer and the polymer.

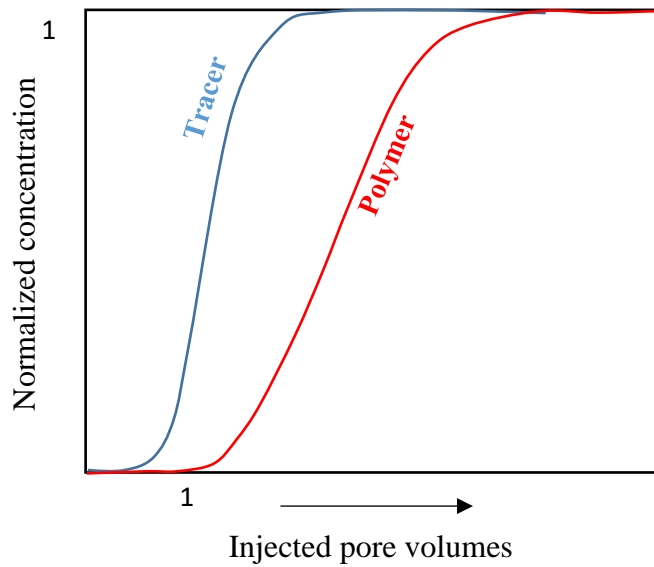


Figure 2-8 Polymer and tracer breakthrough curves in a column test

2.5.1.6. Adsorption kinetic and isotherm models

To describe the rate at which molecules (polymer) in a fluid phase come into contact with and are captured on a solid surface adsorption kinetic models are used. Numerous adsorption kinetic models have been developed to elucidate the adsorption kinetic process. These include the pseudo-first-order (PFO) model (Lagergren, 1898), the pseudo-second-order (PSO) model (Ho Wase DAJ & CF Forster CF, 1996), Ritchie's equation (Ritchie, 1977), and the Elovich model (Elovich and Larinov, 1962). Among the adsorption kinetic models, majority of studies over the last two decades used the classical PFO and PSO rate laws to model their kinetic datasets (Revellame et al., 2020). The PFO model can be described as follows:

$$\ln(q_e - q_t) = \ln q_e - k_1 t \quad \text{Eq 2-24}$$

where q_e and q_t are the amounts of adsorbate adsorbed per unit mass of adsorbent (mg/g) at equilibrium and at any time t (s), respectively, and k_1 (1/s) is the rate constant of the first-order adsorption. This equation is frequently used to fit the kinetics data and to calculate the parameters q_e and k_1 , by plotting $\ln(q_e - q_t)$ versus time.

The PSO model can be expressed as:

$$\frac{t}{q_t} = \frac{1}{k_2 q_e^2} + \frac{t}{q_e} \quad \text{Eq 2-25}$$

where k_2 ($\text{g}\cdot\text{mg}^{-1}\cdot\text{s}^{-1}$) is the rate constant of the pseudo-second order adsorption. The PFO model is best for low initial adsorbate concentrations and early adsorption stages, while the PSO model suits higher concentrations and later stages (Wang and Guo, 2020).

Adsorption isotherms describe how the amount of adsorbate that gets adsorbed on a surface changes with its concentration in the fluid phase at constant temperature. These models provide insights into how adsorbents interact with adsorbates and the adsorption capacities of materials under various conditions. Langmuir, Linear, or Freundlich adsorption isotherm models are the most prevalent models used to represent the equilibrium distribution of surfactants and polymers between the aqueous and solid Phases (Mohammadnejad et al., 2020).

The Langmuir model assumes monolayer adsorption on a homogeneous surface. The mathematical expression is:

$$\frac{q_e}{q_m} = \frac{k_L C_e}{1 + k_L C_e} \quad \text{Eq 2-26}$$

where q_e is the amount of adsorbate adsorbed per unit mass of adsorbent at equilibrium mg/g, C_e (mg/L) is the equilibrium concentration of the adsorbate, q_m is the maximum adsorption capacity mg/g, and k_L (L/mg) is the Langmuir constant which is related to the affinity of binding sites.

2.5.2. Diffusion

Diffusion in porous media refers to the process by which solute molecules move due to a concentration gradient within a porous medium, such as rock or soil. Molecular diffusion is driven by concentration gradient and is described by the Fick's First Law:

$$J_{diff} = -D_0 \nabla c \quad \text{Eq 2-27}$$

where J_{diff} is the diffusive mass flux per unit area (kg/m²/s), c is the concentration of the polymer (kg/m³) and D_0 is the molecular diffusion coefficient (m²/s).

The movement happens within the pore spaces (interstitial spaces) of the medium. Diffusion in porous media is more complex than in free solutions because of factors like pore size distribution, tortuosity (complex path) of the pore channels, and interactions between solute molecules and the solid matrix. When diffusion occurs in porous media, not all the volume is available for solute transport; but only the pore spaces. Then the diffusive transport in porous media can be described by Fick's second law of diffusion, modified to account for the properties of the porous medium (Dullien, 2012; Kantzas et al., 2012):

$$\frac{\partial c}{\partial t} = D_{eff} \nabla^2 c \quad \text{Eq 2-28}$$

where D_{eff} is the effective diffusion coefficient (m²/s) in porous media. Diffusion in porous media differs from diffusion in homogeneous aqueous solutions. Diffusion in porous media occurs through tortuous and irregularly shaped pores, and is therefore slower than that in homogeneous solutions. The effective diffusion coefficient describes diffusion in porous media and can be estimated as:

$$D_{eff} = \frac{D_0}{\tau} \quad \text{Eq 2-29}$$

D_0 is the molecular diffusion coefficient (m²/s), τ is the tortuosity factor accounting for the longer and more twisted pathways solute molecules must navigate in porous media compared to free diffusion.

2.5.3. Dispersion

Mechanical dispersion in porous media refers to the spread of solute caused by variations in the flow velocity within the porous medium. This phenomenon occurs because fluid particles follow different paths through the pore spaces, leading to a range of velocities. The net effect is that solute particles spread out, or disperse, in the direction of flow and perpendicular to it (Bear, 2013; Kantzas et al., 2012). In a one dimensional porous medium the mechanical dispersion can be expressed as:

$$D_m = \alpha u \quad \text{Eq 2-30}$$

where α is dispersivity (m) a property of the porous medium and the fluid, and u is the average velocity (Darcy velocity) of the fluid. The hydrodynamic dispersion is a combination of two primary processes of convective mixing caused by variations in the pore velocities (mechanical dispersion) and molecular diffusion can be expressed as:

$$D = D_{eff} + \alpha u \quad \text{Eq 2-31}$$

For two-dimensional systems, the dispersion tensor can be expressed as (Bear, 2013):

$$\mathbf{D} = (\alpha_T |\mathbf{u}| + D_{eff})\mathbf{I} + (\alpha_L - \alpha_T) \frac{u_x u_y}{|\mathbf{U}|} \quad \text{Eq 2-32}$$

where \mathbf{I} is the identity matrix, u_x and u_y are the longitudinal and transverse components of velocity respectively α_L and α_T are the longitudinal and transverse dispersivities (m), respectively. According to Fick's first law the dispersive flux can be represented as:

$$J_{disp} = -\mathbf{D} \cdot \nabla c \quad \text{Eq 2-33}$$

2.5.4. Advection

Advection is the transport process where solutes flow with the bulk fluid phase. In porous media such as aquifers, this fluid is typically water that flows through the pore spaces of the medium. The solute is carried along by this moving fluid. The terms 'advection' and 'convection' are sometimes used interchangeably. However, more precisely, convection refers to the movement

of fluid, often driven by density differences arising from temperature gradients, while advection describes the transport of substances by the flow of the fluid itself. Mathematically, the advective flux for solute concentration c can be given by (Bear, 2013):

$$J_{adv} = \mathbf{u} \cdot c \quad \text{Eq 2-34}$$

where \mathbf{u} is the velocity vector (m/s).

2.5.5. Advection dispersion reaction

The Advection-Dispersion-Reaction (ADR) equation describes the transport and fate of a solute in a flowing fluid medium, like groundwater. By combining the transport processes outlined above, the expression for the mass conservation of a reactive solute can be expressed as follows:

$$\frac{\partial(\phi S_w c)}{\partial t} + \frac{\rho_B \partial q}{\partial t} = -\nabla \cdot (J_{adv} + J_{disp}) \quad \text{Eq 2-35}$$

where q is the adsorbed mass on the solid surface (g/g), and ρ_B is the density of bulk solid. By substituting the expressions of the advective and dispersive fluxes into this equation, it can be expressed as (Bear, 2013):

$$\frac{\partial(\phi S_w c)}{\partial t} + \frac{\rho_B \partial q}{\partial t} - \nabla \cdot (\phi S_w \mathbf{D} \cdot \nabla c) + \mathbf{u}_w \cdot \nabla c = 0 \quad \text{Eq 2-36}$$

For a homogeneous one-dimensional saturated porous media and non-reactive solute the ADR equation can be analytically solved through (Ogata and Banks, 1961):

$$c = \frac{c_0}{2} \left[\operatorname{erfc} \left(\frac{x - ut}{2\sqrt{Dt}} \right) + \exp \left(\frac{ux}{D} \right) \operatorname{erfc} \left(\frac{x + ut}{2\sqrt{Dt}} \right) \right] \quad \text{Eq 2-37}$$

where c_0 (kg/m³) is the concentration of injected solute in the inlet, x (m) is the length of the column, and erfc is the complementary error function for a variable z defined as:

$$erfc(z) = 1 - \frac{2}{\sqrt{\pi}} \int_0^z e^{-t^2} dt \quad \text{Eq 2-38}$$

For advection dominated regimes, where $\frac{ux}{D} \gg 1$, the second term in analytical solution of ADR equation (2-37) can be neglected and it can be reduced to:

$$c = \frac{c_0}{2} \left[erfc \left(\frac{x - ut}{2\sqrt{Dt}} \right) \right] \quad \text{Eq 2-39}$$

2.6 Rheology

Rheology is the study of how materials flow and deform under applied forces, and it plays a significant role in understanding the behavior of polymer solutions. In the context of polymer solutions, rheology helps us understand how the polymers interact with the solvent and how their properties change under different conditions.

2.6.1. Viscosity

Viscosity is one of the key rheological concepts. It is a fundamental property of fluids that quantifies their resistance to flow. It measures how easily a fluid can be deformed by an applied shear stress. Mathematically, dynamic viscosity can be defined in terms of shear stress and shear rate using the following relationship (Barnes et al., 1989):

$$\tau_f = \mu \frac{du}{dy} \quad \text{Eq 2-40}$$

where τ_f is the shear stress. This expression is referred to as Newton's law of viscosity. In fluid dynamics, kinematic viscosity, occasionally referred to as momentum diffusivity, is defined as the ratio of dynamic viscosity (μ) to the fluid's density (ρ).

Figure 2-9 illustrates the Couette flow to demonstrate the concept of viscosity.

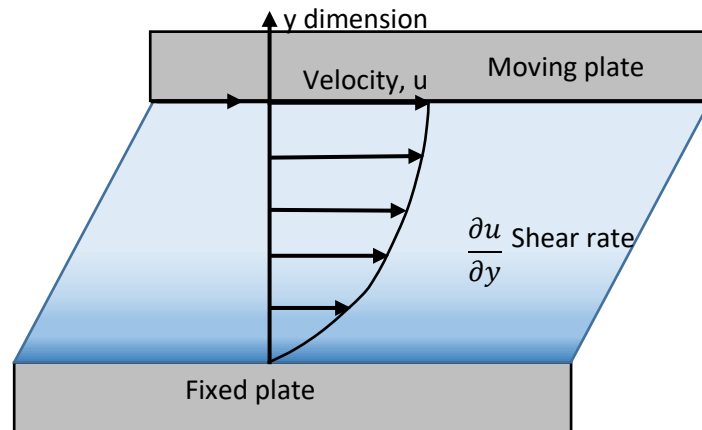


Figure 2-9 Schematic of Couette parallel flow

2.6.2. Non-Newtonian fluids

Non-Newtonian fluids are types of fluids that do not follow the simple linear relationship between shear stress and shear rate that is characteristic of Newtonian fluids. In Newtonian fluids, such as water and many common liquids, the shear stress is directly proportional to the shear rate, and the viscosity remains constant regardless of the applied shear rate. However, non-Newtonian fluids exhibit more a complex and variable behavior, where the viscosity can change with shear rate, time, or other factors (Böhme, 2012). Polymers, foams, and melts are some of the non-Newtonian examples having different characteristics. Characteristics of non-Newtonian fluids can often be categorized into viscoelasticity, time-dependent viscosity, shear-thinning, and shear-thickening behaviors (Chhabra, 2010).

2.6.2.1. Viscoelasticity

Viscoelastic behavior is a combination of both viscous and elastic behaviors. Viscoelastic fluids exhibit time-dependent responses to applied forces. When a force is applied, these fluids can deform and flow like a viscous fluid, but they can also return to their original shape like an elastic solid when the force is removed. Viscoelasticity is commonly observed in polymer solutions, gels, and complex fluids. Elasticity often arises from the stretching of bonds within

ordered crystalline structures. When the stress is removed, these bonds can quickly return to their original configuration. Viscosity, on the other hand, emerges from the movement or diffusion of atoms or molecules within amorphous (non-crystalline) materials (Meyers and Chawla, 2008).

2.6.2.2. Time-dependent viscosity

Some non-Newtonian fluids show changes in viscosity over time when subjected to a constant shear stress. Thixotropic and rheopectic behaviors fall under this category. Thixotropic fluids become less viscous over time under constant shear stress (Mewis and Wagner, 2009), while rheopectic fluids become more viscous over time under the same conditions (O'Neill and Stachowiak, 1996). These time-dependent changes in viscosity are often associated with structural rearrangements within the fluid. The polymer solutions used in this work (xanthan and Carboxymethylcellulose) don't show significant changes in their rheological properties by time.

2.6.2.3. Shear-rate dependent viscosity

Shear-thinning fluids exhibit a decrease in viscosity as the shear rate increases, while shear-thickening fluids show an increase in viscosity with increasing shear rate. These behaviors are often related to the interaction between particles or molecules within the fluid. Shear-thinning is also known as pseudoplastic behavior, and shear-thickening is referred to as dilatant behavior (Barnes et al., 1989). Figure 2-10 demonstrates the Classification of fluids with shear stress as a function shear rate.

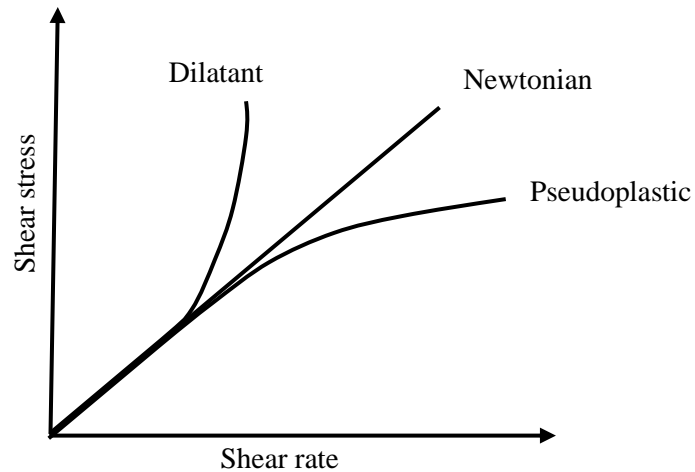


Figure 2-10 Classification of fluids with shear stress as a function shear rate

2.6.2.4. Shear-thinning fluids

Polymers play a crucial role in diverse applications within petroleum engineering and groundwater remediation, often characterized by their shear-thinning behavior (Skauge et al., 2018). These applications benefit from polymers' ability to reduce viscosity under shear stress, enabling efficient injection and flow, while recovering stability and viscosity when shear forces diminish (AlSofi and Blunt, 2010). This occurrence is due to polymer molecules arranging themselves within the shear rate field where internal friction is reduced (Böhme, 2012). In these contexts, polymers are broadly categorized into synthetic and biopolymers (Olajire, 2014). Synthetic polymers are commonly classified into polyacrylamide (PAM), hydrolyzed polyacrylamide (HPAM), and hydrophobically associating polyacrylamide (HAPAM) are designed to exhibit controlled shear-thinning, making them ideal candidates for enhanced oil recovery in petroleum engineering (Gbadamosi et al., 2022). Meanwhile, biopolymers derived from natural sources, including xanthan gum and cellulose derivatives, contribute to environmentally friendly groundwater remediation techniques (Martel et al., 1998, 2004). These polymers can possess neutral or ionic properties, and their interaction with additives like surfactants, salts, suspended particles, and alternative solvents further shapes their behavior

(Carrington et al., 1996; Krstonošić et al., 2019; Nsengiyumva and Alexandridis, 2022; Wyatt and Liberatore, 2009). Figure 2-11 depicts the relationship between viscosity and shear rate for a shear-thinning fluid. The graph demonstrates three distinct regions: lower and upper Newtonian regions at very low and high shear rates, respectively, along with a shear-thinning region in the intermediate shear rate range (Boger, 1977).

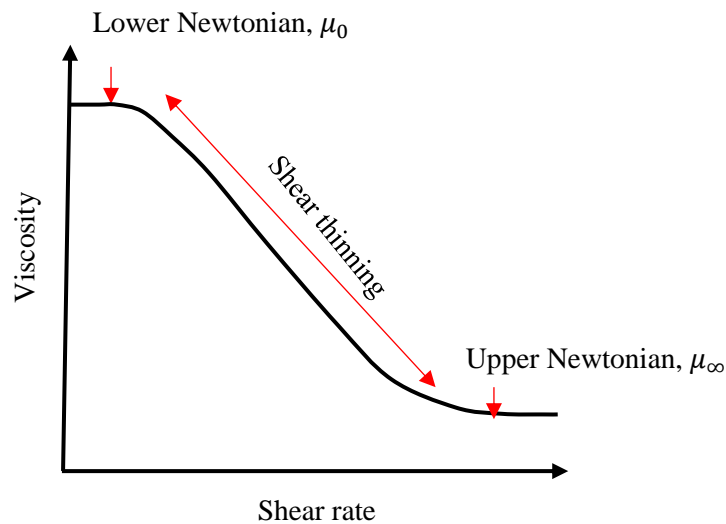


Figure 2-11 Rheological behavior of a shear-thinning fluid

2.6.2.5. Non-Newtonian fluid models

There are several models used to describe non-Newtonian behavior in polymers and other complex fluids. These models aim to capture the relationship between shear stress and shear rate for materials that don't obey the simple linear relationship of Newtonian fluids. Among the renowned models are the Power Law Model (also known as the Ostwald–de Waele Model), Carreau Model (Carreau, 1972), Bingham Plastic Model (Bingham, 1917), Casson Model (Casson, 1959), Herschel-Bulkley Model (Herschel and Bulkley, 1926), and Cross Model (Cross, 1965). There is no single universally accepted model that is describing all the various bulk rheological behaviors (Owens and Phillips, 2002).

Power-law and Carreau models are one of the most suitable models for describing the polymers used in aquifer remediation such as xanthan and cellulose (Benchabane and Bekkour, 2008; Rochefort and Middleman, 2000). The relationship between viscosity and shear rate for power-law model is given by:

$$\mu = \kappa \dot{\gamma}^{n-1} \quad \text{Eq 2-41}$$

where κ is the flow consistency index ($Pa \cdot s^n$), $\dot{\gamma}$ is the shear rate (s^{-1}) and n is the flow behavior index. The values of n less than 1 correspond to a shear-thinning behavior while the values of n more than unity are for shear thickening fluids.

The rheological behavior of non-Newtonian fluids can be described through the Carreau fluid model (Carreau, 1972) expressed as:

$$\mu = \mu_{inf} + (\mu_0 - \mu_{inf}) \left(1 + (\chi \dot{\gamma})^2\right)^{\frac{l-1}{2}} \quad \text{Eq 2-42}$$

where, the viscosities (Pa.s) at zero and infinite shear rate are denoted as μ_0 and μ_{inf} , χ is the relaxation time (s), and l (-) is the power index.

2.6.3. Rheological behavior of xanthan

As it has been aforementioned xanthan as a biopolymer has a variety of application, including aquifer remediation. The performance of the injection of xanthan solutions alone or in combination with other chemical compounds in the recovery of pollutants in contaminated soils has been studied. Several authors have studied the rheological behavior of xanthan gum in the absence or presence of other additives (Bobade et al., 2018; Huang and Sorbie, 1992b; Krstonošić et al., 2019; Zhong et al., 2013). Zhong et al. (2013) characterized the shear thinning behavior of xanthan at various concentrations and observed a linear increase in the viscosity of xanthan solutions as the concentration increased.

The increase of ionic strength through the addition of salts leads to a significant reduction in the intrinsic viscosity of xanthan (Higiro et al., 2007; Zhong et al., 2013). This phenomenon is attributed to the inherent nature of xanthan. In aqueous solutions devoid of introduced ions, the xanthan molecule extends due to the electrostatic repulsion originating from negatively charged acetyl groups (Carrington et al., 1996). The introduction of salt causes the side chains to collapse into the backbone due to charge screening, resulting in a rod-like configuration of the xanthan molecule and a consequent decrease in its hydrodynamic volume (Rocheftort and Middleman, 2000). Due to molecular crosslinking between xanthan and calcium ions, divalent ions like calcium show a more noticeable effect on viscosity reduction compared to monovalent ions. Zhong et al. (2008) observed that above a critical concentration (2 g/L), addition of salt can result in increase in viscosity of the solution. This phenomenon can be ascribed to the pronounced interaction among intermolecular bonds. In such cases, the effect of these interactions on solution viscosity outweighs the influence arising from changes in the hydrodynamic volume of molecules (Dintzis et al., 1970).

Xanthan can be mixed with surfactants for remediation purposes due to their strong abilities in interfacial tension reduction, and dissolution of the pollutants. Understanding the interaction between xanthan and surfactant is necessary. Taylor et al. (2007) attributed the association between similarly charged polymer and surfactant species to strong hydrophobic interactions. Krstonošić et al. (2019) using various chemical techniques investigated the interaction between xanthan and the anionic surfactant SDS and found evidence of both electrostatic and hydrophobic interactions. The dissolution of polymers in water alters the rheological and flow behavior of the aqueous phase.

Krstonošić et al. (2019) investigated the rheological behavior of binary mixtures of xanthan and anionic SDS for various concentrations. They observed that at low SDS concentrations and a fixed xanthan concentration, increasing the surfactant concentration decreased the viscosity to

a minimum value, but higher surfactant concentrations led to higher viscosities. Introducing remedial agents such as phosphate, sodium lactate, and ethyl lactate can diminish the dynamic viscosity of xanthan solutions, while retaining its shear-thinning properties. Adding mono- and divalent salts like Na^+ and Ca^{2+} to enhance the ionic strength of the solution also decreases the dynamic viscosity and the degree of shear thinning in xanthan (Zhong et al., 2013).

The viscosity of xanthan gum decreases when the dissolution temperature rises up to 40°C. However, from 40°C to 60°C, the viscosity goes up as the temperature does. Beyond 60°C, the viscosity drops with rising temperature. This behavior is associated with conformational changes of the xanthan molecule. The conformation shifts from an ordered (low-dissolution temperature) to a disordered (high-dissolution temperature) state (Casas et al., 2000; Sharma et al., 2014).

2.6.4. Rheological behavior of polymer solutions in porous media

Polymer solution rheology in bulk is extensively studied, revealing complex behaviors like shear thinning. However, within porous media, polymer solutions exhibit even more complex behaviors than in viscometers. The complex nature of porous media significantly impacts the local and overall behavior of non-Newtonian fluids. For instance, as polymer solutions flow through pores, they go through contraction-expansion channels that accelerate and decelerate polymer molecules. When flow conditions or pore lengths prevent sufficient relaxation between successive deformations, polymer molecules may exhibit different rheological behaviors (Skauge et al., 2018; Zamani et al., 2015).

The shear rate within porous media at the Darcy scale can be described using the Darcy velocity as (Darby et al., 2017):

$$\dot{\gamma} = \sqrt{\frac{2}{\phi k}} \alpha u \quad \text{Eq 2-43}$$

where, the empirical shifting parameter, α (-), is related to both the tortuosity of the porous medium and the fluid's bulk rheology (Chauveteau and Zaitoun, 1981). Figure 2-12 illustrates the apparent viscosity in porous media alongside bulk viscosity. The horizontal shift is attributed to a conversion factor between in-situ shear rate and Darcy velocity, shown as α .

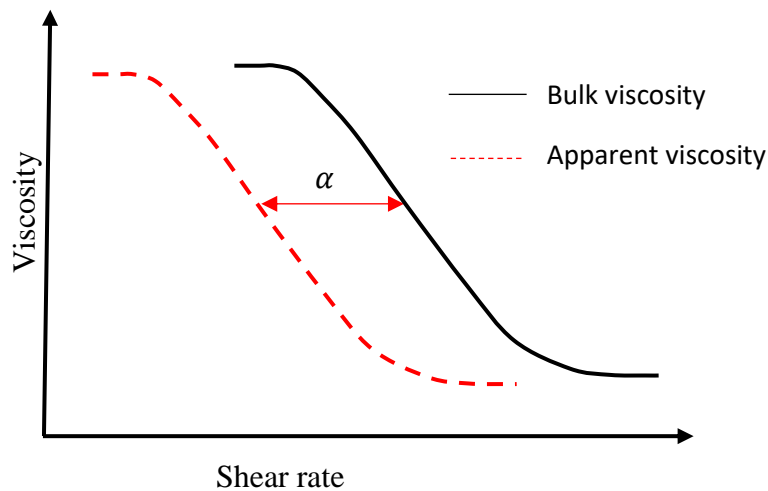


Figure 2-12 Schematic comparison of in-situ and bulk rheology

Chhabra et al. (2001) conducted a comprehensive examination of the extensive literature concerning fluid flow with intricate rheology through unconsolidated packed beds. Similarly, Sochi (2010) undertook an analysis of existing models used to describe non-Newtonian single-phase flow within porous media. Considering no change in rheological behavior in porous media, the shift parameter can be determined, by fitting the Carreau fluid model to the apparent viscosity data. Actually, the apparent shear rate is plotted against the normalized Darcy velocity $\frac{u}{\sqrt{\phi k}}$ and a linear curve passing through the origin is fitted to the data. The slope of this curve is considered to be the shift parameter (Zamani et al., 2015).

Although, α is mostly assumed to be constant and independent of flow rate (Omirbekov et al., 2020b), recently Rodriguez de Castro (2019) showed empirically, in glass-bead packings, the dependence of α on flow rates where $\alpha > 1$ at slow flow rates and $\alpha < 1$ for high flow rates with a constant value at very high velocities. He introduced a methodology involving a differential equation incorporating parameters of porous media like porosity and permeability, alongside parameters of the Herschel-Bulkley fluid model, to determine α . It's important to note that this method is most suitable for homogeneously sized packs of glass spheres.

2.7 Polymer for polluted aquifer remediation

Polymers are high molecular weight chemical agents that can significantly increase the water viscosity by dissolving in aqueous phase even at low concentrations. They have been broadly employed as a promising enhanced-oil-recovery (EOR) method in petroleum industry and an effective technique in soil/groundwater remediation (Alamooti and Malekabadi, 2018; AlSofi and Blunt, 2010; Giese and Powers, 2002). This emerging method is of great interest as they can improve the oil/pollutant recovery, stabilize the displacing front, and reduce the channeling in heterogeneous media (Browne et al., 2020; Sorbie, 2013).

During the last decades, the performance of the injection of the polymer solutions alone and in combination with other chemicals in the recovery of the pollutant in contaminated soil has been studied (Alamooti et al., 2022; Chokeyaroenrat et al., 2014; Giese and Powers, 2002; Robert et al., 2006). Longino and Kueper (1999) evaluated the performance of polymer solution injection on perchloroethylene (PCE) removal from a rough-walled fracture. They found that polymer flood could result in 84% of the recovery factor of the water flood just by injecting 381 pore volumes (PV) of polymer solution in comparison to over 1000 PV of water injection. Wu (2000) using the UTCHEM model, simulated the injection of a polymer solution into the creosote contaminated sandy aquifer. They showed that the volume of DNAPL recovered by polymer

injection was eight times more than water injection after 180 days. Giese and Powers (2002) evaluated the performance of polymer injection on DNAPL recovery in both water and oil wet systems in one dimensional (1D) systems. Their results showed that in an oil wet system the polymer injection could reduce the DNAPL residual saturation to 19% in comparison to 40% for water injection. Chokejaroenrat et al. (2014) used xanthan gum in combination with permanganate and sodium hexametaphosphate to penetrate into trichloroethylene (TCE) contaminated zone in a low permeable layer surrounded by coarse sand. They showed that by this mixture, the permanganate could penetrate 100% into the low permeable contaminated zone and no rind was observed. Bouzid et al. (2022) by means of 2D experiments compared the efficiency of the injection of surfactant, and polymer solutions as well as their mixture on DNAPL recovery and they found that by injecting a mixture of xanthan and surfactant, the recovery factor can reach up to 90%.

Martel et al. (1998) assessed the performance of xanthan on the improvement of surfactant solutions' recovery factor in a heterogeneous system composed of three layers with different permeabilities. They demonstrated that when the surfactant injection was preceded by xanthan pre-flush the surfactant adsorption on the solid surfaces was prevented and the surfactant mobility was controlled. The post-injection of xanthan behind the surfactant solution resulted in a more stable polymer/surfactant front. It also ameliorated the recovery factor of the surfactant by eliminating the viscous fingering and reducing the fluid velocity in the high permeable zone. Robert et al. (2006) in an experimental work evaluated the application of xanthan in surfactant flooding for TCE recovery from a two-dimensional (2D) heterogeneous sand model. They showed that a mixture of xanthan and surfactant could improve recovery factor by minimizing the effect of heterogeneities inside the sand pack. On the contrary, if the polymer solution has been previously injected, the presence of the polymer in the multilayer system zone prevents the surfactant solution invasion into the low permeable zone due to the

unfavorable mobility ratio. Silva et al (2013) simulated the transport of xanthan in a previously water saturated stratified sand pack using UTCHEM. Their results showed that the injection of polymer solution in a multilayer system assists the cross-flow between the layers and consequently the displacement efficiency. They found that polymer solution injection was more efficient than no-polymer tracer, requiring 1.6 PV to completely sweep the 2D multilayer system in comparison to over 6 PV for a dye tracer.

2.8 Density-driven issue during DNAPL displacement

The performance of advanced remediation technologies including surfactant injection, foam injection and polymer can be limited as the density-driven flow affects the recovery of DNAPL. During the remediation of soils contaminated with DNAPL, density-driven flow has been observed. This occurs when a less dense fluid displaces a denser fluid, known as overridden flow, or when a denser fluid displaces a less dense fluid, known as underridden flow. Several studies have investigated density underridden flow in 2D systems for DNAPL remediation purposes, including miscible cosolvent displacement by water injection (Jawitz et al., 1998; Taylor et al., 2001), and water displacement during brine surfactant injection (Lirong Zhong et al., 2008). Zhong et al. (2008) proposed that the addition of the polymer to the densified brine surfactant can control the underridden flow by providing enough viscous forces to overcome gravity; however, the relative density difference has been limited to 1.008. Taylor et al. (2004) in a set of two dimensional experiments observed that a minor density difference (0.008 g/mL) between the injecting ethanol-surfactant mixture and water present near the perchloroethylene (PCE)-contaminated zone can result in density overridden flow. Grubb and Sitar (1999) reported the downward migration of trichloroethylene (TCE) along the water-ethanol interface during ethanol injection in two-dimensional uniform and layered sand packs. They also observed the ethanol gravity override with an increasing inclination angle of the ethanol front

along with invasion progress. The density difference between ethanol and water is 0.211 g/mL, and the density difference between TCE and water is 0.46 g/mL.

Density modification displacement is an approach to control the downward migration of DNAPL by reducing its density through sufficient partitioning of alcohol within DNAPL and turning it to LNAPL (Damrongsiri et al., 2013a; Kibbey et al., 2002; Lunn and Kueper, 1999; Ramsburg and Pennell, 2002a). The density modification by alcohol partitioning can be reversible depending on the equilibrium of alcohol, water and DNAPL (or newly formed LNAPL). Besides, colloidal bilyquid aphron (CBLA), consisting of two surfactants, water, and an oil phase, has been employed to control the downward migration of DNAPL to non-polluted zones by lowering its density (Yang et al., 2020; Yan et al., 2011). CBLA has a foam structure with micron-sized (5-20 microns) droplets consisting of an outer thin aqueous phase and an internal light organic phase. In this approach, the internal light non-aqueous phase is mixed with DNAPL using a demulsifying agent, which transforms it into Light Non-Aqueous Phase Liquids. Although it can influence the downward migration of DNAPL, its efficiency relies on the performance of the demulsifier. Also, propagation of the light colloidal bilyquid aphron flowing over the DNAPL is challenging due to the influence of buoyancy forces.

Miller et al. (2000) in an experimental study used a brine (sodium iodide dissolved in water) solution with a density of 1.79 g/mL to displace the DNAPL (TCE with a density of 1.464 g/mL) pools in a two-dimensional heterogeneous system. They showed that using the densified brine solution around 55% of initial DNAPL was recovered as a direct result of buoyancy forces, however the residual DNAPL was distributed in the entire medium. Jin et al. (2007) in a numerical study examined the downward migration of DNAPL during surfactant flooding. In their numerical approach they considered negligible adsorption of chemical species and dispersion in the transport; focusing mainly on 'body forces' i.e. viscous, buoyancy, and capillary forces. The simulation outcomes indicated that there is a high risk of DNAPL's

downward migration during surfactant flooding if the viscous forces are not dominant. This highlights the crucial role played by viscous forces, which can be supplied by the polymer solution.

2.9 Dimensionless numbers and Lenormand curve

DNAPL (Dense Non-Aqueous Phase Liquid) displacement in soil involves understanding certain dimensionless numbers that describe the physics of the process, including the capillary number (N_{Ca}) and the gravity number (N_G) (Pennell et al., 1996).

The capillary number is a dimensionless number used to quantify the relative effects of viscous forces to capillary forces during the displacement of fluids in porous media. In the context of DNAPL displacement in soil, the capillary number is crucial in determining the efficiency and mechanism of the displacement process. It is defined as:

$$N_{Ca} = \frac{\mu u}{\sigma} \quad \text{Eq 2-44}$$

where μ (Pa.s) is the viscosity of invading phase, u (m/s) is the velocity magnitude of invading phase, and σ (N/m) is the interfacial tension between the phases. The capillary number used to evaluate the performance of DNAPL production during the injection of the polymer solution can be calculated as (Chatzis and Morrow, 1984):

$$N_{Ca} = \frac{k \nabla p}{\sigma} \quad \text{Eq 2-45}$$

where ∇p is the pressure gradient along the system and k (m^2) is the permeability.

To mobilize a DNAPL droplet trapped in pore spaces, the summation of the buoyancy and viscous forces should be more than capillary force (Alamooti et al., 2020; Mansouri-Boroujeni et al., 2023; Pennell et al., 1996). The gravity number is defined as the ratio of the buoyancy and viscous forces showing the balance between them and consequently the direction of flow. It can be considered as (Shook et al., 1998):

$$N_G = \frac{\Delta\rho g k}{v\mu} \quad \text{Eq 2-46}$$

where $\Delta\rho$ is the density difference (kg/m^3), g is the gravitational acceleration (m/s^2), k is the intrinsic permeability (m^2), v is the velocity magnitude of the invading phase (m/s), μ is the viscosity of the invading phase ($Pa.s$). Large negative N_G values correspond to dominant buoyancy forces leading to a vertical migration of the DNAPL if the residence time of the injected phase is large as well (Jin et al., 2007).

The Lenormand curve provides valuable insights into immiscible fluid displacement in porous media. This diagram maps the phase distribution in a porous medium, such as DNAPL and polymer in soil, based on the mobility ratio (M) and capillary number (N_{Ca}), delineating the regions of stable and unstable displacement.

Mobility ratio is a dimensionless number that describes the ratio of mobilities between the displacing fluid and the displaced fluid. It's defined as:

$$M = \frac{k_{rin}/\mu_{in}}{k_{rd}/\mu_d} \quad \text{Eq 2-47}$$

where k_{rin} and k_{rd} are the relative permeabilities of the invading and defending fluids respectively. μ_{in} and μ_d are the viscosities of the invading and defending fluids respectively.

A mobility ratio greater than one indicates that the invading fluid is less mobile than the defending fluid, potentially leading to viscous fingering. Conversely, a mobility ratio less than one denotes a more stable displacement scenario (Lenormand et al., 1988).

On the Lenormand curve (Figure 2-13), the mobility ratio is usually plotted against the capillary number. This curve identifies three main regions:

1. Stable Displacement ($M > 1$): the invading fluid efficiently pushes out the defending fluid without much viscous fingering. The invading fluid fronts are smooth and regular.
2. Viscous Fingering ($M \ll 1$): In this regime, the less viscous invading fluid fingers into the more viscous defending fluid, creating intricate patterns that can decrease sweep efficiency in reservoir recovery or DNAPL remediation.
3. Capillary Fingering (very low N_{Ca}): Dominated by capillary forces, this region is characterized by the irregular invasion of the displacing fluid driven by the pore structure and fluid-fluid interfaces. The patterns here are determined by the porous medium's heterogeneities and can appear similar to viscous fingering, but they are driven by different mechanisms.

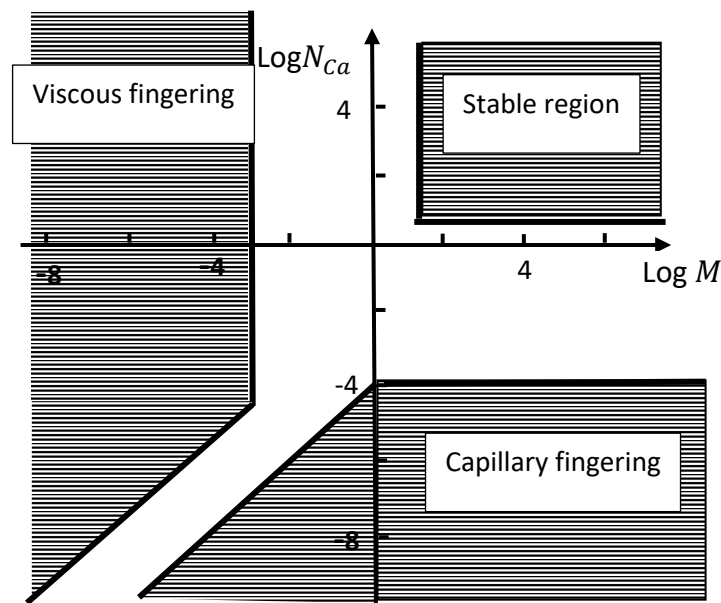


Figure 2-13 Phase-diagram of multiphase domain displacement

2.10 Objectives and structure of the thesis

To sum it up, this chapter delved into the fundamentals of multiphase flow, the transportation of polymers in porous media, and the rheological properties of their solutions. The use of these

polymer solutions in treating DNAPL-contaminated aquifers was explored and the challenges encountered during DNAPL displacement were addressed.

The primary aim of this thesis was to investigate the remediation of aquifers contaminated with DNAPL through the injection of polymer solutions. A range of experimental techniques, including rheological analysis, batch testing, 1D column studies, 2D tank experiments, along with two-phase flow modeling, were employed to primarily address the following objectives:

- Analysis of rheological behavior of polymer solutions when combined with other additives such as surfactants, alcohols, particles, and salts, in both bulk and porous media.
- Evaluation of the transport of polymers in porous media using 1D column experiments, and of their performance on the displacement of DNAPL
- Investigation of the effectiveness of polymer solutions in displacing DNAPL in unconfined and confined, single and multi-layer systems through 2D tank experiments.
- Using two-phase flow modeling to gain a deeper understanding of the physical mechanisms underlying experimental outcomes and assessing different remediation scenarios.

The rest of this thesis is organized as follows:

The 3rd chapter addresses the effectiveness of injecting polymer solutions into DNAPL-saturated multilayered aquifers for remediation purposes. The initial part of this chapter examines DNAPL displacement within saturated multilayered aquifers using polymer solutions with or without surfactants, using both numerical and experimental approaches. Subsequently, the performance of post-injection of polymer-alcohol-surfactant mixtures in improving the remediation of residual DNAPL within multilayered systems is evaluated using various experimental configurations.

In the 4th chapter, the influence of gravity forces on DNAPL displacement through the injection of polymer solutions is investigated, and a gravity-driven remediation approach are introduced. The first part of this chapter discusses the impact of injecting densified polymer suspensions on DNAPL displacement. Subsequently, the remediation of DNAPL using the injection of densified polymer brine is addressed.

In the 5th and last chapter, the general conclusions and prospects are provided.

Chapter 3

3. Remediation of multilayer DNAPL contaminated aquifers by injection of polymer solutions: primary injection of polymer/polymer-surfactant, post-injection of polymer-alcohol mixture

Summary

The presence of DNAPL in heterogeneous aquifers especially for the layered saturated soils, make them challenging for remediation. Polymer solutions through their non-Newtonian behavior can facilitate the penetration into heterogeneous media, by minimizing channeling. To shed light on the performance of polymer solutions on displacement of DNAPL a set of experimental and numerical studies were performed on the multilayered system using the polymer (xanthan) and polymer-surfactant (xanthan-SDBS) solutions. As the complementary study, to minimize the residual saturation of DNAPL in the multilayered aquifer, the performance of post-injection of polymer-surfactant-alcohol mixture was evaluated.

In the first section of this chapter, the rheological analysis of xanthan solutions was analyzed and it was shown that the addition of SDBS to the solution reduced its viscosity due to repulsive electrostatic forces and hydrophobic interactions between the molecules while preserving its shear-thinning behavior. Results of two-phase flow experiments depicted that adding SDBS to the polymer solution led to a reduced differential pressure along the soil and improvements of the DNAPL recovery factor of approximately 0.15 and 0.07 in 1D homogeneous and 2D layered systems, respectively. 2D experiments revealed that the displacement of DNAPL in multilayer zones was affected by permeability difference and density contrast in a heterogeneous soil. Numerical simulations in good agreement with experimental results, showed that for an unconfined soil, the recovery of DNAPL by injection of xanthan solution can be reduced for more than 50%.

In the second section of this chapter, the performance of post-injection of alcohol (1-propanol/1-hexanol)-surfactant (SDBS)-polymer (Xanthan) has been evaluated. Batch experiments revealed that the inclusion of 1-hexanol swelled the DNAPL volume due to alcohol partitioning. Conversely, with only 1-propanol present in the mixture, DNAPL dissolved in the aqueous phase. Column experiments, following primary xanthan-SDBS injections, demonstrated that

mixtures with 1-hexanol underwent a mobilization mechanism. DNAPL appeared in the effluent as an organic phase after the post-injection of 0.3 pore-volumes (PV). In contrast, mixtures with solely 1-propanol exhibited a solubilization mechanism with DNAPL dissolving in the aqueous phase and emerging in the effluent after approximately 1 PV post-injection. 2D tank experiments visualized mobilization and solubilization mechanisms in multilayered systems. Post-injection of the 1-propanol-SDBS-xanthan mixture led to DNAPL solubilization, demonstrated by a dark zone of varied DNAPL concentrations, followed by a clearer white zone indicating significant DNAPL dissolution. Injecting a mixture of 1-propanol, 1-hexanol, SDBS, and xanthan mobilized swollen DNAPL ganglia throughout layers, with these droplets coalescing and migrating to the recovery point.

Section I

3.1. Remediation of multilayer soils contaminated by heavy chlorinated solvents using biopolymer-surfactant mixtures: two-dimensional flow experiments and simulations

Preamble

Authors: Amir Alamooti *, Stéfan Colombano, Zakari Abdullaziz Glabe, Fabien Lion, Dorian Davarzani, Azita Ahmadi-Sénichault

Affiliations: BRGM (French Geological Survey), Orléans, 45000, France; Institut de Mécanique et Ingénierie de Bordeaux (I2M), Arts et Métiers Institute of Technology, CNRS, Talence, 33405, France ; ADEME (Agence de la transition écologique), ANGERS, 49004, France

Published: Yes

Journal: Water Research

Date of publication: 1 September 2023

DOI: <https://doi.org/10.1016/j.watres.2023.120305>

Conference: This work has been presented at 15th annual InterPore2023, 22-25 May 2023 Edinburgh, Scotland.

3.1.1. Abstract

To assess the efficiency of remediating dense non-aqueous phase liquids (DNAPLs), here heavy chlorinated solvents, through injection of xanthan solutions with or without surfactant (sodium dodecylbenzenesulfonate: SDBS), we conducted a comprehensive investigation involving rheological measurements, column (1D) and two-dimensional (2D) sandbox experiments, as well as numerical simulations on two-layers sand packs. Sand packs with grain sizes of 0.2-0.3 mm and 0.4-0.6 mm, chosen to represent the low and high permeable soil layers respectively, were selected to be representative of real polluted field. The rheological analysis of xanthan solutions showed that the addition of SDBS to the solution reduced its viscosity due to repulsive electrostatic forces and hydrophobic interactions between the molecules while preserving its shear-thinning behavior. Results of two-phase flow experiments depicted that adding SDBS to the polymer solution led to a reduced differential pressure along the soil and improvements of the DNAPL recovery factor of approximately 0.15 and 0.07 in 1D homogeneous and 2D layered systems, respectively. 2D experiments revealed that the displacement of DNAPL in multilayer zones was affected by permeability difference and density contrast in a heterogeneous soil. Simulation of multiphase flow in a multilayered system was performed by incorporating non-Newtonian properties and coupling the continuity equation with generalized Darcy's law. The results of modeling and experiments are very consistent. Numerical simulations showed that for an unconfined soil, the recovery of DNAPL by injection of xanthan solution can be reduced for more than 50%. In a large 2D experimental system, the combination of injecting xanthan with blocking the contaminated zone led to a promising remediation of DNAPL-contaminated layered zones, with a recovery of 0.87.

Keywords: chlorinated solvents, biopolymer, polymer-surfactant interaction, Density-driven flow, multilayer soils, modeling

3.1.2. Introduction

Polymer injection is being used as an effective soil/groundwater remediation technology (Alamooti et al., 2022; Bouzid and Fatin-Rouge, 2022; Martel et al., 1998). Polymer flushing has several advantages over other advanced soil remediation technologies such as surfactant flushing (Lee et al., 2005; Pennell and Abriola, 2017; Walker et al., 2022b) or foam injection (Liao et al., 2021; Omirbekov et al., 2020a). Polymer solutions by increasing fluid viscosity, can enhance pollutant recovery, and stabilize the displacement front, minimize channeling, and aid in better control and containment during soil remediation. Shear thinning polymers facilitate the penetration into heterogeneous media, by minimizing channeling (Bouzid and Fatin-Rouge, 2022; Martel et al., 1998, 2004).

The performance of the injection of the polymer solutions alone or in combination with other chemical compounds in the recovery of pollutants in contaminated soils has been studied. Martel et al. (1998) found that pre-flushing with xanthan improved surfactant (Sodium Alkane Sulfonate) transport in a three-layered, heterogeneous system with varying permeabilities by preventing surfactant adsorption and controlling surfactant mobility. Robert et al. (2006) conducted a set of multiphase flow experiments in a heterogeneous 2D sandbox, where trichloroethylene (TCE) was initially distributed in two states; at residual saturation and in pool. They illustrated that the injection of a mixture of xanthan and surfactant could result in 0.90 recovery factor of TCE by minimizing the effect of heterogeneities. They assessed density-driven plume sinking, caused by DNAPL dissolution in a mixture of surfactant and polymer. Density difference and the Darcy velocity magnitude were found to influence downward migration of surfactant polymer mixture containing the dissolved DNAPL. However, the range of density difference between the surfactant mixture and the surrounding groundwater was limited to 0.0045 g/mL. Silva et al (2013) numerically simulated the transport of xanthan in a previously water saturated stratified sand pack. Their results showed that the injection of

xanthan solution in multilayer systems assists the cross-flow between the layers and consequently the displacement efficiency. Bouzid and Fatin-Rouge (2022) through 2D experiments found that by injection of the mixture of xanthan and Sodium dodecyl sulfate (SDS), recovery factor could reach up to 0.90. They used a two-layer porous medium with contrasted permeabilities (composed of glass beads) packed over an impermeable layer. Although, the injection of the xanthan and surfactant mixture shows a promising efficiency, they performed their experiments in a confined sandbox resulting in an unrealistic extra recovery factor.

Alamooti et al. (2022) numerically and experimentally investigated the influence of densified polymer suspension injection on the displacement of DNAPL (same type as this study) in a 2D system composed of sand packs with permeability around 180 Darcy. They showed that the densification of polymer solution to match the density of DNAPL thus nullifying the effect of gravity forces could improve the recovery factor up to four times. For an unconfined system the residual DNAPL saturation after polymer injection was 0.34 compared to 0.11 for a confined one. Density contrast between invading and defending fluids during horizontal displacement can lead to density-driven (overridden/ underridden) flows. Several studies have investigated density-driven flow in 2D systems for DNAPL remediation purposes (Jawitz et al., 1998; Taylor et al., 2004, 2001; L. Zhong et al., 2008). Despite the analysis conducted, in this study we examine the density-overridden flow phenomenon in the context of immiscible two-phase flow displacement involving the use of polymers for DNAPL remediation. Furthermore, our investigation focuses on a multilayer system, considering the potential impact of crossflow between the layers, which has not been addressed in the previously mentioned studies. Modeling of multiphase flow in a multilayer system corresponding to the polymer-DNAPL displacement experiments can shed light on the efficiency of polymer injection, considering the aforementioned parameters.

Understanding the interaction between xanthan and surfactant is necessary as it can affect their rheological properties and consequently their performance for remediation of DNAPL polluted soils. Krstonošić et al. (2019) using various techniques including scanning electron microscopic (SEM) imaging, and viscosity measurements investigated the interaction between xanthan and the anionic surfactant SDS and found evidence of both electrostatic and hydrophobic interactions. Moreover, several authors have studied the rheological behavior of xanthan gum in the absence or presence of other additives (Huang and Sorbie, 1992b; Krstonošić et al., 2019; Zhong et al., 2013). Omirbekov et al. (2023) used an upscaling method and bulk shear viscosity data to study the polymer solution flow. Krstonošić et al. (2019) investigated the rheological behavior of binary mixtures of xanthan and anionic SDS in various concentrations. They observed that at low SDS concentrations and a fixed xanthan concentration, increasing the surfactant concentration decreased the viscosity to a minimum value, but higher surfactant concentrations led to higher viscosities. However, the rheological behavior of xanthan-SDBS mixtures in bulk and in porous media, their interactions and their application for soil remediation remain understudied.

This study aims to describe the performance of xanthan solutions with or without SDBS as an anionic surfactant on remediation of heavy chlorinated solvents from multilayer system. A series of rheological measurements was performed on the xanthan solutions and mixtures of xanthan and SDBS. Interfacial tension analysis and SEM imaging were performed to evaluate the interactions between SDBS and xanthan. Several 1D-column experiments were carried out to quantify the apparent viscosity of polymer solutions and to assess their performance on the removal of DNAPL. Injection of polymer solution into a DNAPL-contaminated multilayered system was conducted through a confined 2D tank where the pressure along the layers was monitored. An unconfined 2D tank was used to launch the experiments in an unconfined system where the contaminated zone was blocked by injection of polymer suspension through a

horizontal well. The numerical modeling was performed by coupling continuity and generalized Darcy's law. The role of the confinement of polluted layers, density difference, and the cross-sectional flow between the layers during the displacement process was assessed using simulation data.

The specific objectives of this study are (i) evaluation of the role of interactions of xanthan and SDBS on their rheological properties; (ii) comparison of the performances of the injection of xanthan solution alone and mixed with SDBS on the remediation of DNAPL from multilayer systems; (iii) using multiphase flow modeling to evaluate of density-driven flow and crossflow during DNAPL remediation by polymer injection in multilayer systems; (iv) assessment of the applicability of polymer injection for the unconfined DNAPL polluted soil (to mimic the real contaminated site).

3.1.3. Materials and methods: experimental and numerical

3.1.3.1. Experimental materials

Two particle-size fractions of marble sand (0.2 to 0.3 mm and 0.4 to 0.6 mm equivalent to absolute permeabilities of 35 ± 5 and 105 ± 10 darcy respectively) have been used as the solid phase in 1D column and 2D tank studies. They were sieved and washed by deionized water and dried in an oven at 105 °C. The composition and properties of DNAPL used in this study is mentioned in supplementary materials. The polymer chosen for the displacement of DNAPL is xanthan gum, an anionic water-soluble biopolymer extracted from xanthomas with the chemical formula of $C_{35}H_{49}O_{29}$. SDBS as a biodegradable surfactant used in this study showing a good efficiency in the improvement of DNAPL recovery by reducing the surface tension and not by solubilization (Colombano et al., 2020). Both xanthan and SDBS powders were supplied by Sigma-Aldrich.

To analyze the rheological behavior of the polymer solutions, the rotational rheometer Haake Mars 60 equipped with the cone-plate geometry was used. The interfacial tension (IFT) between

the polymer solutions and DNAPL was measured through the drop shape analyzer apparatus (DSA-100, KRUSS). The pendant drop method was used to measure the IFT at ambient temperature (22 ± 1 °C). The TOC Shimadzu device was used to measure the effluent's total organic carbon (TOC) concentration to determine the concentration of the polymer solution. The concentration of the bromide ion as tracer was evaluated using ICS 3000 Thermo-Dionex an ionic chromatography apparatus. The morphological analysis of the dried samples of xanthan or xanthan-SDBS solutions was carried out using an Ultra55 Zeiss scanning electron microscope (SEM) operating at a 5 kV acceleration voltage.

3.1.3.2. Column experiments

A series of multiphase and single-phase column experiments were carried out to evaluate the displacement of DNAPL in porous media of two different permeabilities, and analyze the transport of polymer solutions (see the procedure outlined by Alamooti et al. (2022)). Briefly, a glass column (4 cm internal diameter \times 30 cm length) was gradually packed with the dried sand pack while being manually vibrated continuously. Next, CO₂ was injected, which due to its solubility in water allows to avoid trapping of gas bubbles during the water saturation process. Then, degassed deionized water was vertically imbibed through the column for 2 pore volumes (PVs) at a flowrate of 0.1 mL/min. Afterward, the porosity and permeability of the porous media were measured. For the single-phase flow experiments, the polymer solutions or a tracer were introduced into a fully water-saturated sand pack with the flowrate of 1 mL/min and samples were collected from the effluent. For the multiphase flow experiments, DNAPL was initially injected vertically upward into the fully water-saturated column at a flowrate of 1 mL/min until no water was observed in the effluent. Then, the polymer solutions with a flowrate of 1 mL/min were injected into the DNAPL-saturated columns, and the effluent was collected in 15 mL polypropylene tubes while monitoring the pressure at the inlet and outlet of the column using KELLER PR33X pressure transducers. The quantification of DNAPL recovery was

accomplished using volumetric measurement of the effluent samples collected at 15 mL interval thanks to discernible variation in color between the aqueous and DNAPL phases.

3.1.3.3. 2D tank experiments

Two separate two-dimensional systems were employed to conduct the multiphase flow studies in the multilayer system shown in Figure 3.1-8 (appendix). A confined 2D tank, allowing to measure the pressure along the layers, was used to assess the efficiency of injecting polymer solutions into a multilayer heterogeneous system. Another 2D tank was used to mimic the unconfined conditions encountered in a real polluted site (i.e. field pilot) in a laboratory-scale setting. In this case, the contaminated area is confined with a blocking substance (a densified polymer-suspension, same as the one used in Alamooti et al. (2022)) to occupy the pores and resist against the upward movement of the contaminant/remedial polymer. The blocking substance was injected from a horizontal perforated tube with 0.3 cm internal diameter above the contaminated layers. The size of the unconfined 2D tank was 50 cm length×30 cm height×2 cm thickness, while the confined system had dimensions of 15 cm×10 cm×2 cm. To facilitate imaging, the fronts of the tanks were made of glass.

Two separate layers, each with a height of 5 cm, were established in both systems. Sand was compacted inside the tank while water was continuously injected from the bottom. Once the two layers were fully saturated by water, the DNAPL was uniformly injected from three ports located in bottom part through the layers with rate of 3×0.5 mL/min. In the confined tank, the polymer solutions have been injected from two ports in the left side of the tank with the rate of 2×0.5 mL/min, whereas in the unconfined one the polymer solution was injected from the port located in the central bottom of the tank at the rate of 2 mL/min. While in the unconfined system the DNAPL was extracted using Reglo ICC digital peristaltic pump (Ismatec®) from the ports on two sides of the tank at the same rate as the polymer injection rate 2×1 mL/min, in the case of the confined 2D tank the DNAPL was produced naturally in the effluent by injection of the

polymer, similar to the column tests. In the unconfined system, the horizontal perforated line was set above the contaminated zone to inject the polymer suspension. The schematic of polymer injection in 2D systems is depicted in Figure 3.1-8 (appendix).

3.1.3.4. Error and uncertainty estimations

The multiphase flow experiments in 1D column and 2D tank were duplicated. For rheological analysis the experiments have been triplicated. Error bars are calculated by determining the mean (average) of the data points and the standard deviation. The top of the error bar is located at the mean plus the standard deviation, while the bottom is located at the mean minus the standard deviation.

3.1.3.5. Polymer/surfactant solutions

Xanthan gum, widely used in soil remediation, was chosen as a biopolymer exhibiting non-Newtonian behavior in solution form. To avoid fingering (Lenormand et al., 1988), the concentration of xanthan was selected at 0.8 g/mL to provide a stable front for the injection rate of 1 mL/min. The concentration of SDBS used was 1265 mg/L, *i.e.* 5 times the critical micelle concentration, which results in a very slight solubilization of DNAPL at a level of 40 mg/L (Colombano et al., 2021; Rodrigues et al., 2017b), this is while the solubility of DNAPL in aqueous phase without SDBS is around 28 mg/L. This concentration was chosen to ensure that a sufficient amount of surfactant reaches all parts of the porous medium.

3.1.3.6. Numerical modeling

The numerical modeling was employed to simulate the displacement of DNAPL in a multilayer system using a polymer solution. As the dissolution of DNAPL even in the presence of surfactant is negligible, the modeling focused on polymer injection, excluding the influence of DNAPL dissolution in the aqueous phase.

3.1.3.6.1. Two-phase flow in porous media

The contaminated zone is represented as a uniform and isotropic porous medium made up of natural soil, containing two phases that are incompressible and immiscible (water and DNAPL).

The continuity equation of each phase can be expressed as follows (Bear, 2013):

$$\frac{\partial}{\partial t}(\phi \rho_i S_i) + \nabla \cdot (\rho_i \mathbf{u}_i) = 0 \text{ with } i = w, nw \quad \text{Eq 3.1-1}$$

where the subscripts w represents wetting phase composed of water and polymer and nw denotes non-wetting phase, DNAPL. The porosity is denoted by ϕ (-), density by ρ_i (kg/m^3), saturation by S_i (-), Darcy velocity by \mathbf{u}_i (m/s) and the time by t (s). Generalized Darcy's law for two-phase flow in porous media is considered:

$$\mathbf{u}_i = -\frac{k k_{ri}}{\mu_i} (\nabla p_i - \rho_i \mathbf{g}) \quad \text{Eq 3.1-2}$$

where k (m^2) refers to the scalar absolute permeability of the isotropic porous medium, k_{ri} (-) is the relative permeability for phase i . The viscosity and the pressure of phase i as well as the gravity vector are represented by μ_i (Pa.s), p_i (Pa), and \mathbf{g} (m/s^2) respectively. The soil is fully saturated by aqueous and non-aqueous phases; therefore, the summation of the saturations of wetting and non-wetting phases is always equal to unity. As a non-Newtonian polymer, xanthan exhibits shear-thinning behavior; therefore, its rheological behavior in porous media is represented by its viscosity as a function of pressure gradient, which is derived from single-phase flow experiments in the columns. The capillary pressure, difference in pressure between the aqueous and non-aqueous phases, as well as relative permeability curves are considered as Brooks and Corey functions (Brooks and Corey, 1964):

$$p_c = p_{th} S_{we}^{\frac{-1}{\lambda}} \quad \text{Eq 3.1-3}$$

$$k_{rw} = k_{rw}^{max} S_{we}^{\epsilon_w} \quad \text{Eq 3.1-4}$$

$$k_{rnw} = k_{rnw}^{max} S_{nwe}^{\epsilon_{nw}} \quad \text{Eq 3.1-5}$$

where p_{th} is the threshold pressure (Pa) and λ is the index of the pore size distribution. k_{rw}^{max} and k_{rnw}^{max} are the maximum relative permeability values (end points) for the wetting and non-wetting phases, respectively. The saturation exponents for the wetting and non-wetting phases are given by ϵ_w and ϵ_{nw} . The effective saturations of wetting and non-wetting phases are denoted by S_{we} (-) and S_{nwe} (-) and can be expressed as:

$$S_{we} = \frac{S_w - S_{wr}}{1 - S_{nwr} - S_{wr}} \quad \text{Eq 3.1-6}$$

$$S_{nwe} = \frac{S_{nw} - S_{nwr}}{1 - S_{nwr} - S_{wr}} \quad \text{Eq 3.1-7}$$

where, S_{wr} (-) and S_{nwr} (-) are the wetting irreducible and non-wetting residual saturations respectively.

3.1.3.6.2. Polymer transport model

The equation governing polymer transport in porous media, known as the advection-dispersion equation, can be expressed as (O'Carroll et al., 2013; Tsakiroglou et al., 2018):

$$\underbrace{\frac{\partial(\phi S_w c)}{\partial t}}_{\text{Accumulation}} - \underbrace{\nabla \cdot (\phi S_w \mathbf{D} \cdot \nabla c)}_{\text{Dispersion}} + \underbrace{\mathbf{u}_w \cdot \nabla c}_{\text{Advection}} = R_i + \dot{m} \quad \text{Eq 3.1-8}$$

where c is the concentration of the polymer (kg/m^3) and \mathbf{D} the dispersion tensor. R_i is the reaction term for the i -component and the source term is denoted by \dot{m} . As the xanthan is an

anionic polymer, the adsorption on the sand surface is neglected. The principal and cross terms of dispersion tensor can be represented as (Bear, 2013):

$$\mathbf{D} = (\alpha_T |\mathbf{U}| + D_{eff})\mathbf{I} + (\alpha_L - \alpha_T) \frac{U_x U_y}{|\mathbf{U}|} \quad \text{Eq 3.1-9}$$

$$D_{eff} = \frac{D_0}{\tau} \quad \text{Eq 3.1-10}$$

where \mathbf{I} is the identity matrix, D_{eff} is the effective diffusion coefficient (m^2/s) in porous media, D_0 is the molecular diffusion coefficient (m^2/s), τ is the tortusity, α_L and α_T are the longitudinal and transverse dispersivities, respectively.

The molecular diffusion coefficient of xanthan as a polysaccharide can be obtained through (Kono, 2014):

$$D_0 = 8.2 \times 10^{-9} Mw^{-0.49} \quad \text{Eq 3.1-11}$$

where Mw ($\text{g}\cdot\text{mol}^{-1}$) is the molecular weight of xanthan.

The equations 3.1-1, 3.1-2, and 3.1-8 were coupled to simulate the DNAPL displacement by a polymer solution in a multilayer system in a two-dimensional domain. The simulation domain was discretized by 7289 triangular meshes with a maximum element growth rate of 1.2 and maximum and minimum element sizes of 0.3 cm and 0.00112 cm respectively. The mesh is refined near the injection and production ports with the maximum element size of 0.06 cm to improve the convergence of numerical model. MUMPS (multifrontal massively parallel sparse direct solver) in COMSOL (version 5.6) as a finite element solver was used.

COMSOL Multiphysics® has been previously used for modeling two-phase flow problems in the context of soil remediation. Its effectiveness in simulating the coupled flow and transport phenomena in porous media has been successfully demonstrated for both Newtonian (Koohbor et al., 2023) and non-Newtonian fluids (Alamooti et al., 2022; Davarzani et al., 2022a). The

mesh sensitivity was analyzed based on the phase distribution and recovery factor after 70 minutes of injection. The results revealed that three different mesh sizes, consisting of 1338, 2142 and 7289 triangular mesh elements, yielded identical phase distribution and recovery factor. Nevertheless, the finest mesh was chosen due to its acceptably low computational time. A backward differentiation formula (BDF) for time stepping approach with the free time stepping option was used allowing to have flexible time-steps needed to meet the specified tolerance (with tolerance factor of 0.1). For 1D column, the inlet boundary condition for DNAPL displacement by the polymer solution was set as a fixed injection velocity of 1 mL/min, while the outlet boundary condition was set as constant atmospheric pressure (Figure 3.1-9a (appendix)). For 2D tank case, the constant injection rate of 0.5 mL/min for the injection ports and the constant atmospheric pressure in the outlet were considered as the boundary conditions (Figure 3.1-9b (appendix)).

3.1.4. Results and discussion

3.1.4.1. Rheological behavior and polymer surfactant interactions

A rotational rheometer (Haake Mars 60) with a shallow angled rotational cone plate (1°) was used to study the rheological behavior of polymer solutions, specifically xanthan solutions with and without SDBS. The results for the rheological behavior of the mixture of xanthan and SDBS solution at fixed xanthan concentration of 800 mg/L and various concentrations of SDBS are presented in Figure 3.1-1. The rheological behavior of pure xanthan solution and mixture of xanthan & surfactant was described through the Carreau fluid model (Carreau, 1972) expressed as:

$$\mu = \mu_{inf} + (\mu_0 - \mu_{inf})(1 + (\chi\dot{\gamma})^2)^{\frac{l-1}{2}} \quad \text{Eq 3.1-12}$$

where, the viscosities (Pa.s) at zero and infinite shear rate are denoted as μ_0 and μ_{inf} , χ is the relaxation time (s), and l (-) is the power index. The fitted curve and parameters of Carreau model are shown in Figure 3.1-1 and Table 3.1-2 (appendix) respectively.

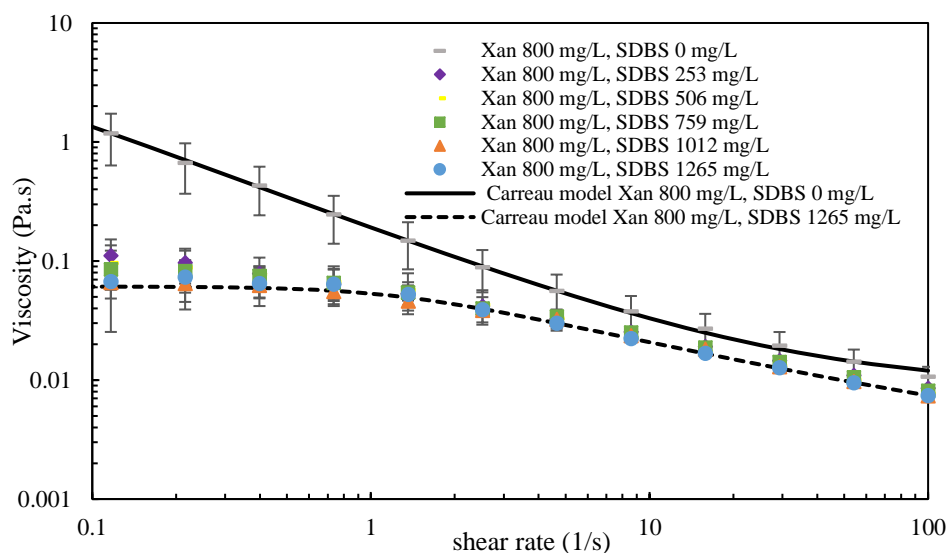


Figure 3.1-1 Rheological behavior of the mixture of xanthan and SDBS solution at fixed xanthan concentration of 800 mg/L and various concentrations of SDBS and Carreau models fitted on experimental data

The results shown in Figure 3.1-10 (appendix) depict that by increasing the concentration of pure xanthan solutions, the viscosity also increases, while exhibiting similar shear thinning behavior. As it can be seen in Figure 3.1-1, the addition of surfactant SDBS to a fixed concentration of xanthan solution decreases the viscosity (mainly at low shear rate). It also expands the range of shear rate where the solution exhibits Newtonian behavior (at low shear rates), but there are no significant changes in the rheological behavior as the concentration of SDBS increases. The decrease in viscosity is explained by the shrinkage of the xanthan chains due to the existence of repulsive electrostatic forces between xanthan and SDBS (Yang and Pal, 2020). As the concentration of SDBS increases, the interaction between the hydrophobic parts of xanthan and SDBS counterbalances the repulsive forces, causing no further noticeable changes in the viscosity of the mixture (Krstonošić et al., 2019).

To gain further insight into the interaction between xanthan and SDBS, additional analysis was conducted using scanning electron microscopy (SEM). The microstructures of solutions of pure xanthan, pure SDBS, and their mixture are presented in Figure 3.1-2. The SEM imaging reveals that the hydrophobic interactions between xanthan and SDBS altered the microstructure of the xanthan gum (Krstonošić et al., 2019).

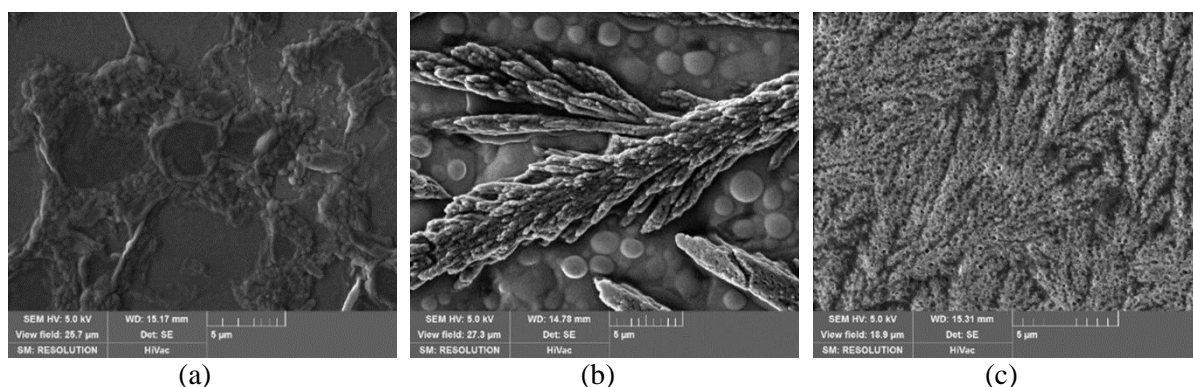


Figure 3.1-2 SEM micrographs. (a) SDBS 1265 mg/L, (b) xanthan 800 mg/L, and (c) mixture of xanthan 800 mg/L and SDBS 1265 mg/L

A series of 1D column experiments were carried out to determine the apparent viscosity of xanthan solutions in the two soils with different permeabilities, with and without the addition of surfactant. The shear rate within porous media at the Darcy scale can be described using the Darcy velocity as (Darby et al., 2017):

$$\dot{\gamma} = \sqrt{\frac{2}{\phi k}} \alpha u \quad \text{Eq 3.1-13}$$

where, the empirical shifting parameter, α (-), is related to both the tortuosity of the porous media and the fluid's bulk rheology (Chauveteau and Zaitoun, 1981). To determine the shift parameter, the apparent shear rate was calculated by fitting the Carreau fluid model to the apparent viscosity data. Actually, the apparent shear rate is plotted against the normalized Darcy velocity $\frac{u}{\sqrt{\phi k}}$ and a linear curve passing through the origin is fitted to the data. The slope of this curve is considered to be the shift parameter (Zamani et al., 2015). The resulting viscosity curves in porous media compared to those at bulk are shown in Figure 3.1-11 (appendix). The

shift parameter for the case of mixture of xanthan-SDBS is close to unity showing that the viscosities at bulk and porous media are close, while for the case of xanthan the shift parameter is more than two (2.9 and 2.41 for low and high permeable media, respectively).

The difference in shift factor in different porous media for the xanthan solution can be explained by the depleted layer concept, which describes a concentration gradient that occurs near the pore wall due to steric hindrances. As the xanthan molecules are relatively large, the steric hindrances caused by the pore walls prevent these molecules from coming too close to the wall, resulting in a gradient from zero concentration at the wall to bulk concentration at a distance close to polymer macromolecular half-length (Chauveteau and Zaitoun, 1981).

For the finer sand as the pore size is smaller, the ratio of the thickness of the depleted layer to the pore size becomes larger, and results in a decrease in apparent viscosity vs bulk viscosity and consequently higher shift factor. The depleted layer effect decreases as the shear rate increases, due to the increase in viscous friction in converging zones of porous medium where the polymer molecules are aligned in the direction of flow.

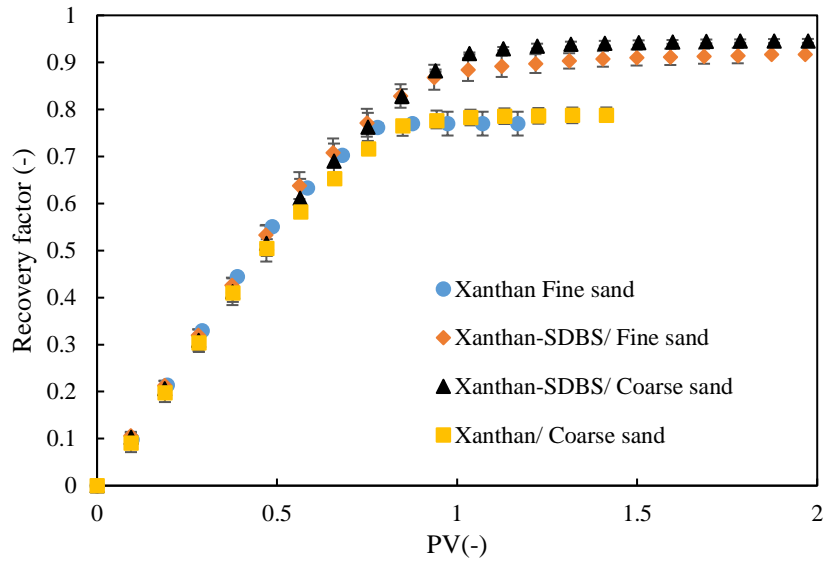
However, when SDBS is present, the mutual presence of the electrostatic repulsion and hydrophobic interactions can cause the xanthan molecule to collapse into a more compact and rod-like shape (Higiro et al., 2007; Rochefort and Middleman, 2000). This results in an alignment of polymer molecules along the direction of flow. This leads to a more uniform distribution of the polymer molecules within the pores, resulting in an increase in the apparent viscosity of the solution. Consequently, the shift factor for the xanthan-SDBS mixture is found to be around unity, implying that there is little or no difference between the bulk viscosity and the apparent viscosity in the porous medium.

3.1.4.2. One dimensional displacement

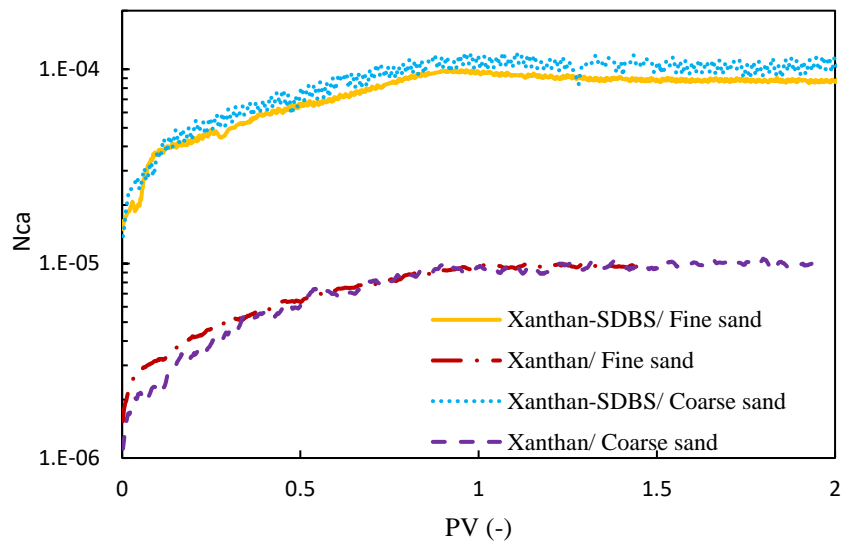
The 1D column experiments were performed to characterize the polymer solutions flow in porous media. This included single-phase and two-phase flow experiments. The single-phase experiments aimed to study the rheological behavior and adsorption/dispersion of polymer solutions in porous media. The results indicate that there is nearly no adsorption of xanthan or SDBS components onto the solid surface, likely due to the repulsive forces between the negative charges on the solid surface and the xanthan/SDBS molecules (Amirmoshiri et al., 2020). The tracer tests and polymer/surfactant injection results are discussed in the supplementary material and the breakthrough curves are shown in Figure 3.1-12 (appendix). The results of 1D column two-phase flow experiments were used to determine relative permeability and capillary pressure curves, through inverse modeling. The xanthan solutions with and without SDBS were injected into the two DNAPL-saturated sand packs and the production data and pressure differences were recorded. The capillary number used to evaluate the performance of DNAPL production during the injection of the polymer solutions was calculated as (Chatzis and Morrow, 1984):

$$N_{ca} = \frac{k\nabla p}{\sigma} \quad \text{Eq 3.1-14}$$

where σ (mN/m) is the interfacial tension (IFT) between the DNAPL and solutions. The IFT for the xanthan solution and the mixture of xanthan-SDBS was found around 21.5 ± 0.05 and 1.5 ± 0.05 mN/m, respectively. Figure 3.1-3 presents the recovery factor $\left(\frac{\text{volume of DNAPL produced}}{\text{initial volume of DNAPL in sand}} \right)$ and capillary numbers against the injected PV of polymer solutions in the two sand packs.



(a)



(b)

Figure 3.1-3 Performance of injection of polymer solutions in two sand packs of different permeabilities. (a) Recovery factor, (b) Capillary number versus injected PV

The recovery factor curves (Figure 3.1-3a) show that the presence of surfactant in the polymer solution enhances the recovery factor by around 0.15 (from 0.77 to 0.91 for fine sand and 0.79 to 0.95 for coarse sand). Additionally, the xanthan-SDBS mixture results in a longer production period after breakthrough due to the reduced interfacial tension with DNAPL. The breakthroughs for a mixture of xanthan-SDBS and xanthan solution are at 0.65 and 0.47 PV for

coarse sand, and at 0.56 and 0.48 PV for fine sand, respectively. The capillary number graphs (Figure 3.1-3b) indicate that the xanthan-SDBS mixture results in a higher capillary number, due to the lower interfacial tension and viscosity leading to a lower differential pressure. The capillary number increases until breakthrough, then remains relatively constant, as the average mobility ratio ($\frac{k_{rw}\mu_{nw}}{k_{rnw}\mu_w}$) decreases with the invasion of polymer solutions.

With the aim of modeling the xanthan-DNAPL flow in multilayered system, the saturation functions (k_{rw} , k_{rnw} , p_c) of the invading polymer and DNAPL for each layer have been determined. The model incorporated the continuity equation and generalized Darcy's law, as well as the non-Newtonian properties of the polymer solution, and viscosity data obtained from single-phase flow experiments (as seen in Figure 3.1-13 (appendix)). Using the inverse modeling method the parameters for the relative permeability and capillary pressure (equations 3.1-3:5) were found. In other words, a mathematical model for two phase flow in porous media, composed of the continuity and the generalized Darcy's law for the two phases and involving the constitutive relationships for relative permeability and capillary pressure is used to simulate two-phase flow. Then, the unknown parameters of relative permeability and capillary pressure curves were adjusted to minimize the mismatch between the model predictions and the experimental data including the differential pressure measurement and the recovery rate.

Figure 3.1-14 (appendix) displays the matched production and differential pressure data, and the parameters of the saturation functions and mean absolute error between the numerical and experimental data can be found in Table 3.1-3 (appendix).

3.1.4.3. Two-Dimensional displacement

Two-dimensional experiments were carried out to study the displacement of DNAPL in a multi-layered system using polymer solutions. A two-phase flow displacement simulation of DNAPL by xanthan solution was also conducted to better understand the mechanisms involved in the displacement process.

3.1.4.3.1. DNAPL removal in multi-layer system, xanthan solutions with/without SDBS

In line with two-phase flow experiments in 1D column, the 2D experiments were carried out in a two-layer system by injection of polymer solutions to displace the DNAPL. The polymer solutions were injected through the contaminated layers, following the steps outlined in Section 2.2. Figure 3.1-4 illustrates the distribution of the polymer solutions and DNAPL at different injected PVs. The average residual DNAPL saturation after xanthan-SDBS injection is 0.13 and for xanthan injection is 0.195 which is consistent with the previous experiments in columns. The displacement of DNAPL for both cases of xanthan solution injection and xanthan-SDBS mixture injection was similar; however, the presence of SDBS in the polymer solution resulted in a lower residual saturation. Also in the presence of SDBS in xanthan solution two fronts in the system can be observed which is likely due to the surfactant's ability to reduce IFT and enhance the mobilization of more DNAPL.

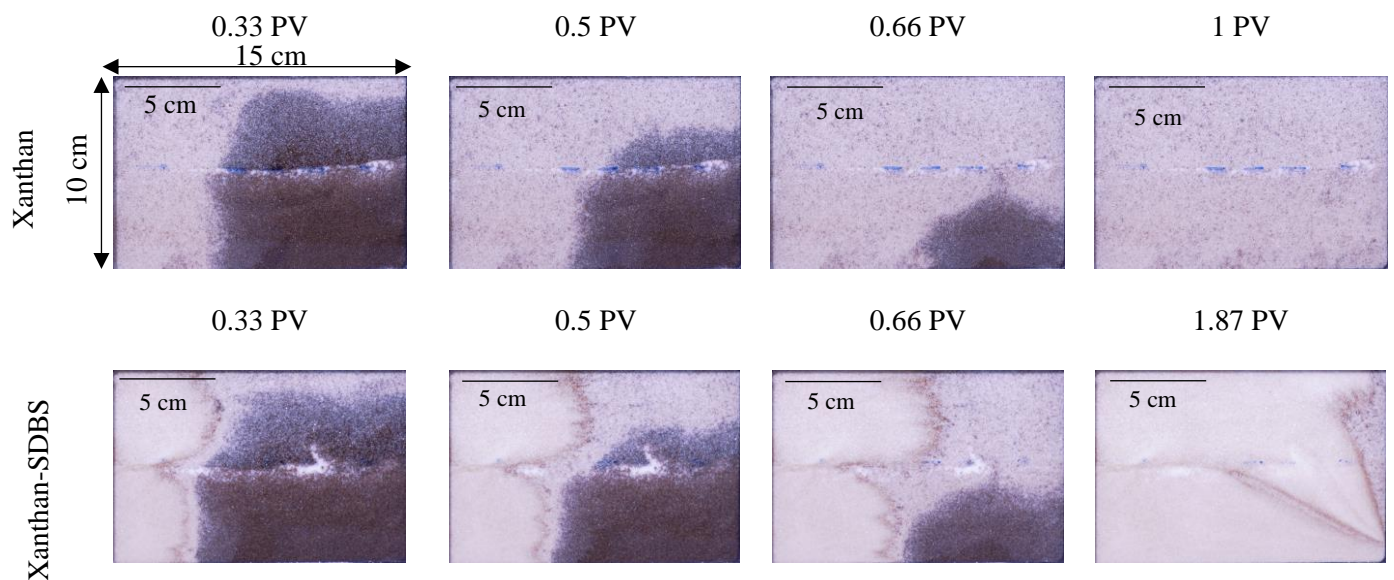


Figure 3.1-4 DNAPL displacement in a 2D multilayer system by injection of xanthan solution (first row) and mixture of xanthan-SDBS (second row) at different pore volumes of injected fluids

The data presented in Figure 3.1-15 (appendix) highlights the impact of surfactant-polymer mixture on the recovery of dense non-aqueous phase liquid (DNAPL) and the pressure gradient

in the layers. The results indicate that the presence of SDBS in the polymer mixture reduces the pressure (~350 Pa for fine sand and ~180 Pa for coarse sand), leading to a higher recovery of DNAPL by 0.07 (0.85 compared to 0.78). The pressure drop is higher in low permeable layer, and the duration of DNAPL production is prolonged after the breakthrough when SDBS is present. The displacement of DNAPL and polymer solutions is influenced not only by the permeability contrast but also by the density difference between the polymer solutions and DNAPL. The invading solution tends to flow on the top of high permeable layers as buoyancy forces favor the vertical movement of the polymer solutions. Indeed, the comparison of dimensionless numbers including capillary and Bond numbers can provide valuable insight into the complex interplay of forces that drive DNAPL displacement by polymer solutions. By evaluating the values of these dimensionless numbers, it is possible to determine the relative influence of gravity, capillary, and viscous forces on the displacement process. The Bond number is defined as (Morrow and Songkran, 1981) :

$$N_{Bo} = \frac{\nabla\rho gk}{\sigma} \quad \text{Eq 3.1-15}$$

The Bond number to capillary number ratio, evaluated at the end of experiment, for the high permeable layer, is 7.15 and 8.57 for injections of xanthan and xanthan-SDBS, respectively. Meanwhile, for the low permeable layer, the ratio is 3.65 and 4.4 for injections of xanthan and xanthan-SDBS, respectively. This shows that gravity forces are stronger than viscous forces for both layers and polymer solutions with or without surfactant. This demonstrates the significance of gravity forces and how they, along with viscous forces, play an active role in the displacement of DNAPL (Zhou et al., 1994). As a result, the flow in the higher permeable layer is faster, and the density difference leads to a preference for flow on top of the DNAPL zone. For the cases where the permeability contrasts are higher, the displacement of the pollutant in the low permeable layer would have a much larger delay compared to the high permeable layer

leading to an uncomplete displacement in the low permeable layer in our experimental conditions.

The simulation of DNAPL displacement in a multilayer system using xanthan solution was performed using the constitutive relationships gathered from 1D column experiments. Figure 3.1-5 shows the close match of saturation profiles obtained numerically and experimentally. The comparison for recovery factor and pressure drop is shown in Figure 3.1-16 (appendix). The dynamic of propagation of the front in both layers influenced by gravity and capillary forces has been relatively well captured by numerical model. The simulation results depicts that the recovery factor for high permeable layer is around 0.79 while for low permeable layer it is approximately 0.74. This model is used for further analysis where the role of densification of polymer solution, the boundary conditions and cross-sectional flow along the layers is evaluated.

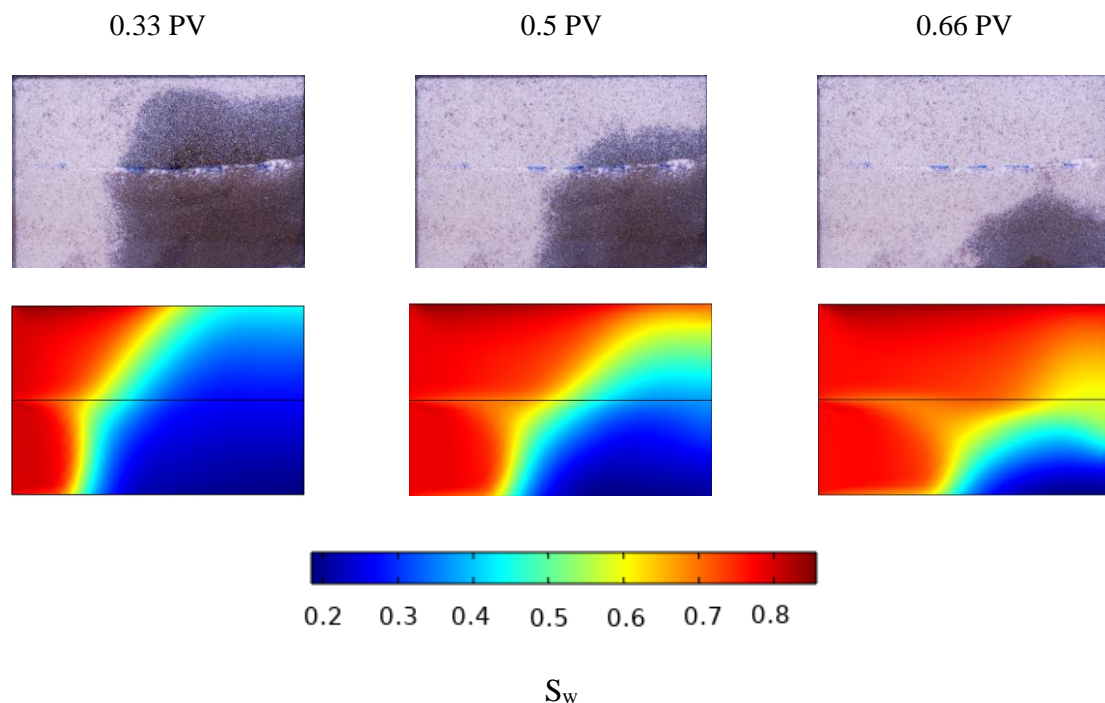


Figure 3.1-5 Comparison between the numerical and experimental results of DNAPL displacement by xanthan solution in a 2D multilayer system, first row: experimental results shown; second row simulation results depicted.

3.1.4.3.2. Cross sectional flow

Nonuniform fluid flow in porous media can occur due to factors such as permeability heterogeneity, adverse mobility ratio, and differences in density between the injected fluid and the contaminant (Debbabi et al., 2017). This type of flow can lead to fluid crossflow between zones of fast and slow flow in the layers, which may be caused by various mechanisms such as viscous crossflow, capillary crossflow, or density-driven crossflow. According to the simulation data analysis, crossflow between the layers occurs during the displacement of DNAPL. As depicted in Figure 3.1-6, the crossflow direction is from the low permeable layer to the high permeable layer near injection points, decreasing to zero at the middle of the horizontal axis. Near the recovery point, the crossflow direction is reversed. These results align with the pressure gradient profile within the layers, where crossflow direction depends on the pressure gradient difference. Higher pressure gradient leads to crossflow from high to low gradient zones. Zero crossflow occurs at the intersection of pressure gradient curves.

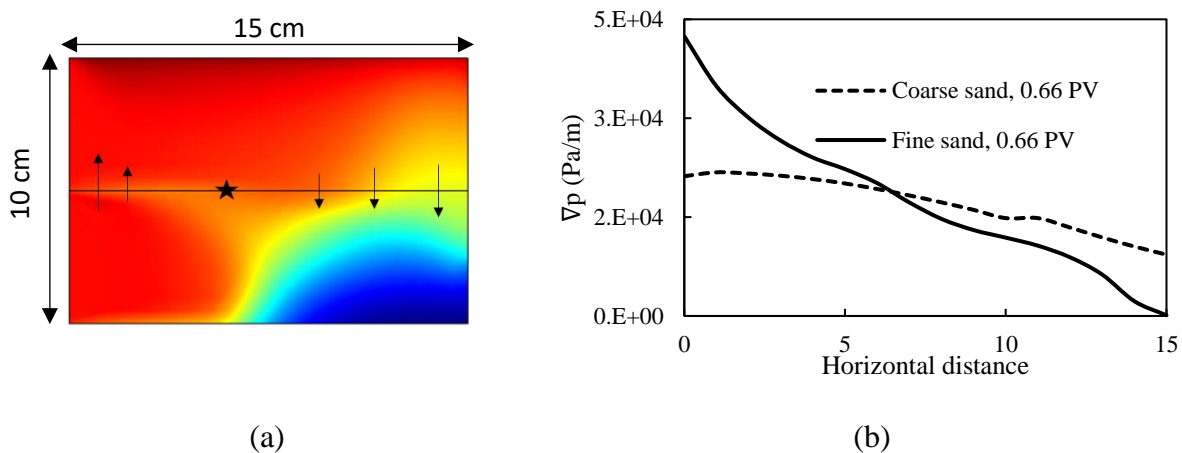


Figure 3.1-6 Crossflow between the layers after 0.66 PV injection of xanthan in a 2D multilayer system. (a) xanthan-DNAPL distribution in the system, the arrows show the

direction of crossflow and the star shows zero cross flow, (b) pressure gradient along the layers

3.1.4.3.3. Evaluation of polymer injection performance in an unconfined polluted site

The displacement of DNAPL by a polymer solution in the subsurface is a complex process that is influenced by several factors, including the density contrast between the two fluids. In traditional soil remediation technologies, the polymer solution is usually less dense than the DNAPL, resulting in an upward flow of the polymer solution due to buoyancy forces. However, recent studies have suggested that the densification of the polymer solution can alter the direction and distribution of DNAPL flow through the soil (Alamooti et al., 2022; Omirbekov et al., 2023).

To numerically assess the densification impact on fluid distribution, the density of the invading polymer solution in the soil is modified to match that of DNAPL, which has a density of 1.66 g/mL. Figure 3.1-17 (appendix) shows that densification reduces vertical movement of the invading fluid while promoting horizontal flow. However, the permeability contrast between the layers still controls the flow in the layers, with faster flow in high permeable layers and slower flow in low permeable layers. These findings highlight the importance of considering density contrast and densification when designing remediation strategies for DNAPL-contaminated sites. For the case of non-densified polymer injection through the DNAPL-contaminated sites where the polluted zone is not confined and is open to adjacent areas, the upward movement of the polymer can negatively impact the remediation of DNAPL. To evaluate this, a simulation analysis was conducted with the upper boundary of the multilayer system considered as an open boundary with constant atmospheric pressure boundary conditions. The results of the simulation, as shown in Figure 3.1-18 (appendix), indicate that

after one PV of injection, the polymer solution has not reached half of the system and has primarily moved upward. The recovery factor is around 0.38 less than half of the recovery factor in a confined system. This indicates that, in a real field, polymer injection alone is much less effective without densification or blocking of the contaminated zone.

To address this issue in a more realistic manner, a larger 2D tank (as shown in Figure 3.1-8a (appendix)) was used, where the contaminated zone was blocked by injection of a densified polymer suspension at the same density as DNAPL. The polymer suspension contained carboxymethyl cellulose at a concentration of 4 g/L and added barite particles to achieve a density of 1.66 g/mL (Alamooti et al., 2022). The blocking suspension was continuously injected above the contaminated layers to prevent the vertical movement of invading polymer solution. Figure 3.1-7 demonstrates that in a system similar to a real polluted site, the injection of the blocking agent can effectively improve remediation during the displacement of DNAPL by polymer solution. DNAPL recovery factor in this system has been 0.87.

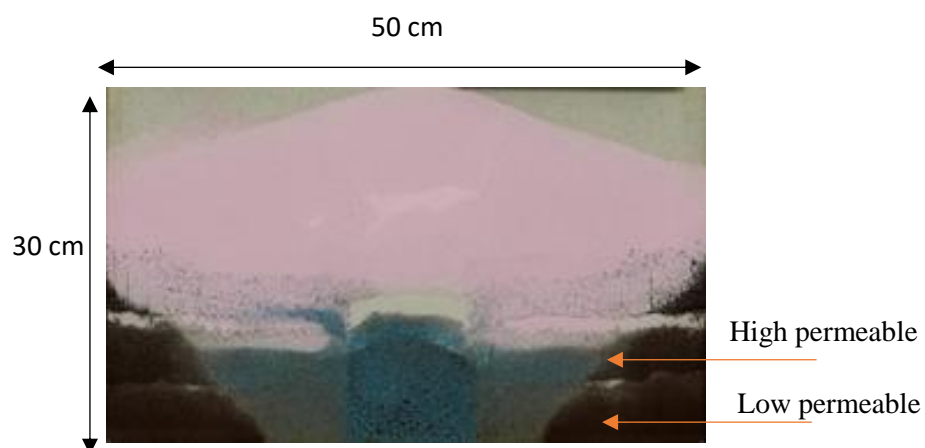


Figure 3.1-7 DNAPL displacement by xanthan solution (black-blue) in a 2D multilayer system where the contaminated zone is blocked by the injection of a densified polymer suspension (pink) through a horizontal well

3.1.5. Conclusion

Experiments were conducted to assess the performance of the injection of xanthan solutions with or without SDBS for remediating DNAPL-contaminated layered zones, including rheological analysis in both bulk and porous media and 1D and 2D multiphase flow. A numerical study was also conducted to understand the mechanisms involved in the removal of DNAPL in heterogeneous soil. The presence of SDBS decreased the viscosity of the xanthan solution, while there are no significant changes in the rheological behavior as the concentration of SDBS increases. The repulsive electrostatic forces and hydrophobic interaction between their molecules were responsible for this behavior.

The addition of SDBS to the xanthan solution resulted in a better recovery of DNAPL by increasing the capillary number during the injection of the mixture, with an improvement of approximately 0.15 in a 1D homogeneous system and 0.07 in a 2D layered system. The 2D experiments revealed that the displacement of DNAPL was affected by permeability difference and density contrast.

Simulation results validated by experimental data showed that, if the invading polymer solution was not densified and the soil above the DNAPL was not confined, the recovery of DNAPL was less than half of the confined system (0.35 compared to 0.78). In a larger 2D experimental system, injection of xanthan led to 0.87 recovery of DNAPL when the contaminated layered zones were impeded by a blocking agent, suggesting that for a field application, the combination of injecting a polymer mixture with blocking the contaminated zone can lead to a promising remediation of DNAPL-contaminated layered zones.

3.1.6. Appendix

3.1.6.1. DNAPL composition and properties

DNAPL used in this study is a multicomponent chlorinated organic compound that is mainly made of hexachlorobutadiene (HBCD) (58%), hexachloroethane (HCA) (14%), and penta-

chlorobenzene (3.5%), carbon tetrachloride (4%), and other conventional chlorinated organic compounds including perchloroethylene (PCE) (8%), and trichloroethylene (TCE) (2%). There are some other components in DNAPL mixture that are not quantifiable. The physical properties of DNAPL are mentioned in Table 3.1-1.

Tables

Table 3.1-1 Physical parameters of the DNAPL

Parameter	Density (kg.L ⁻¹)	Dynamic viscosity (mPa.s)	DNAPL/water interfacial tension (mN.m ⁻¹)	DNAPL/water/sand contact angle (°)
DNAPL, 20 °C	1.66±0.005	4.47±0.15	10.96±0.05	119.33±4.16

Table 3.1-2 Parameters of Carreau model related to rheological behavior of the xanthan solution and the mixture of xanthan-SDBS


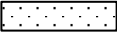
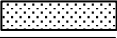




Solution	μ_{inf}	μ_0	χ	l	R ²
[Xanthan] = 800 mg/L	0.0087	4.31	36.75	0.12	0.99
Xanthan-SDBS mixture ([xanthan] = 800 mg/L & [SDBS] = 1265 mg/L)	0.0019	0.061	0.83	0.46	0.97

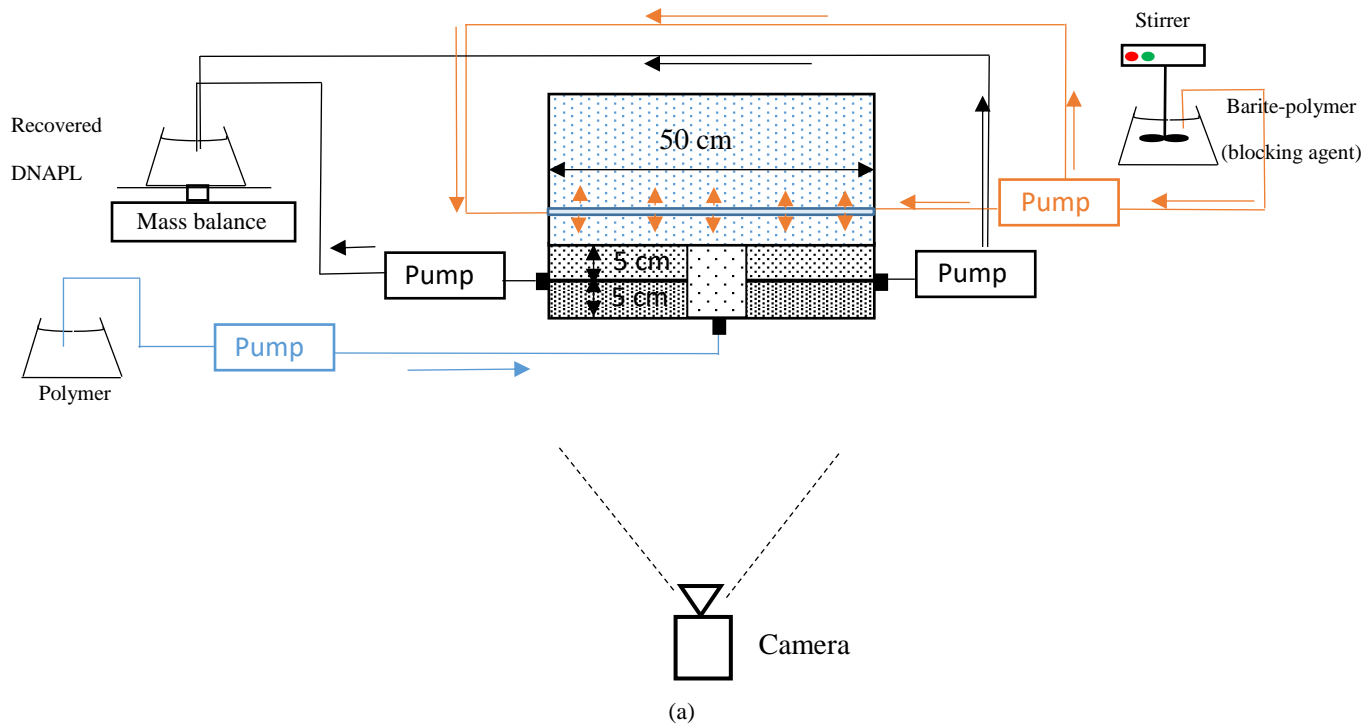
Table 3.1-3 Relative permeability and capillary pressure parameters obtained by inverse modeling and mean average error of experimental and numerical data

Soil	k_{rw}^{max}	k_{rnw}^{max}	ϵ_w	ϵ_{nw}	λ	p_{th} (Pa)	S_{wr}	S_{nwr}	MAE (Mean Absolute Error)
------	----------------	-----------------	--------------	-----------------	-----------	---------------	----------	-----------	---------------------------

Fine	0.6	0.65	2	3	2	500	0.16	0.19	0.0506
Coarse	0.75	0.6	2	3	2	500	0.114	0.188	0.0274

Figures

-  Sand saturated with water, grain size: 0.6-0.8 mm
-  Coarse sand; grain size: 0.8-1 mm
-  High permeable zone; grain size: 0.4-0.6 mm
-  Low permeable zone; grain size: 0.2-0.3 mm
-  Horizontal tube for injection of the blocking substance (polymer suspension)
-  Injection/production port
-  Pressure transducer



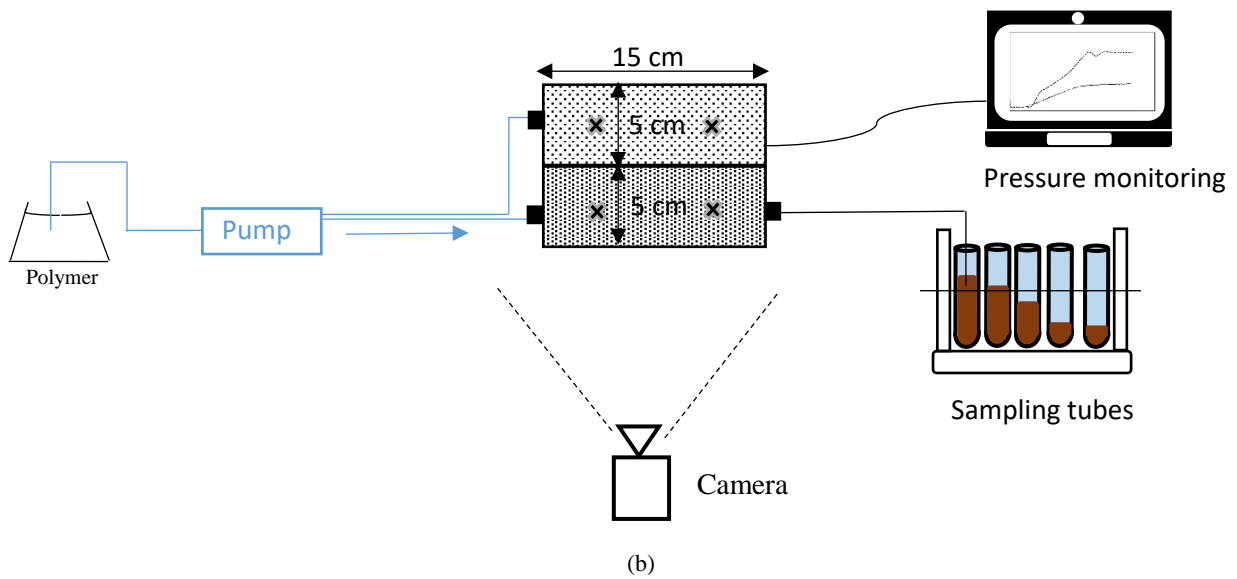


Figure 3.1-8 Schematic of polymer-DNAPL displacement experimental setup (2D tank) as well as the layers configurations. (a) unconfined system, and (b) confined system

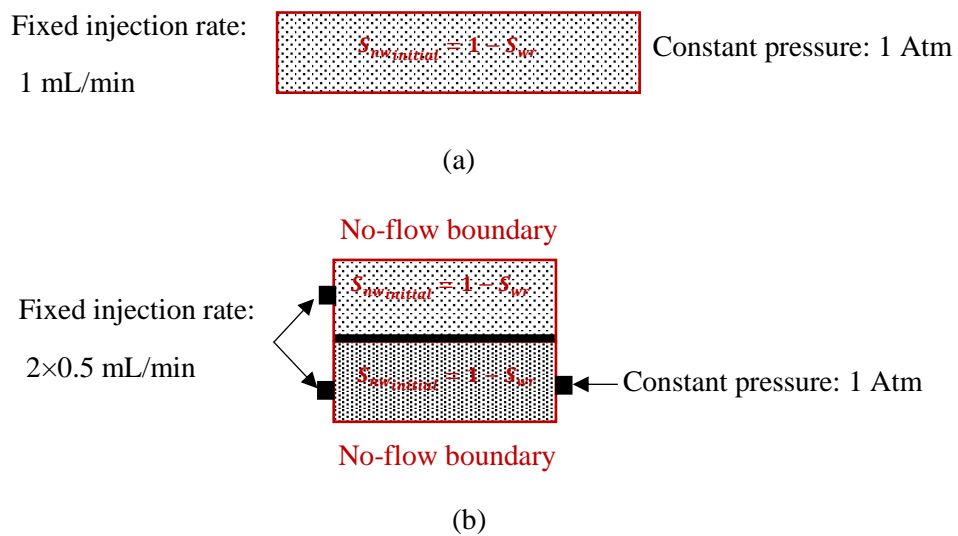


Figure 3.1-9 Schematic of boundary and initial conditions for numerical simulations. (a) 1D column, and (b) 2D tank

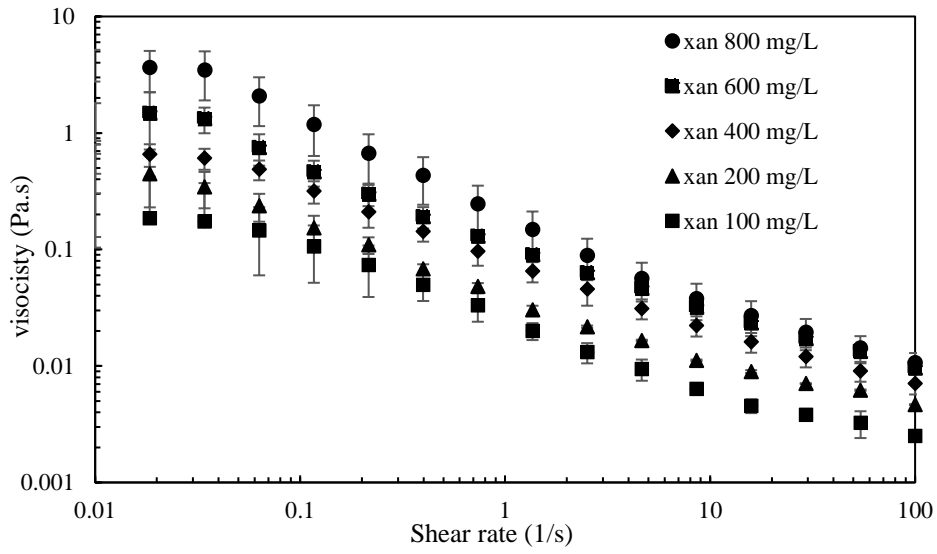
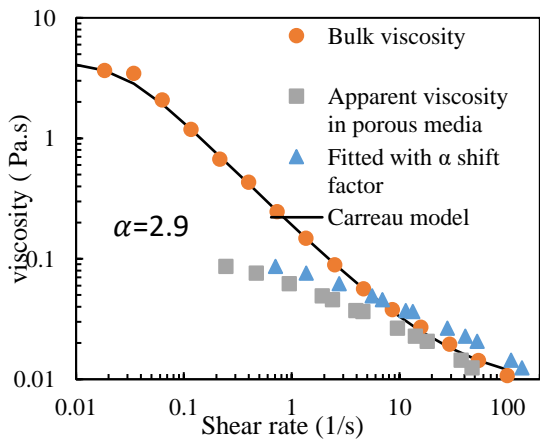
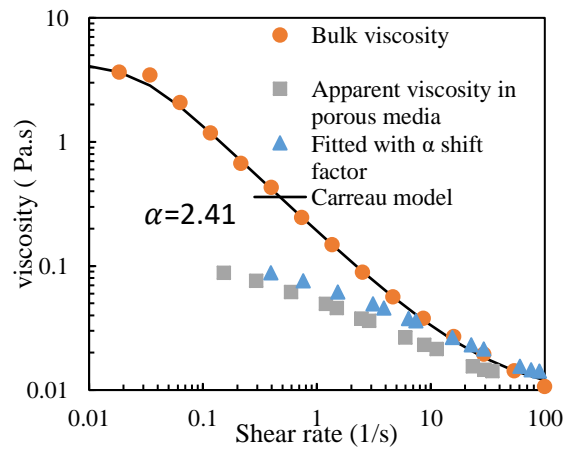


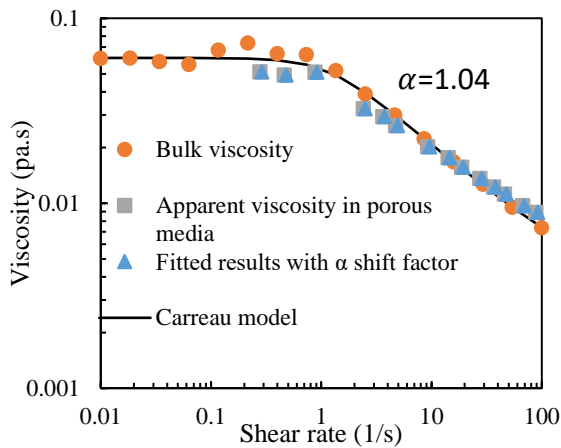
Figure 3.1-10 Rheological behavior of the xanthan solutions at different concentrations



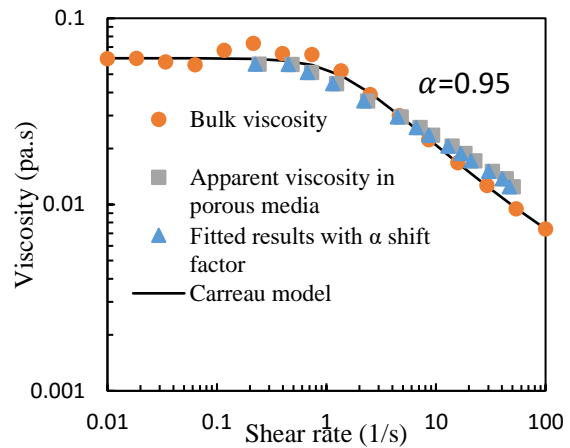
(a)



(b)



(c)



(d)

Figure 3.1-11 Apparent viscosity compared with those obtained from rheometer. (a) pure xanthan solution for the fine sand, (b) pure xanthan solution for coarse sand, (c) mixture of xanthan and SDBS for fine sand, and (d) mixture of xanthan and SDBS for coarse sand

3.1.6.2. Single phase flow experiments

Sodium bromide was utilized as a tracer to assess effluent production, assuming no adsorption of bromide ions. The concentration of these ions was analyzed through ion chromatography. The Total Organic Carbon (TOC) device was used to measure the concentration. In the case of the xanthan-SDBS mixture, both the TOC and conductivity meter were used and the average of the normalized conductivity and TOC was taken as the average normalized concentration of the mixture. The results for breakthrough curves are shown in Figure 3.1-12 (appendix). As it can be seen for both fine and coarse sand the effluent history curves for xanthan and the mixture of xanthan-SDBS has a breakthrough approximately at 1 PV, and there is no noticeable difference between the xanthan and tracer curves. This indicates that there is minimal adsorption of xanthan components onto the solid surface, likely due to the repulsive forces between the negative charges on the solid surface and the xanthan/SDBS molecules (Amirmoshiri et al., 2020). The longitudinal and transverse dispersivities (Eqs. 9-10), were

found to be 0.01 and 0.001 cm, respectively, by using the advection-dispersion equation to match the simulation data from the tracer experiment.

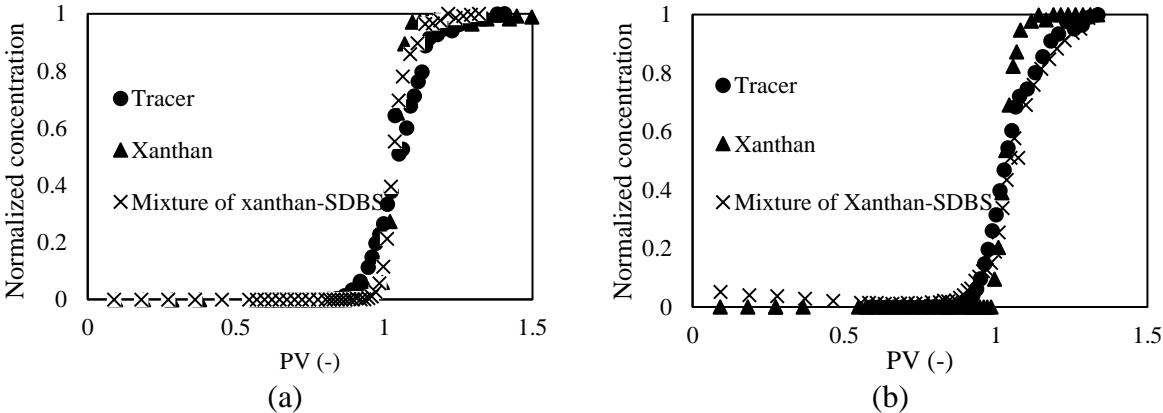


Figure 3.1-12 Breakthrough curves for tracer, xanthan and mixture of xanthan-SDBS in 1D columns. (a) Fine sand, and (b) Coarse sand

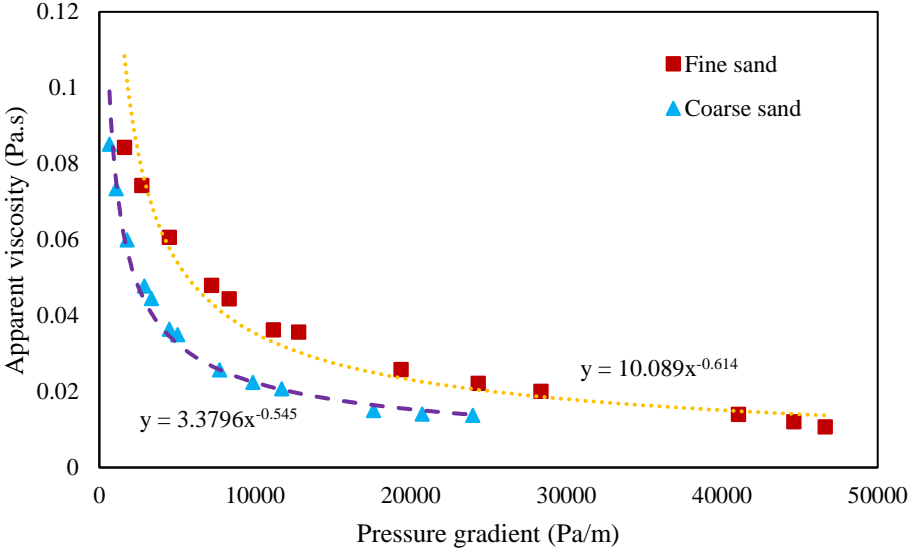


Figure 3.1-13 Apparent viscosity versus pressure gradient for fine and coarse sand in 1D columns

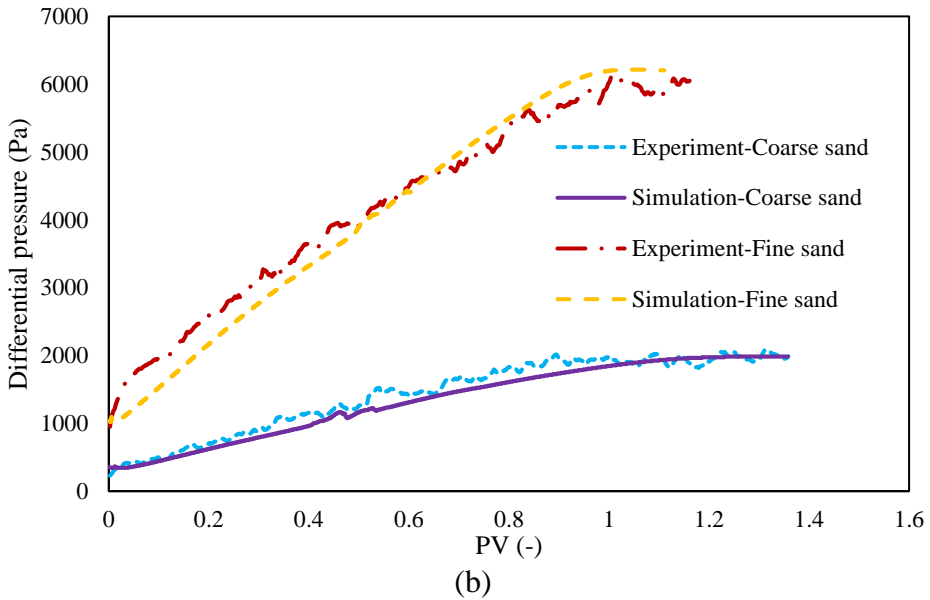
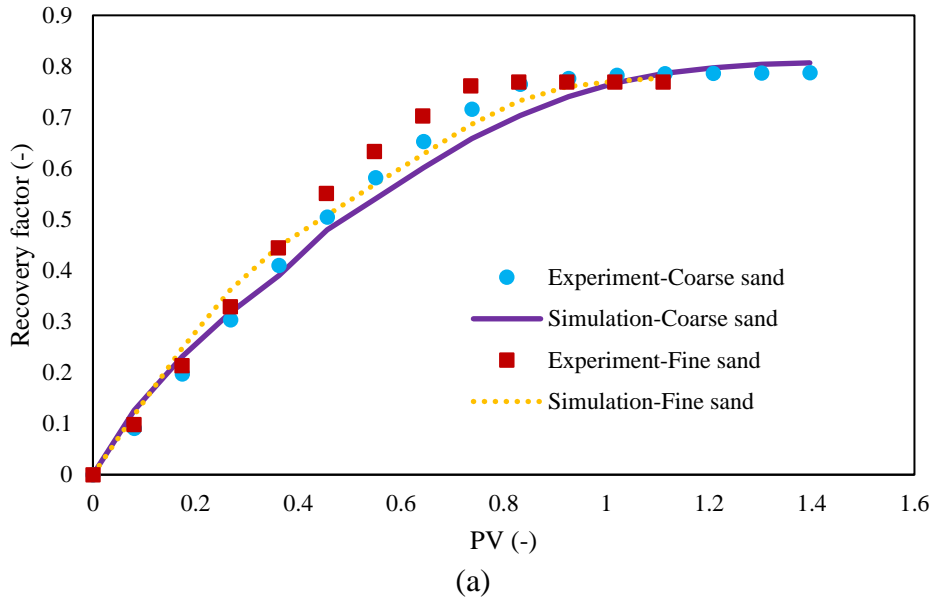
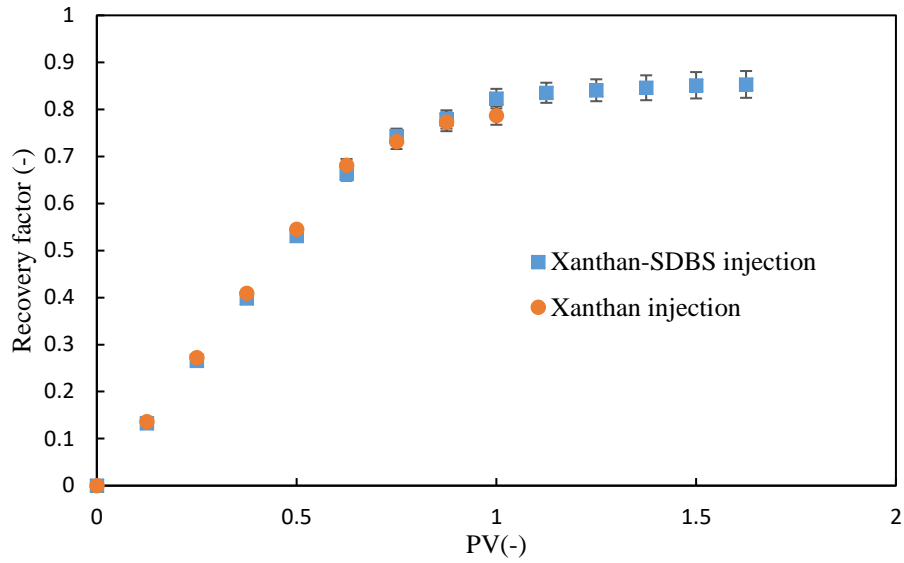
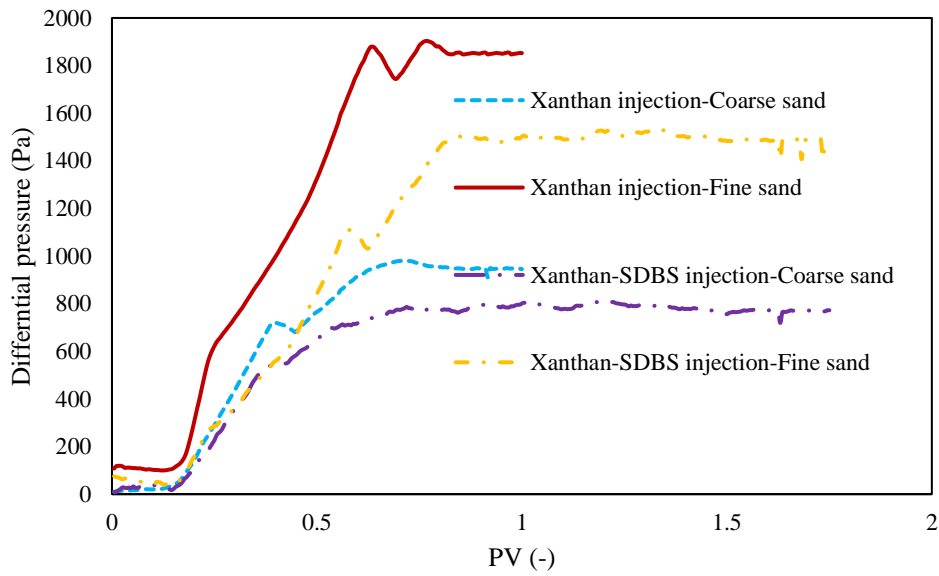


Figure 3.1-14 Comparison of results obtained from experiments and simulations for xanthan-DNAPL displacement for different soils in 1D columns. (a) Recovery factor versus injected PVs, (b) Differential pressure versus injected PVs



(a)



(b)

Figure 3.1-15 Results obtained from injection of polymer solutions into the multilayer 2D system. (a) Recovery factor, (b) Differential pressure

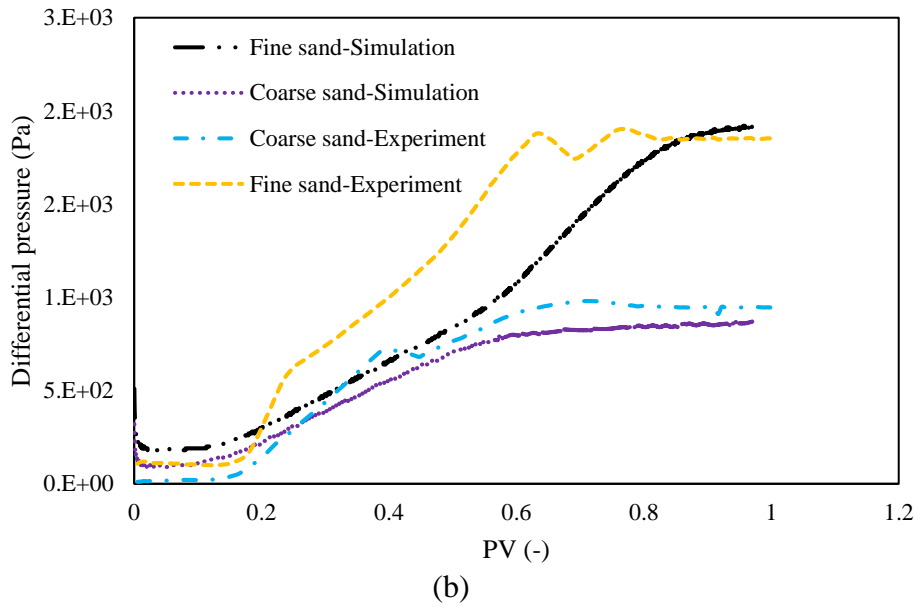
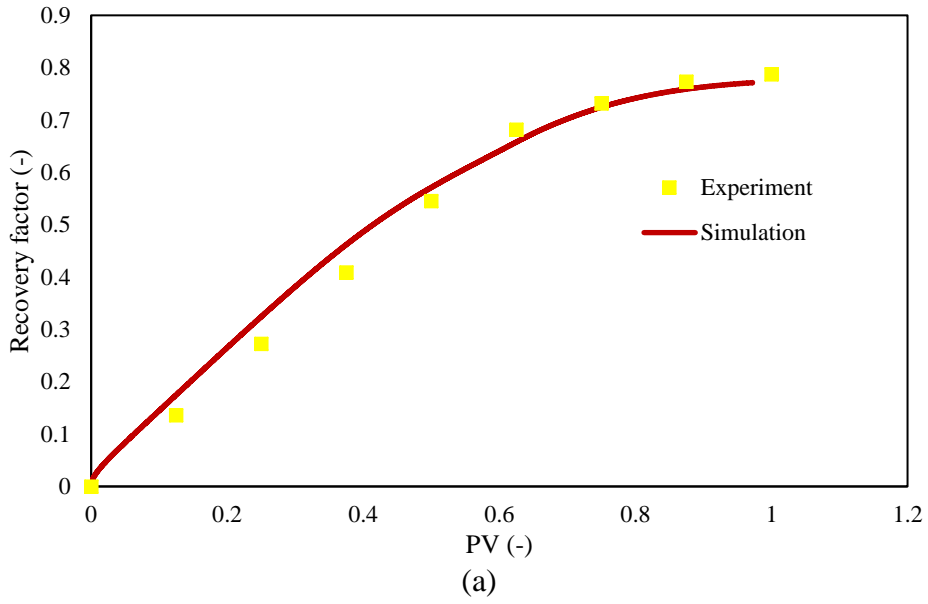


Figure 3.1-16 Comparison between the numerical and experimental results. (a) Recovery factor, (b) differential pressure for xanthan-DNAPL displacement in a confined multilayer 2D system

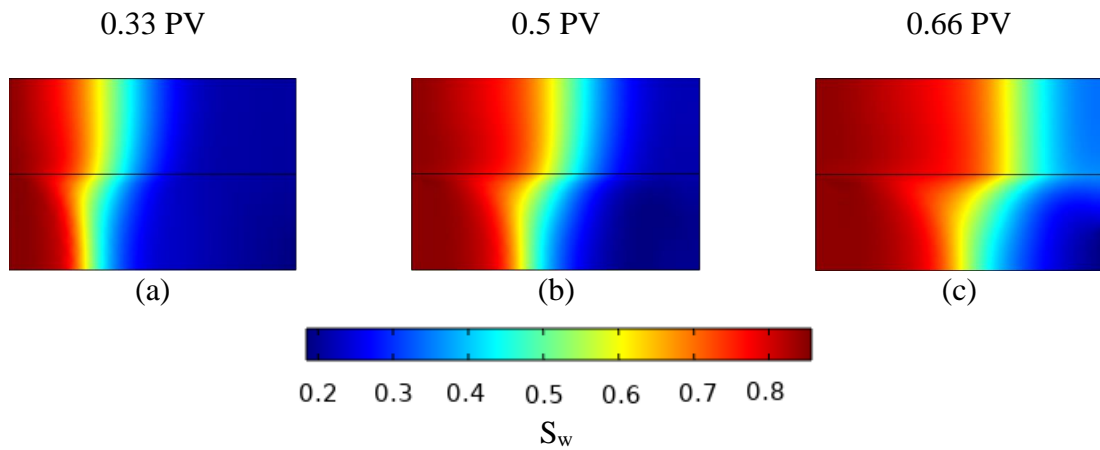


Figure 3.1-17 DNAPL displacement by densified polymer ($\rho= 1.66$ g/mL) solution in a multilayer system after injection period for (a) 0.33 PV, (b) 0.5 PV, and (c) 0.66 PV

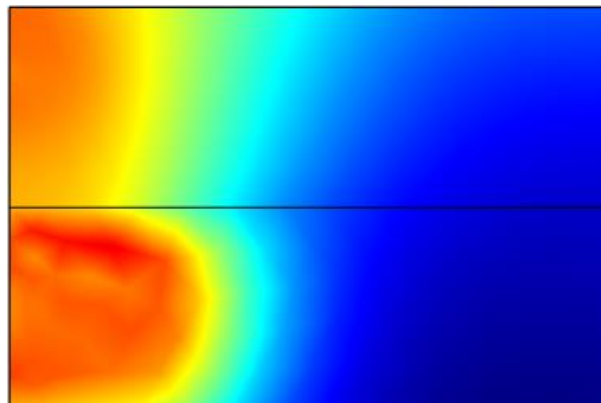


Figure 3.1-18 DNAPL displacement by non-densified polymer ($\rho= 1$ g/mL) injection by considering an open boundary on the upper side (unconfined system) after injection of 1 PV

Section II

3.2. Enhancing Remediation of Residual DNAPL in Multilayer Aquifers: Post-Injection of Alcohol-Surfactant-Polymer Mixtures

Preamble

Authors: Amir Alamooti *, Stéfan Colombano, Abbas Shoker, Azita Ahmadi-Sénichault, Fabien Lion, David Cazaux, Cédric Marion, Jérôme Lagron, Idriss Sawadogo, Dorian Davarzani

Affiliations: BRGM (French Geological Survey), Orléans, 45000, France; Institut de Mécanique et Ingénierie de Bordeaux (I2M), Arts et Métiers Institute of Technology, CNRS, Talence, 33405, France ; ADEME (Agence de la transition écologique), ANGERS, 49004, France, INEOS Inovyn, 39500 Tavaux, France

Published: Yes

Journal: Science of The Total Environment

Date of publication: 05/02/2024

DOI : <https://doi.org/10.1016/j.scitotenv.2024.170680>

Conference: This work has been presented at Aquaconsoil2023 11 to 15 September 2023, Prague.

3.2.1. Abstract

Although polymer-surfactant injection is an effective remediation technology for multilayer aquifers contaminated by Dense Non-Aqueous Phase Liquids (DNAPL), the existence of residual DNAPL after treatment is inevitable. This study evaluates the efficiency of the post-injection of alcohol-surfactant-polymer (ASP) mixtures containing 1-propanol/1-hexanol, sodium dodecylbenzenesulfonate (SDBS), and xanthan in enhancing remediation of residual DNAPL in layered systems. A range of experimental devices, including batch, rheological measurements, centimetric 1D column, and decametric 2D tank experiments, were employed.

Batch experiments revealed that the inclusion of 1-hexanol swelled the DNAPL volume due to alcohol partitioning. Conversely, with only 1-propanol present in the alcohol-surfactant (AS) mixture, DNAPL dissolved in the aqueous phase. The co-presence of 1-hexanol along with 1-propanol in AS mixture favored 1-propanol's partitioning into the DNAPL phase.

Column experiments, following primary xanthan-SDBS (XS) injections, demonstrated that ASP mixtures with 1-hexanol (regardless of presence of 1-propanol) underwent a mobilization mechanism. DNAPL appeared in the effluent as an organic phase after the post-injection of 0.3 pore-volumes (PV), by a reduction trend in its density. In contrast, mixtures with solely 1-propanol exhibited a solubilization mechanism, with DNAPL dissolving in the aqueous phase and emerging in the effluent after approximately 1 PV.

2D tank experiments visualized mobilization and solubilization mechanisms in multilayered systems. Post-injection of the ASP mixture with solely 1-propanol led to DNAPL solubilization, demonstrated by a dark zone of varied DNAPL concentrations, followed by a clearer white zone indicating significant DNAPL dissolution. Injecting ASP mixture containing both 1-propanol and 1-hexanol mobilized swollen DNAPL ganglia throughout layers, with these droplets coalescing and migrating to the recovery point. The darkness of mobilized

droplets was faded as more DNAPL was recovered. The solubilization ASP mixture enhanced the recovery factor by 0.02 while the mobilization ASP mixture led to a 0.08 increase in the recovery factor.

Keywords: DNAPL, biopolymer, alcohol, multilayer, mobilization, solubilization

3.2.2. Introduction

One of the main environmental issues is the spill of chlorinated organic compounds through the soil (You et al., 2020). These highly toxic organic compounds are considered as Dense Non-Aqueous Phase Liquids (DNAPLs). They tend to penetrate downward through the aquifer and form trapped as contaminated lenses (Alamooti et al., 2022; Li et al., 2007; Pennell et al., 1996). The dissolved DNAPL in aqueous phase can enter in low permeability layers by molecular diffusion (Parker et al., 2003; Puigserver et al., 2022). Parker et al. (2003) proposed a framework for understanding the architecture of DNAPL source areas within granular aquifers, highlighting transition zones at the interface of granular aquifers and basal aquitards. These zones, situated at the base of numerous aquifers, exhibit distinct characteristics marked by the presence of numerous thin layers of silty-clay intertwined with coarser-grained layers such as sands and gravels.

In general, DNAPLs are considered as long-lasting contaminants in the groundwater environment. Surfactant injection has proven to be an effective approach in remediation of soil and aquifer contamination caused by DNAPLs (Amanat et al., 2022; Barbati et al., 2023; Colombano et al., 2021, 2020; Pennell et al., 1993; Pennell and Abriola, 2017; Taylor et al., 2001). By introducing a surfactant solution, the recovery of pollutants can be enhanced through two mechanisms: solubilization of DNAPL molecules in the aqueous phase occurring at surfactant concentration higher than critical micelle concentration (CMC) and mobilization of DNAPL by reducing the interfacial tension (IFT) between the pollutant and the aqueous phase. The injection of a flushing solution, comprising either a surfactant or a co-solvent, can effectively reduce the residual saturation of DNAPL by mobilizing or dissolving the DNAPL (St-Pierre et al., 2004). Alcohols with lower molecular weights such as methanol, ethanol, 1-propanol, and 2-propanol, typically function as a co-solvent which preferentially partition into

the aqueous phase when in contact with the DNAPL, thus facilitating the dissolution of DNAPL molecules into the aqueous phase (Agaoglu et al., 2012; Aydin et al., 2011; Mo et al., 2023a; Oostrom et al., 2006). This aids in remediation through a solubilization mechanism. Conversely, alcohols with higher molecular weights or medium chain lengths are typically used as co-surfactants alongside water-soluble surfactants to establish a microemulsion system. When in contact with the DNAPL phase, these alcohols tend to preferentially partition into the organic phase. This leads to an improvement in DNAPL recovery through a mobilization mechanism. As the volume of DNAPL ganglia grows, they merge to create a less viscous, lighter DNAPL bank ahead of the displacement area (Fu et al., 2022; Ramsburg and Pennell, 2002; Zhou and Rhue, 2000).

Experimental studies demonstrate that the injection of these types of alcohols as cosolvents in low-volume fractions (around 1-5% by volume) can enhance NAPL solubilization, although it necessitates numerous pore volumes of the flushing solution to substantially remove NAPL mass. In contrast, flooding with higher volume fractions (70-90%) can lead to a complete NAPL recovery within a single pore volume (Imhoff et al., 1995).

The role of medium chain length or branched short chain alcohols in DNAPL mobilization has been the focus of several studies, particularly their ability to decrease DNAPL density by partitioning into the DNAPL phase (Fu et al., 2022; Kibbey et al., 2002; Ramsburg et al., 2003; Ramsburg and Pennell, 2002; St-Pierre et al., 2004; Wu et al., 2016) . In remedial emulsions, the presence of alcohol swells the DNAPL ganglia by partitioning into the organic phase, which in turn facilitates DNAPL movement by reducing interfacial tension, viscosity, and enhancing flow properties. Experimental studies show that the water present in the alcohol-surfactant emulsion can also partition into the organic phase causing higher swelling of DNAPL (Damrongsiri et al., 2013). This process also serves to limit uncontrolled DNAPL downward

migration, which can occur during surfactant injection, by neutralizing gravitational forces (Ramsburg et al., 2003; Shook et al., 1998).

Numerous studies have assessed the performance of alcohol-surfactant emulsions in remediating DNAPL-contaminated aquifers, taking into account various factors such as the ions present in the aquifer, pH, aquifer temperature, and the temperature of the injected emulsion (Aydin et al., 2011; Mo et al., 2023b, 2023a). Other studies have evaluated the efficacy of the injection of alcohol-surfactant emulsions in heterogeneous systems, particularly where DNAPL is trapped in low permeability layers (Fu et al., 2022; Ramsburg et al., 2003; Ramsburg and Pennell, 2002).

Ramsburg et al. (2003) used a macroemulsion composed of 4.7% Tween 80, 1.3% Span 80, and 15% 1-butanol for in-situ density conversion of trichloroethene (TCE) in a heterogeneous, unconfined aquifer system. After approximately 1.2 pore volumes (PV) injection of the macroemulsion, a low-interfacial-tension (low-IFT) solution with 10% Aerosol MA (sodium bis(1,3-dimethylbutyl) sulfosuccinate which has been obtained from Cytec Industries), 6% 1-butanol, 15 g/L NaCl, and 1 g/L CaCl₂ was used to displace and recover DNAPL. This process resulted in successful TCE-NAPL displacement and 93% recovery of the introduced TCE mass after the injection of a combined 2.4 PV of the macroemulsion and low-IFT solutions. Fu et al. (2022) in an experimental study used sodium dodecyl sulfate (SDS)/1-butanol based in-situ microemulsion as the flushing solution for the remediation of soil contaminated by nitrobenzene as DNAPL, trapped in a low permeable zone surrounded by groundwater. Their findings indicated 15-fold improvement in the recovery of DNAPL compared to the SDS pure solution. Although, the efficiency of the injection of alcohol emulsions in heterogeneous soils has been discussed, their performance for remediation of a multilayer system is still inadequately understood. Indeed, the displacement of these emulsions in these systems presents unique challenges due to the existence of layers with differing permeabilities but nearly the same

thicknesses. The long presence of DNAPL in subsurface can destroy the natural microbiological consortium. Although the alcohols are harmful for the few remaining bacteria, the fast biodegradability of the remaining alcohol at low concentration combined with low residual saturation of DNAPL can accelerate the natural reappearance of the bacteria in the treated zone. If necessary, the post flush of alcohol can be proceeded by injection of polymer slug.

Polymer solutions with shear thinning behavior aid in minimizing channeling and facilitate the movement of surfactant into the different layers of the heterogeneous porous medium (Alamooti et al., 2022; Martel et al., 1998, 2004). By combining polymers and surfactants, DNAPL-saturated multilayer soils can be remediated effectively through the stabilization of the displacement front and a reduction in interfacial tension (Alamooti et al., 2023; Robert et al., 2006). Alamooti et al. (2023) showed in experimental and numerical studies that the addition of surfactant to the polymer solution improved for 0.07 the recovery of the DNAPL in the multilayer system. Nevertheless, even after the initial flushing using these methods, there may still be some DNAPL ganglia trapped in the porous media that cannot be further mobilized. While the back-diffusion of DNAPL from a less permeable zone poses challenges (Parker et al., 2003), employing a polymer solution can enhance pollutant mobilization, particularly when the solution contains alcohol for DNAPL mobilization/solubilization. In practical field applications, along with co-solvent injection, reactive biodegradation combined with polymer injection can be applied (Phenrat et al., 2011; Puigserver et al., 2023). An identified limitation of employing an alcohol-surfactant mixture in a multilayer system is the potential creation of preferential pathways in highly permeable layers; nevertheless, the use of a polymer solution provides control over channeling through these highly permeable layers (Alamooti et al., 2023; Martel et al., 1998; St-Pierre et al., 2004).

This study proposes using a mixture of polymer, surfactant, and alcohols as a post-injection remediation fluid for multilayer systems, taking advantage of the shear thinning feature of

polymers and alcohol's washing properties. Specifically, the shear thinning polymer xanthan, surfactant SDBS, water-soluble alcohol 1-propanol, and water-insoluble alcohol 1-hexanol were employed. Batch experiments were conducted to assess the partitioning and solubilization properties of alcohols, considering varying surfactant concentrations, alcohol volume fractions, and DNAPL volume fractions (vol%). Rheological analyses on different ASP mixtures were also carried out. 1D-column experiments were performed to evaluate the performance of post-injection of ASP mixtures following a primary injection of polymer-surfactant in two individual DNAPL saturated sand packs. A 2D tank with two layers was used to evaluate the efficiency of injecting ASP mixtures on residual DNAPL removal in multilayer systems.

The main objectives of this study are (i) the evaluation of the performance of varying vol% of 1-propanol and 1-hexanol and various concentrations of SDBS on dissolution or swelling of DNAPL; (ii) the assessment and the comparison of the injection of solubilization and mobilization flushing solutions in different injection scenarios (injection scenarios including post-injection, primary injection, several injection consequences, and different vol% of alcohols) in 1D-column; (iii) the comparison of the performance of the post-injection of solubilization and mobilization flushing solutions on remediation of residual DNAPL in a multilayer system.

3.2.3. Materials and methods

3.2.3.1. Experimental materials

In the 1D column and 2D tank experiments, the porous media consisted of two particle-size fractions of marble sand: 0.2-0.3 mm (with a permeability of 35 ± 5 darcy) and 0.4-0.6 mm (with a permeability 105 ± 10 darcy). Prior to use, the sand were washed with deionized water, and oven-dried for 10 hours at 105°C . The DNAPL used in the study is extracted from real polluted site at Tavaux (in France) and is consisted primarily of hexachlorobutadiene-HCBD (58%), hexachloroethane-HCA (14%), and penta-chlorobenzene (3.5%), as well as carbon

tetrachloride (4%). The density and viscosity of the multicomponent DNAPL are 1.66 g/mL and 4.47 mPa.s, respectively (Alamooti et al., 2022; Colombano et al., 2020). Xanthan gum, an anionic, water-soluble biopolymer, and SDBS, a biodegradable surfactant were employed in this study. Additionally, 1-propanol and 1-hexanol were used as water-soluble and water-insoluble alcohols, respectively, both with a 99% purity. Xanthan and SDBS solid powders, and the alcohols were all sourced from Sigma-Aldrich. For analyzing the solutions' rheological behavior, the Haake Mars 60 rotational rheometer with a cone-plate geometry was used. The concentration (mass) of DNAPL in organic phase was determined by density analysis of recovered organic phase and gas chromatography. For density analysis, the density and volume of recovered organic phase was measured and considering the densities of alcohols and DNAPL the DNAPL content was found. For DNAPL concentration in aqueous phase, only gas chromatography was used. For gas chromatography, AGILENT 8890 gas chromatograph with a thermal conductivity detector at 280°C and an injector for chromatograph columns filled at 250 °C. Agilent CP-SIL 5 CB chromatograph columns were used with polydimethylsiloxane as the active phase and helium as the carrier gas. Gas chromatography is able to provide the concentration of alcohols and DNAPL in both aqueous and organic phases.

3.2.3.2. Batch experiment

Batch experiments were conducted to investigate the role of alcohols in the mobilization and solubilization of DNAPL. The experimental materials consisted of solutions prepared with deionized water, a mixture of 1-propanol and 1-hexanol, and the surfactant SDBS. The solutions were mixed with DNAPL, in vol% of 20% and 10%, within 50 mL polyethylene flasks. The SDBS was first dissolved in water at concentrations ranging from 0 to 100 g/L (specifically 0, 1, 5, 10, 25, 50, and 100 g/L) to form the aqueous phase. This aqueous phase was then mixed with the 1-propanol and 1-hexanol mixture at volume percentages of 25% and 50% to prepare the final mixtures. The mixtures of 1-propanol and 1-hexanol was prepared at different volume

proportions of 1:0, 3:1 1:1, 1:3, and 0:1. The AS mixtures were mixed with DNAPL using a Laboshake Gerhardt® shaker and mixed continuously for a period of 24 hours. Subsequently, the Sigma 3-30ks centrifuge was used to separate the phases (organic and aqueous) at a speed of 10,000 rpm for a duration of 30 minutes. The changes of DNAPL volume, which we will refer to as the organic phase post-process, serves as an indicator of the active remediation mechanism. Following the separation, the volume of both the organic and aqueous phases was recorded, and their respective densities were measured using pycnometers.

3.2.3.3. 1D column

The 1D-column experiments aimed to examine the displacement of DNAPL within two separate sand packs of varying permeabilities. The procedure involved an initial injection of a XS (0.8 g/L of xanthan and 1.265 g/L SDBS) mixture, followed by a post-injection of an ASP mixture. The column was made of a glass tube with a 2 cm radius and a 30 cm length (Figure 3.2-1). It was gradually filled with sand, flushed with CO₂ for 30 minutes to remove trapped air, and then saturated with degassed deionized water at a steady flowrate of 0.1 mL/min using an Ismatec® Reglo ICC digital peristaltic pump. Afterward porosity and permeability were measured. Porosity was assessed using the volumetric method, involving measurements of dry weight and the fully saturated water-wet weight of the column. Permeability, on the other hand, was measured by varying the flow rate and recording the pressure drop within the framework of Darcy's law. Next, DNAPL was introduced at a fixed rate of 1 mL/min until residual water saturation was achieved. Then, the XS mixture was injected at a constant flow rate of 1 mL/min until reaching residual DNAPL saturation. Residual saturations were determined when no further recovery of the displaced phase was observed in the effluent. This was followed by the injection of an ASP mixture at the same flow rate for approximately 2 PV. The effluents were collected in 15 mL propylene tubes, while the differential pressure along the column was monitored using KELLER PR33X. The DNAPL recovery during the primary injection was

measured volumetrically. For the ASP mixture post-flush, the organic and aqueous phase volumes were recorded and their densities were measured. Then, the organic and aqueous phases from every 3 to 4 tubes were individually combined, diluted, and analyzed using a gas chromatography apparatus.

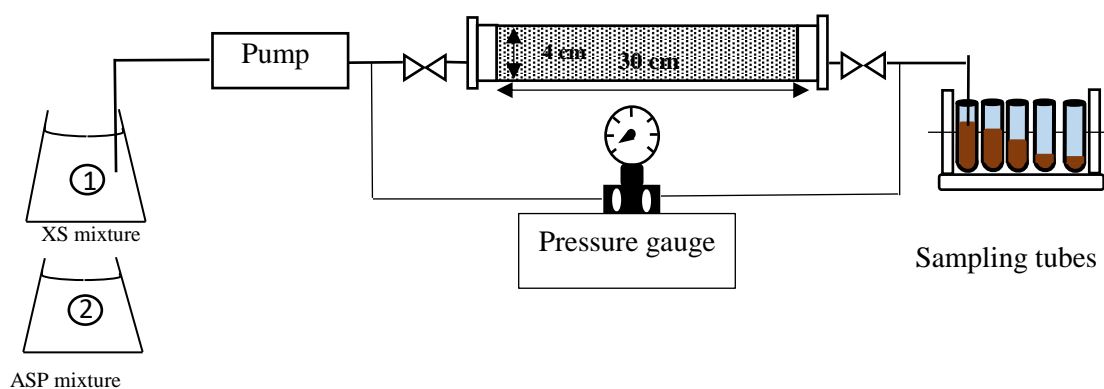


Figure 3.2-1 Schematic of polymer-surfactant injection (container 1) followed by ASP mixture injection (container 2) for DNAPL displacement in 1D column

3.2.3.4. 2D tank

To test the efficiency of the developed flushing solutions on a multilayer system, a confined 2D tank equipped with pressure measurement transducers was employed. The tank measures 15 cm in length, 10 cm in height, and 2 cm in width. It contains two ports on the left side, three ports on the bottom, three ports on the top and one port on the right side. The 2D tank sets up with two distinct layers: a less permeable layer (35 Darcy) at the bottom with a thickness of 5 cm and a more permeable layer (105 Darcy) on top, also with a thickness of 5 cm. The layers were packed under water and then saturated by DNAPL from the ports located at the bottom of the tank, leaving a residual water saturation. In primary injection step, the XS mixture was injected using two ports (in correspondence of layers) located on the left part of the tank at the fixed injection rate of 2×0.5 mL/min, and the DNAPL was naturally recovered through the port located on the right bottom side of the tank at ambient pressure. Then two different ASP mixtures (providing improved recovery by mobilization and solubilization) were individually

injected into the layers at residual DNAPL saturation (in two different experiments with similar experimental setup and initial conditions). The injection processes for the 2D system are visually represented in Figure 3.2-2.

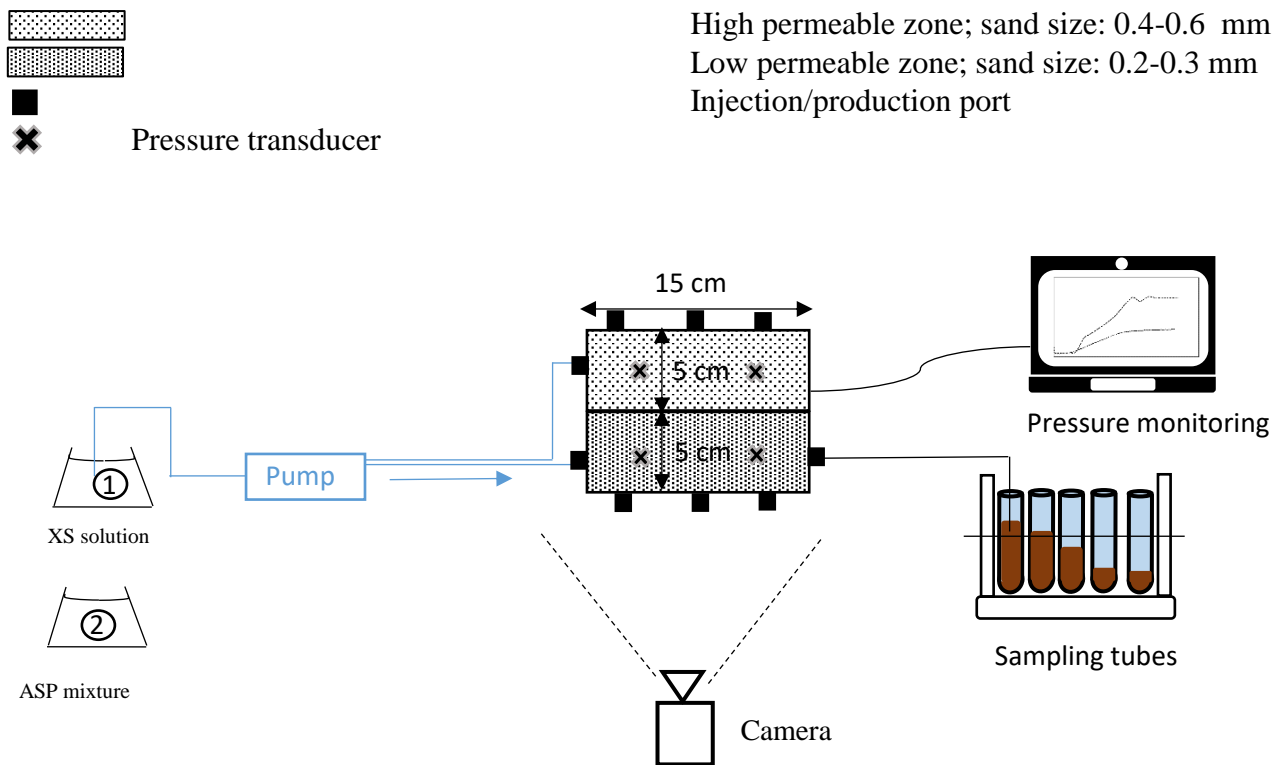


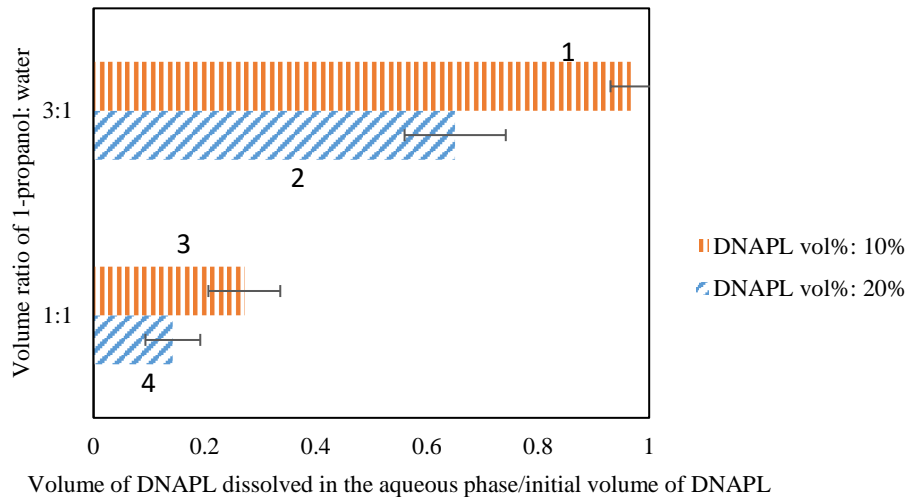
Figure 3.2-2 Schematic of polymer-surfactant injection (container 1) followed by ASP mixture (container 2) injection for DNAPL displacement in the 2D tank (multilayer system)

3.2.4. Results and discussion

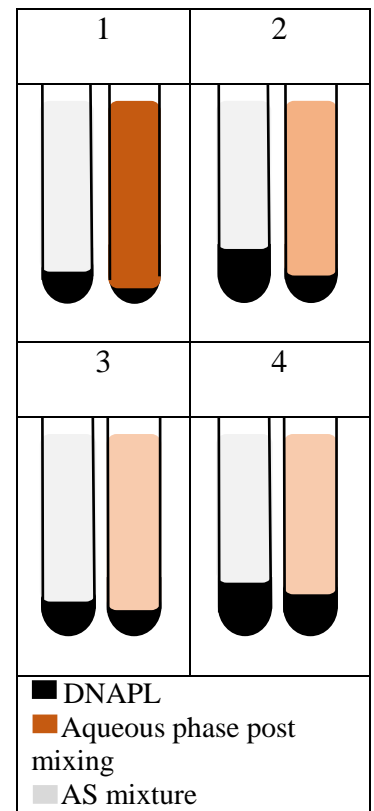
3.2.4.1. Partitioning behavior alcohol-surfactant mixture and DNAPL

Our batch experiments revealed that surfactant concentration does not significantly influence the results. Therefore, for subsequent analyses, the results were averaged across all surfactant concentrations, and the error bars have been displayed on the corresponding graphs. The volumes of the organic and aqueous phases (after mixing and separation in batches) were found to be primarily influenced by the volume fractions of the alcohols, water, and DNAPL. A sort of batch experiments has been performed in the presence polymer. We found that the presence

of polymer in the mixture does not significantly affect the partitioning behavior of alcohols. Also, the separation of phases by centrifuge for the mixtures containing polymer was long; therefore, the batch experiments were performed only with AS mixtures. The batch experiments showed that when 1-propanol is the sole alcohol in the AS mixture, DNAPL dissolves in the aqueous phase. As illustrated in Figure 3a, a higher 3:1 ratio of 1-propanol to water results in increased DNAPL dissolution. Specifically, for initial volume fractions of DNAPL at 10% and 20%, approximately 0.97 and 0.65 of the initial DNAPL dissolves into the aqueous phase, respectively. In contrast, with a lower 1:1 ratio of 1-propanol to water, the same initial volume fractions of DNAPL lead to only about 0.27 and 0.14 dissolution, respectively. When a larger volume of the DNAPL comes in contact with AS mixture, a lower fraction of the organic phase is dissolved, owing to the AS limited solubility capacity. The results show that the solubility of DNAPL in AS mixture is around 0.27 g/mL for higher 3:1 ratio of 1-propanol to water and 0.054 g/mL for lower 1:1 ratio of 1-propanol to water. In Figure 3b, tubes on the left represent the state before mixing, while those on the right depict the state after mixing. The gray color indicates the AS mixture prior to mixing. DNAPL is represented by the black color, and the brownish phase signifies the aqueous phase post-mixing. A darker shade of brown suggests a higher degree of DNAPL dissolution in the AS mixture.



(a)



(b)

Figure 3.2-3 Dissolution of DNAPL in contact with AS mixtures containing solely 1-propanol (a) graph showing the dissolution rates, and (b) schematic of dissolution: tubes on the left represent the state before mixing, while those on the right depict the state after mixing. The gray color indicates the AS mixture prior to mixing. DNAPL is represented by the black color, and the brownish phase signifies the aqueous phase post-mixing

Contrarily, when 1-hexanol is included in the AS mixture, there's an increase in the volume of the organic phase. Figure 3.2-4 presents the swelling factor of the organic phase, defined as the ratio of the volume of the organic phase after contact with the AS mixture (mL) to the initial volume of DNAPL (mL). This is plotted against the volume ratio of 1-propanol to 1-hexanol, for various volume fractions of water in the AS mixture and of DNAPL in contact with the mixture. The results indicate that a lower volume fraction of DNAPL in contact with the AS mixture, such as 10% (5 mL DNAPL and 45 mL AS mixture), leads to a more pronounced increase in the volume of the organic phase. Another significant factor influencing the swelling of the organic phase is the volume fraction of water in the AS mixture. A higher volume fraction

of alcohol results in a greater swelling factor. For instance, when the volume fraction of water in AS mixture is 25% (meaning 75% of alcohol in the AS mixture) and the volume fraction of DNAPL is 10%, a swelling factor of more than 8 can be observed. These findings also suggest that the volume ratio of 1-propanol to 1-hexanol does not noticeably influence the partitioning of alcohols into the organic phase.

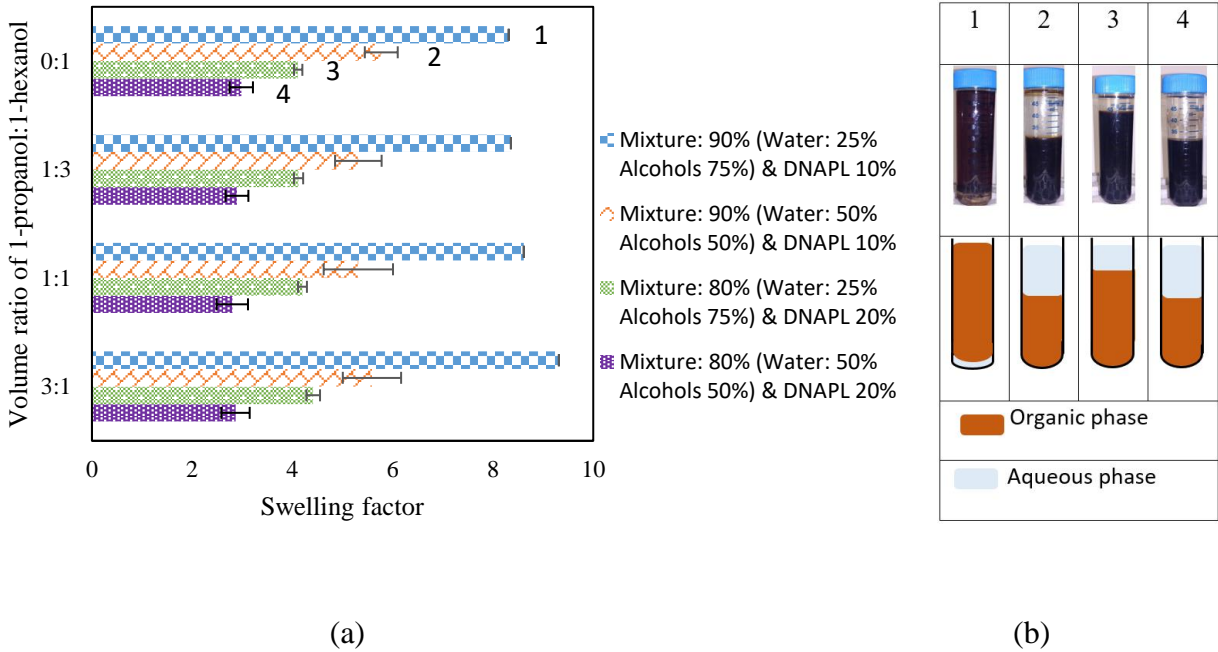


Figure 3.2-4 a) Swelling factor of organic phase versus volume ratio of 1-propanol:1-hexanol for various water/alcohol and DNAPL volume fractions (b) schematic of dissolution for the case 0:1

The results obtained from the swelling factor of the organic phase are consistent with those from the density analysis of the organic phase, as shown in Figure 3.2-9 (in supplementary materials). This analysis demonstrates that samples with a higher swelling factor (i.e., a sign of greater partitioning of alcohols into the NAPL) exhibit lower densities.

As previously mentioned, in the absence of 1-hexanol, DNAPL dissolves into the aqueous phase containing 1-propanol. However, as Figure 3.2-4 demonstrates, when 1-hexanol is

present, a substantial portion of both 1-propanol and 1-hexanol partitions into the NAPL phase, leading to a high swelling factor.

The analysis of alcohol content in the organic and aqueous phases performed by gas chromatography, shown in Figure 3.2-10 (in supplementary materials), reveals that when 1-hexanol is present and the volume fraction of water is lower (i.e., 25%) in the AS mixture, the majority of 1-propanol (between 90% to 100%) partitions into the organic phase. Conversely, when the volume fraction of water is higher (i.e., 50%), a smaller proportion of 1-propanol (~70%) partitions into the organic phase. For all cases, when 1-hexanol is present in the AS mixture, all of the 1-hexanol partitions into the organic phase.

3.2.4.2. Selection of the flushing mixtures

The results obtained from batch experiments indicate that a solution containing only 1-propanol as the alcohol leads to the solubilization mechanism, while AS mixtures containing both 1-propanol and 1-hexanol, or only 1-hexanol, result in the mobilization mechanism. Consequently, three AS mixtures were selected for the remediation of soils at residual DNAPL saturation. These include mixtures consisting of 50% volume fraction of 1-propanol and 50% of surfactant solution, 25% of 1-propanol, 25% of 1-hexanol, and 50% of surfactant solution, and also 50% 1-hexanol and 50% surfactant solution. The surfactant also helped to improve the stability of the mixture of alcohols and water, especially in the presence of 1-hexanol.

Given that the surfactant concentration does not significantly influence the partitioning behavior of alcohols, a low concentration of 1 g/L was chosen. Rheological analysis of these AS mixtures reveals that they exhibit Newtonian behavior, with a viscosity of approximately 3 mPa.s for the AS mixture containing solely 1-propanol as alcohol, and 16 mPa.s for AS mixtures containing 1-hexanol (regardless of presence of 1-propanol).

To enable the injection of the AS mixtures into a multilayer system, a polymer was added to them. The polymers have the non-Newtonian behavior and can help the displacement of DNAPL in layered system where the permeabilities are different. For this purpose, xanthan, a biopolymer, was selected. The stability of the newly formed ASP mixtures with the polymer was evaluated. It was shown that for cases where the volume fraction of water was 25%, the ASP mixture was unstable, either two distinct phases or visually discernible wormlike micelles appeared. While for a 50% volume fraction of water, a highly stable mixture was formed that lasted several days. It's important to note that mixtures without surfactant in contact with the polymer immediately became unstable.

The rheological behavior of the mixtures with a xanthan concentration of 2 g/L in the surfactant solution was evaluated. As seen in Figure 3.2-5, the addition of alcohols to the surfactant-polymer solution (1 g/L of SDBS and 2 g/L of xanthan) resulted in higher viscosities compared to the primary remediation fluid i.e. XS (1.26 g/L of SDBS and 0.80 g/L of xanthan (Alamooti et al., 2023)) mixture that was chosen to be injected into the DNAPL-saturated soil. All ASP mixtures showed a shear thinning behavior, while in the range of working shear rate i.e. around 1-10 1/s, the highest viscosity can be observed for the 25% of 1-propanol, 25% of 1-hexanol and 50% of surfactant-polymer solution (C₃-C₆), and also 50% 1-hexanol and 50% surfactant-polymer solution (C₆), which have a viscosity approximately 17 times that of the XS mixture. The ASP mixture consisting of 50% volume fraction of 1-propanol and 50% of surfactant-polymer solution (C₃) also has a viscosity around 5 times that of the XS mixture.

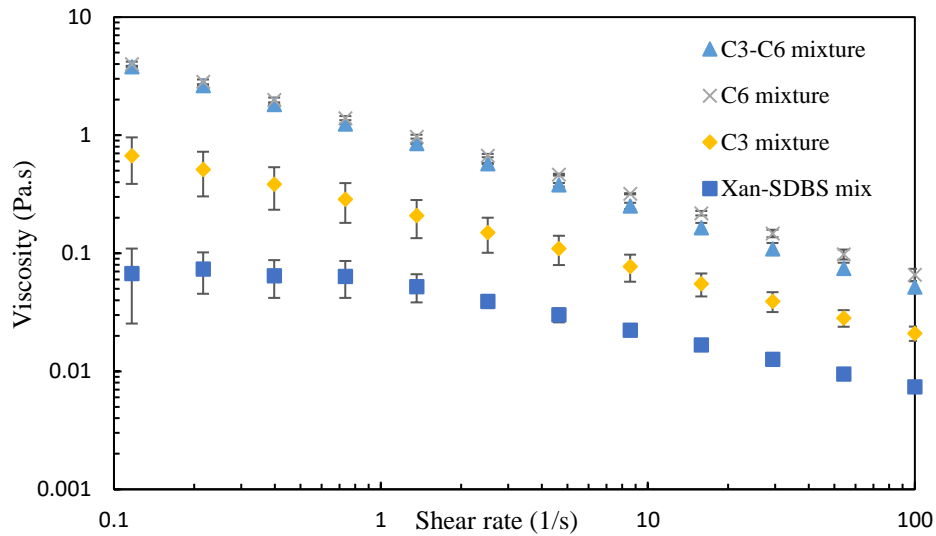


Figure 3.2-5 Viscosities of different ASP mixtures containing xanthan with concentration of 2 g/L, as well as XS mixture

3.2.4.3. 1 D column experiments

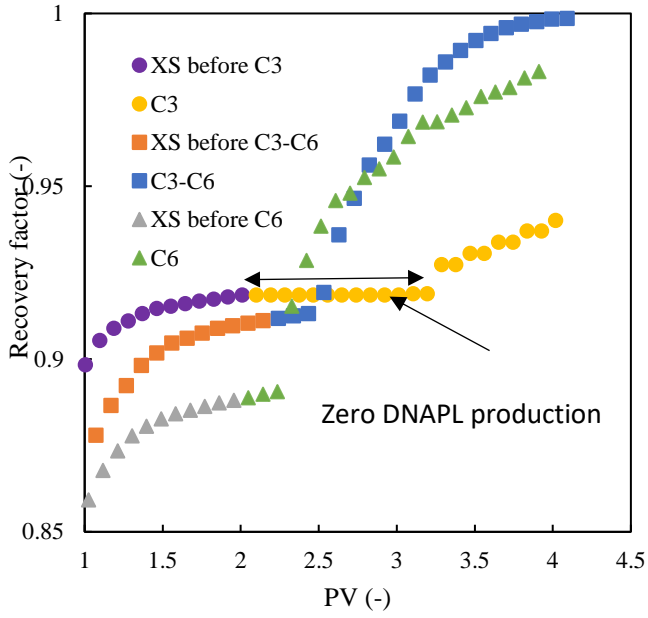
Column experiments were conducted to evaluate the performance of selected ASP mixtures in the remediation of soils of varying permeabilities at residual DNAPL saturation. To this end, the XS solution was first injected into DNAPL-saturated columns packed with both coarse and fine sand. Figure 3.2-6 illustrates the recovery factor $\left(\frac{\text{volume of DNAPL recovered}}{\text{initial volume of DNAPL in porous media}}\right)$ and differential pressure for the period after 1 PV injection of the XS mixture, as well as the subsequent injection of ASP mixtures, displayed against cumulative PV, for both high and low permeable porous media.

These results indicate that the recovery curves for the post-injection of C₃-C₆ and C₆ mixtures follow a similar trend in both high and low permeability 1D columns. In the early stages of injecting alcohol solutions containing 1-hexanol, for approximately 0.3 PV of post injection (between ~2 and 2.3 PV) there is not a noticeable DNAPL recovery. However, DNAPL begins to emerge in the effluent after approximately 0.3 PV of post-injection of ASP mixture. This is attributed to alcohols partitioning into the trapped DNAPL ganglia within the pore space,

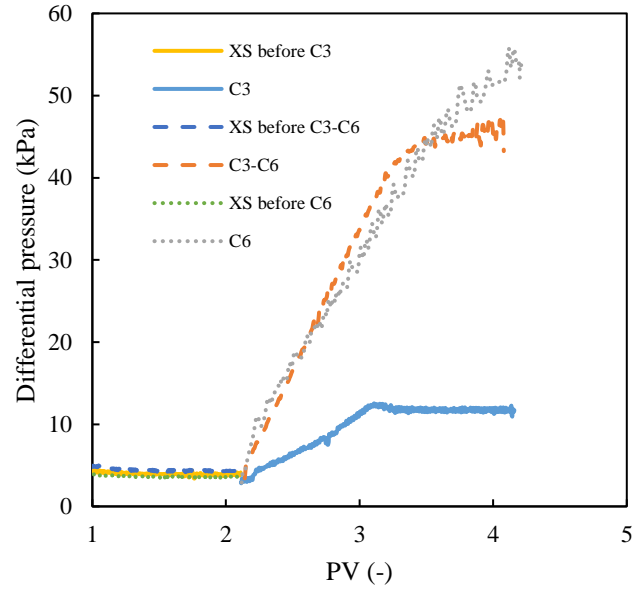
causing them to swell and eventually coalesce to form larger droplets capable of migrating through the porous media (St-Pierre et al., 2004). Consequently, an organic phase, containing both DNAPL and alcohols, starts appearing in the effluent. This phase, having a density lower than the original DNAPL, eventually transitions into a LNAPL. **Figure 3.2-11** (in supplementary materials) visually demonstrates this, as the organic phase progressively lightens in both color and density with the continued injection of the C₃-C₆ mixture in high-permeability layers. The color of the recovered organic phase in individual samples shifts from very dark initially to much lighter by the end. The differential pressure curves for the 1-hexanol containing mixtures are consistent with rheological behavior, reflecting the similar behavior observed in the C₃-C₆ and C₆ mixtures.

In contrast, the C₃ mixture, when introduced into columns at residual DNAPL saturation, leads to the emergence of the organic phase only after 1.3 PV post injection of C₃ mixture, indicating a solubilization mechanism. The C₃ mixture begins dissolving the residual DNAPL into the aqueous phase, moving through the porous media. Once maximum solubility is reached in the aqueous phase, the subsequent slug of the C₃ mixture continues this dissolution process. To see the DNAPL in the effluent, the aqueous phase containing dissolved DNAPL needs to reach the effluent. As a result, DNAPL is absent in the effluent until after 1 PV of post-injection, and then it is recovered at a constant recovery rate (fixed slope). It should be noted that in this case, no DNAPL is recovered as individual organic phase, and all NAPL is recovered through aqueous phase. The mechanisms of DNAPL recovery for different ASP mixtures in both high and low permeable porous media are similar; however, the differential pressure for low permeable porous media is around three times more than high permeable layer corresponding to their permeabilities. XS injection in the higher permeable layer led to a slightly higher recovery rate (~2%), and displacement patterns were consistent between layers. Additionally,

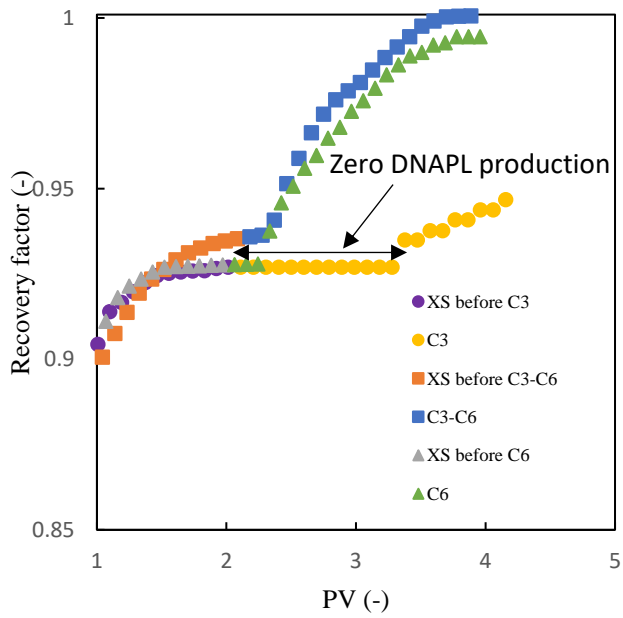
a two-layer system composed of both high and low permeable layers is needed to observe the preferential pathway.



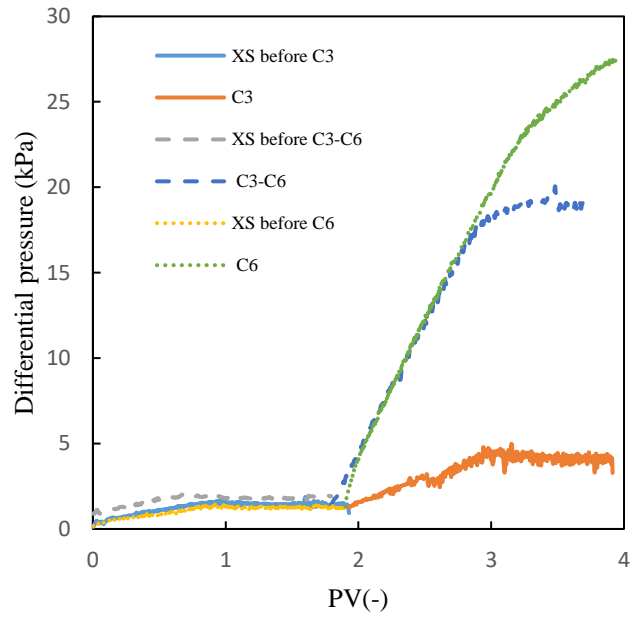
(a)



(b)



(c)



(d)

Figure 3.2-6 Experimental results of post-injection of ASP mixtures in columns: (a) recovery factor for low permeable layer, (b) differential pressure for low permeable layer, (c) recovery factor for high permeable layer, and (d) differential pressure for high permeable layers

As previously noted, the recovery of DNAPL through the post-injection of ASP mixtures in the columns experiences a delay (around 1 PV for the C₃ mixture and 0.3 PV for the C₃-C₆ and C₆ mixtures). **Figure 3.2-12** (in supplementary materials) depicts the DNAPL content in effluent samples against the cumulative injected PV for both solubilization and mobilization mechanisms. The DNAPL content in effluent was determined by analysis of density of recovered organic phase as well as the gas chromatography. For the analysis of recovered DNAPL in aqueous phase, only gas chromatography has been used. The first sample in which DNAPL starts to appear in the effluent, exhibits the highest DNAPL content.

For the solubilization mechanism (using the C₃ mixture), this high DNAPL content can be attributed to the fact that the front of the ASP mixture has the most DNAPL dissolved within it. Meanwhile, for the mobilization mechanism, this elevated DNAPL content is due to the partitioned alcohols. These alcohols increase the size of trapped DNAPL droplets and mobilize a significant portion of it through the coalescence of newly swollen DNAPL ganglia. Consequently, the first sample with DNAPL has the richest DNAPL content. This observation aligns with the density measurements of the organic samples during the mobilization mechanism; samples with a higher DNAPL content show a greater density, which eventually converges to the density of the alcohols (densities of 1-propanol and 1-hexanol are 0.803 and 0.814 g/mL respectively).

3.2.4.4. Evaluating different injection scenarios for DNAPL mobilization mechanism in columns

As it is shown in the previous section, the post-injection of mobilization ASP mixtures (specifically those containing 1-hexanol) leads to a recovery factor improvement of roughly 0.09 and 0.07 for low and high permeable porous media, respectively. Notably, while the post-injection of these mixtures quickly enhanced the recovery factor by recovering more DNAPL, a plateau was observed during the latter stages of ASP mixture injection.

To further investigate, two scenarios using one of the mobilization ASP mixtures (C₃-C₆) were assessed as following;

The mixture was directly introduced to columns saturated with DNAPL at residual water saturation.

A sandwich method was employed: following an initial 2 PV injection of XS mixture, only 0.5 PV of the C₃-C₆ mixture was introduced, which was then flushed with the same XS solution as initially used.

Figure 3.2-13 (in supplementary materials) presents the results. For both low and high permeable layers, a 0.99 recovery efficiency was achieved after the injection of approximately 1.5 PV of direct mixture of C₃-C₆ injection. In contrast, with a full post-injection of C₃-C₆, 1.3 PV was required to attain the same efficiency. In the sandwich method, 0.5 PV of ASP mixture injection improved the recovery factor by 0.03, and subsequent flushing further improved recovery by another 0.02-0.03, after which DNAPL recovery ceased. Interestingly, the sandwich method achieved a ~0.06 recovery factor improvement with just 0.5 PV of ASP between two periods of XS injection. Conversely, for the full post-injection approach, approximately 1 PV was necessary to achieve comparable recovery factor improvements following the initial XS injection.

3.2.4.5. 2D tank experiments

To evaluate the efficiency of ASP mixtures in a multilayered system, 2D tank experiments were carried out as detailed in section 3.2.2.4. To compare the solubilization and mobilization processes, two ASP mixtures were used in the post-injection phase (following an initial injection with the XS mixture) in the multilayer system. To this end, the C₃ as the solubilization and C₃-C₆ as the mobilization mixtures were chosen.

Figure 3.2-7 illustrates the consequences of DNAPL recovery in a multilayer system, first using XS and then the C₃ mixture. This figure shows that the XS solution effectively displaces DNAPL from both layers. This displacement is influenced by density differences, where the invading solution is overriding the DNAPL, in response to density difference between the invading and defending phases (Alamooti et al., 2023). Upon subsequent injection of the C₃ mixture, two distinct zones appear: the dark and white zones. These are highlighted by white and black dashed lines, respectively.

Consistent with observations from the column experiments, the injection of the C₃ mixture initiates the dissolution of DNAPL, forming a dark zone indicative of near-maximum solubility. This dark zone advances thanks to the driving force provided by the continuous injection of C₃ mixture. The ASP mixture in the front of the dark zone is near the maximum solubility of DNAPL, where further DNAPL dissolution becomes negligible, leaving behind residual DNAPL. Behind the front of the dark zone, the ASP mixture continues the dissolution of the remaining DNAPL. This phenomenon gives rise to a transition zone, characterized by a DNAPL concentration gradient in the aqueous phase that descends from its maximum at front to nearly zero at its rear. Subsequent to this transition zone is the white zone, which represents regions where DNAPL has been largely dissolved or flushed out by the C₃ mixture. While the dark zone's propagation correlates directly with the injected pore volume (e.g., at 0.7 PV injection, the dark zone encompasses 60% of the tank's surface area), the white zone's advancement is notably slower, covering only an additional 20% of the surface area between

1.58 and 2.1 PV. This may be attributed to the role of boundary conditions, particularly the presence of a single outlet port. This port seems to cause a significant pressure gradient near the production area, possibly creating a preferential pathway for the C₃ mixture and bypassing some untouched zone in the layers.

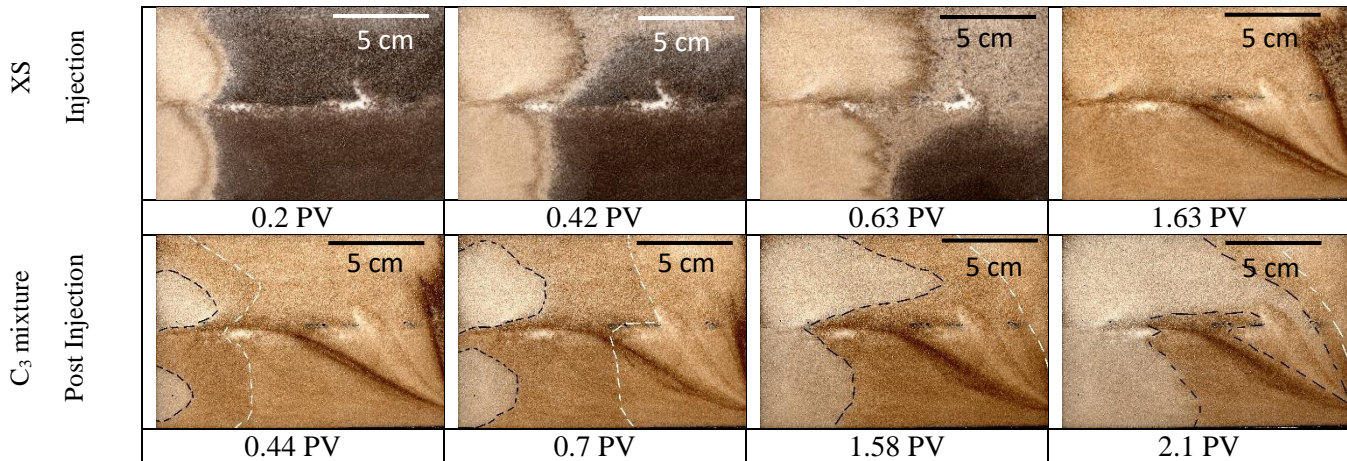


Figure 3.2-7 DNAPL displacement in a 2D multilayer system by injection of XS solution (first row) and subsequent injection of C₃ mixture (second row) against the number of PVs injected of each solution

Figure 3.2-14 (in supplementary materials) displays both the recovery factor and the differential pressure during the initial injection of XS and the subsequent injection of the C₃ mixture into the multilayer system. As observed in the column experiments, DNAPL starts to appear in the effluent after 1 PV of C₃ mixture injection and is recovered at a steady rate. Post-injection of C₃ mixture has improved the recovery factor for approximately 0.02. The differential pressure between the pressure ports in each layer as shown in Figure 3.2-2, curves align with the injection process, showing a higher pressure gradient in the less permeable layer, and a notably higher gradient for the C₃ mixture post-injection compared to the XS injection which is attributed to its higher viscosity. For the case of post-injection of C₃-C₆ mixture in the multilayered system in the 2D tank, in accordance with the column experiments the mobilization mechanism has

been observed. Likewise, the C₃ mixture post-injection, firstly a XS mixture has been injected until no more DNAPL was recovered, then the C₃-C₆ mixture was introduced into the layered system at residual DNAPL saturation. As this mixture was introduced, the alcohols within it began partitioning into the DNAPL ganglia, causing them to move, therefore showing the mobilization mechanism. As it can be seen in Figure 3.2-8, just after the injection of 0.3 PV of the C₃-C₆ mixture mobilized DNAPL droplets have arrived at the recovery point.

These dark droplets gradually lightened as more of the mixture moved into the layers. This is because as the amount of the remaining DNAPL in the layers decreased, the dark color associated with it started to fade.

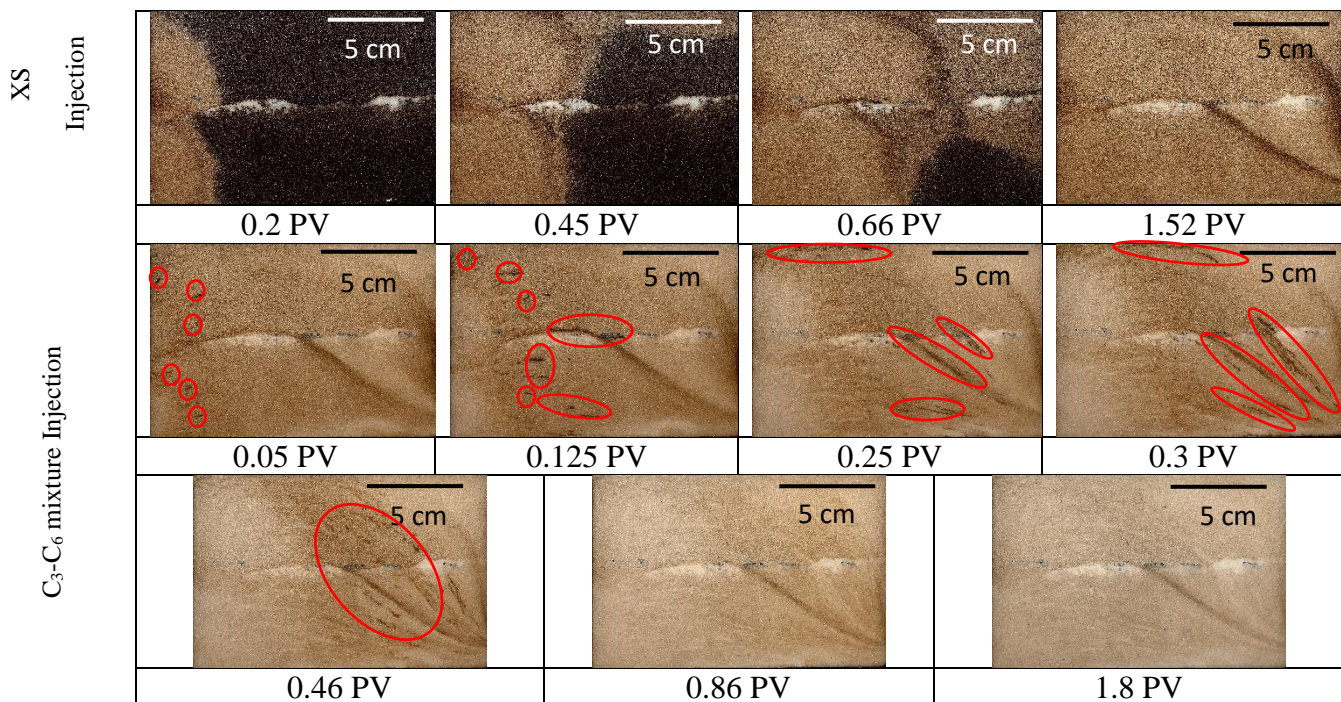


Figure 3.2-8 DNAPL displacement in a 2D multilayer system by injection of XS solution (first row) and subsequent injection of C₃-C₆ mixture (second and third rows) against the number of PVs of each solution injected, mobilized ganglia are shown by red circles

Figure 3.2-15 (in supplementary materials) presents respectively the recovery factor and differential pressure in each layer for the C₃-C₆ mixture's post-injection into the multilayered system. It reveals that the injection of this mixture has enhanced the recovery factor by approximately 0.08. Similarly, the differential pressure curves align with the findings from the column experiments.

The injection of the C₃-C₆ mixture exhibits a higher pressure (around 13 kPa and 8 kPa at the end of post injection for low and high permeable layers respectively) than the injection of the C₃ mixture (around 3.3 kPa and 1.5 kPa at the end of post injection for low and high permeable layers respectively). It can be attributed to the higher viscosity of the C₃-C₆ mixture compared to C₃ mixture.

3.2.5. Conclusion

Experiments were carried out to assess the effectiveness of alcohol-surfactant-polymer mixtures in remediating layers polluted by DNAPL at residual saturation. Xanthan (polymer), SDBS (surfactant), and 1-propanol and 1-hexanol (water-soluble and water-insoluble alcohols) were incorporated in the mixtures. A variety of experimental devices, including batch, column, and 2D tank experiments, as well as rheological analysis, were used.

Batch experiments revealed that the inclusion of 1-hexanol in the AS mixture led to alcohol partitioning in the DNAPL phase, swelling the organic phase. Conversely, when 1-propanol was the sole alcohol in the mixture, DNAPL was dissolved in the aqueous phase. Rheological analysis demonstrated that for AS mixtures with 50% volume fraction of alcohols, those containing 1-hexanol either 25% or 50% volume fraction could yield a viscosity three times

higher than mixtures with only 1-propanol. The rheological analysis showed that by adding the alcohols to the polymer-surfactant solution the non-Newtonian behavior has been retained. Column experiments, performed after primary injection of the XS solution, revealed two unique mechanisms. The post-injection of ASP mixtures with 1-hexanol resulted in DNAPL appearing in the effluent after injecting 0.3 PV, indicating the mobilization mechanism due to alcohol partitioning into trapped DNAPL. In contrast, the post-injection of C₃ mixture initiated DNAPL dissolution, signifying a solubilization mechanism. Here, DNAPL only appeared in the effluent after 1 PV. In a set of individual column experiments, a sandwich method of post-injection of the mobilization mixture was proposed. This method improved the recovery factor by roughly 0.06 with only 0.5 PV injection of the mixture, compared to 1 PV in a full post-injection scenario.

2D tank experiments were conducted to visually compare the solubilization and mobilization processes. Initial injection of the XS mixture effectively displaced DNAPL from both layers. The post-injection of the C₃ mixture initiated DNAPL dissolution, forming a dark zone with the DNAPL concentration gradient, followed by a white zone where DNAPL had been largely dissolved. Post-injection of the C₃-C₆ mixture showcased the mobilization mechanism, with alcohol partitioning into DNAPL causing mobilization. This was illustrated by the formation of moving DNAPL droplets within the layers, where the swollen DNAPL ganglia became interconnected, mobilized and reached the recovery point only after 0.3 PV. As the invasion of new ASP mixture progressed, the dark color of these mobilized droplets gradually faded. The post-injection of the C₃ mixture enhanced the recovery factor by 0.02 and generated a lower pressure gradient compared to the C₃-C₆ mixture. In contrast, the C₃-C₆ mixture led to a larger improvement in the recovery factor, approximately 0.08. These results show that post-injection

of ASP mixture can minimize the residual saturation of DNAPL in layered system and achieve a promising displacement efficiency.

3.2.6. Appendix

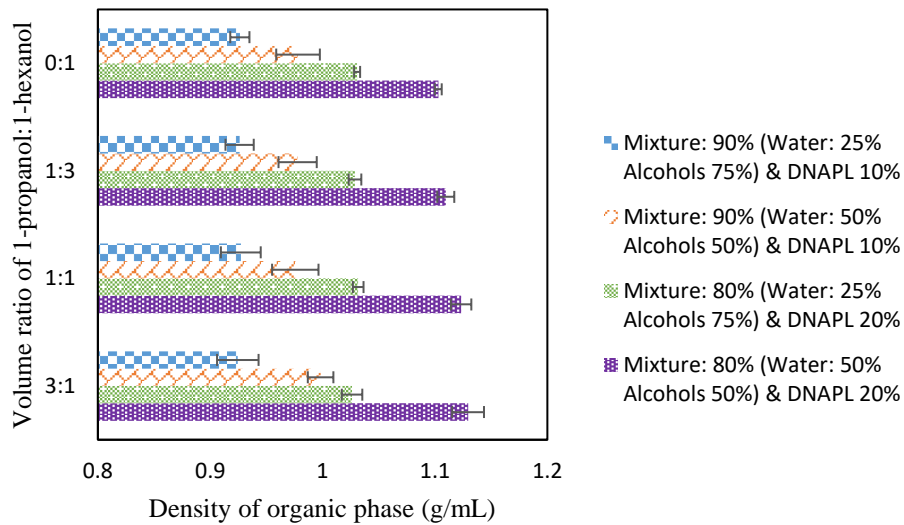


Figure 3.2-9 Densities of organic phase versus volume ratio of 1-propanol:1-hexanol

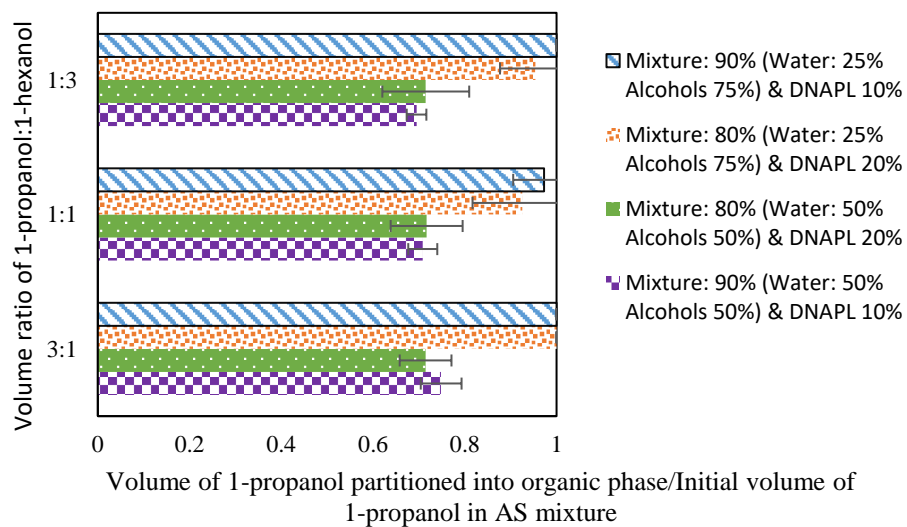


Figure 3.2-10 Partitioning of 1-propanol into organic phase versus volume ratio of 1-propanol: 1-hexanol

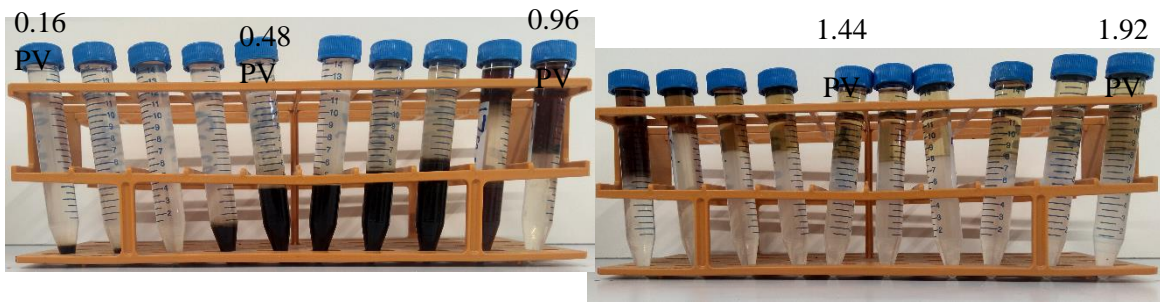
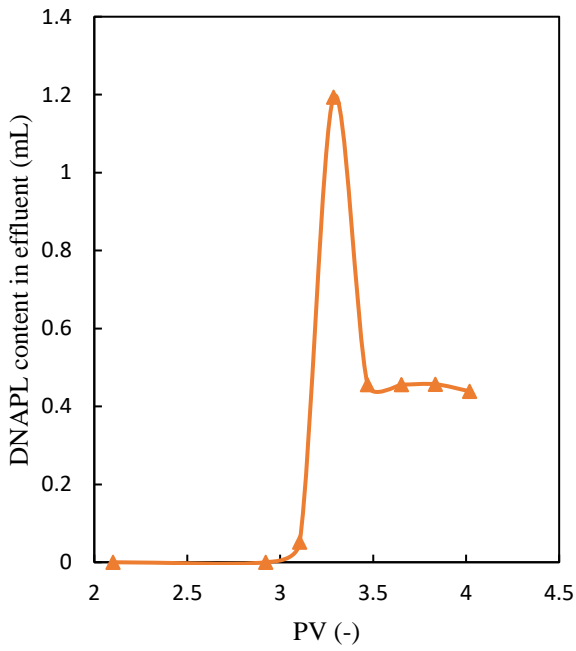
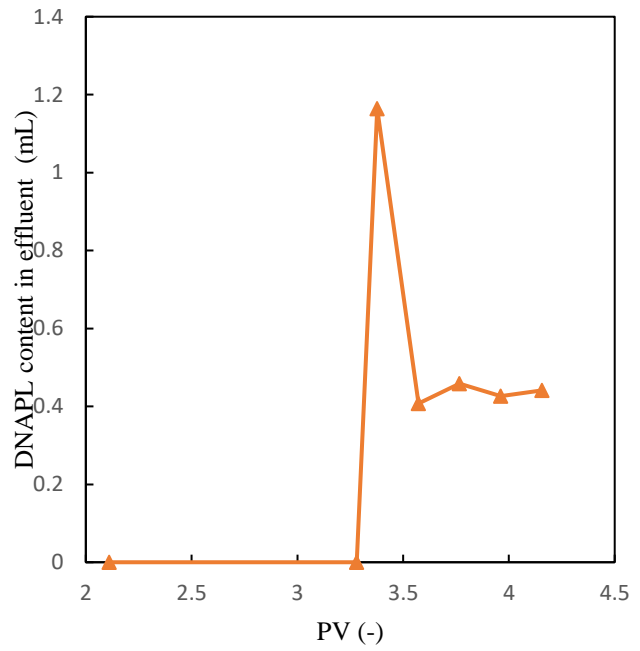


Figure 3.2-11 Samples (from left to right) chronologically obtained from the post-injection of C₃-C₆ mixture in a high-permeability layer at residual DNAPL saturation (the corresponding PVs of post-injection are shown above the samples)



(a)



(b)

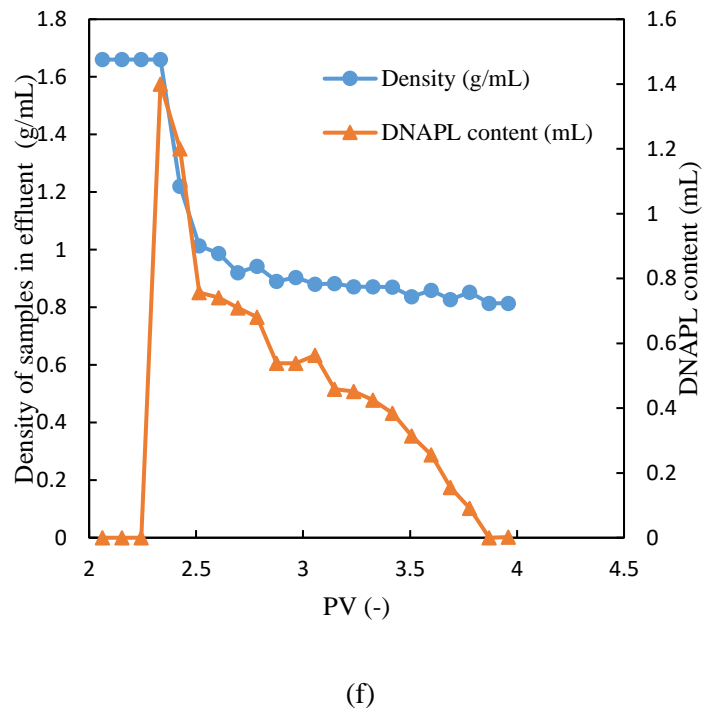
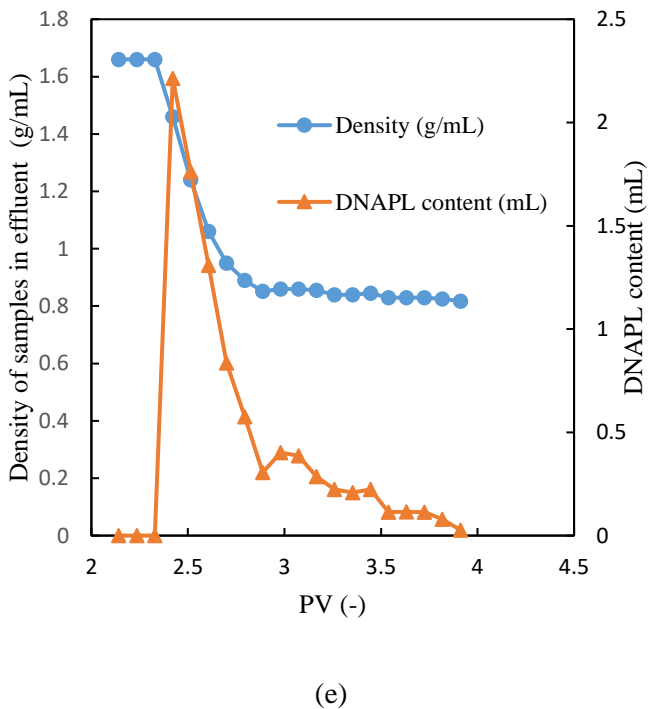
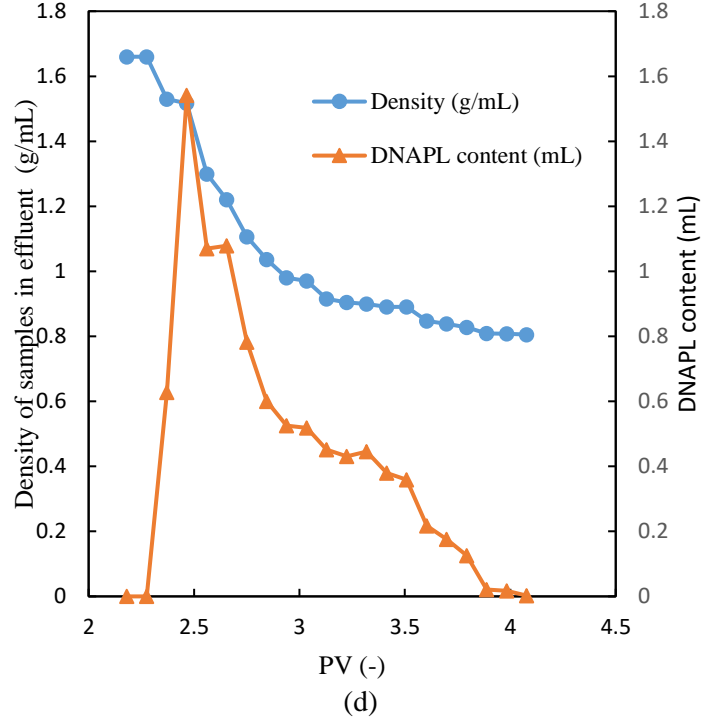
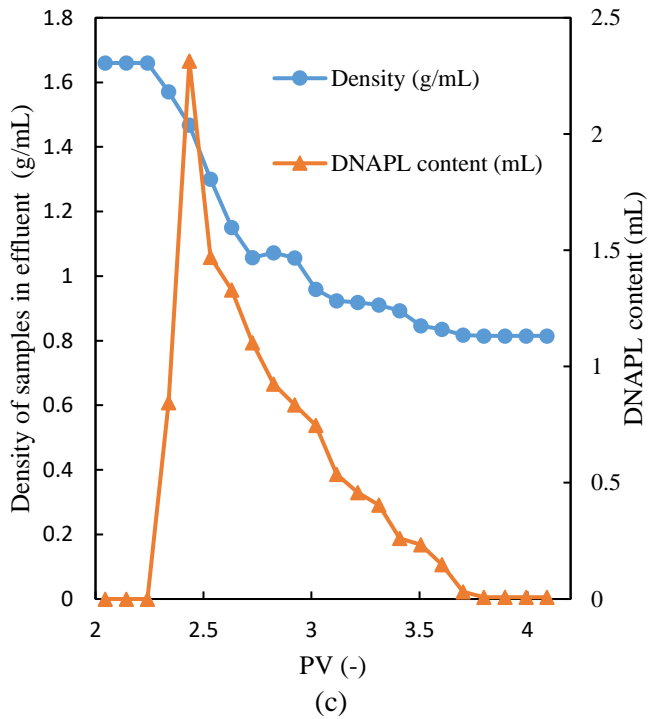
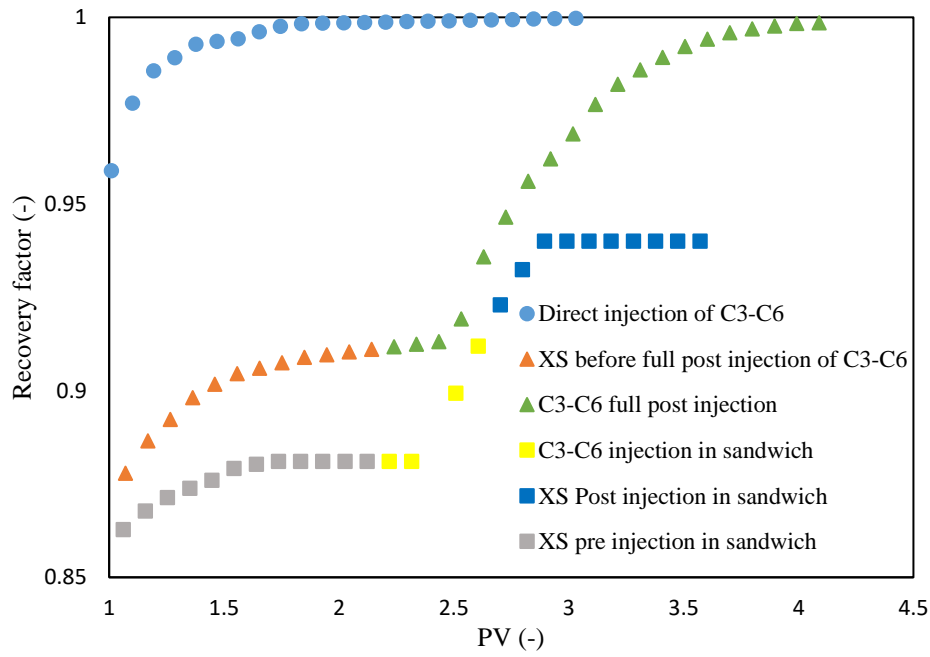
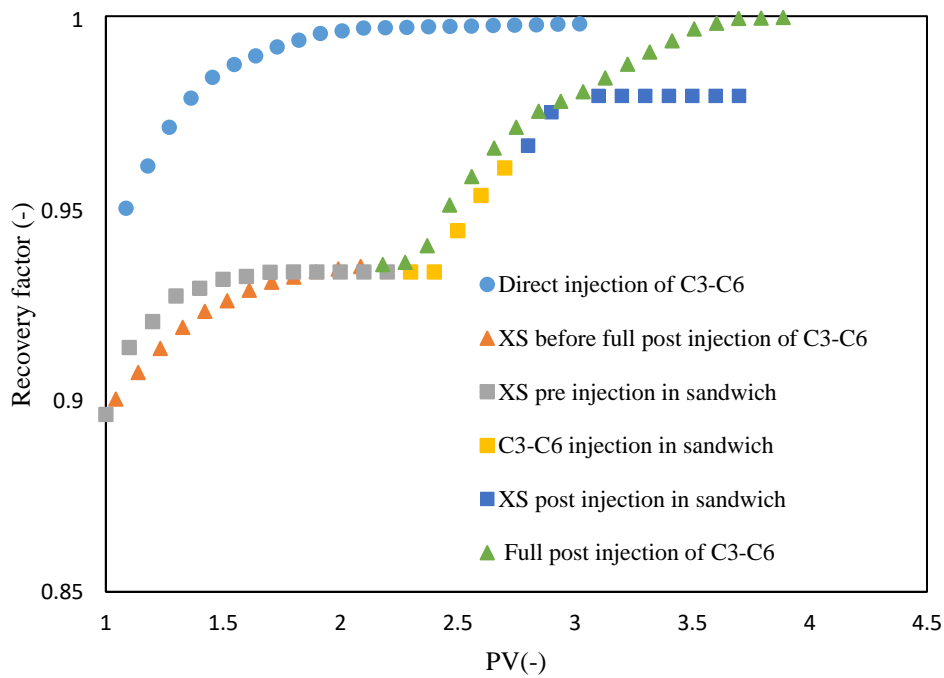


Figure 3.2-12 DNAPL content/densities of organic phase produced during mobilization /solubilization mechanisms. (a) C₃ mixture post-injection in low permeable layer, (b) C₃ mixture post-injection in high permeable layer, (c) C₃-C₆ mixture post-injection in low permeable layer, (d) C₃-C₆ mixture post-injection in high permeable layer, (e) C₆ mixture post-injection in low permeable layer, and (f) C₆ mixture post-injection in high permeable layer

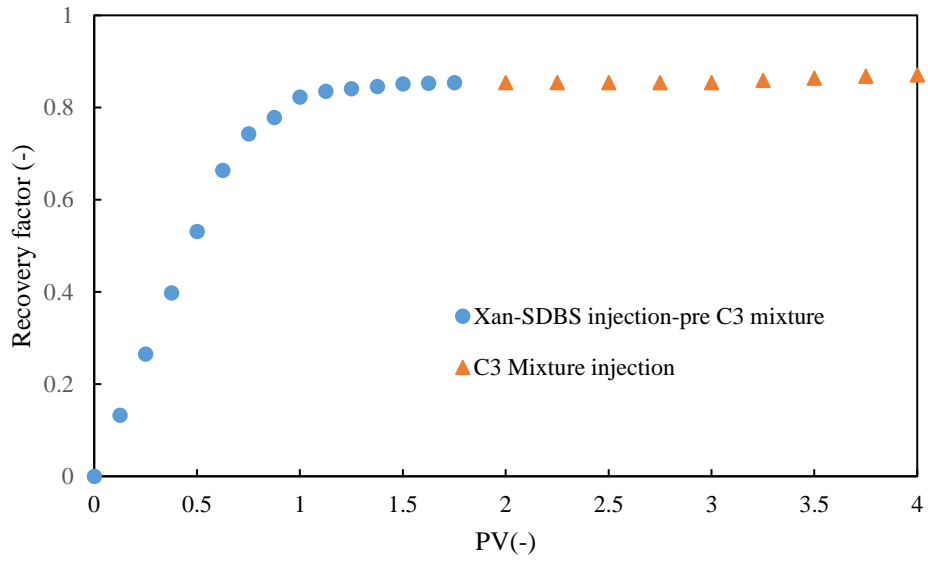


(a)

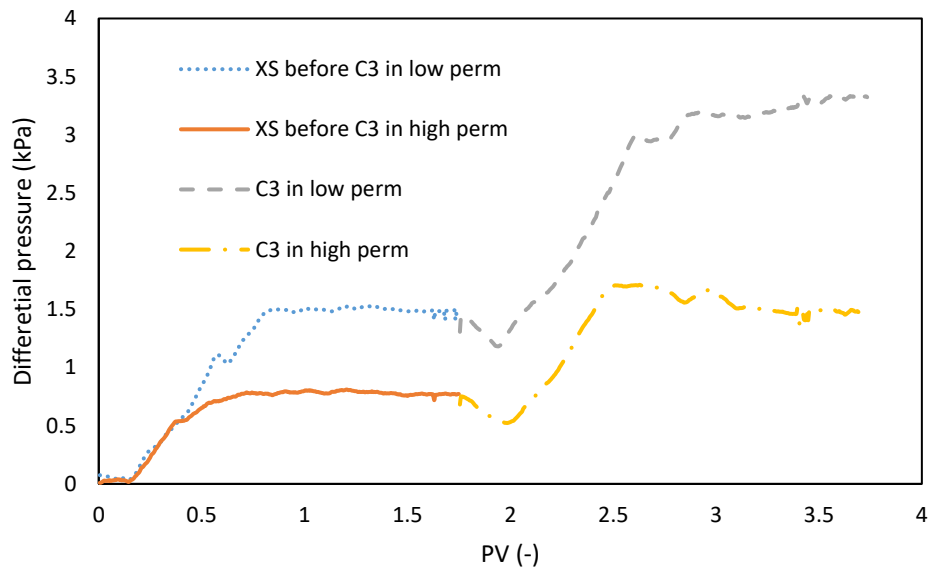


(b)

Figure 3.2-13 Evaluating different injection scenarios for DNAPL mobilization mechanism in columns. (a) Low permeable layer, and (b) High permeable layer

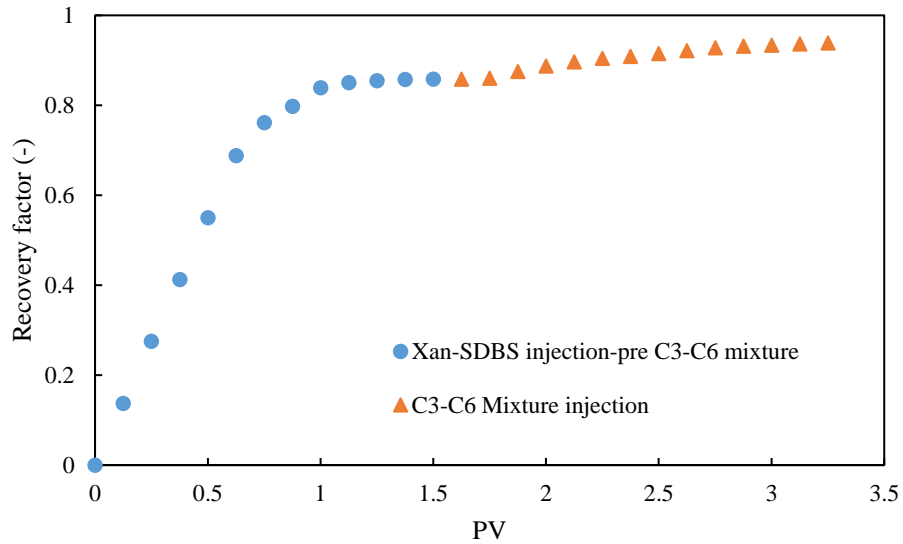


(a)

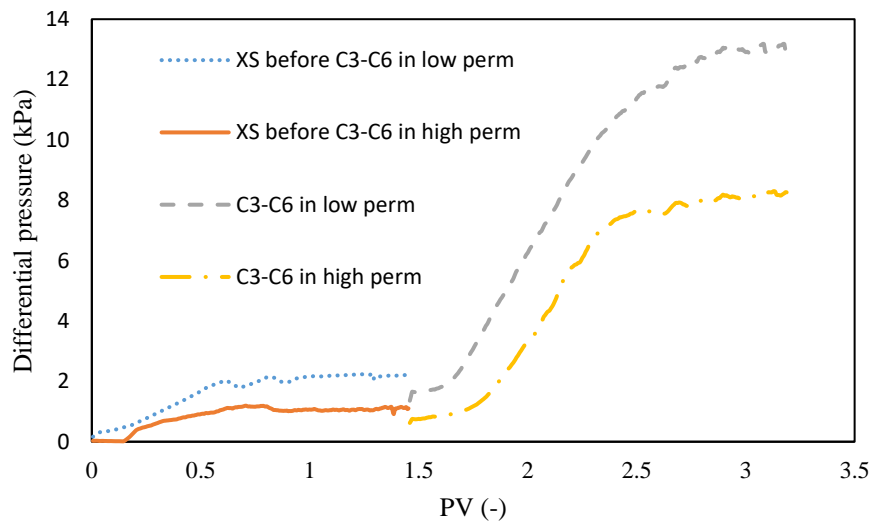


(b)

Figure 3.2-14 Experimental data for primary injection of XS and post injection of C₃ mixture into multilayer system. (a) Recovery factor versus PV, and (b) differential pressure versus PV



(a)



(b)

Figure 3.2-15 Experimental data for primary injection of XS and post injection of C₃-C₆ mixture into multilayer system. (a) Recovery factor versus PV, and (b) differential pressure versus PV

Chapter 4

4. Remediation of DNAPL Polluted Aquifers by injection of Densified Biopolymer Suspension/solution

Summary

One of the primary challenges encountered during the remediation of aquifers polluted with DNAPL is the density-driven phenomenon. This occurs when a less dense fluid displaces a denser one, leading to what is termed "overridden flow". To address the density-driven issue during the displacement of DNAPL, a gravity-driven remediation method is evaluated in which the polymer solution is densified either by suspended barite particles or by salts. It is shown that densifying the polymer solution with suspended matter or soluble salt can improve DNAPL recovery factor up to 4 times.

In the first section of this chapter, the influence of injection of densified polymer suspensions in a DNAPL contaminated aquifer is discussed. Deposition of suspended matter in porous media during densified polymer suspension injection was characterized and a reduction in permeability up to 70% was observed. It is demonstrated that for a confined system, which is not a good representative of real polluted site, a higher unrealistic recovery factor can be obtained. Moreover, the presence of barite particles can result in a higher viscosity of the polymer suspension while keeping a similar rheological behavior.

In the second section of this chapter, gravity-driven remediation of DNAPL polluted aquifers is evaluated by the injection of a densified biopolymer brine solution. Confined column tests show a similar 89% DNAPL recovery for viscous polymer solutions regardless of their density. Unconfined tests mimicking real sites reveal that non-densified viscous polymer solutions yield a mere 0.09 recovery due to density-driven flow. Densified polymer attains radial invasion, boosting recovery to 0.46 with 1.21 aspect ratio. Numerical simulations aligned with experiments, suggesting a near-zero gravity number is necessary to prevent density-driven flow problems.

Section I

4.1. Influence of the injection of densified polymer suspension on the efficiency of DNAPL displacement in contaminated saturated soils

Preamble

Authors: A. Alamooti *, S. Colombano, S. Omirbekov, A. Ahmadi- Sénichault, F. Lion, H. Davarzani

Affiliations: BRGM (French Geological Survey), Orléans, 45000, France; Institut de Mécanique et Ingénierie de Bordeaux (I2M), Arts et Métiers Institute of Technology, CNRS, Talence, 33405, France ; ADEME (Agence de la transition écologique), ANGERS, 49004, France

Published: Yes

Journal: Hazardous Materials

Date of publication: 15 October 2022

DOI: <https://doi.org/10.1016/j.jhazmat.2022.129702>

Conference: This work has been presented at 13th annual InterPore2021, 31 May – 3 June 2021, Online; and 15th Journées d'Etude des Milieux Poreux – JEMP (French Interpore), 26-27 October 2021 Strasbourg; and Aquaconsoil2021 15 to 17 June 2021 2021 Online.

4.1.1. Abstract

Nowadays the remediation of DNAPL contaminated zones near groundwater has gained great prominence in environmental fields due to the high importance of water resources. In this work, we suggest injecting a densified polymer suspension by adding barite particles to displace DNAPL. To evaluate the efficiency of the densification of polymer suspensions on the displacement of DNAPL, various densities of barite-polymer suspension; lower, equal, and higher than the density of DNAPL were prepared and their rheological behavior was analyzed. Then flow experiments were performed using a decimetric-scale 2D tank. The displacement procedure was monitored with an imaging technique and the production and injection process data were recorded by mass balance interpretation. It was shown that the densification of the polymer suspension could improve the recovery factor of DNAPL up to four times. The clogging behavior of barite-polymer suspension was assessed in a 1D column. Generalized Darcy's law and the continuity equation were used to numerically simulate the experimental two-phase flow. To take into account the clogging behavior of the suspension, the transport equation of diluted species was implemented into the model. The simulation results show that the model can properly predicts the experimental consequences.

Keywords: DNAPL, polymer suspension, densification, clogging, two-phase flow

4.1.2. Environmental Implication

Chlorinated DNAPL spills are frequent and due to their high toxicity they can negatively influence the soil and groundwater quality by penetrating through the soil and forming insoluble lenses. This study discusses a novel in situ remediation technique by introducing the densified polymer suspension for displacement of DNAPL from the contaminated zone. The experiments have been done on an unconfined system instead of an idealistic one to represent the real polluted site. This environmentally friendly method can effectively improve the recovery of

DNAPL by overcoming the buoyancy forces caused by high density of the chlorinated compounds.

4.1.3. Introduction

Dense non-aqueous phase liquids (DNAPLs) such as chlorinated organic compounds have been used for several years for various purposes, including but not limited to the cleaning of fabrics and metal degreasing. The vast consumption of these solvents during the last decades, as well as their inappropriate disposal have caused a plethora of environmental issues. Due to the density of these solvents, they can penetrate through the soil and the groundwater and, consequently, shape discontinuous trapped dense non-aqueous phase liquid (DNAPL) zones (Langwaldt and Puhakka, 2000a; Zhang and Smith, 2002). The dissolution of some components of these organic compounds can result in serious groundwater pollution (Roy et al., 2004). Nowadays there are numerous contaminated sites around the world contending with the problems related to the contamination of the groundwater. Displacement and removal of these DNAPLs from their source zones are very challenging and costly (McCarty, 2010). In other words, their high density and interfacial tension as well as their low solubility make the performance of most extraction technologies inefficient (e.g. pump-and-treat-method). The trend in global soil remediation technologies shows that the approach has switched from the pump-and-treat method to more advanced methods, including thermal and chemical enhancement (Colombano et al., 2021, 2020; Stroo et al., 2012).

Among the advanced remediation technologies, invading agents including surfactant, foam and polymer are widely used to displace the residing contaminant (DNAPL as pure phase) from the soil. In the case of the surfactant solution injection, using a high concentration of surfactant (i.e. higher than the critical micelle concentration) can cause the dissolution of the contaminant in the aqueous phase (Johnson et al., 1999). In the event of foam, the foam's stability is one of the

challenging issues in design and performance of foam injection (Ardakani et al., 2020; Kilbane et al., 1997; Wang and Mulligan, 2004).

Polymers have been widely used in the petroleum industry as one of the most effective enhanced oil recovery (EOR) technologies for different reservoir types (Alamooti and Malekabadi, 2018; Littmann, 1988; Liu, 2008; Sandiford, 1964). Although the process of DNAPL remediation of contaminated soils is similar to the EOR methods, there are some main differences. Firstly, the porous media in soils are several orders of magnitudes more permeable than reservoir rocks. In addition, the density of DNAPL is higher than the density of water and the location of these contaminants is close to groundwater and due to the high standards of remediation processes, the amount of residual DNAPLs should not exceed several ppm (Kilbane et al., 1997).

To mobilize the trapped ganglia of DNAPL in pore spaces, several forces including the capillary, viscous, gravity, and buoyancy forces are working simultaneously (Alamooti et al., 2020; Dejam et al., 2014; Mashayekhizadeh et al., 2011). The high surface tension of the DNAPLs makes the mobilization process more difficult but in the case of high permeable porous media, the capillary forces are not dominant. To mobilize ganglia of a non-aqueous phase liquid (here DNAPL) the summation of the viscous and gravity forces should be higher than the capillary forces present in polluted soil (Duffield et al., 2003; Jeong, 2005; Li et al., 2007; Pennell et al., 1996). In general, polymers are used to increase the viscous forces to improve the displacement of DNAPL by reducing the instabilities in the invading phase in porous media. Martel et al. (2004) used a polymer solution before and after a micellar solution (composed of a surfactant (12% Hostapur SAS from Clariant), an alcohol (12% *n*-butanol) and two solvents (19% d-limonene; 5% toluene)) to enhance the recovery factor of DNAPL. They injected polymer as a preflush slug to limit the mobility of the washing solution and avoid the adsorption of surfactant on the solids, and they injected it as postflush slug to push out the

washing solution of porous media. They found that on the one hand using reduced velocity improved the dissolution of the micellar solution by increasing the contact time and on the other hand, it caused less mobilization of DNAPL due to a decrease in capillary number. They also showed that polymer solution (xanthan gum) can positively improve the front stability. Martel et al. (1998) used the xanthan polymer solution for mobility control during the soil remediation of NAPL in a multilayer system, and they found that the injection of a polymer solution after the surfactant increases the mobility of the surfactant in low permeable zones and decreases it in high permeable zones. Silva et al. (2013) used modeling to simulate the flow of the polymer-improved aquifer remediation. They showed that by using a biopolymer the sweep efficiency was improved more than 70%. Smith et al. (2008) illustrated that the polymer-improved remediation technique (xanthan gum and potassium permanganate) can be used as a robust technology for the displacement of contaminants including PCE.

Miller et al. (2000) introduced a density-motivated mobilization approach for the remediation of DNAPL contaminated soils. They elucidated the idea of modifying the balances between the capillary and buoyancy forces. By means of bench-scale columns and a two-dimensional tank, they performed several displacement experiments where they showed that the efficiency of densified brine solution (using NaI) on displacement of DNAPL can reach up to 70%. They also proved that the densified brine solution can be used as a barrier below the DNAPL pool to prevent the downward movement of the DNAPL when a surfactant solution was used as displacement agent.

From the rheological point of view, polymer solutions are considered as non-Newtonian fluids i.e. their viscosity is a function of shear rate. For the study of fluid flow in porous media, to link the shear rate at bulk scale and fluid velocity in porous media (Darcy velocity) the physical parameters of porous media including permeability, porosity, and tortuosity should be considered (Darby et al., 2017; Omirbekov et al., 2020a). For the case of biopolymers such as

xanthan and carboxymethyl cellulose (CMC), a shear thinning behavior is observed (Benchabane and Bekkour, 2008; Zhong et al., 2013).

In the case of chlorinated solvents, as they are much denser than water and mainly isolated near the groundwater resources, if a lighter fluid is injected to remediate the contaminated soil, buoyancy forces work against the displacement. Although polymer solutions can provide higher viscous forces, they are lighter than DNAPL and the gravity forces can influence the recovery factor of DNAPLs.

Despite numerous studies carried out to evaluate the performance of polymer solutions injection on the displacement of the DNAPLs, the question of how to handle the gravity forces in an open system (without no flow boundaries) of the contaminated soil using a polymer solution is not well addressed in the literature. Furthermore, although the performance of the viscous (e.g. polymer) and dense solutions on the displacement of DNAPL have been individually investigated, the literature is bereft of a study in which a single densified high viscosity mixture has been used to overcome the gravity and capillary forces at the same time. Although using only a polymer solution with higher injection rates can improve the viscous forces, but it can result in viscous fingering and soil push up. Therefore, the novelty of this work is the introduction of a new remediation technology in which a densified polymer suspension has been injected to overcome both the gravity and capillary forces. The injection of dense polymers will therefore allow forcing the polymer to remain at the bottom of the aquifer to better displace the DNAPL. To achieve this goal, we analyzed the performance of a densified polymer suspension on the displacement of DNAPL from contaminated soils where gravity forces are working against the sweeping process. Barite (BaSO_4) particles were added to the CMC biopolymer to increase the density (Bern et al., 1996; Hanson et al., 1990) of the polymer suspension and to evaluate the permeability reduction in the displaced zone. Barite has very low solubility in water and is essentially considered nontoxic (Schulz et al., 2018). Also, , it is

normally ingested by patients who are going to do some X-ray tests on their digestive system (Merian et al., 2004). The main achievement of this study is to introduce densified polymer suspension for the improvement of the recovery factor of DNAPL. In addition, it gives insight on not only the application of densified polymer suspension on the displacement of DNAPL but also the role of boundaries on its performance. In this work, the experimental results on rheological behavior of the densified polymer suspension are provided and then the performance of the densification of the polymer suspension on recovery factor of DNAPL is discussed. The role of clogging of suspended particles on the transport of polymer suspension is analyzed. To have better understanding of the displacement process of DNAPL, the two-phase flow was simulated by means of the continuity and Darcy equations (Bear, 2013). The general advection-dispersion-reaction equation was used for the transport of barite and polymer in porous media (O'Carroll et al., 2013).

4.1.4. Material and methods (experimental and numerical)

In this section, first the 1D column and 2D tank experimental setups and procedures are explained. Then the method of image interpretation is presented. Finally, the governing equations are given and the numerical simulation method is described. The properties of experimental materials including the contaminant (DNAPL), barite-polymer suspension, soil physics as well as the suspension preparation are discussed in supplementary material part A.1.

4.1.4.1. 1D column experiments

To measure the permeability and the porosity of sandpacks with the grain size between 0.6 and 0.8 mm and further analyze the clogging process of barite-polymer suspension, one-dimensional calibrated glass columns were used. The diameter and length of the one-dimensional column were 4 cm and 30 cm, respectively.

These experiments were carried out to study the deposition process of barite particles during the barite-polymer suspension injection through the porous media. In this regard, a one-

dimensional column was filled with the same sand as the 2D tank (size between 0.6 and 0.8 mm) and fully saturated with water. The permeability and the porosity of the packed columns were first determined. Next, the barite-polymer suspensions were individually injected at a fixed injection rate of 1 mL/min into the fully water saturated column and the density of the effluents (each 4 mL) was monitored. The experiments were continued to reach the steady state condition by monitoring the pressure gradient. In the end, the columns were flushed at the same injection rate for 24 hours with water to displace the floating barite particles inside, and then the reduced permeability and porosity were determined. The schematic of the experimental setup used for barite-polymer suspension injection in 1D columns is shown in Figure 4.1-1.

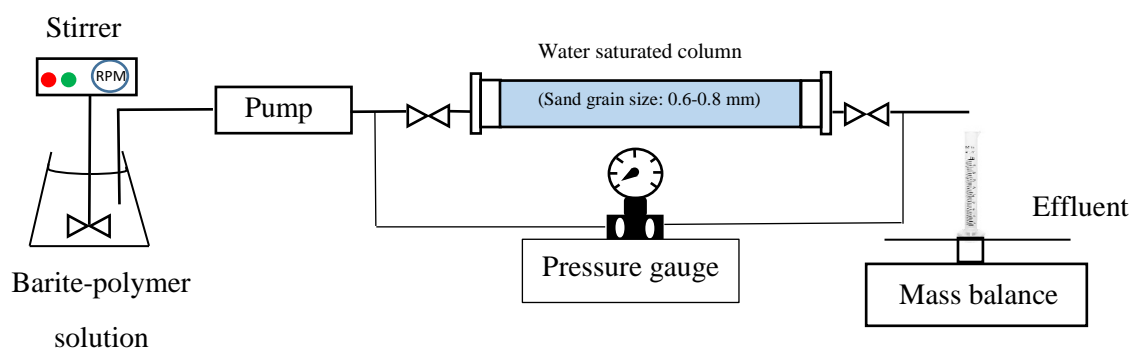
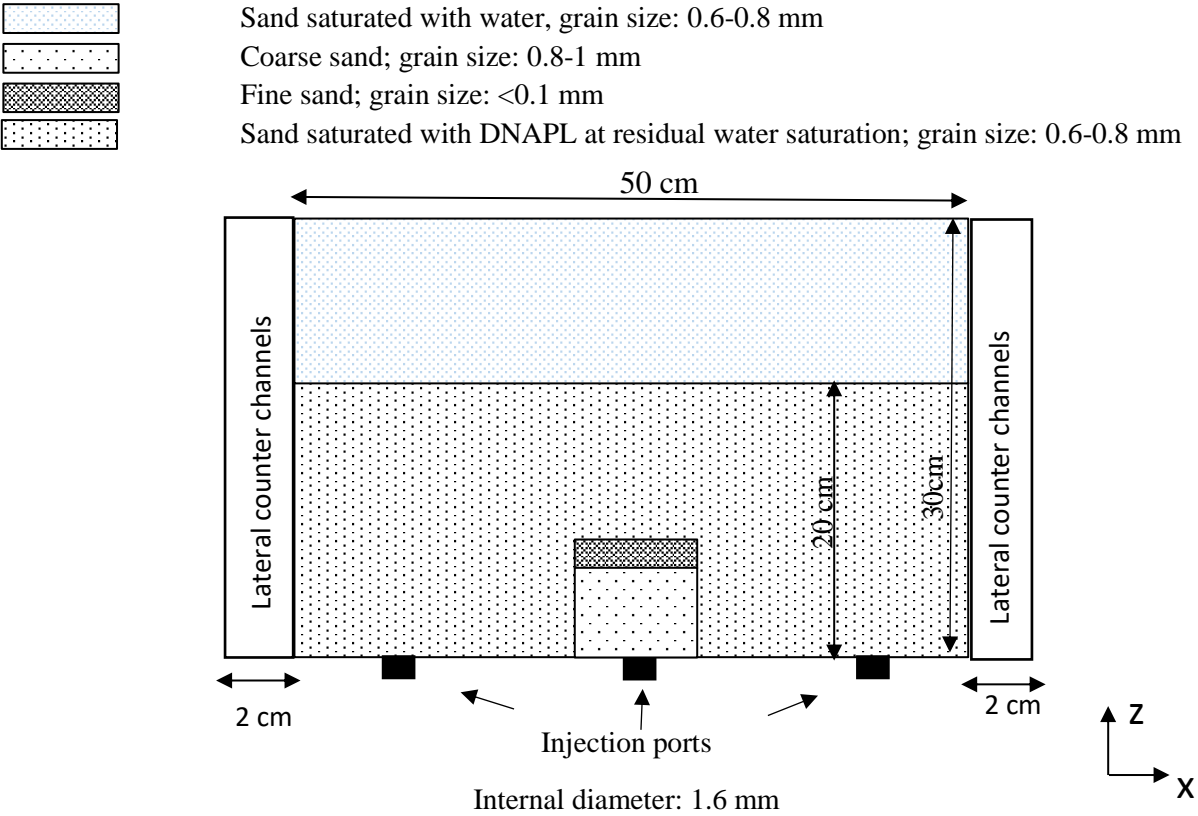


Figure 4.1-1 Schematic of barite-polymer solution injection in 1D column

4.1.4.2. 2D tank experiments

For the DNAPL displacement experiments, a two-dimensional tank with the size of 50 cm length \times 30 cm height \times 2 cm width was used (Figure 2). The front and back of the tank were made of glass to allow the imaging. The tank is filled up to 28 cm with sand of the grain size between 0.6 and 0.8 mm. To inject the suspension uniformly into the porous media a central zone near the injection point (central bottom zone of the tank) is constituted of sandpacks with different permeabilities to represent the injecting well. To fill the 2D tank with sand while injecting water, the central part near the injection point of barite-polymer suspension was

separated using two vertical barrier plates (2 cm × 30 cm). Then the sand of the grain size between 0.6 and 0.8 mm was packed on two lateral sides of tank. Then the coarser sand was packed in central part while the barrier plates were pulled out gradually. When the level of the sandpacks reached a 6 cm height in the entire 2D tank, the coarser sand was covered by 3 cm height of fine sand in the central part. While the sand of the grain size between 0.6 and 0.8 mm was packed everywhere in the 2D tank, the two barrier plates were completely pulled out of the 2D tank. This configuration is close to the field where the polymer is injected using a vertical well into the contaminated zone. Two lateral counter channels (cavities) with the size of 2 cm × 2 cm × 30 cm located at the two sides of the tank were used to regulate the fluid levels during the experiment. The schematic of the tank and the different permeability zones inside are depicted in Figure 4.1-2.



These experiments were performed to investigate the efficiency of the injection of a barite-polymer suspension on the displacement of DNAPL inside porous media. To keep the water level constant during the experiment, demineralized water was recirculated in the tank using two Watson Marlow peristaltic pumps. After the completion of the packing of the sand within the water phase, DNAPL was injected from the three ports ($d= 0.16$ cm) located at the bottom of the tank at the injection rate of 2 mL/min, to reach the height of 20 cm. Then, the barite-polymer suspension was injected from the bottom center of the tank at the constant injection rate of 1.7 mL/min equivalent to an injection velocity of 1 m/day using a peristaltic pump. Using another peristaltic pump, produced DNAPL was pumped out from the cavities and the level of DNAPL inside the cavities was kept constant during the experiments. By means of a mass scale (Sartorius Cubis MSE8201S-000-D0) the mass of recovered DNAPL was measured and a real-time data acquisition was performed. 2D-images of the tank were recorded regularly during the experiments for further analysis of the evolution of the system, using a digital camera (Nikon® D810 with NIKKOR LENS 105). The schematic of barite-polymer suspension/DNAPL displacement is shown in Figure 4.1-3.

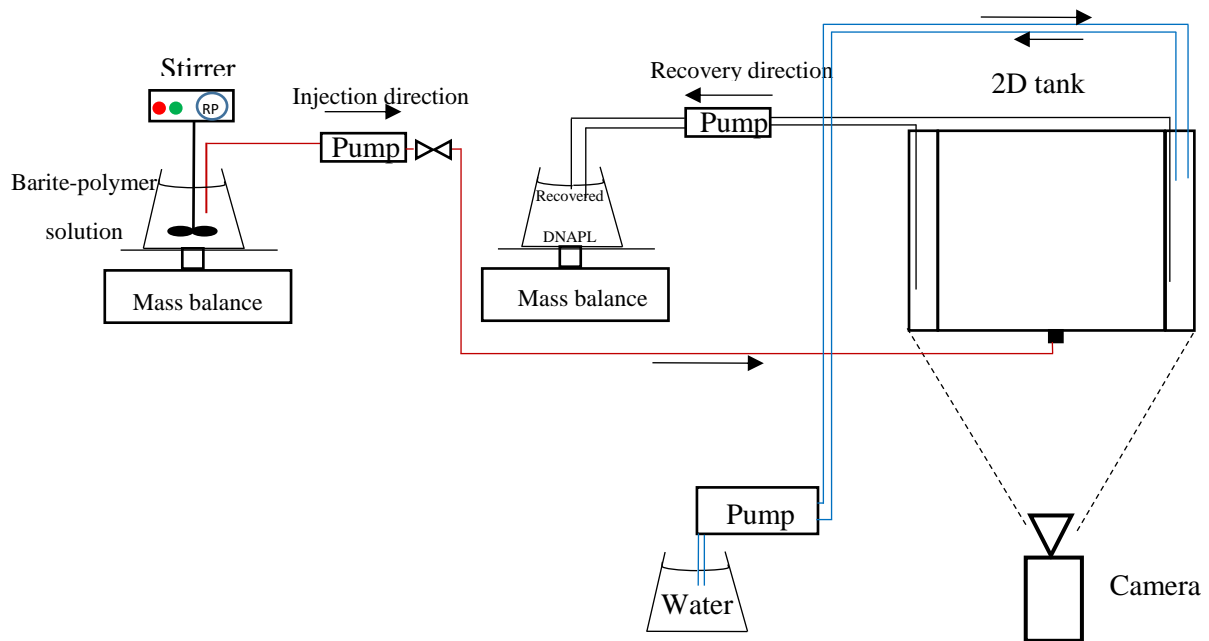


Figure 4.1-3 Schematic of barite-polymer solution-DNAPL displacement experimental setup (2D tank)

4.1.4.3. Suspensions preparation

As the barite particles are almost insoluble in water (Ropp, 2012), the polymer is used, not only to provide a high viscosity but also to cause a stable suspension. In this regard, the role of different polymers on the stability of barite suspension at the same density as the DNAPL ($\rho=1.66$ g/mL) has been examined.

For this purpose, the efficiency of three different biopolymers including xanthan gum, guar gum, and CMC on the stability of the barite suspension was evaluated. The density of the barite-polymer suspensions was kept at the density of the DNAPL (1.66 g/mL) and the concentration of the polymers was set at 4 g/L. The concentration of polymer was selected in a way to provide sufficient viscous forces to displace the DNAPL in soil but not too high to avoid very high injection pressures. Demineralized and degassed water was used to prepare all the suspensions. For the case of polymer solution (without barite particles), polymer powder was added gradually to water, and it was mixed properly using an overhead stirrer (IKA RW14) with 500 RPM for 2 hours. For the barite-polymer suspensions, firstly barite particles were added to

water while stirring at 200 RPM for 15 minutes. Then the polymer powder was added very slowly, and the suspension was stirred for 2 hours at 500 RPM. Using a graduated cylinder, the decantation process of the barite-polymer suspensions was monitored for 48 hours. The results evidenced the sedimentation of a given percentage of the barite particles in the suspension and therefore separation of water from the suspension. When CMC was used as the polymer, 98% of the mixture was kept in the suspension while for xanthan gum and guar gum, this value was 48% and 64% respectively. Therefore, for our study, barite and CMC polymer suspension was chosen to displace the DNAPL inside the soil. For the densities of barite-CMC suspensions of 1.3, 1.66, and 1.9 g/mL, the volume fractions of barite particles inside the suspension were around 8%, 18% and 24%, respectively.

4.1.4.4. Image interpretation

An image analysis tool is used to describe the displacement process during the 2D tank experiments and to evaluate DNAPL saturation. All the experiments were carried out in a darkroom and the lighting was provided by two light spots (2×300 W, Broncolor®). Black and white reflectors were set near the 2D tank to prevent reflections during the photography. A grayscale calibration card was installed on the 2D tank front surface to help regulate the light density for different experiments during image analysis. The lighting differences were adjusted with the 8-grayscale levels. For image interpretation, the area of interest (AOI) was considered almost the same size as the tank glass lateral surface to have a maximum zone of analysis and also to avoid the role of wall shade on the process of the calculation of phases' saturation (Colombano et al., 2021; Davarzani et al., 2021a; Philippe et al., 2021). Next, the size of the pixel area was selected in a way to exclude microscale effect, shadows, and non-uniform lighting effects. To find the relationship between the optical density and DNAPL saturation a

calibration curve was used. The optical density of reflected light, O_d , can be expressed as (Flores et al., 2011; Schincariol et al., 1993).

$$O_d = -\log(\rho_t) \quad \text{Eq 4.1-1}$$

$$\rho_t = \frac{I_r}{I_0} \quad \text{Eq 4.1-2}$$

where O_d is the optical density of reflected light, ρ_t is the ratio of reflected luminous intensity, I_r and the initial luminous intensity, I_0 .

In the next step, the exact optical densities for fully DNAPL-saturated and dry tank (saturation of 1 and 0 respectively), as well as those corresponding to the residual saturations of the wetting and non-wetting phases were determined. With these points, a linear calibration curve has been considered for optical densities and DNAPL saturation (Colombano et al., 2021). To calculate the total DNAPL saturation, the saturation of DNAPL in each pixel was calculated using the average optical density and then for the entire AOI (area of interest) the summation of all saturation was calculated. Indeed, the sum is needed to calibrate the image interpretation vs mass balance data.

4.1.4.5. Governing equations

4.1.4.5.1. Two-phase non-Newtonian flow in porous media

Natural soil in the contaminated zone below the groundwater level is represented as a non-deformable, uniform and isotropic porous medium containing two incompressible, immiscible phases (aqueous and DNAPL). The continuity equation for each phase can be written as follows (Bear, 2013):

$$\frac{\partial}{\partial t}(\phi \rho_i S_i) + \nabla \cdot (\rho_i \mathbf{u}_i) = 0 \text{ with } i = w, nw \quad \text{Eq 4.1-3}$$

where the subscripts w and nw denote wetting and non-wetting phases, respectively. ϕ is the porosity, ρ_i (kg/m^3), S_i and \mathbf{u}_i (m/s) are respectively the fluid density, saturation, and Darcy

velocity vector for phase i , and t is the time (s). For the momentum equation in porous media the generalized Darcy law is considered:

$$\mathbf{u}_i = -\frac{k k_{ri}}{\mu_i} (\nabla p_i - \rho_i \mathbf{g}) \quad \text{Eq 4.1-4}$$

where k (m^2) is the absolute permeability of the isotropic porous medium considered here, k_{ri} , μ_i , and p_i are respectively the relative permeability, viscosity (Pa.s) and the pressure (Pa) of phase i , and \mathbf{g} is the gravity vector. To solve the system of equations for two-phase flow, two other algebraic equations are necessary and are given by:

$$S_w + S_{nw} = 1 \quad \text{Eq 4.1-5}$$

$$p_c = p_{nw} - p_w \quad \text{Eq 4.1-6}$$

where S_w and S_{nw} are wetting and non-wetting phase saturations. p_c is the capillary pressure (Pa) with p_w and p_{nw} , the wetting and non-wetting phase pressures (Pa), respectively. For the relative permeability and capillary pressure curves we used Brooks and Corey functions (Brooks and Corey, 1964):

$$p_c = p_{th} S_{we}^{\frac{-1}{\lambda}} \quad \text{Eq 4.1-7}$$

$$k_{rw} = S_{we}^{(3+\frac{2}{\lambda})} \quad \text{Eq 4.1-8}$$

$$k_{rnw} = S_{nwe}^{2(1-(1-S_{nwe})^{(1+\frac{2}{\lambda})})} \quad \text{Eq 4.1-9}$$

where p_{th} is the threshold pressure (Pa) and λ is the index of the pore size distribution. S_{we} and S_{nwe} are the effective saturations of wetting and non-wetting phases and are defined as follows:

$$S_{we} = \frac{S_w - S_{wr}}{1 - S_{nwr} - S_{wr}} \quad \text{Eq 4.1-10}$$

$$S_{nwe} = \frac{S_{nw} - S_{nwr}}{1 - S_{nwr} - S_{wr}} \quad \text{Eq 4.1-11}$$

where, S_{wr} and S_{nwr} are the wetting irreducible and non-wetting residual saturations respectively. As CMC polymer is soluble in water, it is considered as an aqueous phase and is treated as a species transported by water. Due to the non-Newtonian behaviour of the barite-polymer suspension, several rheological studies were carried out on the barite-polymer suspension with different barite concentrations (discussed in results and discussion part). Among various possible models to describe the non-Newtonian behaviour of the barite-polymer suspension, the power-law model was found to be the most suitable (Benchabane and Bekkour, 2008):

$$\mu = \kappa \dot{\gamma}^{n-1} \quad \text{Eq 4.1-12}$$

where κ is the flow consistency index ($Pa \cdot s^n$), $\dot{\gamma}$ is the shear rate (s^{-1}) and n is the flow behavior index. The values of n less than 1 correspond to a shear-thinning behavior while the values of n more than unity are for shear thickening fluids. The concept of shear rate in porous media, i.e. at the Darcy scale using the Darcy velocity can be expressed as (Darby et al., 2017) :

$$\dot{\gamma} = \frac{4\alpha u/\phi}{R_{eq}} \quad \text{Eq 4.1-13}$$

where α is the empirical shifting parameter depending on the tortuosity of porous media as well as the bulk rheology of the fluid (Chauveteau and Zaitoun, 1981), and R_{eq} (m) is the average pore throat radius which, using a simple bundle of capillary tubes model, can be estimated as:

$$R_{eq} = \sqrt{\frac{8k}{\phi}} \quad \text{Eq 4.1-14}$$

By introducing equations 4.1-(12-14) into equation 4.1-4 the apparent viscosity term for the aqueous phase can be rewritten as:

$$\mu_w = \alpha \kappa \left(\sqrt{\frac{2k}{\phi}} k_{rw} (\nabla p_w - \rho_w \mathbf{g}) \right)^{\frac{n-1}{n}} \quad \text{Eq 4.1-15}$$

4.1.4.5.2. Polymer and barite particle transport model

As the barite-polymer has been used to displace DNAPL in porous media, the modeling of the transport of suspended barite particles and polymer in water is considered. A suspension of barite-polymer was injected at a fixed flow rate into a porous medium. Considering the deposition of the suspended barite particles onto the sand grain surfaces, the advection of the barite-polymer in porous media and the hydrodynamic dispersion of the barite particles, the general advection-dispersion-reaction equation for the transport of barite and polymer in porous media can be written as (O'Carroll et al., 2013; Tsakiroglou et al., 2018):

$$\underbrace{\frac{\partial(\phi S_w c_i)}{\partial t}}_{\text{Accumulation}} - \underbrace{\nabla \cdot (\phi S_w \mathbf{D} \cdot \nabla c_i)}_{\text{Dispersion}} + \underbrace{\mathbf{u}_w \cdot \nabla c_i}_{\text{Advection}} = R_i + \dot{m} \quad \text{Eq 4.1-16}$$

where c_i is the concentration of the i -component (barite or polymer) (kg/m^3), \mathbf{D} is the dispersion tensor, R_i is the reaction term for the i -component and \dot{m} is the source term. Hydrodynamic dispersion determines the behavior of components transport in porous media.

The longitudinal and transverse dispersion coefficients are considered and can be expressed as (Auset and Keller, 2004):

$$D_L = D_0 + \alpha_L u \quad \text{Eq 4.1-17}$$

$$D_T = D_0 + \alpha_T u \quad \text{Eq 4.1-18}$$

where D_L and D_T are the longitudinal and transverse dispersion coefficients respectively, D_0 is the effective diffusion coefficient (m^2/s) in porous media, α_L and α_T are the longitudinal and transverse dispersivities, respectively. Since the barite particles have very low solubility in water, physical clogging happens in porous media as a result of suspended particles retention (De Vries, 1972; Vigneswaran and Suazo, 1987). The same transport properties (dispersion tensor, effective diffusion coefficient) are considered for polymer and barite species. Several theoretical and empirical models have been developed to describe the physical clogging process in porous media (Bedrikovetsky et al., 2012; Boek et al., 2012; Yuan and Shapiro, 2011). While

empirical models focus on the infiltration rate and particle concentrations in suspension and deposition (Pérez Paricio, 2001), theoretical models debate over the dynamics of the attachment and detachment process. The process of clogging is under the influence of the interaction of several forces including gravity, inertia, electrostatic, and viscous forces (Zamani and Maini, 2009).

Here, we use the transition-deposition model in porous media to simulate the physical clogging in soil (Zheng et al., 2014). The clogging process was coupled with density variations inside the displaced zone and permeability/porosity reduction. According to equation 4.1-16, the formulation of barite particle transport in porous media can be described as (Zheng et al., 2014):

$$\frac{\partial(\phi c_b + c_s)}{\partial t} + \mathbf{u}_w \cdot \nabla c_b - \nabla \cdot (\phi S_w \mathbf{D} \cdot \nabla c_b) = 0 \quad \text{Eq 4.1-19}$$

where c_b is the barite particle concentration in the bulk of suspension (kg/m^3), c_s is the concentration of barite particles deposited on the sand grain surfaces per unit pore volume (kg/m^3). To simulate the process of the clogging caused by barite deposition on the surfaces of the sand grains, the continuity equation was coupled with the transport-deposition equation for barite particles. According to the process of attachment and detachment of particles in porous media, the mechanism of deposition of the suspended barite particles can be described as (Herzig et al., 1970):

$$\frac{\partial c_s}{\partial t} = \theta c_b - \beta c_s \quad \text{Eq 4.1-20}$$

where θ is the particle attachment coefficient (s^{-1}) and β is the particle detachment coefficient (s^{-1}). During the injection of barite-polymer suspension the particles of barite can easily be captured by sand grain surfaces, leading to the reduction of pore space (porosity):

$$\phi = \phi_0 - \frac{c_s}{\rho_b} \quad \text{Eq 4.1-21}$$

where ϕ_0 is the initial porosity, ρ_b is the solid barite density (kg/m^3). To correlate the permeability-porosity changes in the displaced zone, the Carman-Kozeny relationship was used (Hommel et al., 2018; Voronov et al., 2010):

$$k = k_0 * CF * \frac{\phi^3}{(1 - \phi)^2} * \frac{(1 - \phi_0)^2}{\phi_0^3} \quad \text{Eq 4.1-22}$$

where k_0 is the initial absolute permeability, and CF is a correction factor to incorporate the changes in sphericity and diameters of sand particles after deposition of barite particles. The degree of clogging is evaluated using the absolute permeability reduction term as $\frac{(k_0 - k)}{k_0}$ (Zheng et al., 2014).

To simulate the system of the partial differential equations (4.1-3, 4.1-16, and 4.1-19) coupled with algebraic equations (4.1-5 and 4.1-6) in a two-dimensional domain. MUMPS (multifrontal massively parallel sparse direct solver) solver in COMSOL Multiphysics as a finite element solver with a BDF (backward differentiation formula) time stepping was used. The relative tolerance was preset at 0.005 and the absolute scaled tolerance with a factor of 0.1 was considered. The triangular meshing tool of COMSOL with maximum element size of 0.77 cm and minimum element size of 0.0029 cm and a maximum element growth rate of 1.2 was used.

4.1.5. Results

Firstly, the rheological behavior of polymer mixture with and without the barite particles was evaluated. Then, the experimental results of the barite particles clogging in the sand is discussed and finally, the results on the efficiency of the barite-polymer suspension on the displacement of the DNAPL is analyzed.

4.1.5.1. Rheological behavior of the densified polymer suspension

For the evaluation of the rheological behavior of the barite-CMC suspension the rotational rheometer, Haake Mars 60 was used. To characterize the rheological behavior of the barite-

CMC suspension with different densities the variation of the viscosity versus the shear rate in the range of 0.1-100 1/s was analyzed. Figure 4.1-4 shows the viscosity of barite-CMC suspensions for different densities as a function of the shear rate in a log-log scale. It can be seen that the viscosity increases with the density of the mixture. For all polymer mixtures with or without barite particles in the shear rate range used in this study, a shear-thinning behavior can be observed which corresponds to less resistance against the flow at higher shear rates. For the case of CMC solution without barite particles ($\rho=1$ g/mL), at low shear rate an initial shear thickening behavior can be noted. This increase in viscosity at low shear rate is still controversial. Liu et al.(2007) have attributed this mechanism to “flow induced formation of macromolecular associations”. Benchabane and Bekkour (2008) observed this behavior for high concentrations of CMC polymer solution at low shear rate. They reported that one of the most probable reasons for this behavior can be the increase in intermolecular interactions due to the increase in shear rate. In other words, this shear thickening behavior is ascribed to stiffer inner structure due to the formation of entanglements of polymer coils as the shear rate increases.

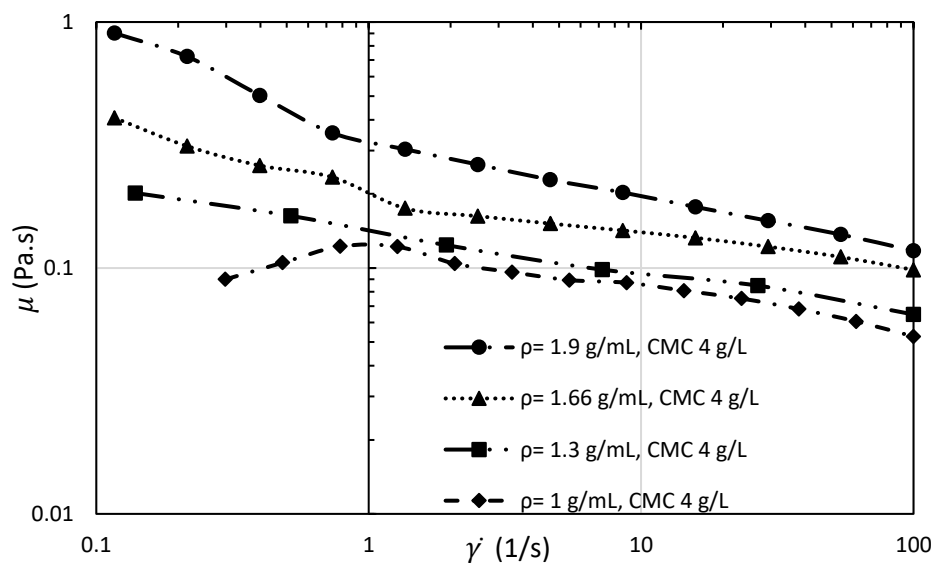


Figure 4.1-4 Rheological behavior of barite-CMC mixtures with different densities

A power-law model as described earlier (Equation 4.1-12) was fitted to the rheological behavior of the barite-CMC suspension. The parameters of the power-law model, the mean relative error (MRE) and R-squared are given in Table 4.1-2 (in appendix). In the case of polymer solution without barite particles a lower R-squared value (corresponding to a worse fit) is due to the shear thickening behavior at very low shear rates.

In addition to power-law model the Carreau fluid model for rheological behavior of the barite-CMC mixtures has been considered (Carreau, 1972). The Carreau model can be expressed as:

$$\mu = \mu_{inf} + (\mu_0 - \mu_{inf})(1 + (\chi\dot{\gamma})^2)^{\frac{l-1}{2}} \quad \text{Eq 4.1-23}$$

where, μ_0 and μ_{inf} are the viscosities (Pa.s) at zero and infinite shear rate, χ is the relaxation time (s), and l is the power index. The parameters of the Carreau model, and R-squared are given in Table 4.1-3 (in appendix). Similar to power-law model for the case of CMC solution without barite particles a lower R-squared value can be seen due to the shear thickening behavior at very low shear rates.

4.1.5.2. Experiments on clogging of barite particles in sandpacks

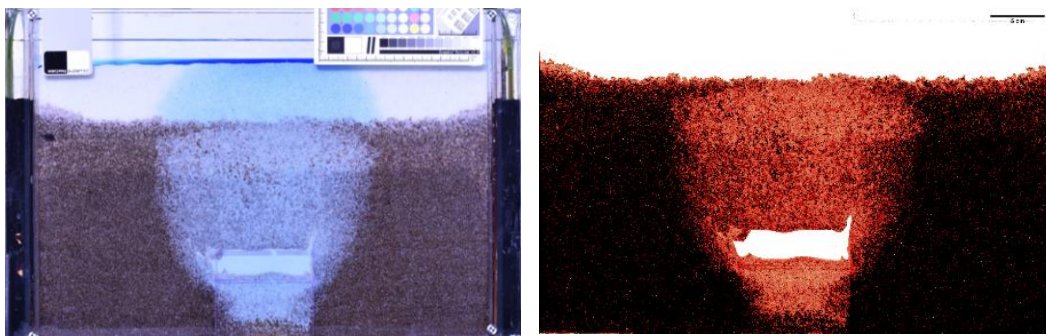
Barite-polymer as a suspension was selected to be injected through the DNAPL saturated zone. The particles suspended in the mixture due to the interaction of several forces can be deposited on the surface of the sand grains. The mass balance analysis of the columns at the end of water postflush after injection of barite-CMC suspensions shows that the mass of retained barite particles for densities of 1.3, 1.66, and 1.9 g/mL were 30.2, 35.5 and 37.3 g, respectively. These quantities of retained barite-particles are quite considerable in comparison to the mass of polymer dissolved in each pore volume of injected suspension (0.5 g). In this regard, the permeability and porosity reductions are mainly attributed to the role of barite particles deposition in sandpacks. In this section, the process of the barite particles clogging in sand for suspensions with different densities is characterized and discussed.

The reduced permeabilities for densities 1.3, 1.66, and 1.9 g/mL are equal to 65, 42, 39.5 Darcy respectively while the initial permeability has been equal to 145 Darcy. Also, The reduced porosities for densities 1.3, 1.66, and 1.9 g/mL are equal to 37.3, 37, 36.9 respectively while the initial porosity has been equal to 39. The degree of clogging for the barite-CMC solution with density of 1.3 g/mL is 0.55 while this value is around 0.71 and 0.73 for densities of 1.66 mL and 1.9 g/mL, respectively. It shows that the capability of the sand grains to retain the barite particles increases by an increase in the concentration of the barite particles in the suspension up to a maximum value. Above this value, there is a weak dependence of deposition of barite particles on the sand grain surfaces on the concentration of the barite in suspension. In addition, the reduction in porosities for various densities of the barite-CMC suspension is in the same trend as the permeability reductions.

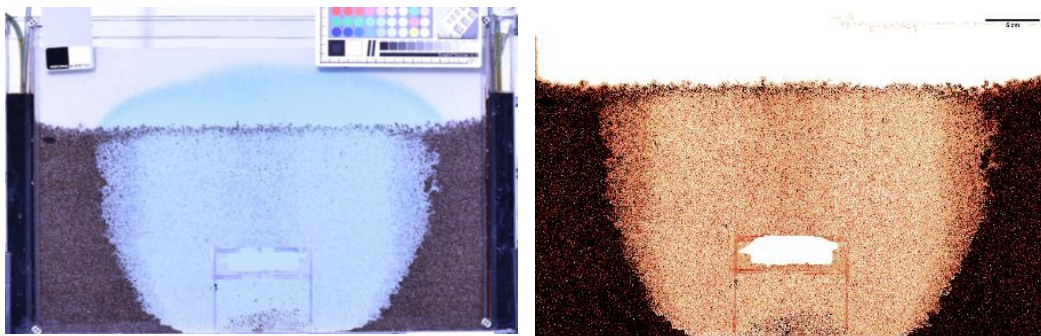
4.1.5.3. Experimental results of DNAPL displacement using barite-CMC suspension

To compare the efficiency of the injection of polymer mixtures with and without barite on the displacement of the DNAPL, three different densities (1.3 g/mL, 1.66 g/mL, and 1.9 g/mL) of barite-CMC suspension were analyzed. In this regard, several polymer mixtures with different densities were injected into the 2D tank saturated with DNAPL in presence of residual water saturation. During the injection of the invading phase, the level of DNAPL in lateral counter channels (Figure 1) was kept constant to recover the same amount of DNAPL as the one displaced in the porous medium. Figure 4.1-5 shows the distribution of the polymer and DNAPL (raw and analyzed images) at the end of the experiment, where either there is no more DNAPL production or the invading phase (barite-CMC suspension) has closely approached to the lateral boundaries. For the case of pure polymer injection in the absence of barite particles, the invading phase has a vertical displacement. By increasing the density of polymer mixture using the barite particles, a more lateral displacement of DNAPL is observed, as the buoyancy

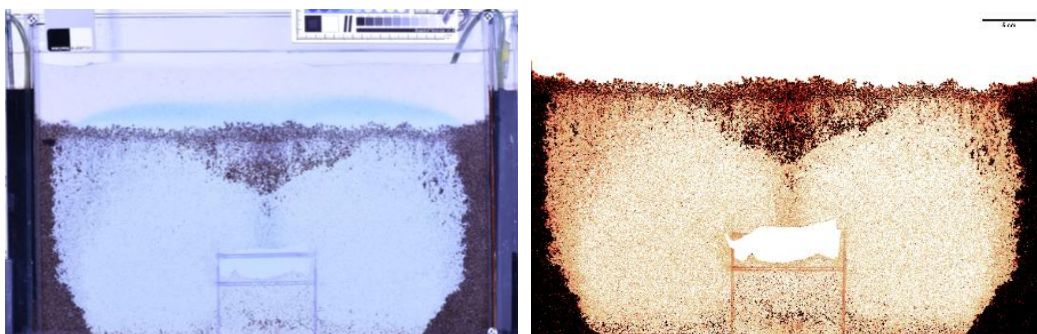
forces are decreased. In addition, the clogging of barite particles in the pores of the tank has led to density variations in the invading phase. This density variation can be visually seen in the images, where near the front, a zone with a density close to the density of water exists, and behind the front, the density increases up to the density of the invading phase. The results obtained from mass balance data show that the final recovery factor $\left(\frac{\text{volume of DNAPL produced}}{\text{initial volume of DNAPL in sand}}\right)$ for the case of only CMC solution without particles is around 0.095 while for barite-CMC suspensions with densities of 1.3, 1.66, and 1.9 g/mL, the recovery factor is around 0.3, 0.45, and 0.44 respectively.



(a)



(b)



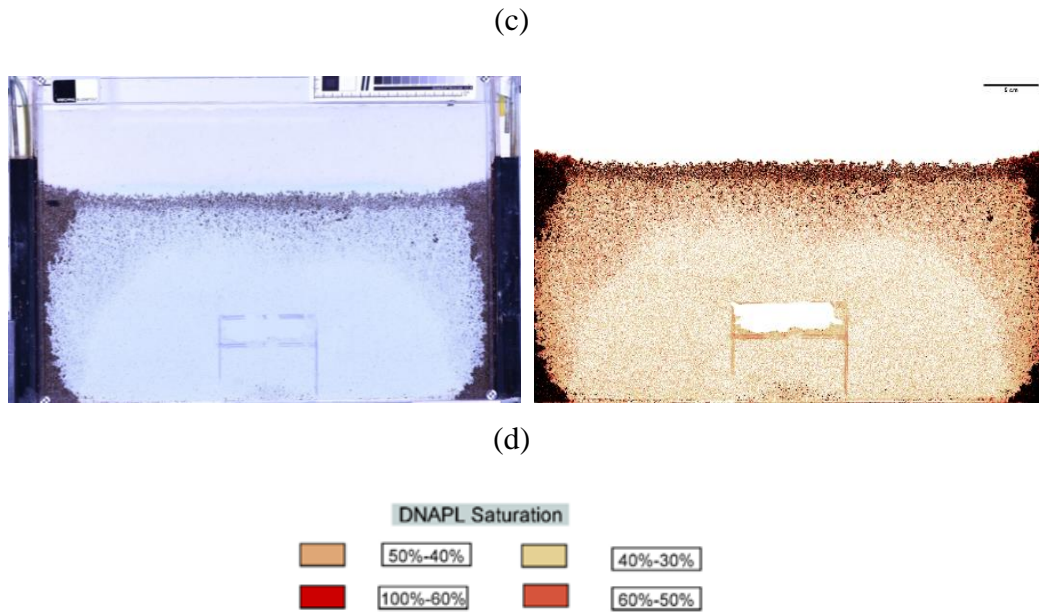


Figure 4.1-5 Comparison of the propagation of the barite-CMC solutions with different densities, the left images are the raw images, and the right images are those interpreted by image analysis. (a) pure polymer injection with density of 1 g/mL, barite-CMC injection with density of (b) 1.3 g/mL, (c) 1.66 g/mL, and (d) 1.9 g/mL. The injection is from bottom

4.1.5.4. Effect of the boundaries on the DNAPL recovery factor (closed or open system)

This section is devoted to a comparison between closed and open systems using both experimental and numerical approaches. Concerning the experiments carried out in the 2D tank and analyzed in previous sections, although the recovery factor is significantly improved (~4 times more) by increasing the density of the polymer mixture, the recovery factor of this technique is still less than that of most other conventional methods (Colombano et al., 2021; Philippe et al., 2020b). To have a better understanding, we designed a new experiment in which the top boundaries are closed to avoid vertical displacement and to force the invading fluid to be displaced in the horizontal direction. The barite-CMC suspension with a density of 1.66 g/mL at an injection flow rate equal to 2.8 mL/min was injected into a similar configuration

used in the previous experiments in the 2D sandpack with minor differences. More precisely, to have a closed zone of interest with a thickness of 5 cm (instead of 20 cm in previous cases), very fine sand (less than 0.1 mm) was used to block the displacing zone shown in Figure 4.1-6. Figure 4.1-11 (in appendix) shows the propagation of the barite-CMC suspension during the displacement in the closed system.

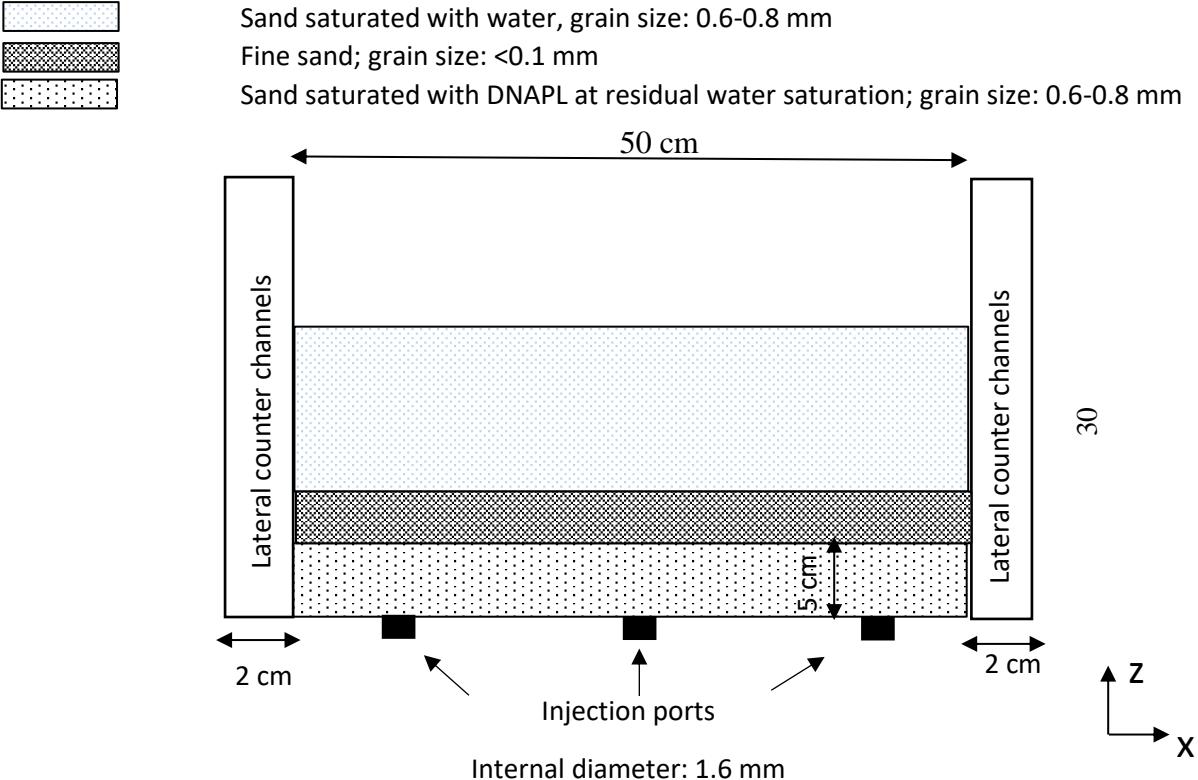


Figure 4.1-6 schematic of configuration and displacement of DNAPL by barite-polymer suspension with the density of 1.66 g/mL in a closed system

The results showed that the recovery factor in the closed system was around 0.88 at the end of the experiment. Some points are of importance to account for this difference: firstly, for the open 2D system, the displacement has been stopped (end of experiment) before reaching the lateral counter channels while in the closed 1D experiment the displacement has been continued to see the invading fluid in the lateral counter channels. Therefore, some parts of the region of interest in the open 2D system are still saturated with DNAPL. Also in comparison to the 1D system, there is a noticeable transition zone in front of fully displaced zone in the 2D system

that has a lower DNAPL saturation. Another point that should be noted is that the comparison of the simulation results for both displacements shows that the residual DNAPL saturation in the fully displaced zone for the open 2D system is around 0.34 while in the closed system is around 0.11.

4.1.6. Discussion

4.1.6.1. Characterization of the clogging of barite particles by finding attachment/detachment parameters

The set of experiments which are explained in section 3.2 have been carried out to find the dispersivity of barite particles and parameters related to attachment and detachment of barite particles. As it is mentioned in material and methods section, the barite-CMC suspensions were injected at fixed injection rate corresponding to 1 m/day to a fully water saturated column of sand. The effluents of the column were monitored during injection until steady state conditions were reached. The effective diffusion coefficient for the CMC polymer is considered 10^{-11} (m²/s) which is quite low (Kono, 2014), and the same value is taken into account for barite particles. To find the unknown values including the dispersivity (α) of barite particles and polymer as well as the attachment and detachment coefficients (θ , β), using an inverse modeling (minimization of the mean squared error), the outlet densities and reduced porosities and permeabilities of the sandpacks from the simulation results were matched with those obtained from the experiment.

It is assumed that the deposited barite particles were retained in their position during water flushing as the hydrodynamic forces of the water were not enough to detach them. In addition, it is considered that the deposition of the barite particles was homogenous along the one-dimensional column and that a maximum concentration of deposited barite particles was reached so that no further deposition on the grain surfaces was possible. To perform the 1D simulations, the appropriate boundary and initial conditions corresponding to the experiments

were applied to the domain: constant injection velocity of 1 m/day at the inlet, atmospheric constant pressure at the outlet, and initially fully water saturation inside the sand column. For solute transport the concentration of barite at the inlet is considered in agreement with the densities of barite-CMC suspension while the initial concentration in the column is equal to zero. To match the porosity values, the concentration of barite particles deposited on the sand grain surfaces per unit pore volume (c_s) from simulation was matched with those calculated from reduced porosities at the end of water postflush after barite-CMC injection (Equation 4.1-21). Then for the reduced permeability values using Carman-Kozeny equation, the correction factors for correlation of porosity and permeability were adjusted. Figure 4.1-7 demonstrates the density curves obtained from the simulations and experiments for different densities of barite-CMC suspensions after breakthrough time. The mean relative error and root mean square error of fitting for all cases are given in Table 4.1-4 (in appendix). As it can be seen, the results show that the transition period (between the breakthrough time and the time of the final plateau) for the lighter barite-CMC suspension is longer than for the two other suspensions. This is because the viscosity of denser fluid is higher therefore, a sharper breakthrough curve is observed. The parameters related to the model including the attachment and detachment coefficients and the dispersivities are listed in Table 4.1-4 (in appendix).

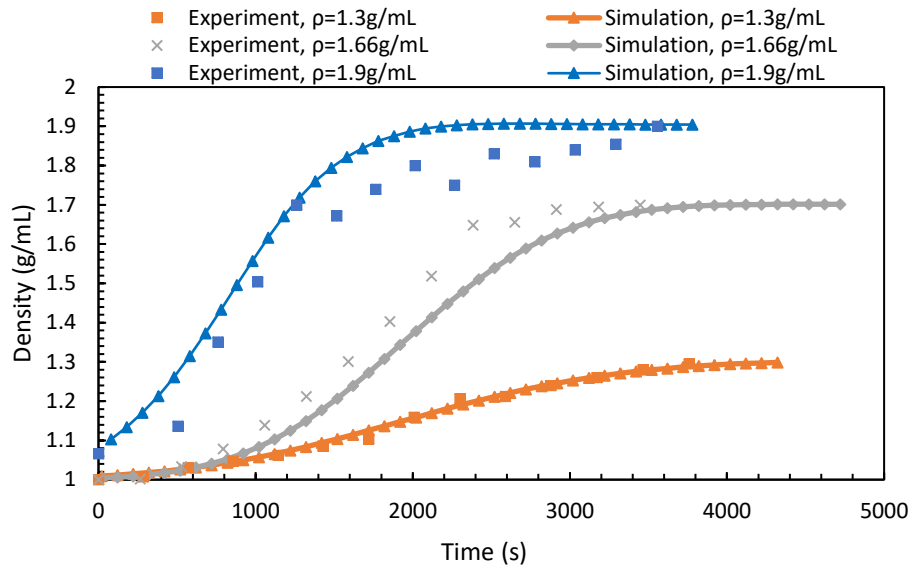
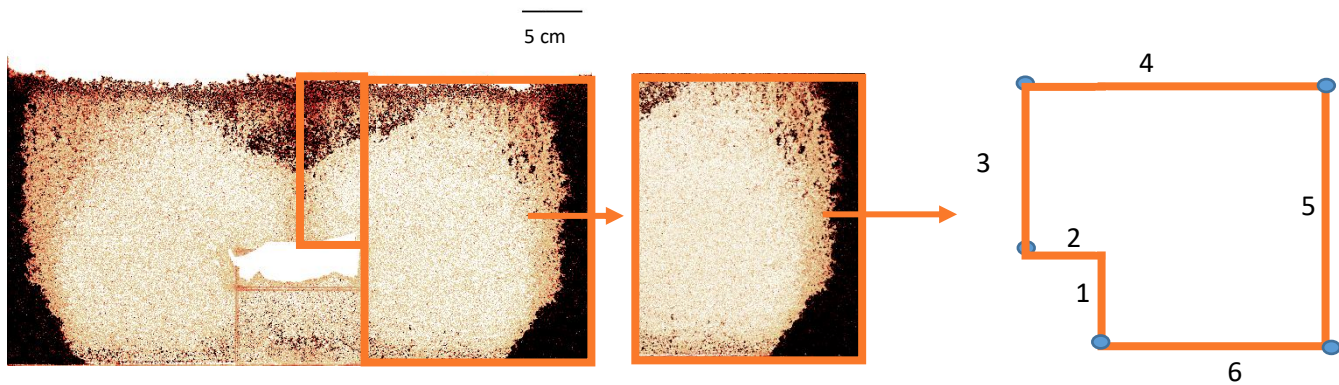


Figure 4.1-7 Comparison between the outlet densities obtained from simulation and experiments after breakthrough time

4.1.6.2. Numerical simulation results of DNAPL displacement using barite-CMC suspension

To simulate the process of DNAPL displacement using the barite-CMC suspensions, the clogging process of barite particles was incorporated into the model to include the density variation and permeability/porosity reduction. In this regard, an area on the right-hand side of the two-dimensional system, as shown in Figure 4.1-8, was considered as the representative zone. It is assumed that the flow in high permeable zone near the injection point has been equally distributed in two lateral parts and there is no vertical flow. The schematic of the boundary conditions and geometry of the model is shown in Figure 4.1-8. For the boundaries 3 and 4 as the level of DNAPL has been kept constant during the experiment the constant pressure condition is considered. In these boundaries z (m) is the vertical axis and P_0 is the pressure caused by water height on the top of DNAPL zone. Boundary 3 is a symmetrical boundary condition is considered and for boundaries 2 and 6 no flow condition and for boundary 1 constant injection velocity (1 m/day) are assumed and the constant pressure boundary conditions for boundaries 4 and 5 are considered.



Boundary conditions
 Boundaries 4, and 5: $P=P_0+\rho_{DNAPL}g(0.2-z)$
 3 : symmetry
 2, and 6: No flux
 1: $u=1$ m/day

Figure 4.1-8 Geometry used for modeling and the corresponding boundary conditions

Figure 4.1-9 shows the comparison between the experimental and numerical results. As can be seen, the shape of the invasion fronts of the barite-CMC suspension for various densities obtained by numerical simulation is in agreement with the ones obtained experimentally. As it was mentioned earlier, the large transient zone near the front of the invading phase is attributed to the role of barite-particles clogging and consequently density variation. The higher degree of clogging can also prohibit the backward diffusion of residual DNAPL, which is in favor of the soil remediation purpose.

In Figure 4.1-10, the displacement efficiencies resulting from experiments for various densities of invading phases are compared with those obtained from numerical simulations. The average

absolute relative errors $\left(\frac{1}{\text{Number of points}} \left| \frac{\text{Displacement efficiency}_{Exp} - \text{Displacement efficiency}_{Sim}}{\text{Displacement efficiency}_{Exp}} \right| \right)$

between the experimental and simulation results are around 0.1, 0.045, 0.083, and 0.158 for densities 1, 1.3, 1.6, and 1.9 g/mL, respectively. The higher error in denser suspensions can be attributed to dependency of saturation functions (capillary pressure and relative permeabilities)

on the concentration of barite particles which are clogging in sand. Also, the other reason can be because of the flow above the low permeable layer observed experimentally while we have considered it as an impermeable zone in our model. It is considered that the injected polymer has been completely invaded laterally on two sides of the high permeable zone and no vertical displacement takes place from low permeable zone.

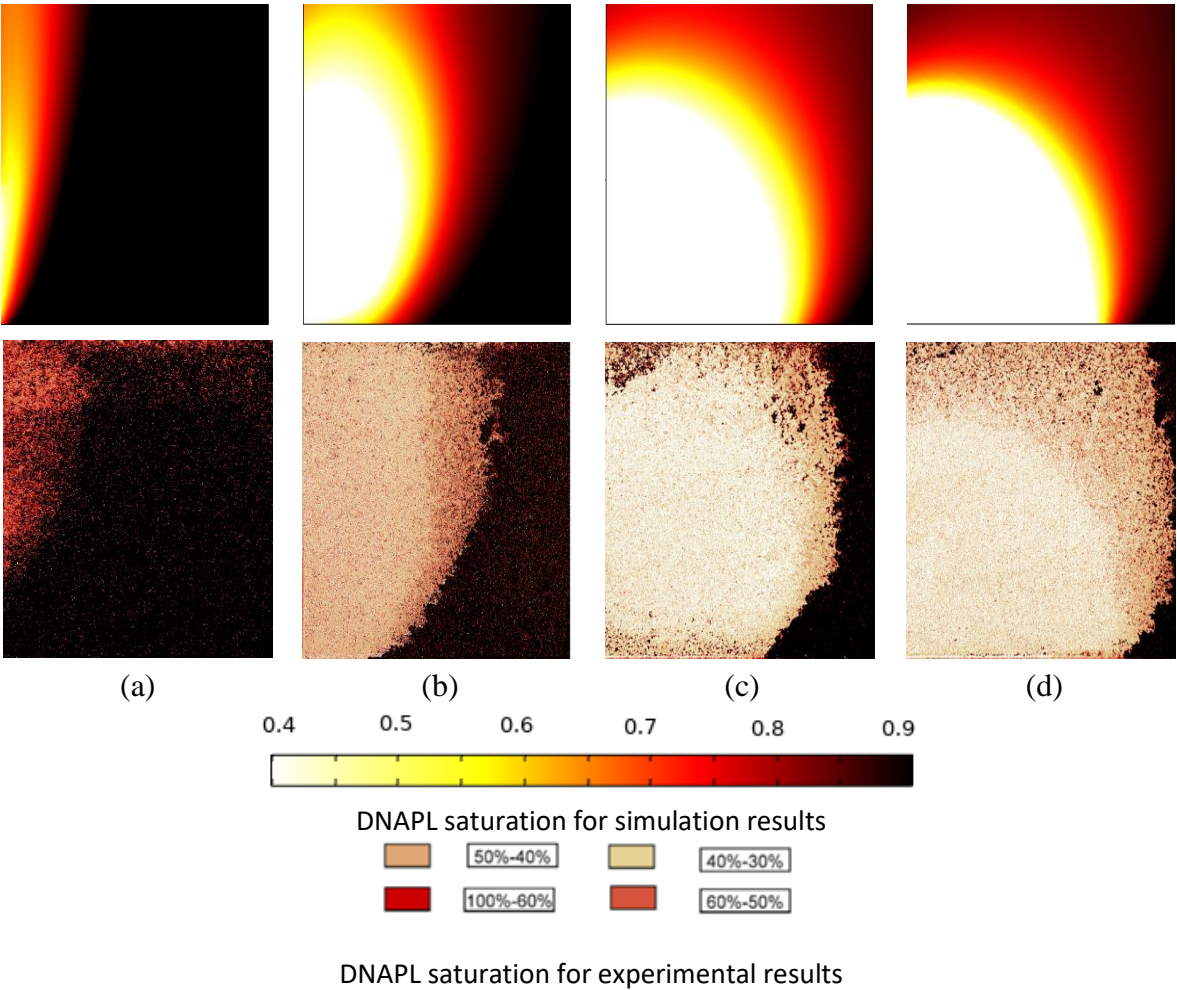


Figure 4.1-9 Comparison between the numerical and experimental results for the end of displacement of DNAPL by barite-CMC suspension, the first row images are from the simulation and the second row images are extracted from the image analysis of experiments. (a) pure polymer injection with density of 1 g/mL after 94 min, barite-CMC injection with

density of (b) 1.3 g/mL after 234 min, (c) 1.66 g/mL after 240 min, and (d) 1.9 g/mL after 220 min

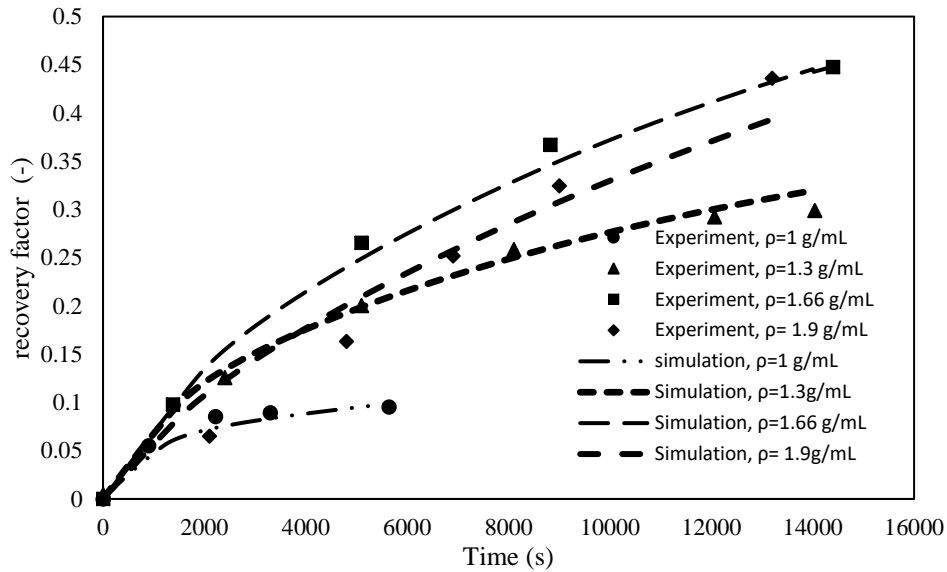


Figure 4.1-10 Comparison between the experimental displacement efficiencies for various densities of invading phases (obtained using mass balance) and those obtained from simulation results

4.1.6.3. Analysis of the transition zone in displaced zone

During the injection of the barite-CMC suspension into the DNAPL saturated zone, due to the deposition of the barite particles onto the sand grain surfaces, and also the mixing with the residual water saturation inside the DNAPL saturated zone, a zone inside the displaced zone near the front has been formed with densities less than the density of invading barite-CMC suspension. Then due to the buoyancy forces, the lighter region has formed a transition zone in front of the fully displaced zone. This transition zone has grown to reach the water zone above the DNAPL saturated zone. To elucidate the diffusive behavior of the segregated fluid from the invading barite-CMC suspension, the evolution of the transition zone, as well as the fully displaced zone (Figure 4.1-12), were analyzed.

The ratio of the transition zone (A_t) to the area of the fully displaced zone (A_d) versus the ratio of the area of the total displaced zone (transition and fully displaced zones, (A_t+A_d)) to the surface area of the region of interest (A_r) is plotted in Figure 4.1-13. At the beginning of the injection, A_t/A_d is at maximum, and then it decreases. In other words, as the front of transition zones reaches the layer of water above the region of interest the transition zone propagation is decelerated. Furthermore, the higher the density of barite-CMC suspension (i.e. higher density difference between the invading fluid and water), the higher is the ratio of A_t/A_d . For example, when half of the region of interest is covered by the invading fluid ($(A_t+A_d)/A_r = 0.5$), A_t/A_d is around 1.38, 0.91, and 0.61 for densities of 1.9, 1.66, and 1.3 g/mL, respectively.

As it was shown in Figure 4.1-12 (in supplementary material), since the beginning of the injection of barite-CMC suspension into the tank, a transition zone was formed in the front of fully displaced zone and it was moving vertically as a sign for a density driven flow. Several factors can influence the transition zone in porous media. In the case of barite-CMC, the deposition and dispersion of barite particles can impact the transition zone.

4.1.6.4. Difference between closed and open systems

There are several studies in which the role of various parameters including boundaries on residual oil saturation, relative permeability and capillary pressure has been investigated (Alamooti et al., 2018; Ataie-Ashtiani et al., 2002; Hollenbeck and Jensen, 1998; Xu et al., 2016). Hollenbeck and Jensen (1998) did several experiments in a vertical column which was homogeneously packed with sand. Various initial capillary pressure heads (from 11.5 to 83.5 cm) have been used. Their results showed that the higher the capillary pressure head, the higher the capillary pressure-saturation curve would lie. Ataie-Ashtiani et al. (2002) by means of numerical experiments investigated the combined effects of boundary conditions and

heterogeneity on capillary pressure and relative permeability. They found that these saturation functions are strongly influenced by heterogeneities and boundary conditions. Xu et al. (2016) did several imbibition experiments at core scale to evaluate the role of displacement pressure gradient on relative permeability curves. They found that at higher displacement pressure gradients the residual oil saturation decreases, the water relative permeability lies higher and oil relative permeability moves to the right. In this regard to match the same production history, residual oil saturation and saturation profile in the closed system, the parameters of capillary pressure and relative permeability curves were redetermined. As a result, the capillary pressure curve lies higher in the case of a closed system in comparison to the open one. For the relative permeabilities when the system is closed the oil and water relative permeability curves have moved to the right.

This ignorance of the difference between the residual saturations in closed and open systems can lead to an overestimation of recovery factor in real field. Thus, it is highly recommended to consider the role of the upper boundary while designing soil remediation methods at the field scale. A way to avoid this problem in real sites could be using a blocking agent to block the upper part of the DNAPL contaminated zone to increase the efficiency of the displacement.

4.1.7. Conclusions

In this study, using two-dimensional tank experiments and corresponding numerical modeling of the displacement process in porous media, the efficiency of the injection of densified polymer suspensions on the displacement of DNAPL was investigated. It was shown that adding barite particles to densify the polymer solution could improve the recovery factor of DNAPL more than 4 times. Using one-dimensional column experiments, it was demonstrated that the barite-CMC suspensions can cause a permeability reduction equal to 55%, 70%, and 72% for different suspensions with densities of 1.3, 1.66, and 1.9 g/mL, respectively. Moreover, the presence of

barite particles can result in a higher viscosity of the polymer suspension while keeping a similar rheological behavior. It was shown that for a confined system which is not a good representative of real polluted site, a higher unrealistic recovery factor can be obtained. The DNAPL displacement by barite-CMC solution was numerically simulated using generalized Darcy's law and the continuity equation. In addition, the clogging of the porous medium by the suspended barite particles was modeled using the transport equation of diluted species. A very good qualitative agreement between the experimental saturation fields and the simulated ones was observed.

4.1.8. Appendix

4.1.8.1. Experimental materials

Here, the properties of materials including the contaminant (DNAPL), barite-polymer suspension and sandpacks, used as the main porous media representative of the real site, are given. Also, the experimental setups in which the different experiments have been carried out are described.

4.1.8.2. DNAPL

The DNAPL used in our study has been extracted from a polluted industrial site (located in the center-east of France). It is mainly composed of heavy chlorinated organic compounds (COC) including hexachlorobutadiene-HCBD (58%), hexachloroethane-HCA (14%), and pentachlorobenzene (3.5%), carbon tetrachloride (4%), and also more conventional COCs such as perchloroethylene-PCE (8%), and trichloroethylene-TCE (2%) (Colombano et al., 2020). The physical properties of DNAPL are given in table 4.1-1.

Table 4.1-1 Physical parameters of the DNAPL (Colombano et al., 2020)

Parameter	Density (kg.L ⁻¹)	Dynamic viscosity (mPa.s)	DNAPL/water interfacial tension (mN.m ⁻¹)	DNAPL/water/sand contact angle (°)
DNAPL, 20 °C	1.66±0.005	4.47±0.15	10.96±0.05	119.33±4.16

4.1.8.3. Barite-polymer suspension

To densify the polymer solution, the barite BariStar® 9015 (average particle size ~ 3.5 microns) was supplied by Mineralia company and consisted of 97.68% of BaSO₄. After preliminary tests with three biopolymers (see section 2.3), the polymer chosen is Carboxymethyl cellulose (CMC), an anionic, water-soluble cellulose derivative polymer containing carboxymethyl groups (-CH₂-COOH) bound to some of the hydroxyl groups. CMC powder as the environmentally friendly biopolymer was supplied by Sigma-Aldrich company. Densities of the powder of CMC polymer and barite particle are 1.6 and 4.72 g/mL respectively. The concentration of barite particles in the suspensions with densities of 1.3, 1.66 and 1.9 g/mL were equal to 381, 838, and 1141 g/L respectively.

4.1.8.4. Soil physics

Sieved white marble sand with the grain size of 0.6 to 0.8 mm was used according to the real polluted site soil properties. The measured permeability of the sand pack is equal to 145 Darcy and the porosity of 39.5%. Also a coarse sand with the grain size between 0.8 and 1 mm and a fine sand of grain size less than 0.1 mm were used during the packing of the 2D tank in order to model the injection zone correctly. To have a consistent and uniform packing, the sand was gradually packed inside the water.

Tables

Table 4.1-2 Parameters of power-law model (Equation 4.1-12) related to rheological behavior of the barite-CMC mixtures (CMC at 4 g/L)

Solution	κ	n	MRE	R ²
Only CMC solution ($\rho=1.0$ g/mL)	0.12	0.8	0.087	0.87
Barite-CMC suspension ($\rho=1.3$ g/mL)	0.13	0.76	0.058	0.93
Barite-CMC suspension ($\rho=1.66$ g/mL)	0.19	0.78	0.066	0.93

Barite-CMC suspension ($\rho=1.9$ g/mL)	0.39	0.61	0.141	0.97
--	------	------	-------	------

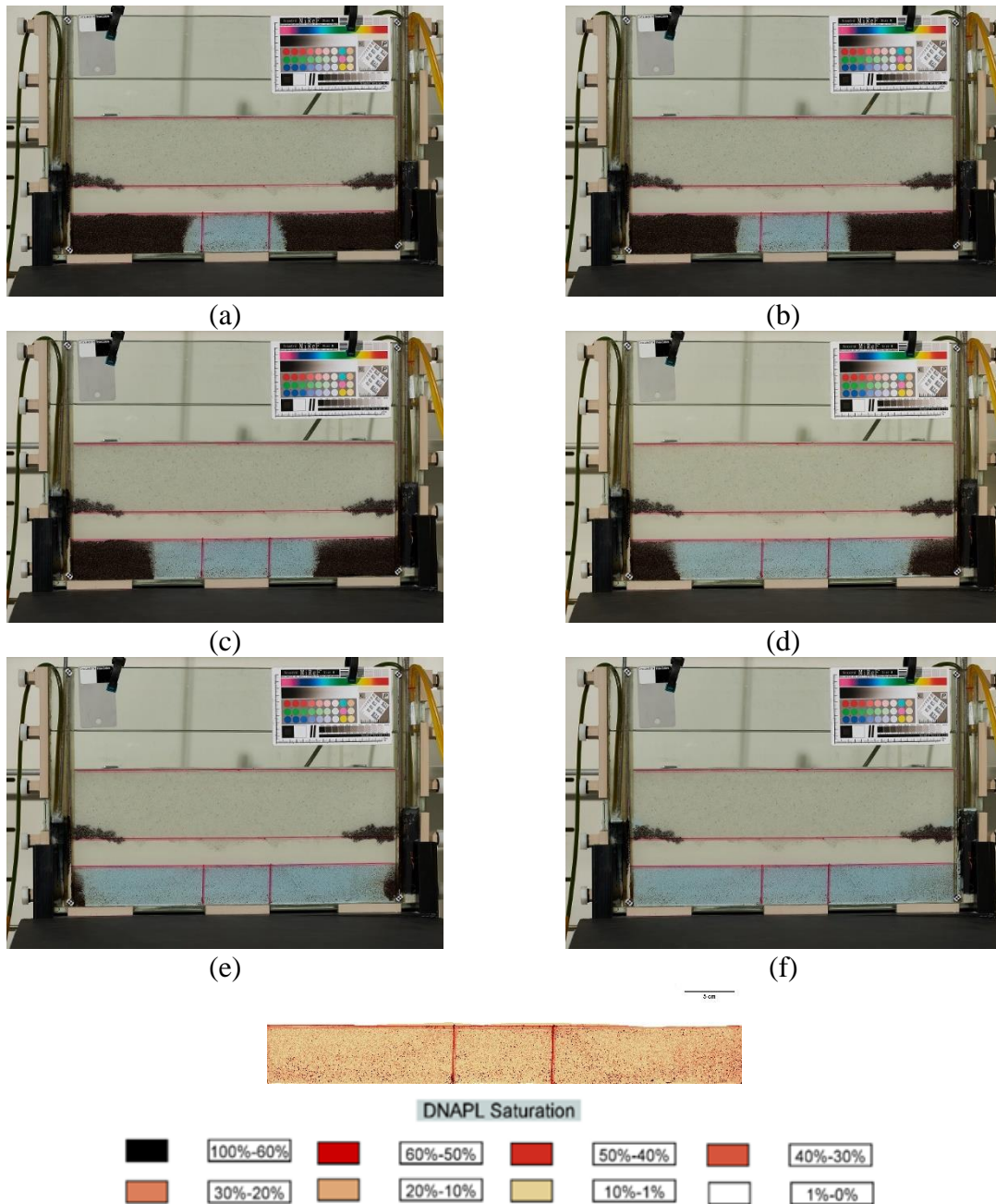
Table 4.1-3 Parameters of Carreau model related to rheological behavior of the barite-CMC mixtures (CMC at 4 g/L)

Solution	μ_{inf}	μ_0	χ	1	R^2
Only CMC solution ($\rho=1.0$ g/mL)	0.04	0.11	1.27	0.83	0.92
Barite-CMC suspension ($\rho=1.3$ g/mL)	0.03	0.21	4.61	0.71	0.99
Barite-CMC suspension ($\rho=1.66$ g/mL)	0.09	0.51	18.96	0.54	0.99
Barite-CMC suspension ($\rho=1.9$ g/mL)	0.12	1.21	12.54	0.42	0.99

Table 4.1-4 Attachment and detachment coefficients and dispersivity for different densities of barite-CMC suspension

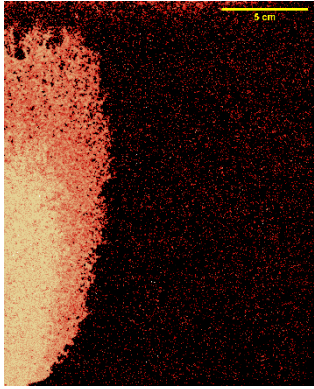
Density of barite-CMC suspension	θ (s^{-1})	β (s^{-1})	α_L (cm)	α_T (cm)	RMSE	MRE (%)
1.3 g/mL	0.1	0.5	0.4	0.04	0.008	0.55
1.66 g/mL	0.1	0.95	0.4	0.04	0.068	3.82
1.9 g/mL	0.1	1.2	0.4	0.04	3.049	5.43

Figures

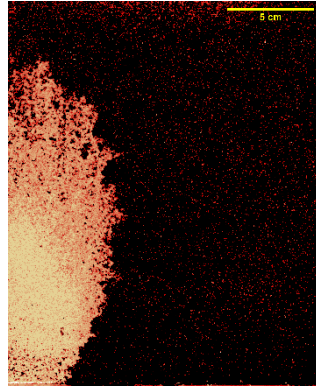


(g)

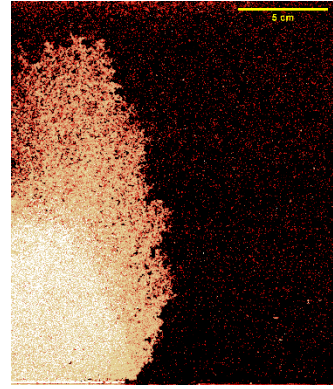
Figure 4.1-11 Propagation of the barite-polymer solutions with density of 1.66 g/mL in a closed system after (a) 20 min, (b) 23 min, (c) 34 min, (d) 49 min, (e) 64 min, (f) 70 min, and (g) the one after 70 min interpreted by image analysis.



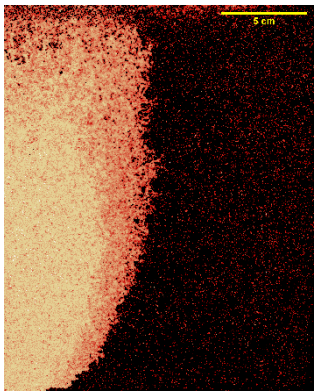
(a-1)



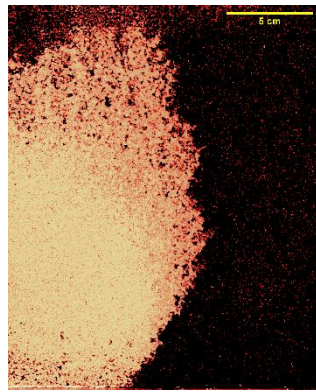
(b-1)



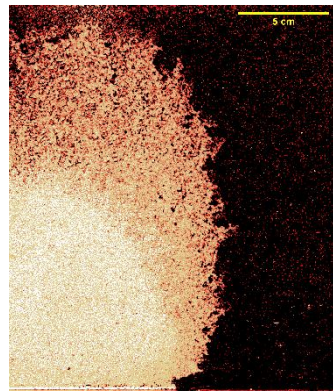
(c-1)



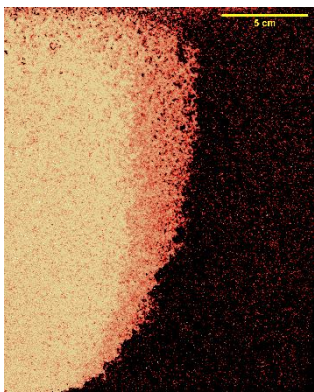
(a-2)



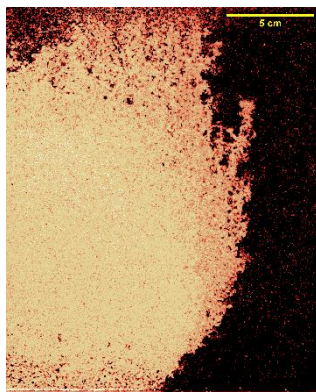
(b-2)



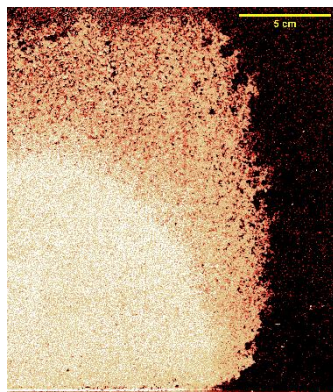
(c-2)



(a-3)



(b-3)



(c-3)

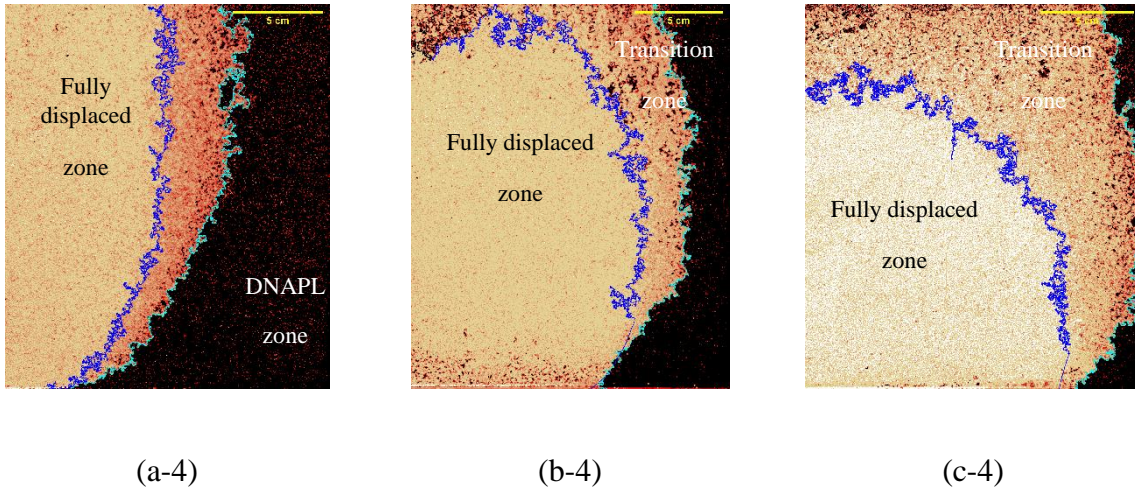


Figure 4.1-12 Images of fully displaced and transition zones in the right hand side of 2D tank for the barite-CMC injection with density (a1-4) 1.3 g/mL at 50, 95, 145, 234 min after injection respectively, (b1-4) 1.66 g/mL 38, 99, 161, 240 min after injection respectively, and (c1-4) 1.9 g/mL 65, 100, 135, 220 min after injection respectively

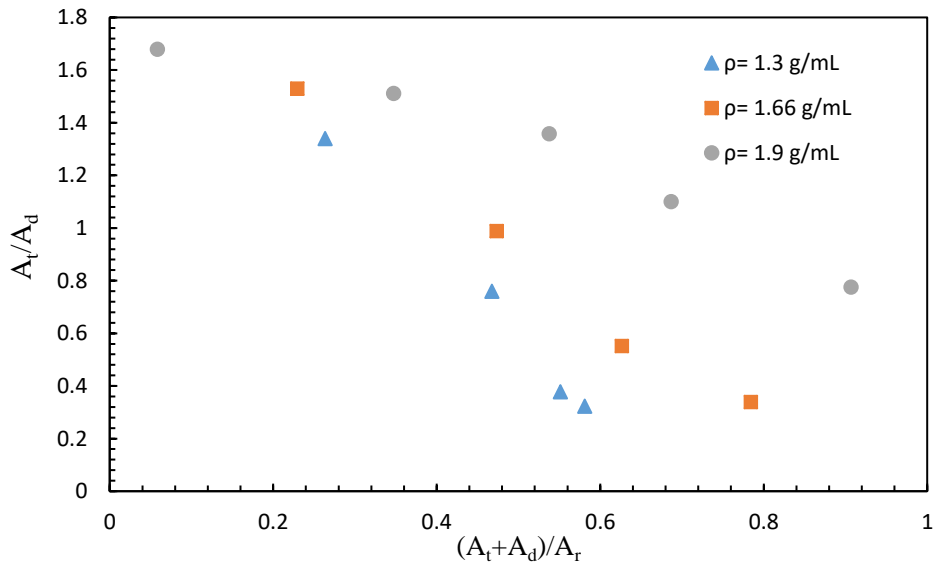


Figure 4.1-13 Dynamics of the growth of the transition zone during the injection of barite-CMC in the 2D tank

Section II

4.2. Gravity-Driven Remediation of DNAPL Polluted Aquifers using Densified Biopolymer Brine Solution: Two-Dimensional Flow Experiments and Simulations

Preamble

Authors: Amir Alamooti *, Stéfan Colombano, Dorian Davarzani, Fabien Lion, Azita Ahmadi-Sénichault

Affiliations: BRGM (French Geological Survey), Orléans, 45000, France; Univ. Bordeaux, CNRS, Bordeaux INP, I2M, UMR 5295, F-33400, Talence, France; Arts et Metiers Institute of Technology, CNRS, Bordeaux INP, Hesam Université, I2M, UMR 5295, F-33400 Talence, France; ADEME (Agence de la transition écologique), ANGERS, 49004, France

Published: Yes

Journal: Advances in Water Resources

Date of publication: 03 February 2024

DOI: <https://doi.org/10.1016/j.advwatres.2024.104643>

Patent: A patent application of this work has been filed with the reference: FR 2305516.

Conference: This work has been presented at Aquaconsoil2023 11 to 15 September 2023, Prague.

4.2.1. Abstract

Polymer solutions aid DNAPL (Dense Non Aqueous Phase Liquid)-contaminated soil remediation but are impacted by gravity and viscous forces. This study assesses the interplay between buoyancy and viscous forces in influencing the distribution of DNAPL and the invading phase, by introducing a densified brine (NaI) biopolymer (xanthan) solution as remediation fluid. A matrix of experiments was conducted, encompassing rheological measurements, multiphase flow tests in 1D-columns and 2D-tanks. Numerical modeling was used to assess polymer and DNAPL propagation under different conditions. NaI addition maintains xanthan's shear-thinning yet lowers mid-range shear viscosity 2.6 times. Confined column tests show similar 89% performance for viscous polymer solutions regardless of density. Unconfined tests mimicking real sites reveal non-densified viscous polymer solution yield mere 0.09 recovery due to density-driven flow. Densified polymer attains radial invasion, boosting recovery to 0.46 with 1.21 aspect ratio. Numerical simulations aligned with experiments, suggesting a near-zero gravity number is necessary to prevent density-driven flow problems. The multiphase flow experiments in confined multilayer system are performed and using the numerical modeling the effects of the permeability contrast and dimensions of the layers on the shape of front are analyzed.

Keywords

DNAPL, remediation, xanthan, sodium iodide, rheology, density-driven flow, two-phase flow modelling

4.2.2. Introduction

Spills of heavy chlorinated solvents (DNAPL) through the soils is one of the main environmental issues in many industrial sites (Alamooti et al., 2022; Colombano et al., 2020; Maire et al., 2019; Santos et al., 2018). DNAPLs can penetrate through the soil and form polluted pools under the groundwater level due to gravity forces (Taghavy et al., 2010; Yang et

al., 2020). Several advanced technologies including surfactant injection (Lee et al., 2005; Pennell and Abriola, 2017; Walker et al., 2022), foam injection (Fitzhenry et al., 2022; Longpré-Girard et al., 2020; Maire et al., 2019) and polymer injection have been developed for the remediation of DNAPL polluted soils (Alamooti et al., 2023, 2022; Martel et al., 1998; Omirbekov et al., 2023). However, the efficiency of these methods for DNAPL remediation can be limited as the density-driven flow affects the recovery of DNAPL. During the remediation of soils contaminated with DNAPL, density-driven flow has been observed. This occurs when a less dense fluid displaces a denser fluid, known as overridden flow, or when a denser fluid displaces a less dense fluid, known as underridden flow. Several studies have investigated density underridden flow in 2D systems for DNAPL remediation purposes, including miscible cosolvent displacement by water injection (Jawitz et al., 1998; Taylor et al., 2001), and water displacement during brine surfactant injection (Zhong et al., 2008). Zhong et al. (2008) proposed that the addition of the polymer to the densified brine surfactant can control the underridden flow by providing enough viscous forces to overcome gravity; however, the relative density difference has been limited to 1.008. Taylor et al. (2004) in a set of two dimensional experiments observed that a minor density difference (0.008 g/mL) between the injecting ethanol-surfactant mixture and water present near the perchloroethylene (PCE)-contaminated zone can result in density overridden flow. Grubb and Sitar (1999) reported the downward migration of trichloroethylene (TCE) along the water-ethanol interface during ethanol injection in two-dimensional uniform and layered sand packs. They also observed the ethanol gravity override with an increasing inclination angle of the ethanol front along with invasion progress. The density difference between ethanol and water is 0.211 g/mL, and the density difference between TCE and water is 0.46 g/mL.

Density modification displacement is an approach to control the downward migration of DNAPL by reducing its density through sufficient partitioning of alcohol within DNAPL and

turning it to LNAPL (Damrongsiri et al., 2013; Kibbey et al., 2002; Lunn and Kueper, 1999; Ramsburg and Pennell, 2002). The density modification by alcohol partitioning can be reversible depending on the equilibrium of alcohol, water and DNAPL (or newly formed LNAPL). Besides, colloidal biliquid aphron (CBLA), consisting of two surfactants, water, and an oil phase, has been employed to control the downward migration of DNAPL to non-polluted zones by lowering its density (Yang et al., 2020; Yan et al., 2011). CBLA has a foam structure with micron-sized (5-20 microns) droplets consisting of an outer thin aqueous phase and an internal light organic phase. In this approach, the internal light non-aqueous phase is mixed with DNAPL using a demulsifying agent, which transforms it into Light Non-Aqueous Phase Liquids LNAPL. Although it can influence the downward migration of DNAPL, its efficiency relies on the performance of the demulsifier. Also, propagation of the light colloidal biliquid aphron that can flow over the DNAPL is challenging due to the influence of buoyancy forces. To mobilize a DNAPL droplet trapped in pore spaces, the summation of the buoyancy and viscous forces should be more than capillary force (Alamooti et al., 2020; Mansouri-Boroujeni et al., 2023; Pennell et al., 1996). The gravity number is defined as the ratio of the buoyancy and viscous forces showing the balance between them and consequently the direction of flow. It can be considered as (Shook et al., 1998):

$$N_G = \frac{\Delta\rho g k}{v\mu} \quad \text{Eq 4.2-1}$$

where $\Delta\rho$ is the density difference (kg/m^3), g is the gravitational acceleration (m/s^2), k is the intrinsic permeability (m^2), v is the velocity magnitude of the invading phase (m/s), μ is the viscosity of the invading phase (Pa s). Large negative N_G values correspond to dominant buoyancy forces leading to a vertical migration of the DNAPL if the residence time of the injected phase is large as well (Jin et al., 2007).

Miller et al. (2000) in an experimental study used a brine (sodium iodide dissolved in water) solution with a density of 1.79 g/mL to displace the DNAPL (TCE with a density of 1.464 g/mL) pools in a two-dimensional heterogeneous system. They showed that using the densified brine solution around 55% of initial DNAPL was recovered as a direct result of buoyancy forces, however the residual DNAPL was distributed in the entire medium. Jin et al. (2007) in a numerical study examined the downward migration of DNAPL during surfactant flooding. In their numerical approach they considered negligible adsorption of chemical species and dispersion in the transport; focusing mainly on 'body forces' i.e. viscous, buoyancy, and capillary forces. The simulation outcomes indicated that there is a high risk of DNAPL's downward migration during surfactant flooding if the viscous forces are not dominant. This highlights the crucial role played by viscous forces, which can be supplied by the polymer solution.

The performance of the injection of the polymer solutions for recovery of pollutants in contaminated soils have been widely investigated (Alamooti et al., 2022; Bouzid and Fatin-Rouge, 2022; Giese and Powers, 2002; Martel et al., 1998, 2004; Omirbekov et al., 2023; Robert et al., 2006; Wu et al., 2000).

Robert et al. (2006) evaluated density-driven plume sinking during the injection of a xanthan-surfactant mixture for displacement of TCE in a heterogeneous 2D sandbox. Their results indicated that to prevent downward migration of surfactant polymer mixture containing the dissolved DNAPL, it is important to avoid excessive increase in the density of the mixture during DNAPL dissolution. They stated that the density plume sinking can be prevented by a strong hydraulic gradient that can be provided by a polymer.

Recent studies have shown that the injection of a densified polymer suspension can improve up to four times the recovery of a multicomponent DNAPL compared to a non-densified polymer solution (Alamooti et al., 2022; Omirbekov et al., 2023). Alamooti et al. (2022) conducted

numerical and experimental investigations, revealing that densifying the polymer (carboxymethyl cellulose) with barite particles to match the DNAPL density (same DNAPL as in this study) can counteract buoyancy forces and improve DNAPL recovery. The lateral displacement of DNAPL decreased as the density of the barite-polymer suspension decreased. The study showed that the presence of barite particles in the polymer suspension can reduce soil permeability by up to 70% due to barite particle deposition. While the presence of barite particles in the polymer suspension can reduce the back-diffusion of residual DNAPL to the groundwater zone, it can result in higher injection pressures and hinder the ability of subsequent remediation reagents to fully react with DNAPL.

In addition to studies about density-driven flow in the context of soil remediation, substantial research has investigated this phenomenon within porous media, commonly known as gravity currents (Anderson et al., 2003; Di Federico et al., 2014; Huppert et al., 2013; Longo et al., 2015). These currents play a crucial role in various environmental scenarios, such as seawater intrusion in coastal aquifers, where they manifest at the interface of fresh water and brine (Koohbor et al., 2019). This process is also observed in applications like CO₂ sequestration, where the interaction between CO₂-rich brine and CO₂-free brine induces natural convection. This, in turn, leads to the descent of dense CO₂-rich brine fingers under gravity, facilitating the transport of aqueous CO₂ into deep saline aquifers (Du et al., 2023). The propagation of density driven flow in natural porous formations is strongly affected by heterogeneity. In a theoretical study, density-driven fluid drainage from an edge of a heterogeneous system, exemplified by a V-shaped Hele-Shaw cell where permeability varies transverse to the flow direction, reveals that profile shapes and the remaining mass in the medium are influenced by variations in both vertical porosity and permeability (Zheng et al., 2013). Ciriello et al. (2013) developed an analytical formulation to describe the propagation of plane viscous gravity currents in porous media, considering varying permeability conditions transverse or parallel to the propagation

direction. Their study reveals that spatial variations in permeability not only influence the rate of spreading but also affect the current profile, steepness, and average height.

Huppert et al. (2013) investigated the gravitational flow of a dense fluid in a two-layered porous medium, considering experimental and theoretical analyses. When the upper layer is more permeable than the lower one, gravity and flow focusing initially counteract. At low input flux, flow confines to the lower layer; however, beyond a critical flux, the fluid preferentially spreads horizontally in the upper layer before draining back down. Above this critical flux, increased resistance in the higher permeability upper layer dominates, causing the denser current to override the less dense fluid in the lower layer, leading to a gravitationally unstable state susceptible to Rayleigh–Taylor instability.

Di Federico et al. (2014) formulated a closed-form solution for radial gravity currents involving power-law fluids in porous media with deterministic vertical permeability variation. Their results highlight the substantial impact of the rheological properties of the intruding fluid and permeability variations on the radius and profile of gravity-driven currents within porous media. In this work, we analyze the efficiency of the injection of a densified polymer brine solution to remediate the DNAPL-contaminated soil. This solution contains xanthan gum as the polymer and sodium iodide salt as a soluble densifier. We conducted several experiments, including rheological measurements, 1D column tests, unconfined single layer and confined two-layer 2D sandbox experiments aimed at investigating the impact of saline densification on DNAPL recovery efficiency. Additionally, we employed numerical simulations to assess the propagation of the polymer solution and DNAPL under various gravity numbers.

The main objectives of this study are (i) to assess the individual and combined effects of increasing viscosity and densification of remediation fluid on the displacement of DNAPL, (ii) to compare the efficiency of these technologies in both confined 1D and unconfined 2D media, (iii) to analyze the competition between buoyancy and viscous forces on the distribution of

DNAPL and the invading phase and (IV) to evaluate the efficiency of densified polymer solution on displacement of DNAPL from two-layer system. This study aims to make a valuable contribution to the remediation of DNAPL contamination in groundwater environments.

4.2.3. Materials and methods (experimental and numerical)

4.2.3.1. Experimental materials

The soil used in this study was made up of marble sand packs that were sieved and washed with deionized water, and then dried at a temperature of 105 °C. Three particle-size fractions of marble sand (0.2 to 0.3 mm, 0.4 to 0.6 mm, and 0.6-0.8 mm equivalent to absolute permeabilities of 0.34 ± 0.05 , 1.05 ± 0.1 , and $1.8 \pm 0.1 \cdot 10^{-10} \text{ m}^2$ respectively) have been used as the solid phase in 1D column and 2D tank studies.

Xanthan gum, a biopolymer with the chemical formula $\text{C}_{35}\text{H}_{49}\text{O}_{29}$ (purity >99%), and sodium iodide salt (NaI) (purity >99%) were provided in powder by Sigma-Aldrich, and solutions were prepared using deionized water. The DNAPL used in the study consisted primarily of hexachlorobutadiene-HCBD (58%), hexachloroethane-HCA (14%), and penta-chlorobenzene (3.5%), as well as carbon tetrachloride (4%). There are some other components in DNAPL mixture that are not quantifiable. The density and viscosity of the multicomponent DNAPL have been 1.66 g/mL and 4.47 mPa s, respectively (Alamooti et al., 2022; Colombano et al., 2020; Rodrigues et al., 2017). A rotational rheometer Haake Mars 60 equipped with the cone-plate geometry was used to assess the rheological behavior of the polymer solutions. Acknowledging the potential impact of wall slip on polymer rheology (Di Federico et al., 2017), we varied the gap between rotating and fixed plates, yet observed no significant changes in rheological behavior at different gap distances. The drop shape analyzer apparatus (DSA-100, KRUSS) was employed to measure the interfacial tension (IFT) between the polymer solutions and DNAPL. The IFT was determined using the pendant drop method at ambient temperature ($22 \pm 1 \text{ }^\circ\text{C}$).

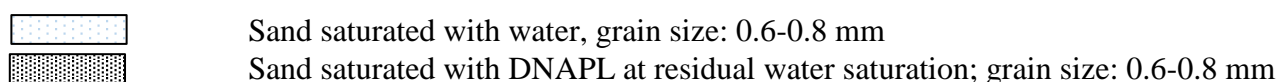
4.2.3.2. Column and 2D tank experiments

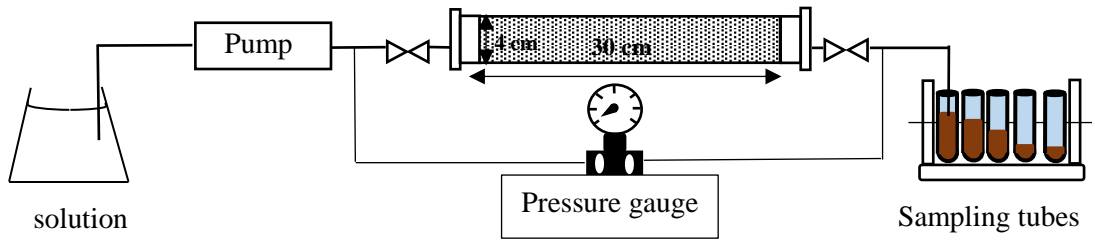
Column experiments were conducted to investigate the displacement of DNAPL by various solutions in a one-dimensional (1D) system. The experimental procedure, as described previously by Alamooti et al. (2022), involved using glass columns that were 4 cm in diameter and 30 cm in length. The columns were flushed with CO₂ gas, and then vertically saturated with deionized water at a flow rate of 0.1 mL/min for 2 PV. Next, DNAPL was injected vertically upward into the column at a flow rate of 1 mL/min until no water production was observed. Finally, the solutions were individually horizontally injected into the columns at a flow rate of 1 mL/min using a Reglo ICC digital peristaltic pumps (Ismatec®). The pressure at the inlet and outlet were monitored. A schematic of the multiphase flow in the 1D column experiments can be seen in Figure 1a.

The unconfined 2D experiments were conducted to assess the efficiency of DNAPL displacement using different solutions in a system close to the real polluted site. The experiments were carried out in a 2D sandbox measuring 50 cm in length, 30 cm in height, and 2 cm in thickness. Initially, sand packs were compacted under water, and then DNAPL was injected into the water-saturated porous media until it reached a height of 20 cm. Next, different solutions were individually injected into the DNAPL-contaminated zone using a port located in the bottom central part of the sandbox at a flow rate of 2 mL/min. The level of DNAPL in the system was maintained constant during the injection of remediation fluids using peristaltic pumps connected to cavities on two sides of the sandbox. The injection of the solutions were continued until no more DNAPL was recovered or the solution fronts reached the lateral boundaries of the system. The mass of the recovered DNAPL was measured using a mass scale (Sartorius Cubis MSE8201S-000-D0), and real-time data (pressure and mass balance)

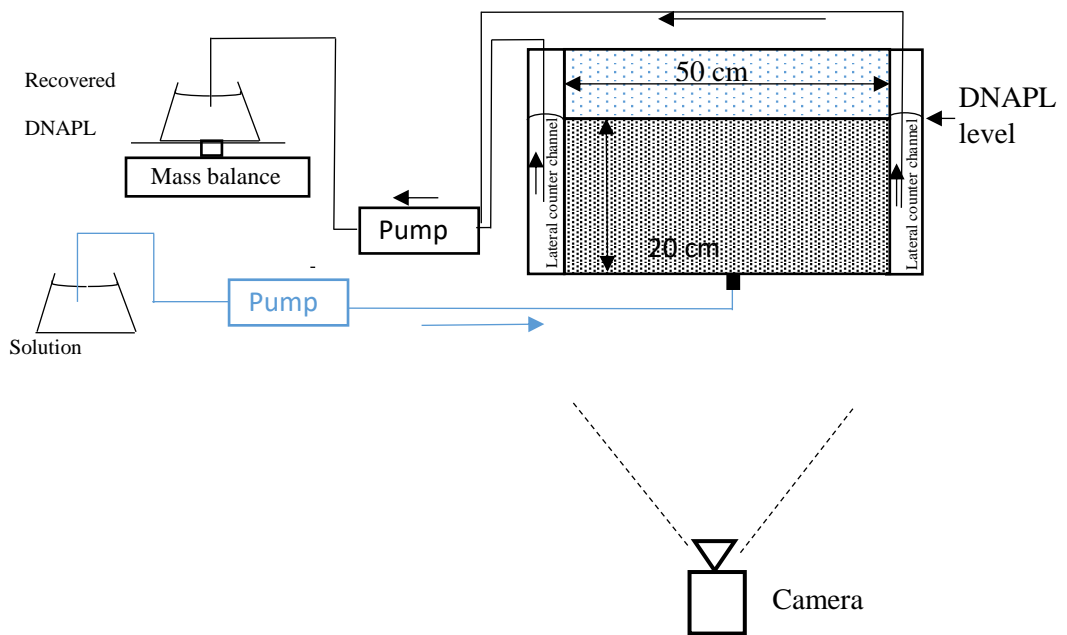
acquisition was performed. To further analyze the propagation of the fluids, 2D images of the tank were regularly captured using a Nikon D810 camera equipped with a NIKKOR 105 lens. A schematic of the multiphase experiments in the unconfined 2D sandbox can be seen in Figure 1b. This unconfined setup, designed to mimic the fluid configuration of a real polluted site (featuring DNAPL-saturated soil at the bottom and water on top) and lacking confinement on the upper boundary, facilitates a clear visualization of how polymer solutions perform in displacing DNAPL within a polluted zone, notably without the presence of a blocking layer on top.

A confined 2D tank was used to evaluate the efficiency of injecting polymer solutions into a multilayer heterogeneous system. The tank's dimensions were 15 cm × 10 cm × 2 cm, with glass fronts for imaging. Two distinct layers, each 5 cm in height, were established within the tank, and sand was compacted inside, while water was continuously injected from the bottom. Upon complete saturation of the two layers with water, DNAPL was uniformly injected from three ports located at the bottom, through the layers, at a rate of 3×0.5 mL/min. Polymer solutions (un/densified) were injected from two ports on the left side of the tank at a rate of 2×0.5 mL/min. The injection of polymer led to the natural production of DNAPL in the effluent, similar to the column tests. The schematic of confined multilayer 2D tank is shown in Figure 1c. This system facilitates monitoring the displacement of DNAPL, influenced by both permeability contrast and density differences, within a well-controlled multilayer porous media. It achieves this by preventing the vertical migration of the polymer solution (which is a scenario commonly observed in an unconfined 2D system).

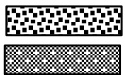




(a)



(b)



Sand saturated with DNAPL at residual water saturation, grain size: 0.4-0.6 mm
 Sand saturated with DNAPL at residual water saturation; grain size: 0.2-0.3 mm

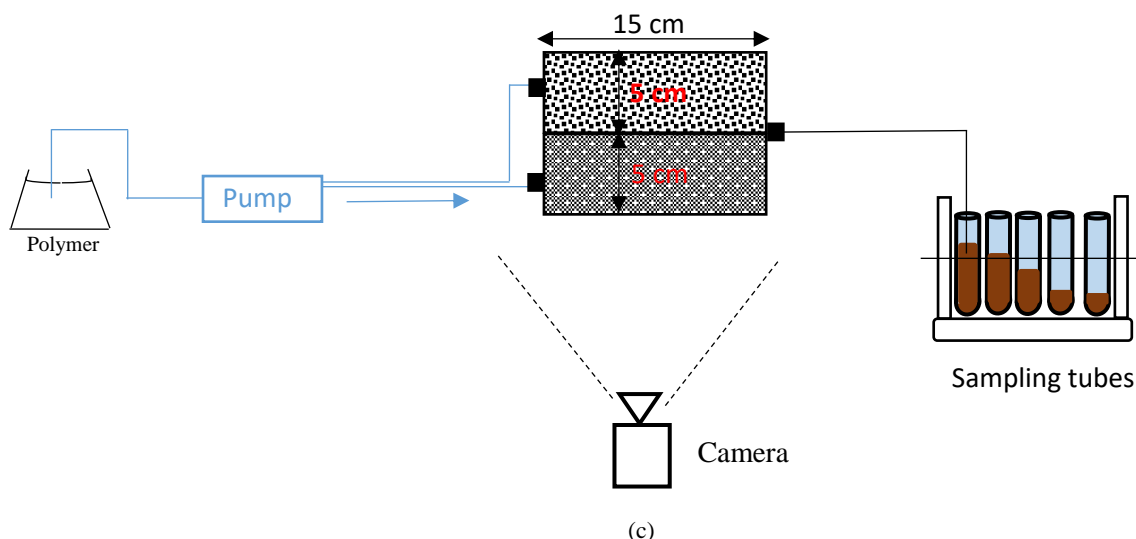


Figure 4.2-1 Schematic of polymer-DNAPL displacement experimental setup. (a) 1D column setup, (b) unconfined 2D tank, and (c) confined multilayer 2D tank

4.2.3.3. Xanthan-NaI solutions

The concentration of xanthan in the polymer solution was chosen at 0.8 g/L to provide a stable front during displacement of DNAPL for the injection rate of 1 mL/min in the column (Lenormand et al., 1988). A dense brine solution was prepared by mixing sodium iodide with water to achieve a density close to that of DNAPL at 1.7 g/mL. The xanthan-NaI mixture was used to achieve the appropriate viscosity for a stable front, favorable mobility ratio, and to counteract buoyancy forces during DNAPL displacement. To prepare the mixture, the xanthan solution with a concentration of 0.8 g/L was initially prepared. Next, sodium iodide powder was added to the solution to reach a density of 1.7 g/mL, which is equivalent to a concentration of 960.11 g/L (considering the solubility of sodium iodide in water is around 1842 g/L at 25 °C). Consequently, the resulting mixture had a lower concentration of xanthan of 0.59 g/L. The descriptive parameters for each experiment is shown in Table 1.

Table 1 Parameters used in all experiments

Dimensions D: diameter L: Length W: Width H: Height	Number of layers	Displacing phase	Displaced phase	$\Delta\rho \left(\frac{Kg}{L}\right)$ Displacing - Displaced	Injection rate (mL/min)	Grain size (mm)	Permeability ($10^{-10} m^2$)
1D column (D 4 cm × L 30 cm)	1	Xanthan	Water	0	1	0.6-0.8	1.8
1D column (D 4 cm × L 30 cm)	1	Xanthan- NaI	water	700	1	0.6-0.8	1.8
1D column (D 4 cm × L 30 cm)	1	Xanthan	DNAPL	-660	1	0.6-0.8	1.8
1D column (D 4 cm × L 30 cm)	1	Xanthan- NaI	DNAPL	34	1	0.6-0.8	1.8
1D column (D 4 cm × L 30 cm)	1	NaI	DNAPL	34	1	0.6-0.8	1.8
2D tank (L 50 cm × H 30 cm × 2 cm)	1	Xanthan	DNAPL	-660	2	0.6-0.8	1.8
2D tank (L 50 cm × H 30 cm × 2 cm)	1	Xanthan- NaI	DNAPL	34	2	0.6-0.8	1.8
2D tank (L 50 cm × H 30 cm × 2 cm)	1	NaI	DNAPL	34	2	0.6-0.8	1.8
2D tank (L 15 cm × H 10 cm × 2 cm)	2	Xanthan	DNAPL	-700	2×0.5	0.4-0.6 0.2-0.3	1.03 0.34
2D tank (L 15 cm × H 10 cm × 2 cm)	2	Xanthan- NaI	DNAPL	34	2×0.5	0.4-0.6 0.2-0.3	1.03 0.34

4.2.3.4. Numerical modeling

4.2.3.4.1. Two-phase flow in porous media

The soil is considered as a uniform and isotropic porous medium containing water and DNAPL as incompressible and immiscible phases. The continuity equation for each phase can be considered as follows (Bear, 2013):

$$\frac{\partial}{\partial t} (\phi \rho_i S_i) + \nabla \cdot (\rho_i \mathbf{u}_i) = 0 \text{ with } i = w, nw \quad \text{Eq 4.2-2}$$

where the subscripts "w" and "nw" refer to the wetting and non-wetting phases, respectively.

The porosity is represented by the symbol ϕ (-), time by t (s), while the density, saturation, and the Darcy velocity of the i-phase are denoted by ρ_i (kg/m^3), S_i (-) and \mathbf{u}_i (m/s) respectively. The generalized Darcy's law for the flow of two phases in isotropic porous media is given by:

$$\mathbf{u}_i = -\frac{k k_{ri}}{\mu_i} (\nabla p_i - \rho_i \mathbf{g}) \quad \text{Eq 4.2-3}$$

where k (m^2) represents the scalar absolute permeability of the isotropic porous medium, and k_{ri} (-) denotes the relative permeability for phase i . The viscosity and pressure of the phase i are represented by μ_i ($Pa.s$), p_i (Pa) respectively, and the gravity vector is represented by \mathbf{g} (m/s^2). As the volume of the void space in a rigid porous medium is considered constant, it is exclusively occupied by aqueous and non-aqueous phases; therefore, the sum of the saturations of wetting and non-wetting phases always equals one. To present the capillary pressure, which reflects the difference in the pressure between the aqueous and non-aqueous phases, as well as the relative permeability curves in the model, Brooks and Corey functions are used (Brooks and Corey, 1964):

$$p_c = p_{th} S_{we}^{-\frac{1}{\lambda}} \quad \text{Eq 4.2-4}$$

$$k_{rw} = k_{rw}^{max} S_{we}^{\epsilon_w} \quad \text{Eq 4.2-5}$$

$$k_{rnw} = k_{rnw}^{max} S_{nwe}^{\epsilon_{nw}} \quad \text{Eq 4.2-6}$$

where the index of the pore size distribution is represented by λ (-) and p_{th} denotes the threshold pressure (Pa). The maximum relative permeability values, or end points, for the wetting and non-wetting phases are indicated by k_{rw}^{max} and k_{rnw}^{max} , respectively. ϵ_w and ϵ_{nw} indicate the saturation exponents for the wetting and non-wetting phases, respectively. The effective saturations of wetting and non-wetting phases are denoted by S_{we} (-) and S_{nwe} (-) and can be expressed as:

$$S_{we} = \frac{S_w - S_{wr}}{1 - S_{nwr} - S_{wr}} \quad \text{Eq 4.2-7}$$

$$S_{nwe} = \frac{S_{nw} - S_{nwr}}{1 - S_{nwr} - S_{wr}} \quad \text{Eq 4.2-8}$$

where the wetting irreducible and non-wetting residual saturations are represented by S_{wr} (-) and S_{nwr} (-), respectively.

4.2.3.4.2. Solute transport model

In porous media, the transport of solute is described by the classical differential advection-dispersion equation (O'Carroll et al., 2013; Tsakiroglou et al., 2018):

$$\underbrace{\frac{\partial(\phi S_w c_i)}{\partial t}}_{\text{Accumulation}} - \underbrace{\nabla \cdot (\phi S_w \mathbf{D} \cdot \nabla c_i)}_{\text{Dispersion}} + \underbrace{\mathbf{u}_w \cdot \nabla c_i}_{\text{Advection}} = R_i + \dot{m} \quad \text{Eq 4.2-9}$$

where the concentration of the i -component (kg/m^3) is represented by c_i , \mathbf{D} denotes the dispersion tensor, the reaction term for the i -component is indicated by R_i and \dot{m} signifies the source term. The adsorption of xanthan as an anionic polymer and NaI as an inherent tracer on the sand surface is neglected. The principal and cross terms of dispersion tensor for an isotropic porous medium can be represented as (Auset and Keller, 2004; Bear, 2013):

$$\mathbf{D} = (\alpha_T |\mathbf{U}_w| + D_{eff})\mathbf{I} + (\alpha_L - \alpha_T) \frac{U_{wx}U_{wy}}{|\mathbf{U}|} \quad \text{Eq 4.2-10}$$

$$D_{eff} = \frac{D_0}{\tau} \quad \text{Eq 4.2-11}$$

where the identity matrix is denoted as \mathbf{I} , the effective diffusion coefficient in porous media is represented as D_{eff} (m^2/s). The molecular diffusion coefficient is indicated as " D_0 (m^2/s), and τ refers to the tortuosity. Furthermore, α_L and α_T are used to represent the longitudinal and transverse dispersivities, respectively.

Through the following formula, it is possible to derive the molecular diffusion coefficient of xanthan, a polysaccharide (Kono, 2014):

$$D_0 = 8.2 \times 10^{-9} M_w^{-0.49} \quad 5$$

where the coefficient 8.2×10^{-9} is in $(\text{m}^2 \text{s}^{-1} \text{g}^{0.49} \text{mol}^{-0.49})$ and M_w (g mol^{-1}) is the molecular weight of xanthan. Diffusion coefficients of sodium and iodide ions at 25 °C are 1.33×10^{-9} and $2 \times 10^{-9} \text{ m}^2/\text{s}$ respectively (Yuan-Hui and Gregory, 1974).

By coupling the equations 2, 3 and 9, the displacement of DNAPL and solute transport through two-dimensional domains was simulated. A total of 10598 triangular meshes were used to discretize the simulation domain. The parameters used for simulating two-phase flow in 2D tank including the relative permeability, capillary pressure and dispersivities have been shown in Table 2 for three solutions. The maximum element growth rate used was 1.1, while the maximum and minimum sizes of the elements were 0.48 cm and 0.00094 cm, respectively. To enhance the convergence of the numerical model, the mesh was refined in the vicinity of the injection port, with a maximum element size of 0.11 cm. The finite element solver used was MUMPS (multifrontal massively parallel sparse direct solver) within COMSOL Multiphysics. For the time-stepping approach, a backward differentiation formula (BDF) was employed, along with the free time-stepping option, enabling flexible time steps to meet the specified tolerance. The tolerance factor used was 0.1. The boundary conditions for 2D tank, the constant injection rate of 2 mL/min and injection concentration of each component for the injection port and constant pressure for the lateral and upper boundaries were considered (Figure 4.2-2).

Table 4.2-6 Relative permeability and capillary pressure parameters used in modeling and mean average error of experimental and numerical data for 2D tank

System	Solution	k_{rw}^{max} (-)	k_{rnw}^{max} (-)	ϵ_w (-)	ϵ_{nw} (-)	λ	p_{th} (Pa)	S_{wr} (-)	S_{nwr} (-)	α_L (cm)	α_T (cm)	MAE (Mean Absolute Error)
Unconfined	Mixture	0.5	0.7	2.5	3	2	500	0.12	0.3	0.1	0.001	0.102

	NaI	0.5	0.7	2.5	3	0.12	0.32	0.103
	Xanthan	0.8	0.55	2.3	3	0.12	0.48	0.084
Confined multilayer	Mixture	0.7	0.6	2.3	3.2	0.08	0.22	0.018

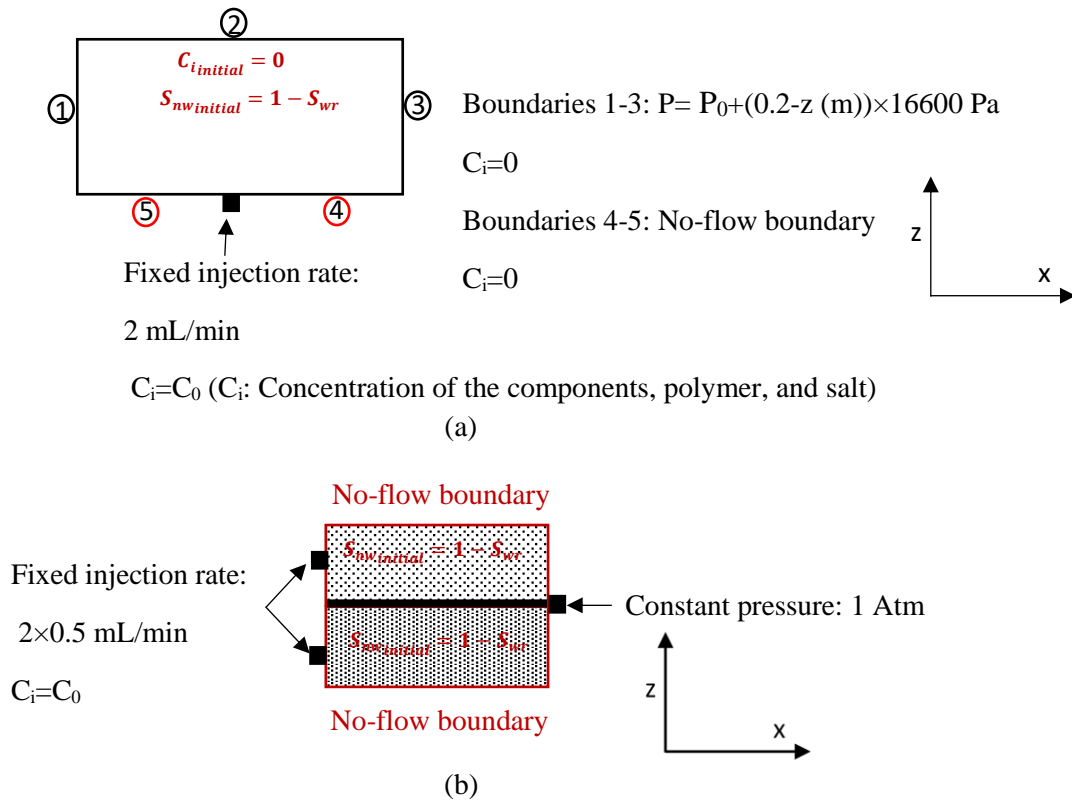


Figure 4.2-2 Schematic of boundary and initial conditions for numerical simulations in 2D tank. (a) unconfined single layer 2D tank, (b) confined two-layer 2D tank

4.2.3.5. Image analysis

Image analysis was used to track changes in the two-phase flow inside the porous medium over time and estimate DNAPL saturation. To capture high-quality images, a Nikon® D810 was used in a dark room, illuminated by two 300 W (Broncolor®) floodlights. To reduce reflections and optimize contrast, black and white reflectors were placed at precise locations in the laboratory. A grayscale calibration card was positioned on the front surface of the 2D tank to regulate the light density during image analysis. Using the 8-grayscale levels the lighting variances were modified. To minimize the impact of wall shading on the phases' saturation

calculation, the size of the area of interest (AOI) was chosen to be almost the same as the lateral surface of the tank glass (Alamooti et al., 2022; Colombano et al., 2021; Philippe et al., 2020b).

The optical density of reflected light O_d , is considered as (Flores et al., 2011):

$$O_d = -\log(\rho_t) \quad \text{Eq 4.2-12}$$

$$\rho_t = \frac{I_r}{I_0} \quad \text{Eq 4.2-13}$$

where optical density of reflected light is denoted as $O_d(-)$, and the ratio of reflected luminous intensity $I_r(-)$ to the initial luminous intensity $I_0(-)$ is represented as $\rho_t(-)$.

Next, optical densities were measured at four points: points where the porous medium was fully saturated with water and DNAPL, as well as points with known residual saturations of DNAPL and water. A linear calibration curve was used to correlate the optical densities with DNAPL saturation (Alamooti et al., 2022; Colombano et al., 2020). The average DNAPL saturation for the entire area of interest (AOI) was determined by summing the individual saturations for each pixel, which were obtained from the optical density measurements. The calculated saturation was then compared to those obtained through mass balance calibration.

4.2.4. Results and discussion

4.2.4.1. Rheological behavior in bulk and porous media

Figure 4.2-3 displays the rheological behaviour of xanthan solution with and without NaI, along with the fitted Carreau fluid model (Carreau, 1972) expressed as:

$$\mu = \mu_{inf} + (\mu_0 - \mu_{inf})(1 + (\chi\dot{\gamma})^2)^{\frac{l-1}{2}} \quad \text{Eq 4.2-14}$$

where, μ_0 and μ_{inf} represent the viscosities (Pa.s) at zero and infinite shear rate respectively, χ denotes the relaxation time (s), and l (-) indicates the power index. The parameters of Carreau model for xanthan solutions in the presence and absence of NaI are shown in Table 4.2-2. As it can be seen the results from Carreau model is properly fit with experimental results.

Table 4.2-7 parameters of Carreau model for pure xanthan and mixture of xanthan and NaI

solution	μ_{inf} (Pa.s)	μ_0 (Pa.s)	χ (s)	l (-)	R^2
Xanthan solution	0.0087	4.310	36.755	0.1237	0.988
Mixture of xanthan and NaI	0.0072	3.214	67.330	0.0515	0.988

The experimental results show that xanthan exhibit a shear thinning behavior which is preserved in the presence of NaI while the viscosity of the solution is reduced (Najjari et al., 2016). This can be justified by the lower concentration of xanthan in the mixture due to the increase in volume of solution by dissolution of NaI. Also, xanthan as a long-chain polysaccharide contains negatively charged chemical groups, such as acetyl and pyruvate groups. The electrostatic repulsion between these negative charges cause the xanthan molecules to extend and form a coiled shape due to electrostatic repulsion (Carrington et al., 1996). However, when salt ions are present, they reduce the electrostatic repulsion and cause the xanthan molecule to collapse into a more compact and rod-like shape. As a result, the negatively charged groups are positioned closer to the molecule's backbone, which leads to a decrease in its hydrodynamic volume (Higiro et al., 2007; Rochefort and Middleman, 2000). The lower the hydrodynamic volume the easier xanthan molecules can move in the solution; resulting in a reduction in viscosity. As a result the viscosity of mixture of NaI and xanthan is lower than the one for pure xanthan solution. This difference is most pronounced in the intermediate range of shear rates, where an average reduction in viscosity by a factor of 2.6 is observed. However, at very high or low shear rates, the viscosity decrease is approximately by a factor of 1.5.

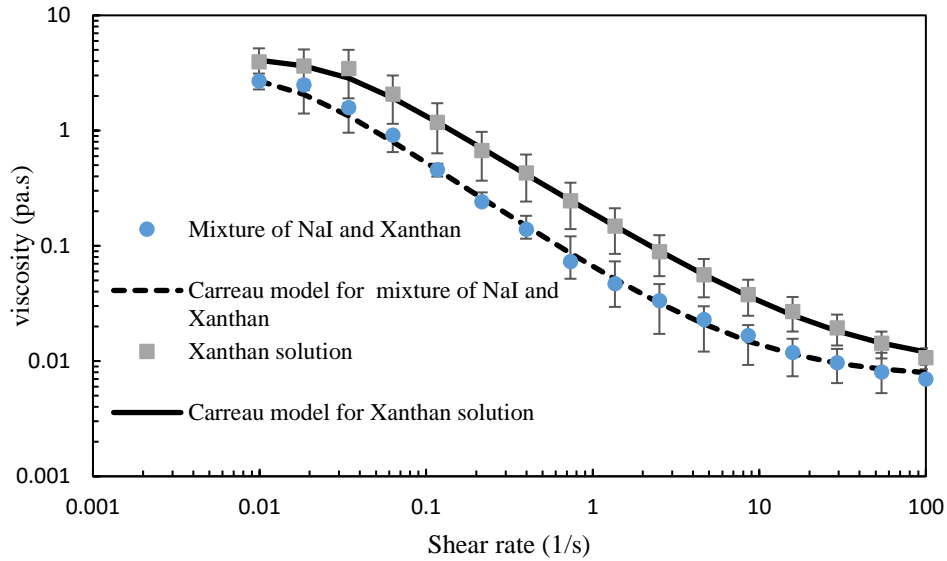


Figure 4.2-3 Rheological behavior of xanthan solution at a concentration of 800 mg/L and mixture of xanthan and NaI with xanthan concentration of 590 mg/L and NaI concentration of 960.11 g/L as well as Carreau models fitted on experimental data. Experiments have been triplicated and error bars are calculated by determining the mean (average) of the data points and the standard deviation.

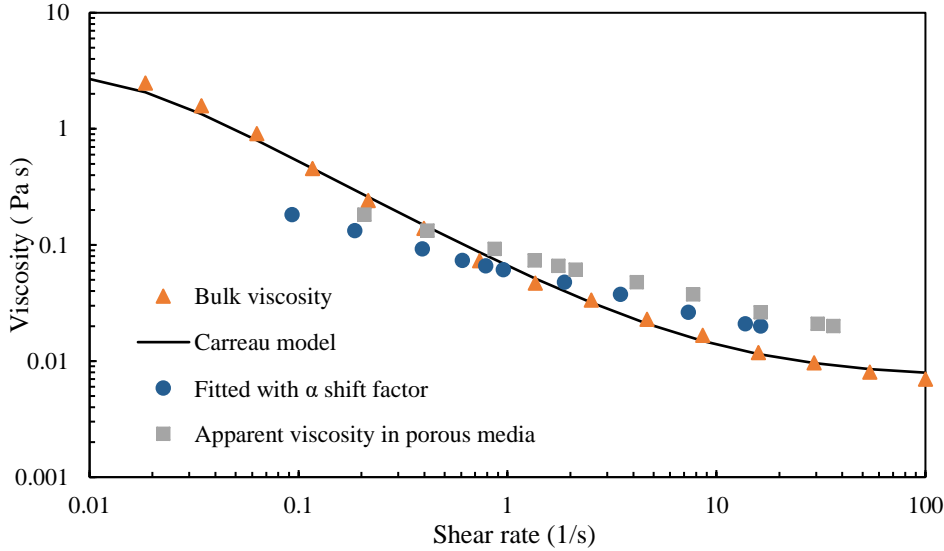
Single-phase flow 1D column experiments were performed to assess the rheological behavior of xanthan solutions with and without NaI in porous media. The shear rate in porous media can be expressed as (Darby et al., 2017):

$$\dot{\gamma} = \sqrt{\frac{2}{\phi k}} \alpha u \quad \text{Eq 4.2-15}$$

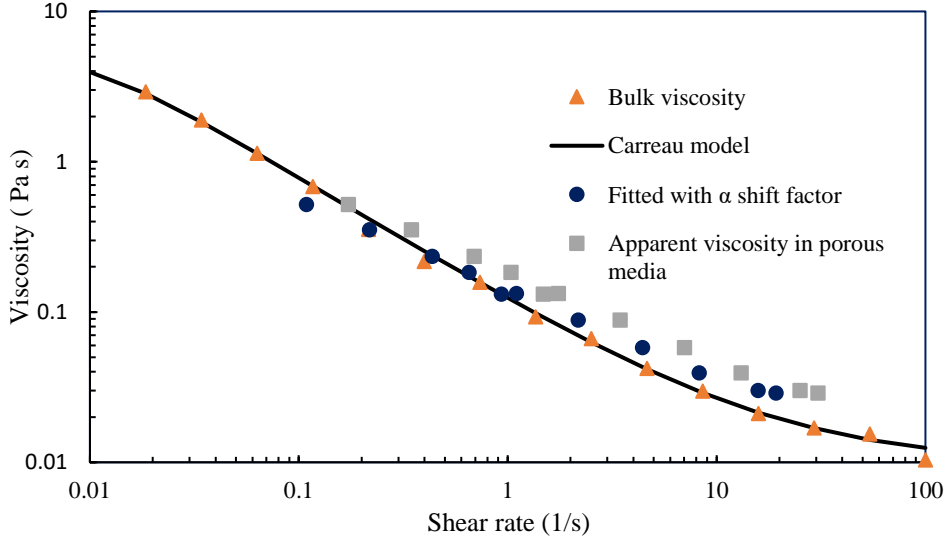
The shift factor, α (-), is associated with the properties of the porous medium and the rheological properties of the fluid at bulk (Chauveteau and Zaitoun, 1981).

The apparent shear rate is obtained using the apparent viscosity derived from the column experiment, after rearranging the Carreau fluid model based on its determined parameters. Then the apparent shear rate is plotted against the Darcy velocity $\frac{u}{\sqrt{\phi k}}$. The slope of the fitted linear

curve passing through the origin was then found and considered as the shift parameter (Zamani et al., 2015). The viscosity data obtained from the porous media experiments compared with those at bulk are shown in Figure 4.2-4.



(a)



(b)

Figure 4.2-4 Apparent viscosity compared with those obtained from rheometer. (a) mixture of xanthan and NaI, (b) pure xanthan solution

The shift parameter is 0.6 and 0.45 for xanthan solution and the mixture of xanthan and NaI, showing that the apparent viscosity in our porous medium is globally higher than that in bulk fluid. The flow of polymers in porous media can be understood by looking at the pore and throat

structure as a sequence of expanding and contracting channels. The polymer molecules deform as they pass through the contractions, causing an increase in resistance to flow (Holmberg et al., 2002). When NaI is present in the polymer solution can lead to a decrease in electrostatic repulsion, causing the xanthan molecule to condense into a compact, rod-like structure. As a result, polymer molecules align along the flow direction. This leads to a smaller shift factor compared to that of a pure xanthan solution. The influence of the depleted layer near the pore wall is relatively insignificant due to the high permeability of the porous media (Chauveteau and Zaitoun, 1981).

4.2.4.2. Two-phase flow columns experiments

Two-phase flow column experiments were conducted to assess the efficiency of injecting various solutions for displacing DNAPL in a closed horizontal system. The termination criterion for the experiments was reached when no further DNAPL was observed in the effluents. The 1D column results shown in Figure 4.2-5a indicate that the recovery efficiency $\left(\frac{\text{volume of DNAPL recovered}}{\text{initial volume of DNAPL in sand}} \right)$ as a function of PV for xanthan solutions, with or without NaI, are nearly identical, whereas the recovery efficiency is slightly higher for pure xanthan solution due to its higher viscosity compared to the mixture of xanthan and NaI. The recovery efficiency for pure NaI solution is lower, at around 0.74, as its viscosity is significantly lower than that of the polymer solutions. During the injection of various solutions, the capillary number was calculated using the following equation to evaluate their effectiveness in displacing DNAPL (Chatzis and Morrow, 1984):

$$N_{ca} = \frac{k\nabla p}{\sigma} \quad \text{Eq 4.2-16}$$

where σ (N/m) is the interfacial tension (IFT) between the DNAPL and the different solutions. The IFT between DNAPL and a mixture of xanthan and NaI, pure NaI solution and xanthan solution were measured as 10.87 ± 0.05 , 10.14 ± 0.05 , and 21.5 ± 0.05 mN/m, respectively. The

capillary number plots (Figure 4.2-5b) show that the capillary number at the end of the experiment as a function of PV is almost identical for injection of xanthan and the mixture of xanthan and NaI. Moreover, it is higher compared to the pure NaI solution, which is in line with the recovery efficiency results. The oscillations in capillary number plot of pure NaI solution is attributed to the pressure fluctuations caused by peristaltic pump which is directly detected by pressure sensors as there is no polymer inside the solution to dampen it.

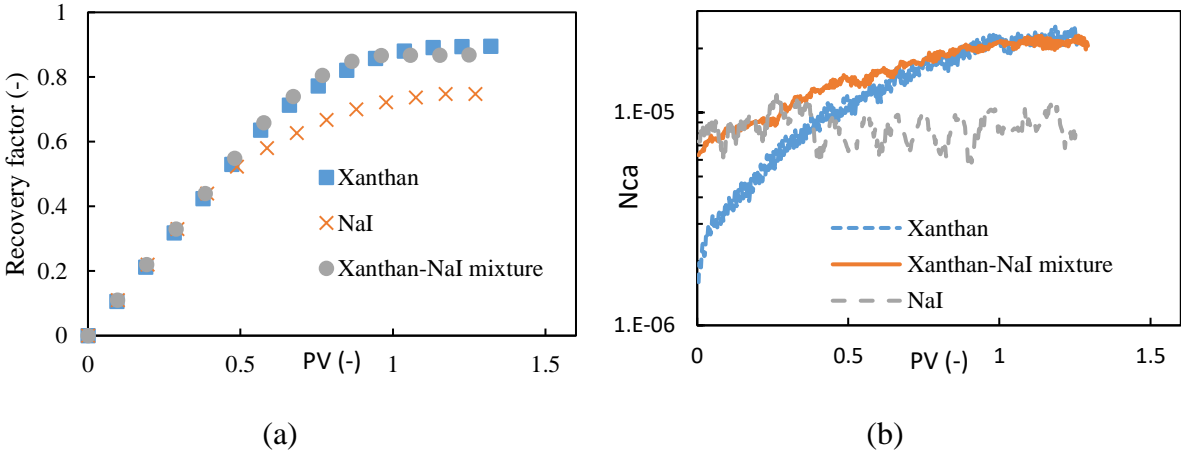


Figure 4.2-5 Performance of injection of different solutions. (a) Recovery efficiency, (b) Capillary number versus injected PV

4.2.4.3. Two-dimensional flow (2D tank)

The role of gravity cannot be accurately observed in a horizontal 1D column system, as the thickness of the polluted zone (diameter of the column) is too small, and the system is closed, prohibiting vertical movement. The 2D experiments were performed to evaluate the efficiency of the injection of the three aforementioned solutions on the displacement of DNAPL layer in an unconfined system where the gravity can significantly influence the propagation of the invaded fluid. The solutions containing a colorant were individually injected into the tank saturated with DNAPL in presence of residual water following the steps mentioned in section

2.1. Figure 4.2-6 shows the propagation of different solutions at the end of the experiments. The interface between the invading solution and DNAPL is depicted by the white dashed lines. In the case of a mixture of xanthan and NaI (Figure 4.2-6a), two white lines are present, representing the interface for the fully and partially displaced zones.

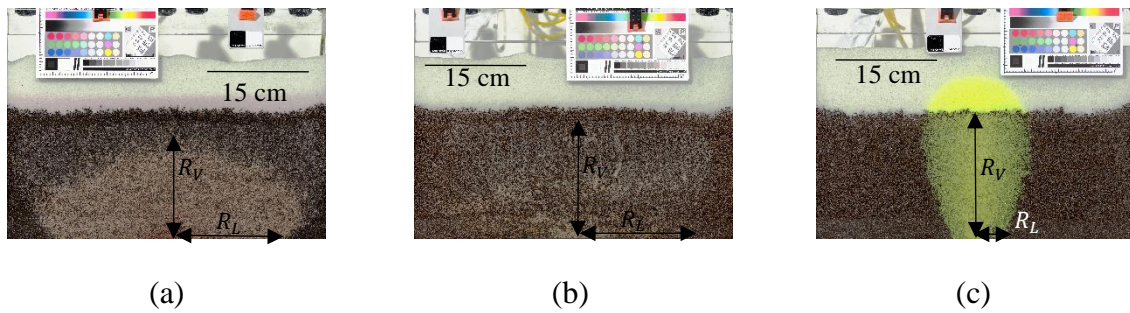
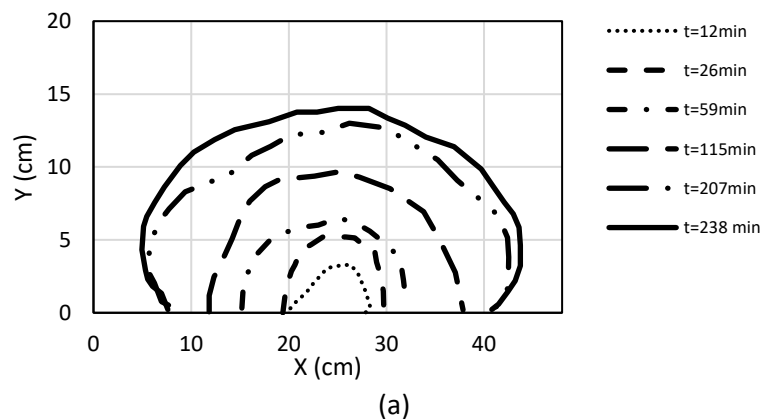


Figure 4.2-6 Comparison of the propagation of three solutions at the end of injection through the contaminated zone, DNAPL appears black and displaced zone is bright. (a) Mixture of xanthan and NaI, (b) pure NaI brine, and (c) xanthan solution

When NaI is present in the polymer solution, a lateral displacement can be observed (Figure 4.2-6a); however, in the absence of xanthan in NaI solution the displacement is less effective and there are areas where the black color of the DNAPL remains more prominent (Figure 4.2-6b). Injection of pure xanthan results in a main vertical movement (Figure 4.2-6c). The evolution of the front propagation of the injected fluid through the contaminated zone is shown in Figure 4.2-7.



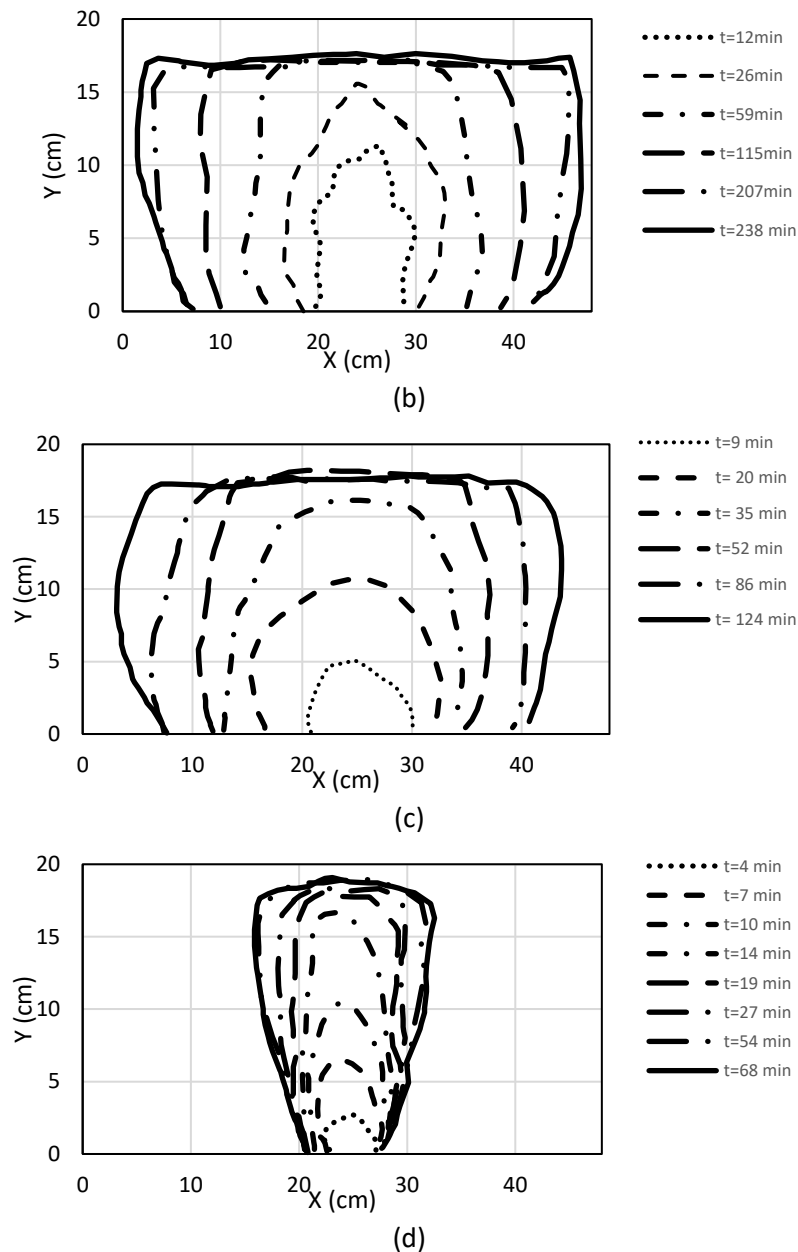


Figure 4.2-7 Dynamic of propagation of the fluids during injection through the DNAPL contaminated zone. (a) fully displaced zone for injection of mixture of xanthan and NaI, (b) transition displaced zone for injection of mixture of xanthan and NaI, (c) displaced zone for injection of NaI brine solution, and (d) displaced zone for injection of xanthan solution

The observations in Figure 4.2-7 indicate that in cases where NaI is present in the solution, the solution propagations exhibit similar radial/lateral patterns through the contaminated zone. In contrast, when using pure xanthan, the lateral propagation becomes limited over time, and the movement is predominantly vertical. For the case of injection of the mixture, a fully displaced

zone and a transition zone can be observed (Figure 4.2-6a). The recovery efficiency curves for injection of each solution are shown in Figure 4.2-8, which exhibit values around 0.46, 0.24, and 0.09 at the end of the displacement for the mixture of xanthan and NaI, pure NaI, and xanthan solutions, respectively. The propagation of the invading solution in the contaminated zone can be described through aspect ratio values (see Figure 4.2-6) which is defined as the ratio of the lateral radius R_L to vertical radius R_V (Davarzani et al., 2021). When both transition and fully displaced zones are present in the system, for the determination of the aspect ratio, R_L and R_V correspond to the radii of the fully displaced zone. The aspect ratios are around 1.21, 1 and 0.38 for the mixture of xanthan and NaI, pure NaI, and xanthan solutions, respectively. The low recovery efficiency even when the aspect ratio favors the displacement of DNAPL is attributed to the unconfined nature of the system which is close to the real polluted site (Alamooti et al., 2022).

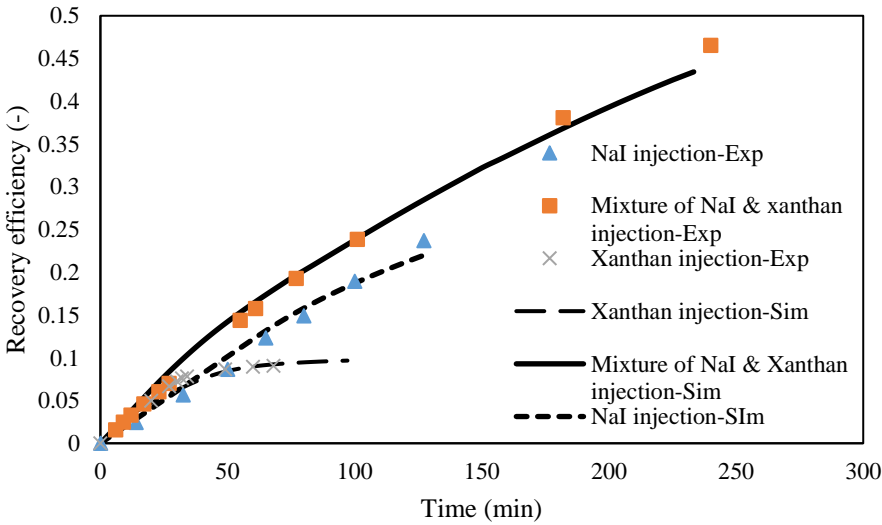


Figure 4.2-8 Comparison of recovery factor obtained from experiments and simulations for injection of different solutions including mixture of xanthan and NaI solution, pure NaI solution, and xanthan solution

Numerical modeling was performed to have a better understanding of the underlying physics behind the experiments. Using the data obtained from 1D column experiments (directly and indirectly through inverse modeling), the displacement of DNAPL through the 2D tank was simulated. Figure 4.2-9 shows the comparison between the numerical and experimental results after image analysis. The recovery efficiency curves obtained from the experiments and modeling are shown in Figure 4.2-10. These results demonstrate that the numerical modeling can properly predict the experimental consequences, where the mean absolute error between the numerical and experimental results is around 0.1. Also, the dynamic of propagation of the invading phases for different solution during the experiments has been appropriately captured by simulation results which are shown in Figure 10.

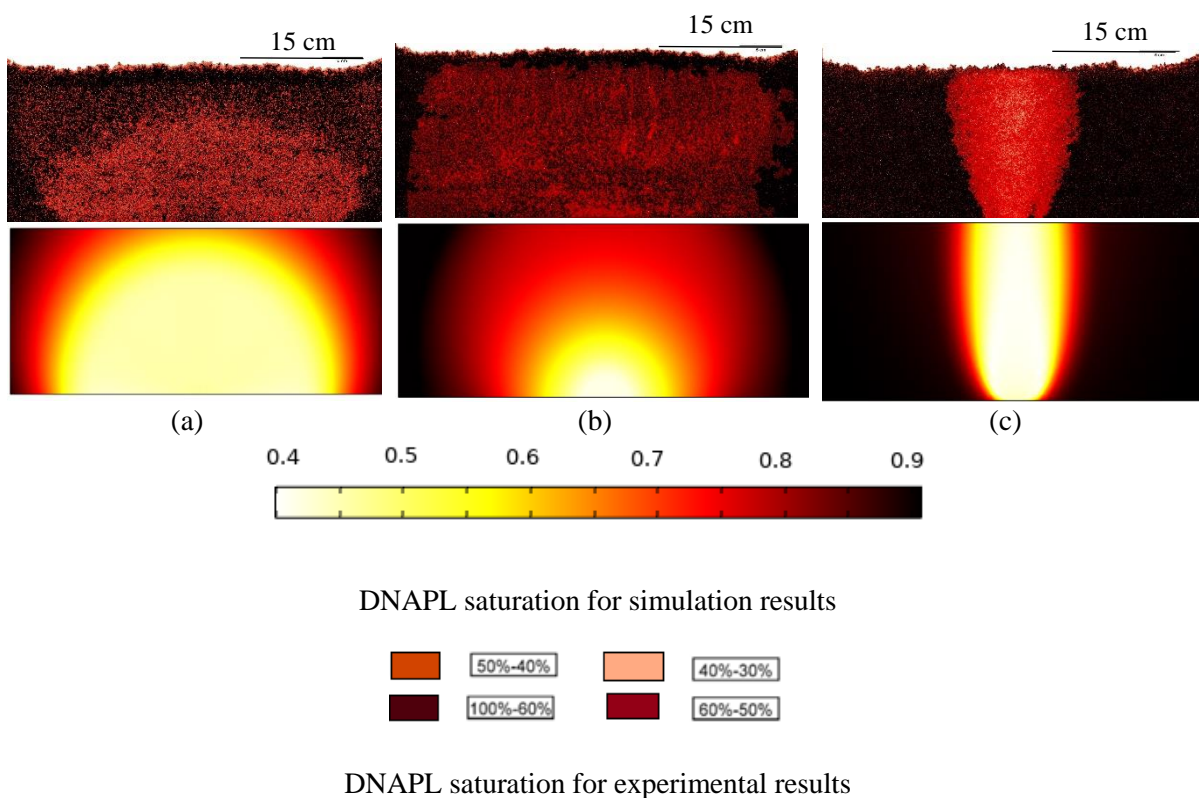
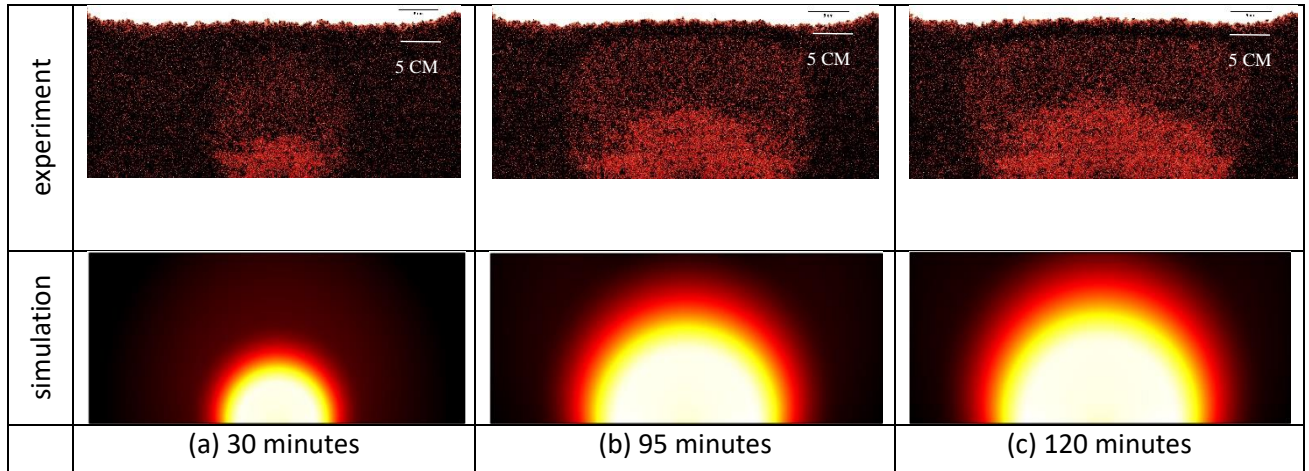
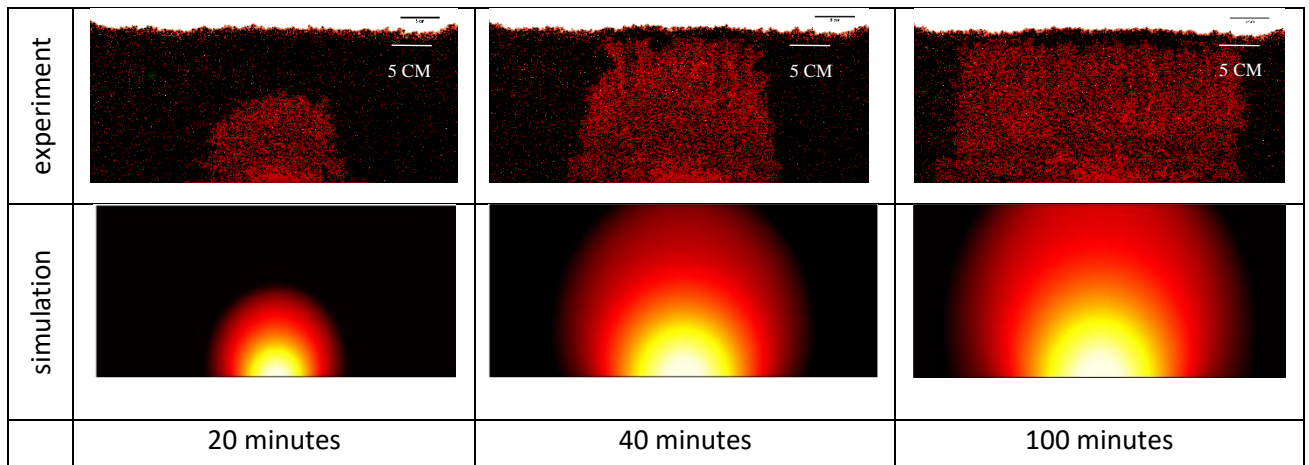


Figure 4.2-9 Comparison between the numerical and experimental results at the end of the displacement of DNAPL by different solutions, the first row images are extracted from the image analysis of experiments and the second row images are from the simulation. (a)

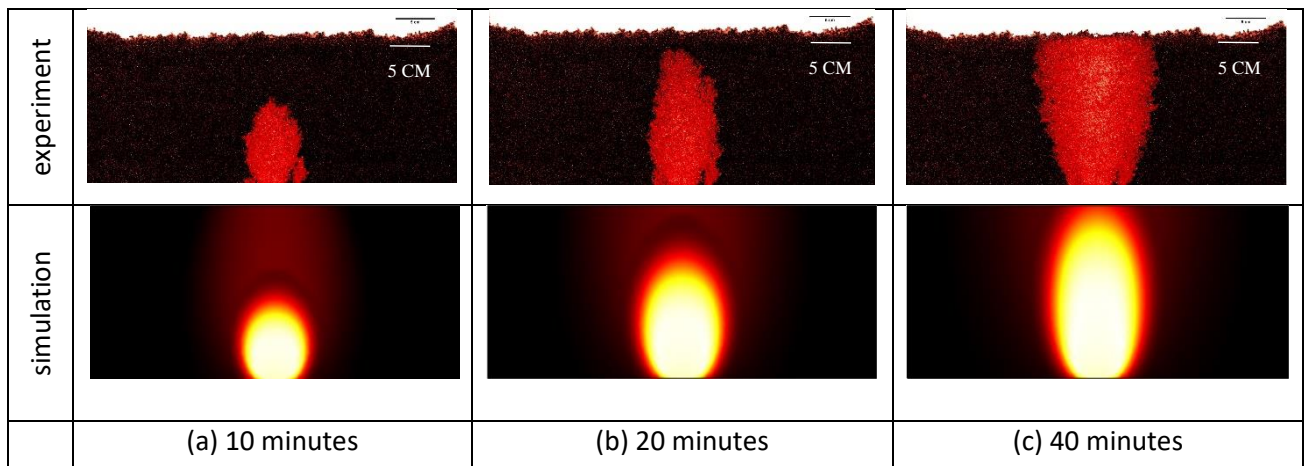
Mixture of NaI and xanthan (b) pure NaI, (c) and pure xanthan



(a)



(b)



(c)

Figure 4.2-10 Comparison of the propagation of invading solutions and DNAPL in 2D tank at different times, (a) mixture of xanthan and NaI solution, (b) pure NaI solution, and (c) pure xanthan solution

4.2.4.4. Gravity number analysis

The displacement of DNAPL through the 2D system is influenced by gravity, viscous and capillary forces. The gravity number given by Eq. 1 can show how effectively gravity and viscous forces are playing a role on the propagation of the injected fluids in the contaminated zone. Using the developed numerical model that has properly captured experimental consequences, an analysis was performed to evaluate the changes in aspect ratio of the invading fluid versus the changes in gravity number (Cochennec et al., 2022). To investigate this, a range of injection velocities and different densities of the invading phase were considered. The corresponding viscosity was determined by establishing a relationship between the apparent viscosity of the invading phase and the pressure gradient obtained from column experiments. Figure 11 displays the results, showing that for gravity numbers less than -0.25, a very slight increase in aspect ratio is observed, indicating a preference for vertical migration of the invading phase when the density of the invading phase is lower than that of the DNAPL. Then, a sharp increase in aspect ratio for the gravity numbers between -0.25 and 0.25 can be observed, demonstrating a favorable displacement where a radial displacement can be observed. For higher gravity numbers, the slope of increase in aspect ratio decreases as the denser invading phase reaches the lateral boundaries and its lateral movement stops (Cochennec et al., 2022). The results showing that an increase in the gravity number due to densification of the polymer solution can hinder vertical movement of the invading fluid, but may result in an underridden flow where the invading fluid flows below the contaminated zone.

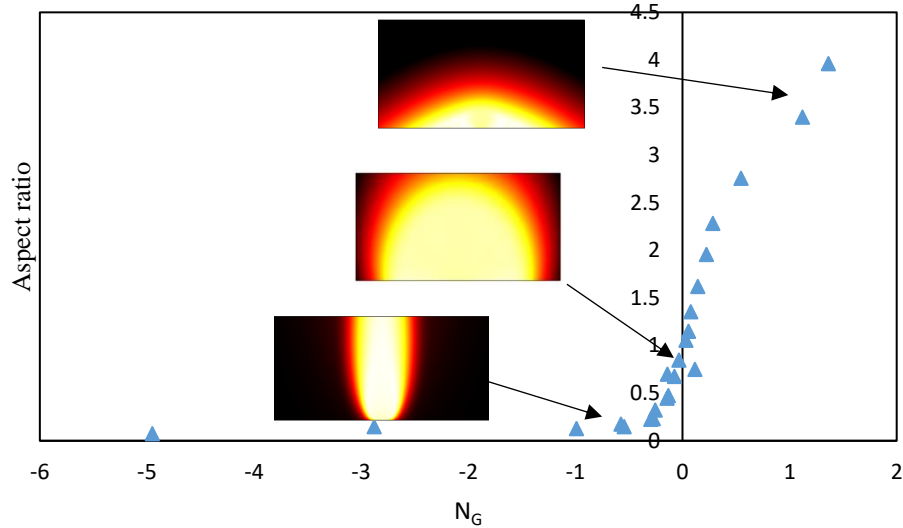


Figure 4.2-11 Changes in aspect ratio of invaded fluid based on gravity number using numerical simulations in 2D tank domain

4.2.4.5. DNAPL displacement in confined two-layer system by densified polymer solution

Multiphase flow experiments were conducted in a two-layer 2D system, following the procedures outlined in section 4.2.2.2. Xanthan solutions, both with and without NaI, were injected individually through contaminated layers to displace DNAPL. In Figure 4.2-12, the propagation of polymer solutions in DNAPL-saturated layers is illustrated at different injected PVs. The experimental results indicate similar DNAPL displacement for both non-densified and densified polymer solutions. This similarity can be attributed to the role of the closed upper boundary, which hinders the vertical movement of the non-densified polymer solution. Additionally, irrespective of the density of invading polymer solutions, a density-overridden flow is observed.

In the case of xanthan-NaI, this overridden flow can be explained by the mixing of the invading densified solution and residual water in the system, resulting in a reduction in the density of the

flowing aqueous phase. Consequently, a preference for flowing on the top of the layers is observed. The permeability contrast influences the flow as DNAPL is initially drained from the higher permeable layer. The results for the distribution of xanthan-NaI and DNAPL by numerical simulation are also depicted in the third line of Figure 4.2-12, capturing the experimental consequences, including the density-overridden flow.

Figure 4.2-13 illustrates the recovery curves obtained from 2D experiments for both polymer solutions, indicating a higher recovery efficiency for pure xanthan solution. This finding is consistent with 1D column results and is attributed to its slightly higher viscosity. Additionally, the recovery efficiency curve obtained from simulation for the xanthan-NaI case is demonstrated in Figure 4.2-13, showing good consistency with the experimental results.

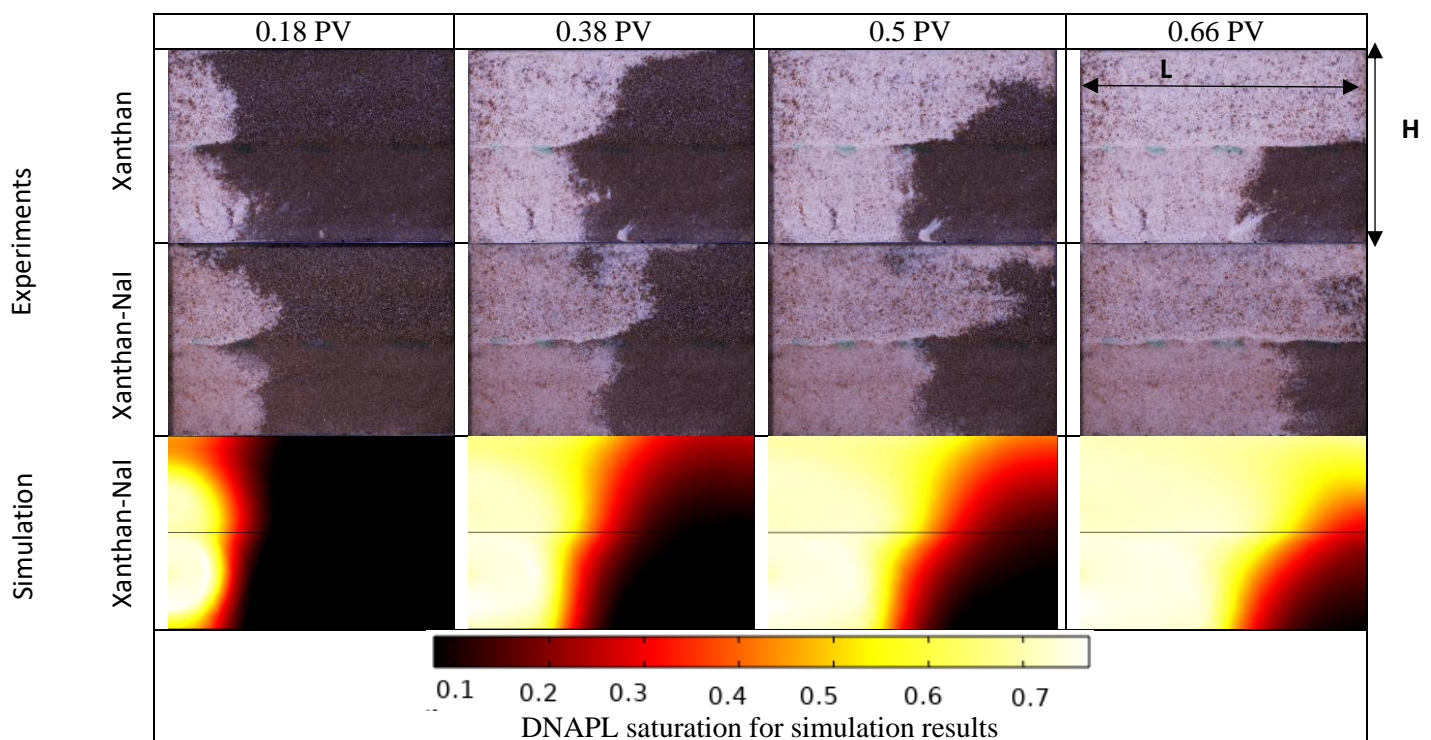


Figure 4.2-12 DNAPL displacement in a 2D multilayer system by injection of pure xanthan

solution (first row), mixture of xanthan-NaI (second row) and numerical simulation for

xanthan-NaI (third row) at different pore volumes of injected fluids

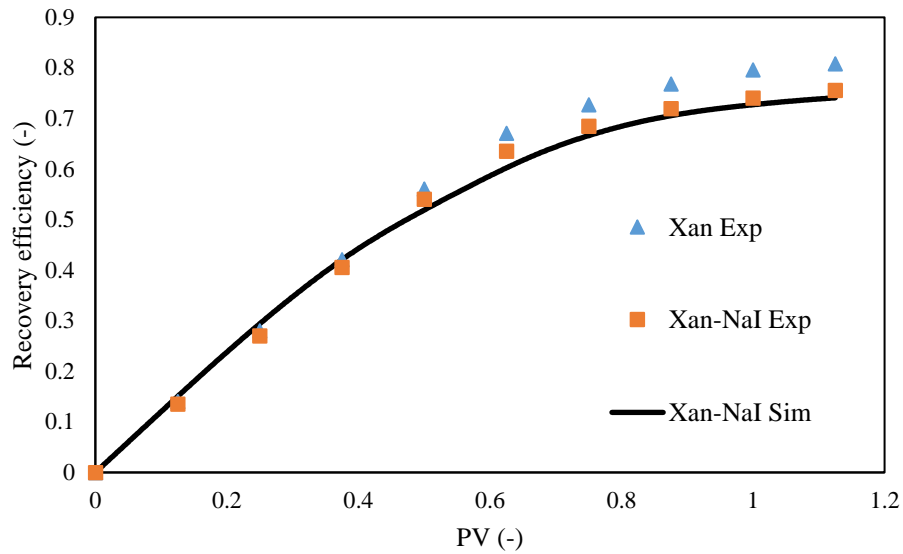


Figure 4.2-13 Recovery efficiency curve for experiments of injection of pure xanthan and xanthan-NaI mixture into multilayer system and results from numerical simulation for xanthan-NaI mixture injection

To assess the impact of permeability contrast on the displacement of DNAPL, we conducted numerical simulations by varying the permeability ratios of two layers. These simulations were compared with experimental results, where the DNAPL in the bottom layer reached half of the horizontal axis. The front shape from simulation results were specifically extracted from the middle of the transition zone and compared to the experimental data. Figure 4.2-14 illustrates the propagation of fronts for various permeability ratios ($K_{\text{upper}}/K_{\text{lower}}$) in a 2D system with a vertical axis of relative height (y/H) and a horizontal axis of relative length (x/L). The results indicate that increasing the values of $K_{\text{upper}}/K_{\text{lower}}$ leads to a rapid breakthrough, where both permeability contrast and density-driven flow synergistically contribute to the flow in the upper layer. Simultaneously, a significant amount of DNAPL can remain untouched in the lower layer. Conversely, lower values of $K_{\text{upper}}/K_{\text{lower}}$ demonstrate an opposing influence of density difference and permeability contrast on the flow. Even at a $K_{\text{upper}}/K_{\text{lower}}$ ratio equal to 1/10, the front in the bottom layer remains considerably distant from the recovery point. Notably, when there is no permeability contrast between the layers, a slightly inclined front is observed.

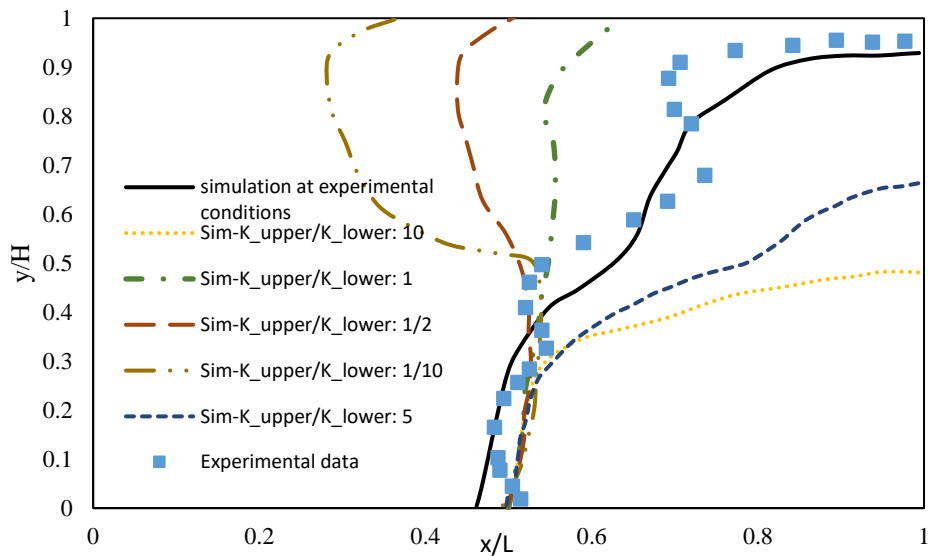


Figure 4.2-14 Effect of permeability contrast on propagation of invading xanthan-NaI solution in DNAPL saturated two-layer system

Another crucial factor influencing the front shape in a multilayer system is the ratio of the length to height of the tank (L/H). In this context, the length of the system was varied in numerical simulations to cover the range of L/H from 0.5 to 20. Similar to the previous case, these simulations were then compared with experimental results where the DNAPL in the bottom layer reached half of the horizontal axis.

The results depicted in Figure 4.2-15 reveal that as the length of the system increases to achieve higher L/H ratios, the influence of density difference on the flow diminishes. A steep front, without a noticeable preference for flow on the top, becomes apparent. Conversely, for lower L/H values, density-driven flow can lead to a rapid breakthrough, with a front inclined toward the recovery point and propagation occurring in the upper parts of the system.

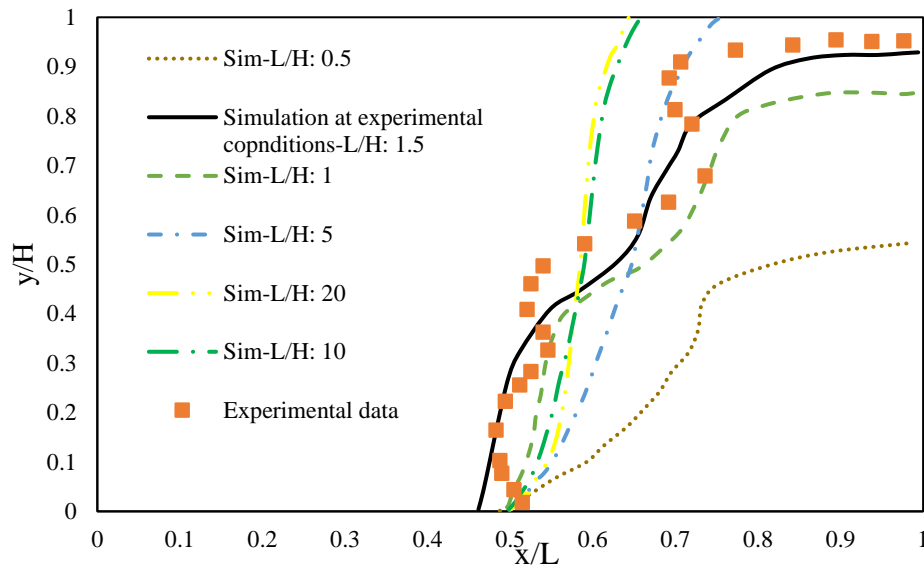


Figure 4.2-15 Effect of L/H ratios on propagation of invading xanthan-NaI solution in DNAPL saturated two-layer system

4.2.4.6. Sensitivity analysis

The injection of NaI-xanthan mixture into the unconfined two-dimensional aquifer sandbox was selected as the experimental setup to explore the impact of various numerical modeling parameters on the shape of the fully displaced zone's front at the 115th minute. The optimal front shape for each parameter was compared with simulations employing higher or lower values of that specific parameter, while keeping other numerical modeling parameters constant at the fitted values detailed in Table 2. The results, depicted in Figure 4.2-16, highlight that among the relative permeability terms, the saturation exponents exert a more pronounced influence on the front shape than the maximum relative permeability values. Regarding capillary pressure terms, a lower threshold pressure and a higher pore size distribution lead to a more invaded front compared to the experimental results. Similarly, excluding the transport equation in numerical simulations results in a larger (expanded) front.

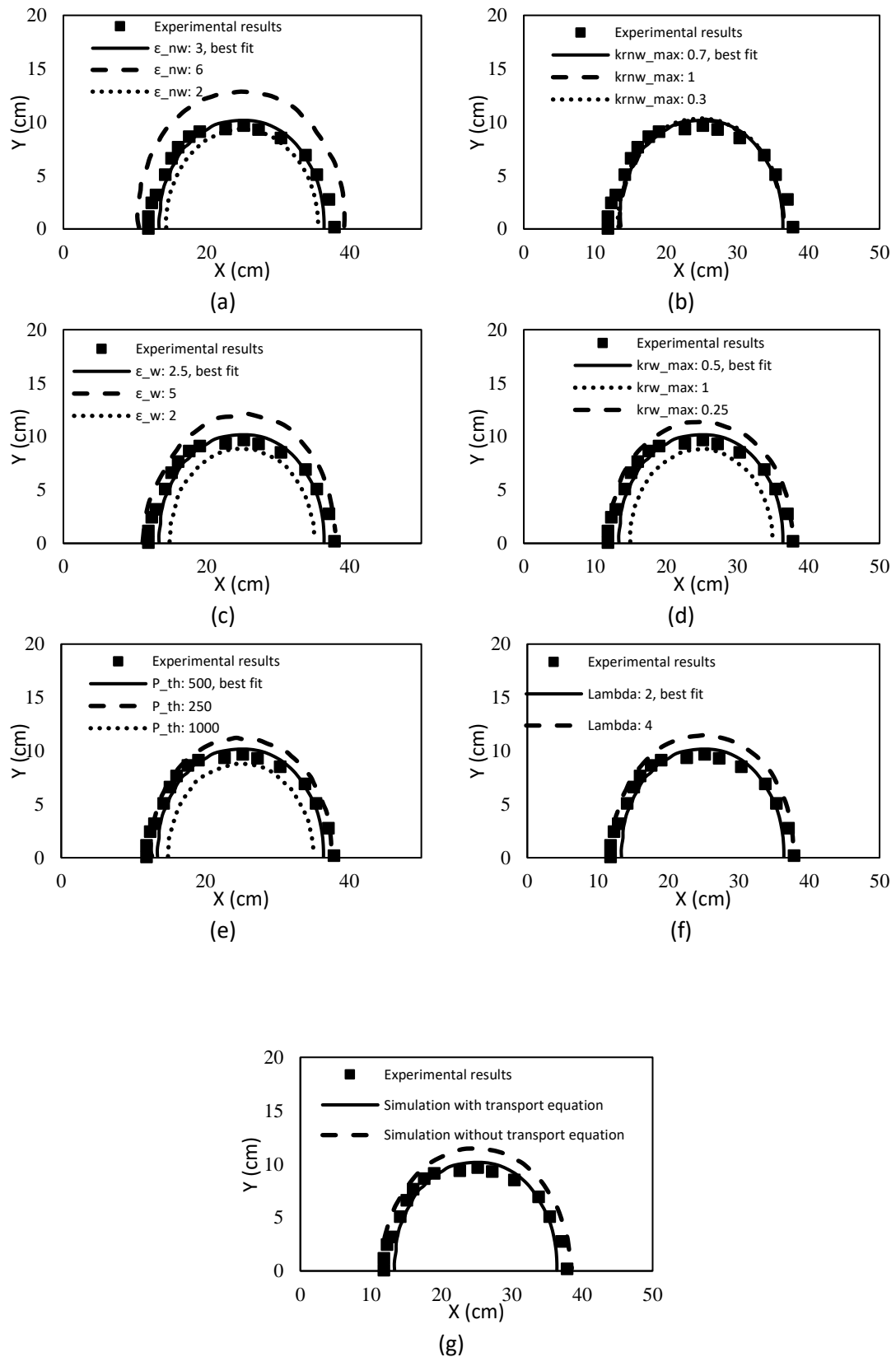


Figure 4.2-16 Sensitivity analysis of numerical simulation parameters compared with selected experiment. (a) non wetting phase relative permeability saturation exponent, (b) non wetting phase maximum relative permeability, (c) wetting phase relative permeability

saturation exponent, (d) wetting phase maximum relative permeability, (e) threshold pressure, (f) pore size distribution, and (g) transport equation

4.2.5. Conclusions

A set of experiments including rheological measurement in the bulk fluid and in porous media, as well as two-phase flow in 1D columns and 2D tanks was performed to evaluate the efficiency of the injection of densified NaI solutions with and without xanthan and a pure xanthan solution on the displacement of DNAPL. A numerical simulation consistent with the experimental consequences was also performed to analyze the role of gravity and viscous forces on the propagation of the polymer solution (with different degrees of densification) in 2D systems.

Rheological measurements showed that the addition of NaI as a densifier did not affect the shear-thinning behavior of xanthan, but the presence of ions reduced the viscosity by a factor of 2.6 for intermediate range of shear rate. The shift factor for apparent viscosity was less than unity, indicating a deformation of polymer molecules and an increased flow resistance due to contractions and expansions in porous media. Confined column experiments revealed similar recovery efficiencies of around 0.89 for xanthan solutions regardless of density, while the pure brine solution had a lower recovery efficiency of around 0.74, consistent with capillary number analysis.

In open 2D tank experiments, gravity and viscous forces cooperatively influenced DNAPL displacement efficiency. Pure xanthan solution injection showed vertical displacement with an aspect ratio of 0.38 and recovery efficiency of 0.09, while densified polymer solution invaded the contaminated zone radially with an aspect ratio of 1.21 with a recovery efficiency of 0.46. Pure brine solution reached most of the contaminated zone, but the black color of the DNAPL remained more prominent in displaced zone resulted in recovery efficiency of 0.24. Numerical simulations indicated that a gravity number close to zero is needed to achieve an aspect ratio around unity and avoid density-driven flow issues.

Injection of both densified and non-densified polymer solutions resulted in a preferential flow on top of multilayer system. In the case of xanthan-NaI, this overridden flow can be explained by the mixing of the invading densified solution and residual water in the system, resulting in a reduction in the density of the flowing aqueous phase. The numerical simulation results indicate that increasing the values of $K_{\text{upper}}/K_{\text{lower}}$ leads to a rapid breakthrough, where both permeability contrast and density-driven flow synergistically contribute to the flow in the upper layer.

Chapter 5

5. Conclusions and perspectives

5.1. Conclusions

This thesis aimed to provide new insights into the study of polymer injection for remediation of aquifers polluted by DNAPL (Dense Non-Aqueous Phase Liquid). The performance of polymer injection in multilayer systems is comprehensively examined, and the gravity-driven remediation of DNAPL polluted aquifers using densified polymer solution/suspension is evaluated.

For the cases where a pool of DNAPL is present, particularly in heterogeneous aquifers, the use of polymer solution injections can offer a promising improvement in recovery rates. Nonetheless, some residual DNAPL will remain in the aquifer after soil traditional treatment techniques. As such, it is recommended to use polymer solution injections as a primary remediation technology, which should then be supplemented by other remediation techniques to address the residual DNAPL. In these scenarios, the polymer solution can act as a delivery fluid, transporting the necessary remedial agents to the contaminated zone. The possible remedial agents include oxidants, microbes, surfactants, and alcohols. This thesis has specifically explored the injection of mixtures of polymer, surfactant, and alcohols that can be post-injected into the aquifers at residual DNAPL saturation.

A key topic discussed in detail is the impact of density-driven flow on DNAPL displacement in both single-layer and multilayer systems. A combination of experimental and numerical analyses was conducted to illuminate the two-phase flow dynamics of DNAPL displacement by polymer injection, taking into account the non-Newtonian properties of polymer solutions in both bulk fluid and porous media. To tackle the density-driven issue in either layered or homogeneous systems, various approaches such as increasing the density of the polymer solution by adding barite particles or soluble salts, as well as isolating contaminated zones, were evaluated.

In the case of multilayer systems, the initial focus was on evaluating the effectiveness of injecting xanthan solutions, either with or without a surfactant (SDBS), for remediation of DNAPL-polluted layered aquifer. The findings indicated that the mixture of xanthan and SDBS yielded superior recovery rates in both single and multilayer systems. Consequently, this mixture was selected as the primary injection fluid for a subsequent study that assessed the performance of the post-injection of alcohol mixtures in reducing DNAPL's residual saturation.

Here are the main conclusions of the studies on multilayer systems:

- The presence of SDBS decreased the viscosity of the xanthan solution, while there are no significant changes in the rheological behavior as the concentration of SDBS increases. The repulsive electrostatic forces and hydrophobic interaction between their molecules were responsible for this behavior.
- The addition of SDBS to the xanthan solution resulted in a better recovery of DNAPL by increasing the capillary number during the injection of the mixture, with an improvement in the recovery factor of approximately 0.15 in a 1D homogeneous system and 0.07 in a 2D layered system. The 2D experiments revealed that the displacement of DNAPL was affected by permeability difference and density contrast.
- Simulation results validated by experimental data showed that, if the invading polymer solution was not densified and the soil above the DNAPL was not confined, the recovery of DNAPL was less than half of the confined system (0.35 compared to 0.78). In a larger 2D experimental system, injection of xanthan led to 0.87 recovery of DNAPL when the contaminated layered zones were impeded by a blocking agent above the DNAPL, suggesting that for a field application, the combination of injecting a polymer mixture with blocking the contaminated zone can lead to a promising remediation of DNAPL-contaminated layered zones.

- Batch experiments revealed that the inclusion of 1-hexanol in the alcohol mixture led to alcohol partitioning in the DNAPL phase, swelling the organic phase. Conversely, when 1-propanol was the sole alcohol in the mixture, DNAPL was dissolved in the aqueous phase. Rheological analysis demonstrated that for alcohol mixtures with 50% volume fraction of alcohols, those containing 1-hexanol either at 25% or 50% volume fraction could yield a viscosity three times higher than mixtures with only 1-propanol. We found that by adding the alcohols to the polymer-surfactant solution the non-Newtonian behavior has been retained.
- Column experiments, performed after the primary injection of the xanthan-SDBS solution, revealed two unique mechanisms. The post-injection of mixtures with 1-hexanol resulted in DNAPL appearing in the effluent after injecting 0.3 PV, indicating the mobilization mechanism due to alcohol partitioning into trapped DNAPL. In contrast, the post-injection of C₃ mixture (consisting of 50% volume fraction of 1-propanol and 50% of surfactant-polymer solution) initiated DNAPL dissolution, signifying a solubilization mechanism. Here, DNAPL only appeared in the effluent after 1 PV injected. In a set of individual column experiments, a sandwich method of post-injection of the mobilization mixture was proposed. This method improved the recovery factor by roughly 0.06 with only 0.5 PV injection of the mixture, compared to 1 PV in a full post-injection scenario.
- 2D tank experiments were conducted to visually compare the solubilization and mobilization processes. Initial injection of the xanthan-SDBS mixture effectively displaced DNAPL from both layers. The post-injection of the C₃ mixture initiated DNAPL dissolution, forming a dark zone with the DNAPL concentration gradient, followed by a white zone where DNAPL had been largely dissolved. Post-injection of the C₃-C₆ mixture (25% of 1-propanol, 25% of 1-hexanol and 50% of surfactant-

polymer solution) showcased the mobilization mechanism, with alcohol partitioning into DNAPL causing mobilization. This was illustrated by the formation of moving DNAPL droplets within the layers, where the swollen DNAPL ganglia became interconnected, mobilized and reached the recovery point only after 0.3 PV injected. As the invasion of new alcohol mixture progressed, the dark color of these mobilized droplets gradually faded. The post-injection of the C₃ mixture enhanced the recovery factor by 0.02 and generated a lower pressure gradient compared to the C₃-C₆ mixture. In contrast, the C₃-C₆ mixture led to a larger improvement in the recovery factor, approximately 0.08. These results show that post-injection of alcohol-surfactant-polymer mixture can minimize the residual saturation of DNAPL in layered system and achieve a promising displacement efficiency.

In the gravity-driven remediation study, the interplay between buoyancy and viscous forces that influence the distribution of DNAPL and the aquifer remediation using polymer solution-based was investigated. We achieved this by introducing a densified polymer (carboxymethyl cellulose, CMC) suspension (barite particles) and a polymer (xanthan) brine (NaI) solution to remediate DNAPL polluted aquifers.

Here are the main findings of these studies:

- It was shown that using a polymer solution individually cannot yield the proper recovery factor in a system similar to the real conditions. Adding barite particles to densify the polymer solution could improve the recovery factor of DNAPL more than 4 times.
- Using one-dimensional column experiments, the clogging behavior of suspended barite particles in the densified polymer suspensions was analyzed and the parameters related to the clogging of the barite particles were found. Moreover, it was shown that the barite-polymer suspensions can cause a permeability reduction in sandpacks up to 55%,

70%, and 72% for different suspensions with increasing densities of 1.3, 1.66, and 1.9 g/mL, respectively. It was shown that the viscosity of the polymer suspension increased with the density of the mixture. For all polymer mixtures with or without barite particles, a shear-thinning behavior was observed which corresponds to less resistance against the flow at higher shear rates.

- It was shown that for a confined system which is not a good representative of real polluted site, a higher unrealistic recovery factor can be obtained. The results of numerical simulations, using generalized Darcy's law and the continuity equation, in agreement with experimental findings, showed that saturation functions for the open and closed systems are different. The capillary pressure curve lies higher in the case of a closed system in comparison to the open one. When the system is closed, the oil and water relative permeability curves have moved to the right. This ignorance of the difference between the residual saturations in closed and open systems can lead to an overestimation of the recovery factor in real field. Thus, it is highly recommended to consider the role of the upper boundary while designing soil remediation methods in laboratory-scale to mimic the field scale.
- The addition of the sodium iodide (NaI) as a densifier did not affect the shear-thinning behavior of xanthan, but the presence of ions reduced the viscosity by a factor of 2.6, for the intermediate range of shear rate. The shift factor for apparent viscosity was less than unity, indicating a deformation of polymer molecules, leading to increased flow resistance caused by contractions and expansions in porous media. Confined column experiments revealed similar recovery efficiencies of around 0.89 for xanthan solutions regardless of density, while the pure brine solution of NaI had a lower recovery factor of around 0.74, consistent with capillary number analysis.

- In open 2D tank experiments, gravity and viscous forces cooperatively influenced DNAPL displacement efficiency. Pure xanthan solution injection showed vertical displacement with an aspect ratio of 0.38 and recovery factor of 0.09, while the densified polymer solution invaded the contaminated zone radially with an aspect ratio of 1.21 with a recovery factor of 0.46. Pure brine (NaI) solution reached most of the contaminated zone, but the black color of the DNAPL remained more prominent in the displaced zone and resulted in a recovery factor of 0.24. For the field case study, densified polymer solution could be more interesting, avoiding the clogging issues in soil and providing lower injection pressure. Numerical simulations indicated that a gravity number close to zero is needed to achieve an aspect ratio around unity and avoid density-driven flow issues.

These results shed light on density driven flows for the remediation of soils contaminated with heavy chlorinated DNAPL. It is proved that an increase in both the viscosity and the density of the displacing fluid leads to a significant improvement of the efficiency of the remediation of heavy chlorinated DNAPL in soils.

5.2. Perspectives

One of the main applications of the injection of polymer solutions is to transport remedial amendments to targeted contaminated areas. This thesis assessed the injection, both initial and subsequent, of polymer-surfactant mixtures, as well as polymer-surfactant-alcohol combinations. It is noteworthy that polymers can effectively transport agents, such as nanomaterials (e.g., Nano zero valent iron), to these contaminated regions. Future research can delve into the retention mechanisms of the compounds in these mixtures, especially concerning the remediation of DNAPL-contaminated aquifers.

Another critical consideration is the type of polymers used, as they can significantly affect the displacement performance on DNAPL. In this thesis, we focused on two polymers: xanthan and CMC. However, other synthetic polymers such as PAMs or Polyethylene oxide (PEO), which possess varying molecular weights, can also be utilized. Their unique rheological properties and varying interfacial tensions when in contact with DNAPL differentiate them in performance.

The experiments conducted in this thesis were under ambient conditions. Nevertheless, temperature's influence could be significant, impacting the properties of both DNAPL and the polymer, as well as their interfacial characteristics. A detailed examination, such as injecting hot polymers, would be of great interest. This could include analyzing the rheological behavior of the polymer solution at varying temperatures, assessing the interfacial tension between the polymer and DNAPL, and observing any viscosity alterations in DNAPL.

Within this thesis, we explored the blocking of the contaminated zone by injecting a polymer suspension via a horizontal well situated above this zone. The results indicated that the polymer suspension effectively hinders the vertical flow of fluids (both DNAPL and the injected polymer solution). However, a more detailed examination may be necessary to assess the various factors influencing the efficiency of the blocking aspect of the polymer suspension. This could encompass the impact of the injection pressure of the remedial polymer solution, the introduction rate of the polymer suspension through the horizontal well, and an assessment of potential fracturing in the region above the contamination.

Density-driven challenges are significant during DNAPL displacement. It has been demonstrated that employing gravity-driven remediation with densified polymer solutions or suspensions can enhance DNAPL recovery. During DNAPL displacement, both gravity and viscous forces are interplaying. The gravity-driven remediation proposed in this thesis,

primarily aims to counteract gravity forces by densifying the polymer solution. An alternative approach might involve augmenting the viscosity of the polymer solution, by raising its concentration, to overcome these gravity forces. A thorough evaluation is needed to elucidate various aspects of increasing viscous forces, including considerations related to the injection pressure and potential soil push-up or fracturing.

For the simulation of DNAPL displacement by polymer injection in heterogeneous aquifers, where layers with different permeability exist, the influence of capillarity between the two layers could be thoroughly studied. Also, the effect of various boundary conditions including no-flow boundaries, constant-pressure, and/or different injection rates on two-phase flow parameters or more precisely the saturation-dependent functions is needed to be analyzed. The rate dependency of the shift factor, α , for apparent viscosity in porous media can be thoroughly analyzed as well. A comprehensive numerical study is necessary, to simulate the mobilization and solubilization of DNAPL by alcohol-surfactant-polymer mixtures considering the swelling/dissolution of DNAPL, its influence on saturation functions, as well as rheological behavior of polymer mixture in porous media.

This study concentrates on using polymer injection to displace DNAPL from pools in its free phase. Nonetheless, examining the efficiency of polymer solutions when combined with other additives, such as surfactants, for the remediation of heterogeneous aquifers polluted with dissolved DNAPL could be intriguing.

Evaluation of the suggested methods in this thesis for the remediation of real DNAPL polluted fields would be necessary, as the other parameters like groundwater flow, well locations and spacing and the aquifer geological characteristics can affect the performance of polymer injection.

List of Publications

Scientific papers

1- **Alamooti A.**, Colombano, S., Ahmadi-Sénichault, A., Lion, F., Cazaux, D., Marion, C., Lagron, J., Davarzani, D., “Enhancing Remediation of Residual DNAPL in Multilayer Aquifers: Post-Injection of Alcohol-Surfactant-Polymer Mixtures” **Science of The Total Environment**, (2024)

2- **Alamooti, A.**, Colombano, S., Lion, F., Davarzani, D., & Ahmadi-Sénichault, A., “Gravity-Driven Remediation of DNAPL Polluted Aquifers using Densified Biopolymer Brine Solution: Two-Dimensional Flow Experiments and Simulations.” **Advances in Water Resources**, (2024)

3- **Alamooti, A.**, Colombano, S., Glabe, Z. A., Lion, F., Davarzani, D., & Ahmadi-Sénichault, A. “Remediation of multilayer soils contaminated by heavy chlorinated solvents using biopolymer-surfactant mixtures: Two-dimensional flow experiments and simulations.” **Water Research**, (2023). 243, 120305.

4- **Alamooti, A.**, Colombano, S., Omirbekov, S., Ahmadi, A., Lion, F., & Davarzani, H., “Influence of the injection of densified polymer suspension on the efficiency of DNAPL displacement in contaminated saturated soils.” **Journal of Hazardous Materials**, (2022). 440, 129702.

5- Omirbekov, S., Colombano, S., **Alamooti, A.**, Batikh, A., Cochenec, M., Amanbek, Y., ... & Davarzani, H “Experimental study of DNAPL displacement by a new densified polymer solution and upscaling problems of aqueous polymer flow in porous media.” **Journal of Contaminant Hydrology**, (2023). 252, 104120

Patent

Procédé d'extraction de liquides denses en phase non aqueuse, **Alamooti, A.**, Colombano, S., Lion, F., Davarzani, D., & Ahmadi-Sénichault, A

Conferences

- 1- Assessment of the role of densification on displacement of DNAPL in high permeable porous media using polymer solution, **Alamooti, A.**, Colombano, S., Glabe, Z. A., Lion, F., Davarzani, D., & Ahmadi-Sénichault, A. **Interpore 2021**, Online
- 2- Assessment of the role of densification on displacement of DNAPL in high permeable porous media using polymer solution, **Alamooti, A.**, Colombano, S., Glabe, Z. A., Lion, F., Davarzani, D., & Ahmadi-Sénichault, A. **Aquaconsoil 2021**, Online

- 3- Analysis of the displacement behavior of DNAPL from contaminated soils by injecting densified polymer suspension. **Alamooti, A.**, Colombano, S., Omirbekov, S., Ahmadi, A., Lion, F., & Davarzani, H. **JEMP (French Interpore) 2021**, Strasbourg, France
- 4- In situ flushing of multilayer DNAPL contaminated soils using a polymer/alcohol/surfactant mixture, , **Alamooti A.**, Colombano, S., Ahmadi-Sénichault, A., Lion, F., Cazaux, D., Marion, C., Lagron, J., Davarzani, D., **Aquaconsoil 2023**, Prague, Czech Republic
- 5- DNAPL Remediation through injection of densified polymer by sodium iodide: balancing gravity and buoyancy forces, **Alamooti, A.**, Colombano, S., Davarzani, D., & Ahmadi-Sénichault, A., **Aquaconsoil 2023**, Prague, Czech Republic
- 6- Remediation of multilayer soils contaminated by heavy chlorinated solvents using biopolymer surfactant mixture, **Alamooti, A.**, Colombano, S., Davarzani, D., & Ahmadi-Sénichault, A. **Interpore 2023**, Edinburgh, Scotland

Contribution of authors in research papers in this thesis

- 1- Influence of the injection of densified polymer suspension on the efficiency of DNAPL displacement in contaminated saturated soils

Amir Alamooti: Methodology, Conceptualization, Visualization, Experimental and numerical analysis, Writing – original draft.

Stéfan Colombano: Supervision, Funding acquisition, Project administration, Writing – review & editing. **Sagyn Omirbekov:** Methodology, Conceptualization, **Azita Ahmadi:** Supervision, Validation, Writing – review & editing. **Fabien lion:** Resources, Visualization. **Dorian Davarzani:** Supervision, Writing – review & editing, Visualization.

- 2- Remediation of multilayer soils contaminated by heavy chlorinated solvents using biopolymer-surfactant mixtures: Two-dimensional flow experiments and simulations

Amir Alamooti: Methodology, Conceptualization, Visualization, Experimental and numerical analysis, Writing – original draft.

Stéfan Colombano: Supervision, Funding acquisition, Project administration, Writing – review & editing. **Zakari Abdullaziz Glabe:** Methodology, Conceptualization, **Fabien lion:** Resources, Visualization. **Dorian Davarzani:** Supervision, Writing – review & editing, Visualization. **Azita Ahmadi:** Supervision, Validation, Writing – review & editing.

- 3- Gravity-Driven Remediation of DNAPL Polluted Aquifers using Densified Biopolymer Brine Solution: Two-Dimensional Flow Experiments and Simulations

Amir Alamooti: Methodology, Conceptualization, Visualization, Experimental and numerical analysis, Writing – original draft.

Stéfan Colombano: Supervision, Funding acquisition, Project administration, Writing – review & editing. **Dorian Davarzani:** Supervision, Writing – review & editing, Visualization. **Fabien lion:** Resources, Visualization. **Azita Ahmadi:** Supervision, Validation, Writing – review & editing.

4- Enhancing Remediation of Residual DNAPL in Multilayer Aquifers: Post-Injection of Alcohol-Surfactant-Polymer Mixtures

Amir Alamooti: Methodology, Conceptualization, Visualization, Experimental analysis, Writing – original draft.

Stéfan Colombano: Supervision, Funding acquisition, Project administration, Writing – review & editing. **Abbas Shoker:** Methodology, Conceptualization, **Azita Ahmadi:** Supervision, Validation, Writing – review & editing. **Fabien lion:** Resources, Visualization. **David Cazaux:** Experimental analysis. **Cédric Marion:** Experimental analysis. **Jérôme Lagron:** Experimental analysis. **Idriss Sawadogo:** Experimental analysis. **Dorian Davarzani:** Supervision, Writing – review & editing, Visualization.

References

- Adebanjo, F.O., Olusegun, O., 2015. Evaluating the application of foam injection as an enhanced oil recovery in unconsolidated sand. *Journal of Petroleum and Gas Engineering* 6, 22–37.
- ADEME, 2023. URBANISME DURABLE [WWW Document]. URL <https://expertises.ademe.fr/urbanisme-durable/sols-pollues> (accessed 8.15.23).
- Agaoglu, B., Scheytt, T., Copty, N.K., 2012. Laboratory-scale experiments and numerical modeling of cosolvent flushing of multi-component NAPLs in saturated porous media. *J Contam Hydrol* 140–141, 80–94. <https://doi.org/https://doi.org/10.1016/j.jconhyd.2012.07.005>
- Alamooti, A., Colombano, S., Davarzani, D., Lion, F., Ahmadi-Sénichault, A., 2024a. Gravity-Driven Remediation of DNAPL Polluted Aquifers using Densified Biopolymer Brine Solution. *Adv Water Resour* 104643. <https://doi.org/https://doi.org/10.1016/j.advwatres.2024.104643>
- Alamooti, A., Colombano, S., Glabe, Z.A., Lion, F., Davarzani, D., Ahmadi-Sénichault, A., 2023. Remediation of multilayer soils contaminated by heavy chlorinated solvents using biopolymer-surfactant mixtures: Two-dimensional flow experiments and simulations. *Water Res* 243, 120305. <https://doi.org/https://doi.org/10.1016/j.watres.2023.120305>
- Alamooti, A., Colombano, S., Omirbekov, S., Ahmadi, A., Lion, F., Davarzani, H., 2022. Influence of the injection of densified polymer suspension on the efficiency of DNAPL displacement in contaminated saturated soils. *J Hazard Mater* 440, 129702. <https://doi.org/https://doi.org/10.1016/j.jhazmat.2022.129702>
- Alamooti, A., Colombano, S., Shoker, A., Ahmadi-Sénichault, A., Lion, F., Cazaux, D., Marion, C., Lagron, J., Sawadogo, I., Davarzani, D., 2024b. Enhancing remediation of residual DNAPL in multilayer aquifers: Post-injection of alcohol-surfactant-polymer mixtures. *Science of The Total Environment* 170680. <https://doi.org/https://doi.org/10.1016/j.scitotenv.2024.170680>
- Alamooti, A., Ghazanfari, M.H., Masihi, M., 2018. Investigating the relative permeability behavior in presence of capillary effects in composite core systems. *J Pet Sci Eng* 160, 341–350. <https://doi.org/10.1016/j.petrol.2017.10.051>
- Alamooti, A.H., Azizi, Q., Davarzani, H., 2020. Direct numerical simulation of trapped-phase recirculation at low capillary number. *Adv Water Resour* 145, 103717. <https://doi.org/10.1016/j.advwatres.2020.103717>
- Alamooti, A.M., Malekabadi, F.K., 2018. An Introduction to Enhanced Oil Recovery, in: *Fundamentals of Enhanced Oil and Gas Recovery from Conventional and Unconventional Reservoirs*. Elsevier Inc., pp. 1–40. <https://doi.org/10.1016/B978-0-12-813027-8.00001-1>
- Alexandra, R., Gerhard, J.I., Kueper, B.H., 2012. Hydraulic displacement of dense nonaqueous phase liquids for source zone stabilization. *Groundwater* 50, 765–774.
- Alexandridis, P., Ghasemi, M., Furlani, E.P., Tsianou, M., 2018. Solvent processing of cellulose for effective bioresource utilization. *Curr Opin Green Sustain Chem* 14, 40–52. <https://doi.org/https://doi.org/10.1016/j.cogsc.2018.05.008>
- AlSofi, A.M., Blunt, M.J., 2010. Streamline-Based Simulation of Non-Newtonian Polymer Flooding. *SPE Journal* 15, 895–905. <https://doi.org/10.2118/123971-PA>

- Amirmoshiri, M., Zhang, L., Puerto, M.C., Tewari, R.D., Bahrim, R.Z.B.K., Farajzadeh, R., Hirasaki, G.J., Biswal, S.L., 2020. Role of Wettability on the Adsorption of an Anionic Surfactant on Sandstone Cores. *Langmuir* 36, 10725–10738. <https://doi.org/10.1021/acs.langmuir.0c01521>
- Anderson, W.G., 1987. Wettability literature survey part 5: the effects of wettability on relative permeability. *Journal of petroleum technology* 39, 1453–1468.
- Ardakani, A.G., Mohammadi Alamooti, A.H., Rasaei, M.R., Javadi, A., Ghazanfari, M.H., Davarzani, H., 2020. Monitoring Polymer-Enhanced Foam Displacements Through Heterogeneous Porous Media: A Pore-Scale Study. *J Energy Resour Technol* 142. <https://doi.org/10.1115/1.4046943>
- Ataie-Ashtiani, B., Hassanizadeh, S.M., Celia, M.A., 2002. Effects of heterogeneities on capillary pressure–saturation–relative permeability relationships. *J Contam Hydrol* 56, 175–192.
- Auset, M., Keller, A.A., 2004. Pore-scale processes that control dispersion of colloids in saturated porous media. *Water Resour Res* 40. <https://doi.org/10.1029/2003WR002800>
- Aydin, G.A., Agaoglu, B., Kocasoy, G., Coptu, N.K., 2011. Effect of temperature on cosolvent flooding for the enhanced solubilization and mobilization of NAPLs in porous media. *J Hazard Mater* 186, 636–644. <https://doi.org/https://doi.org/10.1016/j.jhazmat.2010.11.046>
- Barnes, H.A., Hutton, J.F., Walters, K., 1989. *An introduction to rheology*. Elsevier.
- Barrere, G.C., Barber, C.E., Daniels, M.J., 1986. Molecular cloning of genes involved in the production of the extracellular polysaccharide xanthan by *Xanthomonas campestris* pv. *campestris*. *Int J Biol Macromol* 8, 372–374.
- Bear, J., 2013. *Dynamics of fluids in porous media*. Courier Corporation.
- Bedrikovetsky, P., Zeinijahromi, A., Siqueira, F.D., Furtado, C.A., de Souza, A.L.S., 2012. Particle Detachment Under Velocity Alternation During Suspension Transport in Porous Media. *Transp Porous Media* 91, 173–197. <https://doi.org/10.1007/s11242-011-9839-1>
- Benchabane, A., Bekkour, K., 2008. Rheological properties of carboxymethyl cellulose (CMC) solutions. *Colloid Polym Sci* 286, 1173–1180. <https://doi.org/10.1007/S00396-008-1882-2/FIGURES/5>
- Bern, P.A., Zamora, M., Slater, K.S., Hearn, P.J., 1996. The influence of drilling variables on barite sag, in: *SPE Annual Technical Conference and Exhibition*. OnePetro.
- Beyke, G., Fleming, D., 2005. In situ thermal remediation of DNAPL and LNAPL using electrical resistance heating. *Remediation Journal: The Journal of Environmental Cleanup Costs, Technologies & Techniques* 15, 5–22.
- Bezemer, L., Ubbink, J.B., de Kooker, J.A., Kuil, M.E., Leyte, J.C., 1993. On the conformational transitions of native xanthan. *Macromolecules* 26, 6436–6446.
- Bingham, E.C., 1917. *An investigation of the laws of plastic flow*. US Government Printing Office.
- Bobade, V., Cheetham, M., Hashim, J., Eshtiaghi, N., 2018. Influence of gas injection on viscous and viscoelastic properties of Xanthan gum. *Water Res* 134, 86–91. <https://doi.org/https://doi.org/10.1016/j.watres.2018.01.071>

- Boek, E.S., Hall, C., Tardy, P.M.J., 2012. Deep Bed Filtration Modelling of Formation Damage Due to Particulate Invasion from Drilling Fluids. *Transp Porous Media* 91, 479–508. <https://doi.org/10.1007/s11242-011-9856-0>
- Boger, D. V, 1977. Demonstration of upper and lower Newtonian fluid behaviour in a pseudoplastic fluid. *Nature* 265, 126–128. <https://doi.org/10.1038/265126a0>
- Böhme, G., 2012. *Non-Newtonian fluid mechanics*. Elsevier.
- Bossa, N., Carpenter, A.W., Kumar, N., de Lannoy, C.-F., Wiesner, M., 2017. Cellulose nanocrystal zero-valent iron nanocomposites for groundwater remediation. *Environ Sci Nano* 4, 1294–1303. <https://doi.org/10.1039/C6EN00572A>
- Bouزيد, I., Fatin-Rouge, N., 2022. Assessment of shear-thinning fluids and strategies for enhanced in situ removal of heavy chlorinated compounds-DNAPLs in an anisotropic aquifer. *J Hazard Mater* 432, 128703. <https://doi.org/https://doi.org/10.1016/j.jhazmat.2022.128703>
- Brooks, R.H., Corey, A.T., 1964. Hydraulic properties of porous media and their relation to drainage design. *Transactions of the ASAE* 7, 26–28.
- Browne, Christopher A, Shih, Audrey, Datta, Sujit S, Browne, C A, Shih, A, Datta, S S, 2020. Pore-Scale Flow Characterization of Polymer Solutions in Microfluidic Porous Media. *Small* 16, 1903944. <https://doi.org/10.1002/SMLL.201903944>
- Carreau, P.J., 1972. Rheological equations from molecular network theories. *Transactions of the Society of Rheology* 16, 99–127. <https://doi.org/https://doi.org/10.1122/1.549276>
- Carrington, S., Odell, J., Fisher, L., Mitchell, J., Hartley, L., 1996. Polyelectrolyte behaviour of dilute xanthan solutions: Salt effects on extensional rheology. *Polymer (Guildf)* 37, 2871–2875. [https://doi.org/10.1016/0032-3861\(96\)87653-1](https://doi.org/10.1016/0032-3861(96)87653-1)
- Casas, J.A., Mohedano, A.F., García-Ochoa, F., 2000. Viscosity of guar gum and xanthan/guar gum mixture solutions. *J Sci Food Agric* 80, 1722–1727.
- Casson, N., 1959. Flow equation for pigment-oil suspensions of the printing ink-type. *Rheology of disperse systems* 84–104.
- Cazaux, D., Colombano, S., Dumestre, A., Joubert, A., Lecuelle, G., 2014. Optimized physical recovery of DNAPL using upwelling technique and geostatistical analysis at large field scale, in: *Ninth International Conference on Remediation of Chlorinated and Recalcitrant Compounds*. p. x.
- Challen, I.A., 1994. Xanthan gum: a multifunctional stabiliser for food products, in: *Food Hydrocolloids: Structures, Properties, and Functions*. Springer, pp. 135–140.
- Chatzis, I., Morrow, N.R., 1984. Correlation of capillary number relationships for sandstone. *Society of Petroleum Engineers Journal* 24, 555–562. <https://doi.org/https://doi.org/10.2118/10114-PA>
- Chauveteau, G., Kohler, N., 1974. Polymer flooding: The essential elements for laboratory evaluation, in: *SPE Improved Oil Recovery Conference? SPE*, p. SPE-4745.
- Chauveteau, G., Zaitoun, A., 1981. Basic rheological behavior of xanthan polysaccharide solutions in porous media: effects of pore size and polymer concentration, in: *Proceedings of the First European Symposium on Enhanced Oil Recovery*, Bournemouth, England, Society of Petroleum Engineers, Richardson, TX. pp. 197–212.

- Cheng, S.-F., Wu, S.-C., 2000. The enhancement methods for the degradation of TCE by zero-valent metals. *Chemosphere* 41, 1263–1270. [https://doi.org/https://doi.org/10.1016/S0045-6535\(99\)00530-5](https://doi.org/https://doi.org/10.1016/S0045-6535(99)00530-5)
- Cheraghian, G., Khalili Nezhad, S.S., Kamari, M., Hemmati, M., Masihi, M., Bazgir, S., 2014. Adsorption polymer on reservoir rock and role of the nanoparticles, clay and SiO₂. *Int Nano Lett* 4, 1–8.
- Chhabra, R.P., 2010. Non-Newtonian fluids: an introduction. *Rheology of complex fluids* 3–34.
- Chiappa, L., Mennella, A., Lockhart, T.P., Burrafato, G., 1999. Polymer adsorption at the brine/rock interface: the role of electrostatic interactions and wettability. *J Pet Sci Eng* 24, 113–122.
- Chokejaroenrat, C., Comfort, S., Sakulthaew, C., Dvorak, B., 2014. Improving the treatment of non-aqueous phase TCE in low permeability zones with permanganate. *J Hazard Mater* 268, 177–184. <https://doi.org/https://doi.org/10.1016/j.jhazmat.2014.01.007>
- Cochennec, M., Davarzani, H., Davit, Y., Colombano, S., Ignatiadis, I., Masselot, G., Quintard, M., 2022. Impact of gravity and inertia on stable displacements of DNAPL in highly permeable porous media. *Adv Water Resour* 162, 104139. <https://doi.org/https://doi.org/10.1016/j.advwatres.2022.104139>
- Cohen, Y., Christ, F.R., 1986a. Polymer retention and adsorption in the flow of polymer solutions through porous media. *SPE Reservoir Engineering* 1, 113–118.
- Cohen, Y., Christ, F.R., 1986b. Polymer retention and adsorption in the flow of polymer solutions through porous media. *SPE Reservoir Engineering* 1, 113–118.
- Colombano, S., Davarzani, H., van Hullebusch, E.D., Huguenot, D., Guyonnet, D., Deparis, J., Ignatiadis, I., 2020. Thermal and chemical enhanced recovery of heavy chlorinated organic compounds in saturated porous media: 1D cell drainage-imbibition experiments. *Science of the Total Environment* 706, 135758. <https://doi.org/10.1016/j.scitotenv.2019.135758>
- Colombano, S., Davarzani, H., van Hullebusch, E.D., Huguenot, D., Guyonnet, D., Deparis, J., Lion, F., Ignatiadis, I., 2021. Comparison of thermal and chemical enhanced recovery of DNAPL in saturated porous media: 2D tank pumping experiments and two-phase flow modelling. *Science of the Total Environment* 760, 143958. <https://doi.org/10.1016/j.scitotenv.2020.143958>
- CRAIG JR, F.F., 1972. THE RESERVOIR ENGINEERING. *Society of Petroleum Engineers Journal* 12, 80.
- Crane, R.A., Scott, T.B., 2012. Nanoscale zero-valent iron: Future prospects for an emerging water treatment technology. *J Hazard Mater* 211–212, 112–125. <https://doi.org/https://doi.org/10.1016/j.jhazmat.2011.11.073>
- Cross, M.M., 1965. Rheology of non-Newtonian fluids: a new flow equation for pseudoplastic systems. *J Colloid Sci* 20, 417–437.
- Damrongsiri, S., Tongcumpou, C., Sabatini, D.A., 2013a. Partition behavior of surfactants, butanol, and salt during application of density-modified displacement of dense non-aqueous phase liquids. *J Hazard Mater* 248, 261–267.
- Damrongsiri, S., Tongcumpou, C., Sabatini, D.A., 2013b. Partition behavior of surfactants, butanol, and salt during application of density-modified displacement of dense non-aqueous phase liquids. *J Hazard Mater* 248–249, 261–267. <https://doi.org/https://doi.org/10.1016/j.jhazmat.2012.12.059>

- Dang, T.Q.C., Chen, Z., Nguyen, T.B.N., Bae, W., 2014. Investigation of isotherm polymer adsorption in porous media. *Pet Sci Technol* 32, 1626–1640.
- Darby, Ronald, Darby, Ron, Chhabra, R.P., 2017. *Chemical engineering fluid mechanics, revised and expanded*. CRC Press. <https://doi.org/https://doi.org/10.1201/9781315274492>
- Davarzani, H., Aranda, R., Colombano, S., Laurent, F., Bertin, H., 2022a. Modeling and monitoring of foam propagation in highly permeable porous media under lateral water flow. *Adv Water Resour* 166, 104225. <https://doi.org/10.1016/J.ADVWATRES.2022.104225>
- Davarzani, H., Aranda, R., Colombano, S., Laurent, F., Bertin, H., 2021a. Experimental study of foam propagation and stability in highly permeable porous media under lateral water flow: Diverting groundwater for application to soil remediation. *J Contam Hydrol* 243, 103917. <https://doi.org/10.1016/J.JCONHYD.2021.103917>
- Davarzani, H., Aranda, R., Colombano, S., Laurent, F., Bertin, H., 2021b. Experimental study of foam propagation and stability in highly permeable porous media under lateral water flow: Diverting groundwater for application to soil remediation. *J Contam Hydrol* 243, 103917. <https://doi.org/10.1016/J.JCONHYD.2021.103917>
- Davarzani, H., Philippe, N., Cochenec, M., Colombano, S., Dierick, M., Ataie-Ashtiani, B., Klein, P.-Y., Marcoux, M., 2022b. Numerical simulations of high viscosity DNAPL recovery in highly permeable porous media under isothermal and non-isothermal conditions. *J Contam Hydrol* 251, 104073.
- Debbabi, Y., Jackson, M.D., Hampson, G.J., Fitch, P.J.R., Salinas, P., 2017. Viscous crossflow in layered porous media. *Transp Porous Media* 117, 281–309. <https://doi.org/https://doi.org/10.1007/s11242-017-0834-z>
- Dejam, M., Hassanzadeh, H., Chen, Z., 2014. Reinfiltration through liquid bridges formed between two matrix blocks in fractured rocks. *J Hydrol (Amst)* 519, 3520–3530. <https://doi.org/10.1016/j.jhydrol.2014.10.050>
- Denys, K., Fichen, C., Zaitoun, A., 2001. Bridging adsorption of cationic polyacrylamides in porous media, in: *SPE International Conference on Oilfield Chemistry? SPE*, p. SPE-64984.
- De Vries, J., 1972. Soil filtration of wastewater effluent and the mechanism of pore clogging. *J Water Pollut Control Fed* 565–573.
- Dintzis, F.R., Babcock, G.E., Tobin, R., 1970. Studies on dilute solutions and dispersion of the polysaccharide from *Xanthomonas campestris* NRRL B-1459. *Carbohydr Res* 13, 257–267.
- Dominguez, J.G., Willhite, G.P., 1977. Retention and flow characteristics of polymer solutions in porous media. *Society of Petroleum Engineers Journal* 17, 111–121.
- Duffield, A.R., Ramamurthy, R.S., Campanelli, J.R., 2003. Surfactant enhanced mobilization of mineral oil within porous media. *Water Air Soil Pollut* 143, 111–122. <https://doi.org/10.1023/A:1022829204883>
- Dullien, F.A.L., 2012. *Porous media: fluid transport and pore structure*. Academic press.
- Elovich, S.Y., Larinov, O.G., 1962. Theory of adsorption from solutions of non electrolytes on solid (I) equation adsorption from solutions and the analysis of its simplest form,(II) verification of the

- equation of adsorption isotherm from solutions. *Izv. Akad. Nauk. SSSR, Otd. Khim. Nauk* 2, 209–216.
- Falls, A.H., Hirasaki, G.J., Patzek, T.W. et al, Gauglitz, D.A., Miller, D.D., Ratulowski, T., 1988. Development of a mechanistic foam simulator: the population balance and generation by snap-off. *SPE reservoir engineering* 3, 884–892.
- Farajzadeh, R., Bedrikovetsky, P., Lotfollahi, M., Lake, L.W., 2016. Simultaneous sorption and mechanical entrapment during polymer flow through porous media. *Water Resour Res* 52, 2279–2298.
- Fittolani, G., Seeberger, P.H., Delbianco, M., 2020. Helical polysaccharides. *Peptide Science* 112, e24124.
- Fitzhenry, E., Martel, R., Robert, T., 2022. Foam injection for enhanced recovery of diesel fuel in soils: Sand column tests monitored by CT scan imagery. *J Hazard Mater* 434, 128777.
- Flores, G., Katsumi, T., Inui, T., Kamon, M., 2011. A simplified image analysis method to study LNAPL migration in porous media. *Soils and foundations* 51, 835–847.
- French Ministry of Ecological Transition, 2022. Bilan environnemental de la France.
- French Ministry of Ecological Transition, 2015. Sols et environnement Chiffres clés.
- Fu, Y., Qin, C., Gao, S., Lv, C., Zhang, C., Yao, Y., 2022. Aquifer flushing using a SDS/1-butanol based in-situ microemulsion: Performance and mechanism for the remediation of nitrobenzene contamination. *J Hazard Mater* 424, 127409.
<https://doi.org/https://doi.org/10.1016/j.jhazmat.2021.127409>
- García-Ochoa, F., Santos, V.E., Casas, J.A., Gómez, E., 2000. Xanthan gum: production, recovery, and properties. *Biotechnol Adv* 18, 549–579. [https://doi.org/https://doi.org/10.1016/S0734-9750\(00\)00050-1](https://doi.org/https://doi.org/10.1016/S0734-9750(00)00050-1)
- Gbadamosi, A., Patil, S., Kamal, M.S., Adewunmi, A.A., Yusuff, A.S., Agi, A., Oseh, J., 2022. Application of polymers for chemical enhanced oil recovery: a review. *Polymers (Basel)* 14, 1433.
- Gerhard, J.I., Pang, T., Kueper, B.H., 2007. Time scales of DNAPL migration in sandy aquifers examined via numerical simulation. *Groundwater* 45, 147–157.
- Giese, S.W., Powers, S.E., 2002. Using polymer solutions to enhance recovery of mobile coal tar and creosote DNAPLs. *J Contam Hydrol* 58, 147–167. [https://doi.org/10.1016/S0169-7722\(02\)00009-8](https://doi.org/10.1016/S0169-7722(02)00009-8)
- Grubb, D.G., Sitar, N., 1999. Mobilization of trichloroethene (TCE) during ethanol flooding in uniform and layered sand packs under confined conditions. *Water Resour Res* 35, 3275–3289.
<https://doi.org/https://doi.org/10.1029/1999WR900222>
- Hanson, P.M., Trigg, T.K., Rachal, G., Zamora, M., 1990. Investigation of barite sag in weighted drilling fluids in highly deviated wells, in: *SPE Annual Technical Conference and Exhibition*. OnePetro.
- Heinemann, Z., Mittermeir, G., 2013. Fluid flow in porous media.
- Herschel, W.H., Bulkley, R., 1926. Konsistenzmessungen von Gummi-Benzollösungen. *Kolloid-Zeitschrift* 39, 291–300. <https://doi.org/10.1007/BF01432034>

- Herzig, J.P., Leclerc, D.M., Le Goff, P.L., 1970. Flow of Suspensions through Porous Media— Application to Deep Filtratio. *Ind Eng Chem* 62, 8–35. <https://doi.org/10.1021/ie50725a003>
- Higiro, J., Herald, T.J., Alavi, S., Bean, S., 2007. Rheological study of xanthan and locust bean gum interaction in dilute solution: Effect of salt. *Food Research International* 40, 435–447. <https://doi.org/10.1016/J.FOODRES.2006.02.002>
- Hirasaki, G.J., Miller, C.A., Szafranski, R., Lawson, J.B., Akiya, N., 1997a. Surfactant/foam process for aquifer remediation, in: *SPE International Conference on Oilfield Chemistry? SPE*, p. SPE-37257.
- Hirasaki, G.J., Miller, C.A., Szafranski, R., Tanzil, D., Lawson, J.B., Meinardus, H., Jin, M., Londergan, J.T., Jackson, R.E., Pope, G.A., 1997b. Field demonstration of the surfactant/foam process for aquifer remediation, in: *SPE Annual Technical Conference and Exhibition? SPE*, p. SPE-39292.
- Hollenbeck, K.-J., Jensen, K.H., 1998. Experimental evidence of randomness and nonuniqueness in unsaturated outflow experiments designed for hydraulic parameter estimation. *Water Resour Res* 34, 595–602.
- Holmberg, K., Jönsson, B., Kronberg, B., Lindman, B., 2002. *Surfactants and Polymers in Aqueous Solution*. Wiley-Blackwell. <https://doi.org/10.1002/0470856424>
- Holzwarth, G., 1976. Conformation of the extracellular polysaccharide of *Xanthomonas campestris*. *Biochemistry* 15, 4333–4339.
- Hommel, J., Coltman, E., Class, H., 2018. Porosity–Permeability Relations for Evolving Pore Space: A Review with a Focus on (Bio-)geochemically Altered Porous Media. *Transp Porous Media*. <https://doi.org/10.1007/s11242-018-1086-2>
- Ho Wase DAI & CF Forster CF, Y.S., 1996. Removal of lead ions from aqueous solution using sphagnum moss peat as adsorbent. *Water SA* 22, 219–224.
- Huang, Y., Sorbie, K.S., 1992a. The adsorption and in-situ rheological behavior of xanthan solution flowing through porous media, in: *SPE Improved Oil Recovery Conference? SPE*, p. SPE-24153.
- Huang, Y., Sorbie, K.S., 1992b. The adsorption and in-situ rheological behavior of xanthan solution flowing through porous media, in: *SPE/DOE Enhanced Oil Recovery Symposium. OnePetro*. <https://doi.org/https://doi.org/10.2118/24153-MS>
- Huling, S.G., Pivetz, B.E., 2006. In-situ chemical oxidation (EPA/600/R-06/072). US EPA.
- Imhoff, P.T., Gleyzer, S.N., McBride, J.F., Vancho, L.A., Okuda, I., Miller, C.T., 1995. Cosolvent-enhanced remediation of residual dense nonaqueous phase liquids: Experimental investigation. *Environ Sci Technol* 29, 1966–1976.
- Ishiguro, M., Koopal, L.K., 2016. Surfactant adsorption to soil components and soils. *Adv Colloid Interface Sci* 231, 59–102. <https://doi.org/https://doi.org/10.1016/j.cis.2016.01.006>
- Jamshidian, M., Savary, G., Grisel, M., Picard, C., 2014. Stretching properties of xanthan and hydroxypropyl guar in aqueous solutions and in cosmetic emulsions. *Carbohydr Polym* 112, 334–341.
- Jansson, P., Kenne, L., Lindberg, B., 1975. Structure of the extracellular polysaccharide from *Xanthomonas campestris*. *Carbohydr Res* 45, 275–282.

- Jawitz, J.W., Annable, M.D., Rao, P.S.C., 1998. Miscible fluid displacement stability in unconfined porous media: Two-dimensional flow experiments and simulations. *J Contam Hydrol* 31, 211–230. [https://doi.org/https://doi.org/10.1016/S0169-7722\(97\)00062-4](https://doi.org/https://doi.org/10.1016/S0169-7722(97)00062-4)
- Jeong, S.W., 2005. Evaluation of the use of capillary numbers for quantifying the removal of DNAPL trapped in a porous medium by surfactant and surfactant foam floods. *J Colloid Interface Sci* 282, 182–187. <https://doi.org/10.1016/j.jcis.2004.08.108>
- Jin, M., Hirasaki, G.J., Jackson, R.E., Kostarelos, K., Pope, G.A., 2007. Control of downward migration of dense nonaqueous phase liquid during surfactant flooding by design simulations. *Water Resour Res* 43. <https://doi.org/https://doi.org/10.1029/2006WR004858>
- Johansson, C., Bataillard, P., Biache, C., Lorgeoux, C., Colombano, S., Joubert, A., Défarge, C., Faure, P., 2022. Permanganate oxidation of polycyclic aromatic compounds (PAHs and polar PACs): column experiments with DNAPL at residual saturation. *Environmental Science and Pollution Research* 1–17.
- Johansson, C., Bataillard, P., Biache, C., Lorgeoux, C., Colombano, S., Joubert, A., Pigot, T., Faure, P., 2020. Ferrate VI oxidation of polycyclic aromatic compounds (PAHs and polar PACs) on DNAPL-spiked sand: degradation efficiency and oxygenated by-product formation compared to conventional oxidants. *Environmental Science and Pollution Research* 27, 704–716.
- Johnson, E.F., Bossler, D.P., Bossler, V.O.N., 1959. Calculation of relative permeability from displacement experiments. *Transactions of the AIME* 216, 370–372.
- Johnson, J.C., Sun, S., Jaffé, P.R., 1999. Surfactant Enhanced Perchloroethylene Dissolution in Porous Media: The Effect on Mass Transfer Rate Coefficients. *Environ Sci Technol* 33, 1286–1292. <https://doi.org/10.1021/ES980908D>
- Jones, S.C., Roszelle, W.O., 1978. Graphical techniques for determining relative permeability from displacement experiments. *Journal of Petroleum Technology* 30, 807–817.
- Kantzas, A., Bryan, J., Taheri, S., 2012. Fundamentals of fluid flow in porous media. Pore size distribution.
- Kavanaugh, M.C., Rao, P.S.C., Abriola, L., Cherry, J., Destouni, G., Falta, R., Major, D., Mercer, J., Newell, C., Sale, T., 2003. The DNAPL remediation challenge: Is there a case for source depletion? *US Environmental Protection Agency, National Risk Management Research*
- Keykhosravi, A., Vanani, M.B., Aghayari, C., 2021. TiO₂ nanoparticle-induced Xanthan Gum Polymer for EOR: Assessing the underlying mechanisms in oil-wet carbonates. *J Pet Sci Eng* 204, 108756. <https://doi.org/https://doi.org/10.1016/j.petrol.2021.108756>
- Kibbey, T.C.G., Ramsburg, C.A., Pennell, K.D., Hayes, K.F., 2002. Implications of alcohol partitioning behavior for in situ density modification of entrapped dense nonaqueous phase liquids. *Environ Sci Technol* 36, 104–111. <https://doi.org/https://doi.org/10.1021/es010966q>
- Kilbane, J.J., Chowdiah, P., Kayser, K.J., Misra, B., Jackowski, K.A., Srivastava, V.J., Sethu, G.N., Nikolov, A.D., Wasan, D.T., Hayes, T.D., 1997. Remediation of contaminated soils using foams. *Land Contamination and Reclamation* 5, 41–54.
- Kim, H., Cho, M.-Y., Annable, M.D., 2022. Analysis of facilitated air intrusion during surfactant-enhanced air sparging using surface tension-reducing chemicals: surfactants and alcohols. *Soil and Sediment Contamination: An International Journal* 31, 133–151.

- Kjosavik, A., Ringen, J.K., Skjaeveland, S.M., 2000. Relative permeability correlation for mixed-wet reservoirs, in: SPE Improved Oil Recovery Conference? SPE, p. SPE-59314.
- Kono, H., 2014. Characterization and properties of carboxymethyl cellulose hydrogels crosslinked by polyethylene glycol. *Carbohydr Polym* 106, 84–93.
<https://doi.org/10.1016/j.carbpol.2014.02.020>
- Koohbor, B., Colombano, S., Harrouet, T., Deparis, J., Lion, F., Davarzani, D., Ataie-Ashtiani, B., 2023. The effects of water table fluctuation on LNAPL deposit in highly permeable porous media: A coupled numerical and experimental study. *J Contam Hydrol* 256, 104183.
- Kovalick Jr, W.W., 2008. Review of Characterization and Remediation Technologies for NAPL's in Groundwater. *Methods and techniques for cleaning-up contaminated sites* 165–175.
- Králík, M., 2014. Adsorption, chemisorption, and catalysis. *Chemical Papers* 68, 1625–1638.
- Krstonošić, V., Milanović, M., Dokić, L., 2019. Application of different techniques in the determination of xanthan gum-SDS and xanthan gum-Tween 80 interaction. *Food Hydrocoll* 87, 108–118.
[https://doi.org/https://doi.org/10.1016/S0169-7722\(97\)00062-4](https://doi.org/https://doi.org/10.1016/S0169-7722(97)00062-4)
- Kueper, B.H., Frind, E.O., 1988. An overview of immiscible fingering in porous media. *J Contam Hydrol* 2, 95–110.
- Kueper, B.H., Redman, D., Starr, R.C., Reitsma, S., Mah, M., 1993. A field experiment to study the behavior of tetrachloroethylene below the water table: Spatial distribution of residual and pooled DNAPL. *Groundwater* 31, 756–766.
- Kueper, B.H., Stroo, H.F., Vogel, C.M., Ward, C.H., 2014. Chlorinated solvent source zone remediation. Springer.
- Lagergren, S.K., 1898. About the theory of so-called adsorption of soluble substances. *Sven. Vetenskapsakad. Handlingar* 24, 1–39.
- Langwaldt, J.H., Puhakka, J.A., 2000a. On-site biological remediation of contaminated groundwater: A review, in: *Environmental Pollution*. Elsevier, pp. 187–197. [https://doi.org/10.1016/S0269-7491\(99\)00137-2](https://doi.org/10.1016/S0269-7491(99)00137-2)
- Langwaldt, J.H., Puhakka, J.A., 2000b. On-site biological remediation of contaminated groundwater: A review, in: *Environmental Pollution*. Elsevier, pp. 187–197. [https://doi.org/10.1016/S0269-7491\(99\)00137-2](https://doi.org/10.1016/S0269-7491(99)00137-2)
- Lee, M., Kang, H., Do, W., 2005. Application of nonionic surfactant-enhanced in situ flushing to a diesel contaminated site. *Water Res* 39, 139–146.
<https://doi.org/https://doi.org/10.1016/j.watres.2004.09.012>
- Lenormand, R., Touboul, E., Zarcone, C., 1988. Numerical models and experiments on immiscible displacements in porous media. *J Fluid Mech* 189, 165–187.
<https://doi.org/https://doi.org/10.1017/S0022112088000953>
- Letey, J., 1994. Adsorption and desorption of polymers on soil. *Soil Sci* 158, 244–248.
- Liao, S., Saleeba, Z., Bryant, J.D., Abriola, L.M., Pennell, K.D., 2021. Influence of aqueous film forming foams on the solubility and mobilization of non-aqueous phase liquid contaminants in quartz sands. *Water Res* 195, 116975. <https://doi.org/https://doi.org/10.1016/j.watres.2021.116975>

- Li, K., Shen, P., Qing, T., 1994. A new method for calculating oil-water relative permeabilities with consideration of capillary pressure. *Mechanics and Practice* 16, 46–52.
- Littmann, W., 1988. *Polymer flooding*. Elsevier.
- Liu, S., 2008. *Alkaline Surfactant Polymer enhanced oil recovery process*. Rice University.
- Liu, W.H., Yu, T.L., Lin, H.L., 2007. Shear thickening behavior of dilute poly(diallyl dimethyl ammonium chloride) aqueous solutions. *Polymer (Guildf)* 48, 4152–4165.
<https://doi.org/10.1016/J.POLYMER.2007.05.012>
- Li, Y., Abriola, L.M., Phelan, T.J., Ramsburg, C.A., Pennell, K.D., 2007. Experimental and numerical validation of the total trapping number for prediction of DNAPL mobilization. *Environ Sci Technol* 41, 8135–8141. <https://doi.org/10.1021/es070834i>
- Lomeland, F., Ebeltoft, E., Thomas, W.H., 2005. A new versatile relative permeability correlation, in: *International Symposium of the Society of Core Analysts, Toronto, Canada*.
- Longino, B.L., Kueper, B.H., 1999. Effects of capillary pressure and use of polymer solutions on dense, non-aqueous-phase liquid retention and mobilization in a rough-walled fracture. *Environ Sci Technol* 33, 2447–2455. <https://doi.org/https://doi.org/10.1021/es980752h>
- Longpré-Girard, M., Martel, R., Robert, T., Lefebvre, R., Lauzon, J.-M., Thomson, N., 2020. Surfactant foam selection for enhanced light non-aqueous phase liquids (LNAPL) recovery in contaminated aquifers. *Transp Porous Media* 131, 65–84.
- Lunn, S.R.D., Kueper, B.H., 1999. Manipulation of density and viscosity for the optimization of DNAPL recovery by alcohol flooding. *J Contam Hydrol* 38, 427–445.
[https://doi.org/https://doi.org/10.1016/S0169-7722\(99\)00008-X](https://doi.org/https://doi.org/10.1016/S0169-7722(99)00008-X)
- Maire, J., Coyer, A., Fatin-Rouge, N., 2015. Surfactant foam technology for in situ removal of heavy chlorinated compounds-DNAPLs. *J Hazard Mater* 299, 630–638.
<https://doi.org/https://doi.org/10.1016/j.jhazmat.2015.07.071>
- Maire, J., Davarzani, H., Colombano, S., Fatin-Rouge, N., 2019. Targeted delivery of hydrogen for the bioremediation of aquifers contaminated by dissolved chlorinated compounds. *Environmental Pollution* 249, 443–452. <https://doi.org/10.1016/j.envpol.2019.03.033>
- Malik, M., Letey, J., 1991. Adsorption of polyacrylamide and polysaccharide polymers on soil materials. *Soil Science Society of America Journal* 55, 380–383.
- Mansouri-Boroujeni, M., Soulaïne, C., Azaroual, M., Roman, S., 2023. How interfacial dynamics controls drainage pore-invasion patterns in porous media. *Adv Water Resour* 171, 104353.
<https://doi.org/https://doi.org/10.1016/j.advwatres.2022.104353>
- Martel, K.E., Martel, R., Lefebvre, R., Gélinas, P.J., 1998. Laboratory study of polymer solutions used for mobility control during in situ NAPL recovery. *Ground Water Monit Remediat* 18, 103–113.
<https://doi.org/10.1111/j.1745-6592.1998.tb00734.x>
- Martel, R., Hébert, A., Lefebvre, R., Gélinas, P., Gabriel, U., 2004. Displacement and sweep efficiencies in a DNAPL recovery test using micellar and polymer solutions injected in a five-spot pattern. *J Contam Hydrol* 75, 1–29. <https://doi.org/10.1016/j.jconhyd.2004.03.007>

- Mashayekhizadeh, V., Ghazanfari, M.H., Kharrat, R., Dejam, M., 2011. Pore-Level Observation of Free Gravity Drainage of Oil in Fractured Porous Media. *Transp Porous Media* 87, 561–584. <https://doi.org/10.1007/s11242-010-9701-x>
- McCarty, P.L., 2010. *Groundwater Contamination by Chlorinated Solvents: History, Remediation Technologies and Strategies*. Springer, New York, NY, pp. 1–28. https://doi.org/10.1007/978-1-4419-1401-9_1
- McGuire, T.M., McDade, J.M., Newell, C.J., 2006. Performance of DNAPL source depletion technologies at 59 chlorinated solvent-impacted sites. *Groundwater Monitoring & Remediation* 26, 73–84.
- Mewis, J., Wagner, N.J., 2009. Thixotropy. *Adv Colloid Interface Sci* 147–148, 214–227. <https://doi.org/https://doi.org/10.1016/j.cis.2008.09.005>
- Meyers, M.A., Chawla, K.K., 2008. *Mechanical behavior of materials*. Cambridge university press.
- Miller, C.T., Hill, E.H., Moutier, M., 2000. Remediation of DNAPL-contaminated subsurface systems using density-motivated mobilization. *Environ Sci Technol* 34, 719–724.
- Mohammadnejad, H., Liao, S., Marion, B.A., Pennell, K.D., Abriola, L.M., 2020. Development and Validation of a Two-Stage Kinetic Sorption Model for Polymer and Surfactant Transport in Porous Media. *Environ Sci Technol* 54, 4912–4921. <https://doi.org/10.1021/acs.est.0c00123>
- Morrow, N.R., Songkran, B., 1981. Effect of viscous and buoyancy forces on nonwetting phase trapping in porous media, *Surface phenomena in enhanced oil recovery*. Springer. https://doi.org/https://doi.org/10.1007/978-1-4757-0337-5_19
- Mortensen, A., Aguilar, F., Crebelli, R., Di Domenico, A., Frutos, M.J., Galtier, P., Gott, D., Gundert-Remy, U., Lambré, C., 2017. Re-evaluation of xanthan gum (E 415) as a food additive. *EFSA Journal* 15, e04909.
- Mo, Y., Dong, J., Liang, X., Bai, J., 2023a. Influencing of hydrogeochemical conditions and engineering parameters on phase behaviors and remediation performance of in-situ microemulsion for residual PCE in aquifers. *Science of The Total Environment* 872, 162253. <https://doi.org/https://doi.org/10.1016/j.scitotenv.2023.162253>
- Mo, Y., Dong, J., Li, Y., Liang, X., Bai, J., 2023b. Formation of in-situ microemulsion and its efficiency for residual PCE removal in low temperature aquifers. *Colloids Surf A Physicochem Eng Asp* 656, 130461. <https://doi.org/https://doi.org/10.1016/j.colsurfa.2022.130461>
- Muhammed, N.S., Haq, M.B., Al-Shehri, D., Rahaman, M.M., Keshavarz, A., Hossain, S.M.Z., 2020. Comparative study of green and synthetic polymers for enhanced oil recovery. *Polymers (Basel)* 12, 2429.
- Najjari, M.R., Hinke, J.A., Bulusu, K. V., Plesniak, M.W., 2016. On the rheology of refractive-index-matched, non-Newtonian blood-analog fluids for PIV experiments. *Exp Fluids* 57, 1–6. <https://doi.org/10.1007/S00348-016-2185-X/FIGURES/4>
- Nono, F., Bertin, H., Hamon, G., 2014. An experimental investigation of the oil recovery in the transition zone of carbonate reservoirs taking into account wettability change, in: *IPTC 2014: International Petroleum Technology Conference*. European Association of Geoscientists & Engineers, p. cp-395.

- Nsengiyumva, E.M., Alexandridis, P., 2022. Xanthan gum in aqueous solutions: Fundamentals and applications. *Int J Biol Macromol* 216, 583–604.
<https://doi.org/https://doi.org/10.1016/j.ijbiomac.2022.06.189>
- O'Carroll, D., Sleep, B., Krol, M., Boparai, H., Kocur, C., 2013. Nanoscale zero valent iron and bimetallic particles for contaminated site remediation. *Adv Water Resour* 51, 104–122.
<https://doi.org/10.1016/J.ADVWATRES.2012.02.005>
- Ogata, A., Banks, R.B., 1961. A solution of the differential equation of longitudinal dispersion in porous media. US Government Printing Office.
- Olajire, A.A., 2014. Review of ASP EOR (alkaline surfactant polymer enhanced oil recovery) technology in the petroleum industry: Prospects and challenges. *Energy* 77, 963–982.
- Omirebekov, S., Colombano, S., Alamooti, A., Batikh, A., Cochennec, M., Amanbek, Y., Ahmadi-Senichault, A., Davarzani, H., 2023. Experimental study of DNAPL displacement by a new densified polymer solution and upscaling problems of aqueous polymer flow in porous media. *J Contam Hydrol* 252, 104120. <https://doi.org/https://doi.org/10.1016/j.jconhyd.2022.104120>
- Omirebekov, S., Davarzani, H., Ahmadi-Senichault, A., 2020a. Experimental Study of Non-Newtonian Behavior of Foam Flow in Highly Permeable Porous Media. *Ind Eng Chem Res* 59, 12568–12579.
<https://doi.org/10.1021/acs.iecr.0c00879>
- Omirebekov, S., Davarzani, H., Colombano, S., Ahmadi-Senichault, A., 2020b. Experimental and numerical upscaling of foam flow in highly permeable porous media. *Adv Water Resour* 146, 103761. <https://doi.org/10.1016/j.advwatres.2020.103761>
- O'Neill, P.L., Stachowiak, G., 1996. The inverse thixotropic behaviour of synovial fluid. *Journal of Orthopaedic Rheumatology* 9, 222–228.
- Oostrom, M., Dane, J.H., Wietsma, T.W., 2006. A review of multidimensional, multifluid intermediate-scale experiments: nonaqueous phase liquid dissolution and enhanced remediation. *Vadose Zone Journal* 5, 570–598.
- Owens, R.G., Phillips, T.N., 2002. *Computational rheology*. World Scientific.
- Pennell, K.D., Abriola, L.M., 2017. Surfactant-enhanced aquifer remediation: fundamental processes and practical applications, in: *Fundamentals and Applications*. Routledge, pp. 693–750.
- Pennell, K.D., Abriola, L.M., Weber Jr, W.J., 1993. Surfactant-enhanced solubilization of residual dodecane in soil columns. 1. Experimental investigation. *Environ Sci Technol* 27, 2332–2340.
- Pennell, K.D., Pope, G.A., Abriola, L.M., 1996. Influence of viscous and buoyancy forces on the mobilization of residual tetrachloroethylene during surfactant flushing. *Environ Sci Technol* 30, 1328–1335. <https://doi.org/10.1021/es9505311>
- Pérez Paricio, A., 2001. Integrated modelling of clogging processes in artificial groundwater recharge. Universidad Politécnica de Cataluña.
- Philippe, N., Davarzani, H., Colombano, S., Dierick, M., Klein, P.-Y., Marcoux, M., 2021. Experimental study of thermally enhanced recovery of high-viscosity DNAPL in saturated porous media under non-isothermal conditions. *J Contam Hydrol* 243, 103861.
- Philippe, N., Davarzani, H., Colombano, S., Dierick, M., Klein, P.-Y., Marcoux, M., 2020a. Experimental study of the temperature effect on two-phase flow properties in highly permeable porous

- media: Application to the remediation of dense non-aqueous phase liquids (DNAPLs) in polluted soil. *Adv Water Resour* 146, 103783.
- Philippe, N., Davarzani, H., Colombano, S., Dierick, M., Klein, P.Y., Marcoux, M., 2020b. Experimental study of the temperature effect on two-phase flow properties in highly permeable porous media: Application to the remediation of dense non-aqueous phase liquids (DNAPLs) in polluted soil. *Adv Water Resour* 146, 103783. <https://doi.org/10.1016/j.advwatres.2020.103783>
- Pourhakkak, P., Taghizadeh, A., Taghizadeh, M., Ghaedi, M., Haghdoust, S., 2021. Fundamentals of adsorption technology, in: *Interface Science and Technology*. Elsevier, pp. 1–70.
- Ramsburg, C.A., Pennell, K.D., 2002a. Density-modified displacement for dense nonaqueous-phase liquid source-zone remediation: Density conversion using a partitioning alcohol. *Environ Sci Technol* 36, 2082–2087. <https://doi.org/https://doi.org/10.1021/es011357l>
- Ramsburg, C.A., Pennell, K.D., 2002b. Density-modified displacement for dense nonaqueous-phase liquid source-zone remediation: Density conversion using a partitioning alcohol. *Environ Sci Technol* 36, 2082–2087. <https://doi.org/https://doi.org/10.1021/es011357l>
- Ramsburg, C.A., Pennell, K.D., Kibbey, T.C.G., Hayes, K.F., 2003. Use of a Surfactant-Stabilized Emulsion To Deliver 1-Butanol for Density-Modified Displacement of Trichloroethene. *Environ Sci Technol* 37, 4246–4253. <https://doi.org/10.1021/es0210291>
- Reddy, K.R., Tekola, L., 2004. Remediation of DNAPL source zones in groundwater using air sparging. *Land Contamination & Reclamation* 12, 67–84.
- Revellame, E.D., Fortela, D.L., Sharp, W., Hernandez, R., Zappi, M.E., 2020. Adsorption kinetic modeling using pseudo-first order and pseudo-second order rate laws: A review. *Clean Eng Technol* 1, 100032. <https://doi.org/https://doi.org/10.1016/j.clet.2020.100032>
- Richmond, P.C., Watson, A.T., 1990. Estimation of multiphase flow functions from displacement experiments. *SPE Reservoir Engineering* 5, 121–127.
- Ritchie, A.G., 1977. Alternative to the Elovich equation for the kinetics of adsorption of gases on solids. *Journal of the Chemical Society, Faraday Transactions 1: Physical Chemistry in Condensed Phases* 73, 1650–1653.
- Robert, T., Martel, R., Conrad, S.H., Lefebvre, R., Gabriel, U., 2006. Visualization of TCE recovery mechanisms using surfactant-polymer solutions in a two-dimensional heterogeneous sand model. *J Contam Hydrol* 86, 3–31. <https://doi.org/10.1016/j.jconhyd.2006.02.013>
- Rochefort, W.E., Middleman, S., 2000. Rheology of Xanthan Gum: Salt, Temperature, and Strain Effects in Oscillatory and Steady Shear Experiments. *J Rheol (N Y N Y)* 31, 337. <https://doi.org/10.1122/1.549953>
- Rodrigues, R., Betelu, S., Colombano, S., Masselot, G., Tzedakis, T., Ignatiadis, I., 2017a. Reductive Dechlorination of Hexachlorobutadiene by a Pd/Fe Microparticle Suspension in Dissolved Lactic Acid Polymers: Degradation Mechanism and Kinetics. *Ind Eng Chem Res* 56, 12092–12100. <https://doi.org/10.1021/acs.iecr.7b03012>
- Rodrigues, R., Betelu, S., Colombano, S., Masselot, G., Tzedakis, T., Ignatiadis, I., 2017b. Influence of temperature and surfactants on the solubilization of hexachlorobutadiene and hexachloroethane. *J Chem Eng Data* 62, 3252–3260. <https://doi.org/https://doi.org/10.1021/acs.jced.7b00320>

- Rodríguez de Castro, A., 2019. Extending Darcy's law to the flow of yield stress fluids in packed beds: Method and experiments. *Adv Water Resour* 126, 55–64. <https://doi.org/https://doi.org/10.1016/j.advwatres.2019.01.012>
- Roy, J.W., Smith, J.E., Gillham, R.W., 2004. Laboratory evidence of natural remobilization of multicomponent DNAPL pools due to dissolution. *J Contam Hydrol* 74, 145–161. <https://doi.org/10.1016/j.jconhyd.2004.02.009>
- Sandiford, B.B., 1964. Laboratory and field studies of water floods using polymer solutions to increase oil recoveries. *Journal of Petroleum Technology* 16, 917–922.
- Schincariol, R.A., Herderick, E.E., Schwartz, F.W., 1993. On the application of image analysis to determine concentration distributions in laboratory experiments. *J Contam Hydrol* 12, 197–215.
- Schulz, K.J., DeYoung, J.H., Seal, R.R., Bradley, D.C., 2018. Critical mineral resources of the United States: economic and environmental geology and prospects for future supply. Geological Survey.
- Sharma, A., Gautam, S., Wadhawan, S., 2014. Xanthomonas, in: Batt, C.A., Tortorello, M. Lou (Eds.), *Encyclopedia of Food Microbiology (Second Edition)*. Academic Press, Oxford, pp. 811–817. <https://doi.org/https://doi.org/10.1016/B978-0-12-384730-0.00359-1>
- Shook, G.M., Pope, G.A., Kostarelos, K., 1998. Prediction and minimization of vertical migration of DNAPLs using surfactant enhanced aquifer remediation at neutral buoyancy. *J Contam Hydrol* 34, 363–382. [https://doi.org/https://doi.org/10.1016/S0169-7722\(98\)00090-4](https://doi.org/https://doi.org/10.1016/S0169-7722(98)00090-4)
- Siegrist, R.L., Crimi, M., Simpkin, T.J., 2011. *In situ chemical oxidation for groundwater remediation*. Springer Science & Business Media.
- Silva, J.A.K., Liberatore, M., Mccray, J.E., Asce, M., 2013. Characterization of Bulk Fluid and Transport Properties for Simulating Polymer-Improved Aquifer Remediation. [https://doi.org/10.1061/\(ASCE\)EE.1943-7870.0000616](https://doi.org/10.1061/(ASCE)EE.1943-7870.0000616)
- Singhvi, G., Hans, N., Shiva, N., Dubey, S.K., 2019. Xanthan gum in drug delivery applications, in: *Natural Polysaccharides in Drug Delivery and Biomedical Applications*. Elsevier, pp. 121–144.
- Skauge, A., Zamani, N., Gausdal Jacobsen, J., Shaker Shiran, B., Al-Shakry, B., Skauge, T., 2018. Polymer flow in porous media: Relevance to enhanced oil recovery. *Colloids and Interfaces* 2, 27.
- Skjaeveland, S.M., Siqveland, L.M., Kjosavik, A., Thomas, W.L., Virnovsky, G.A., 2000. Capillary pressure correlation for mixed-wet reservoirs. *SPE Reservoir Evaluation & Engineering* 3, 60–67.
- Smith, M.M., Silva, J.A.K., Munakata-Marr, J., Mccray, J.E., 2008. Compatibility of polymers and chemical oxidants for enhanced groundwater remediation. *Environ Sci Technol* 42, 9296–9301. <https://doi.org/10.1021/es800757g>
- Sorbie, K.S., 2013. *Polymer-improved oil recovery*. Springer Science & Business Media.
- Sorbie, K.S., Seright, R.S., 1992. Gel placement in heterogeneous systems with crossflow, in: *SPE Improved Oil Recovery Conference? SPE*, p. SPE-24192.
- St-Pierre, C., Martel, R., Gabriel, U., Lefebvre, R., Robert, T., Hawari, J., 2004. TCE recovery mechanisms using micellar and alcohol solutions: phase diagrams and sand column experiments. *J Contam Hydrol* 71, 155–192. <https://doi.org/10.1016/J.JCONHYD.2003.09.010>

- Stroo, H.F., Leeson, A., Marqusee, J.A., Johnson, P.C., Ward, C.H., Kavanaugh, M.C., Sale, T.C., Newell, C.J., Pennell, K.D., Lebrón, C.A., Unger, M., 2012. Chlorinated ethene source remediation: Lessons learned. *Environ Sci Technol*. <https://doi.org/10.1021/es204714w>
- Taghavy, A., Costanza, J., Pennell, K.D., Abriola, L.M., 2010. Effectiveness of nanoscale zero-valent iron for treatment of a PCE–DNAPL source zone. *J Contam Hydrol* 118, 128–142. <https://doi.org/10.1016/J.JCONHYD.2010.09.001>
- Taylor, T.P., Pennell, K.D., Abriola, L.M., Dane, J.H., 2001. Surfactant enhanced recovery of tetrachloroethylene from a porous medium containing low permeability lenses: 1. Experimental studies. *J Contam Hydrol* 48, 325–350. [https://doi.org/https://doi.org/10.1016/S0169-7722\(00\)00185-6](https://doi.org/https://doi.org/10.1016/S0169-7722(00)00185-6)
- Taylor, T.P., Rathfelder, K.M., Pennell, K.D., Abriola, L.M., 2004. Effects of ethanol addition on micellar solubilization and plume migration during surfactant enhanced recovery of tetrachloroethene. *J Contam Hydrol* 69, 73–99. [https://doi.org/https://doi.org/10.1016/S0169-7722\(03\)00151-7](https://doi.org/https://doi.org/10.1016/S0169-7722(03)00151-7)
- Thombare, N., Jha, U., Mishra, S., Siddiqui, M.Z., 2016. Guar gum as a promising starting material for diverse applications: A review. *Int J Biol Macromol* 88, 361–372. <https://doi.org/https://doi.org/10.1016/j.ijbiomac.2016.04.001>
- Toth, J., Bodi, T., Szucs, P., Civan, F., 2002. Convenient formulae for determination of relative permeability from unsteady-state fluid displacements in core plugs. *J Pet Sci Eng* 36, 33–44. [https://doi.org/https://doi.org/10.1016/S0920-4105\(02\)00249-8](https://doi.org/https://doi.org/10.1016/S0920-4105(02)00249-8)
- Travis, C., Doty, C., 1990. ES&T views: can contaminated aquifers at superfund sites be remediated? *Environ Sci Technol* 24, 1464–1466.
- Tsakiroglou, C.D., Sikinioti-Lock, A., Terzi, K., Theodoropoulou, M., 2018. A numerical model to simulate the NAPL source zone remediation by injecting zero-valent iron nanoparticles. *Chem Eng Sci* 192, 391–413. <https://doi.org/10.1016/J.CES.2018.07.037>
- Tsitonaki, A., Petri, B., Crimi, M., Mosbaek, H., Siegrist, R.L., Bjerg, P.L., 2010. In situ chemical oxidation of contaminated soil and groundwater using persulfate: a review. *Crit Rev Environ Sci Technol* 40, 55–91.
- Unger, A.J.A., Sudicky, E.A., Forsyth, P.A., 1995. Mechanisms controlling vacuum extraction coupled with air sparging for remediation of heterogeneous formations contaminated by dense nonaqueous phase liquids. *Water Resour Res* 31, 1913–1925.
- USEPA, 2009. DNAPL Remediation: Selected Projects Where Regulatory Closure Goals Have Been Achieved. EPA/542/R-09/008. Washington, DC, USA.
- Vafai, K., 2015. Handbook of porous media. Crc Press.
- Van Genuchten, M.T., 1980. A closed-form equation for predicting the hydraulic conductivity of unsaturated soils. *Soil science society of America journal* 44, 892–898.
- Vigneswaran, S., Suazo, R.B., 1987. A detailed investigation of physical and biological clogging during artificial recharge. *Water Air Soil Pollut* 35, 119–140. <https://doi.org/10.1007/BF00183848>

- Voronov, R., VanGordon, S., Sikavitsas, V.I., Papavassiliou, D. V., 2010. Computational modeling of flow-induced shear stresses within 3D salt-leached porous scaffolds imaged via micro-CT. *J Biomech* 43, 1279–1286. <https://doi.org/10.1016/j.jbiomech.2010.01.007>
- Walker, D.I., Cápiro, N.L., Chen, E., Anderson, K., Pennell, K.D., 2022a. Micellar solubilization of binary organic liquid mixtures for surfactant enhanced aquifer remediation. *J Surfactants Deterg.* <https://doi.org/https://doi.org/10.1002/jsde.12637>
- Walker, D.I., Cápiro, N.L., Chen, E., Anderson, K., Pennell, K.D., 2022b. Micellar solubilization of binary organic liquid mixtures for surfactant enhanced aquifer remediation. *J Surfactants Deterg.*
- Wang, J., Guo, X., 2020. Adsorption kinetic models: Physical meanings, applications, and solving methods. *J Hazard Mater* 390, 122156. <https://doi.org/https://doi.org/10.1016/j.jhazmat.2020.122156>
- Wang, S., Mulligan, C.N., 2004. An evaluation of surfactant foam technology in remediation of contaminated soil. *Chemosphere* 57, 1079–1089. <https://doi.org/https://doi.org/10.1016/j.chemosphere.2004.08.019>
- Wei, C., Zheng, J., Xiong, L., Li, Z., Yang, J., Zhang, J., Lin, S., Zhou, L., Fang, L., Ding, Y., 2020. Evaluation and utilization of nano-micron polymer plug for heterogeneous carbonate reservoir with thief zones. *Advances in Polymer Technology* 2020.
- Wever, D.A.Z., Picchioni, F., Broekhuis, A.A., 2011. Polymers for enhanced oil recovery: a paradigm for structure–property relationship in aqueous solution. *Prog Polym Sci* 36, 1558–1628.
- Willhite, G.P., 1986. Waterflooding.
- Wu, B., Li, H., Du, X., Zhong, L., Yang, B., Du, P., Gu, Q., Li, F., 2016. Correlation between DNAPL distribution area and dissolved concentration in surfactant enhanced aquifer remediation effluent: A two-dimensional flow cell study. *Chemosphere* 144, 2142–2149. <https://doi.org/https://doi.org/10.1016/j.chemosphere.2015.11.005>
- Wu, W., Delshad, M., Oolman, T., Pope, G.A., 2000. Remedial Options for Creosote-Contaminated Sites. *Groundwater Monitoring & Remediation* 20, 78–86. <https://doi.org/https://doi.org/10.1111/j.1745-6592.2000.tb00268.x>
- Wyatt, N.B., Liberatore, M.W., 2009. Rheology and viscosity scaling of the polyelectrolyte xanthan gum. *J Appl Polym Sci* 114, 4076–4084.
- Xie, Q., Mumford, K.G., Kueper, B.H., Zhao, C., 2019. A numerical model for estimating the removal of volatile organic compounds in laboratory-scale treatability tests for thermal treatment of NAPL-impacted soils. *J Contam Hydrol* 226, 103526.
- Xu, J., Guo, C., Jiang, R., Wei, M., 2016. Study on relative permeability characteristics affected by displacement pressure gradient: Experimental study and numerical simulation. *Fuel* 163, 314–323. <https://doi.org/10.1016/J.FUEL.2015.09.049>
- Yang, C., Offiong, N.A., Chen, X., Zhang, C., Liang, X., Sonu, K., Dong, J., 2020. The role of surfactants in colloidal biliquid aphrons and their transport in saturated porous medium. *Environmental Pollution* 265, 114564. <https://doi.org/10.1016/J.ENVPOL.2020.114564>

- Yang, J., Pal, R., 2020. Investigation of Surfactant-Polymer Interactions Using Rheology and Surface Tension Measurements. *Polymers* 2020, Vol. 12, Page 2302 12, 2302. <https://doi.org/10.3390/POLYM12102302>
- Yan, Y.-L., Deng, Q., He, F., Zhang, X.-Q., Liu, Y.-P., 2011. Remediation of DNAPL-contaminated aquifers using density modification method with colloidal liquid aphrons. *Colloids Surf A Physicochem Eng Asp* 385, 219–228. <https://doi.org/https://doi.org/10.1016/j.colsurfa.2011.06.012>
- You, X., Liu, S., Dai, C., Guo, Y., Zhong, G., Duan, Y., 2020. Contaminant occurrence and migration between high- and low-permeability zones in groundwater systems: A review. *Science of The Total Environment* 743, 140703. <https://doi.org/10.1016/J.SCITOTENV.2020.140703>
- Yuan, H., Shapiro, A.A., 2011. A mathematical model for non-monotonic deposition profiles in deep bed filtration systems. *Chemical Engineering Journal* 166, 105–115. <https://doi.org/10.1016/j.cej.2010.10.036>
- Zamani, A., Maini, B., 2009. Flow of dispersed particles through porous media - Deep bed filtration. *J Pet Sci Eng* 69, 71–88. <https://doi.org/10.1016/j.petrol.2009.06.016>
- Zamani, N., Bondino, I., Kaufmann, R., Skauge, A., 2015. Effect of porous media properties on the onset of polymer extensional viscosity. *J Pet Sci Eng* 133, 483–495. <https://doi.org/https://doi.org/10.1016/j.petrol.2015.06.025>
- Zhang, Z.F., Smith, J.E., 2002. Visualization of DNAPL fingering processes and mechanisms in water-saturated porous media. *Transp Porous Media* 48, 41–59. <https://doi.org/10.1023/A:1015675404195>
- Zheng, X.L., Shan, B.B., Chen, L., Sun, Y.W., Zhang, S.H., 2014. Attachment-detachment dynamics of suspended particle in porous media: Experiment and modeling. *J Hydrol (Amst)* 511, 199–204. <https://doi.org/10.1016/j.jhydrol.2014.01.039>
- Zhong, L., Oostrom, M., Truex, M.J., Vermeul, V.R., Szecsody, J.E., 2013. Rheological behavior of xanthan gum solution related to shear thinning fluid delivery for subsurface remediation. *J Hazard Mater* 244–245, 160–170. <https://doi.org/10.1016/J.JHAZMAT.2012.11.028>
- Zhong, L., Oostrom, M., Wietsma, T.W., Covert, M.A., 2008. Enhanced remedial amendment delivery through fluid viscosity modifications: Experiments and numerical simulations. *J Contam Hydrol* 101, 29–41. <https://doi.org/https://doi.org/10.1016/j.jconhyd.2008.07.007>
- Zhong, L., Oostrom, M., Wietsma, T.W., Covert, M.A., 2008. Enhanced remedial amendment delivery through fluid viscosity modifications: Experiments and numerical simulations. *J Contam Hydrol* 101, 29–41.
- Zhou, D., Fayers, F.J., Orr, F.M., 1994. Scaling of multiphase flow in simple heterogeneous porous media, in: *SPE/DOE Improved Oil Recovery Symposium*. OnePetro. <https://doi.org/https://doi.org/10.2118/27833-MS>
- Zhou, M., Rhue, R.D., 2000. Effect of interfacial alcohol concentrations on oil solubilization by sodium dodecyl sulfate micelles. *J Colloid Interface Sci* 228, 18–23.
- Zitha, P.L.J., Botermans, C.W., 1998. Bridging adsorption of flexible polymers in low-permeability porous media. *SPE production & facilities* 13, 15–20.

Zitha, P.L.J., Chauveteau, G., Léger, L., 2001. Unsteady-state flow of flexible polymers in porous media. *J Colloid Interface Sci* 234, 269–283.

Zitha, P.L.J., Van Os, K.G.S., Denys, K.F.J., 1998. Adsorption of Linear Flexible Polymers During Laminar Flow Through Porous Media, in: *SPE Improved Oil Recovery Conference? SPE*, p. SPE-39675.